DEVELOPMENT OF A THREE DIMENSIONAL NUMERICAL WATER QUALITY MODEL FOR CONTINENTAL SHELF APPLICATIONS

By

Malcolm Spaulding

David Hunter

Ocean Engineering Department

University of Rhode Island

Kingston, Rhode Island 02881

Sponsored by:

National Aeronautics and Space Administration Grant NSG 1008

Langley Research Center

Hampton, Virginia 23665

ABSTRACT

A model to predict the distribution of water quality parameters in three dimensions has been developed, and applied to several theoretical and real problems. The mass transport equation is solved using a non-dimensional vertical axis and an alternating-direction-implicit finite difference technique. The reaction kinetics of the constituents are incorporated into a matrix method which permits computation of the interactions of multiple constituents.

Extensive literature reviews were made to determine the most appropriate methods available for the computation of dispersion coefficients and coliform bacteria decay rates. Numerical investigations of dispersive and dissipative effects showed that the three-dimensional model performed as predicted by the analysis of simpler cases. The mass transport was then linked to a two-dimensional vertically averaged tidal dynamics model for the Providence River. A uniform field was simulated, indicating mass conservation errors of less than 0.1 %. Modeling coliform concentrations in the area revealed a mass conservation error of as much as 3.5 %, due to an extrapolated, time-varying boundary condition. However, the model compared quite closely to a set of field data when no decay was

specified.

Additional effort was devoted to the extension of the model to a steady-state application, by replacing the time step with an iteration sequence. This was verified by comparison to analytical solutions, and demonstrated by application to a river confluence situation. Another application of the time-varying model was to point sources in Block Island Sound. A two-dimensional model prediction was compared to the three-dimensional distribution for the vertically well-mixed case, and found very similar after several tidal cycles.

TABLE OF CONTENTS

LIST OF FIGURES

LIST OF FIGURES (CONT.)

LIST OF FIGURES (CONT.)

LIST OF FIGURES (CONT.)

LIST OF FIGURES (CONT.)

LIST OF FIGURES (CONT.)

LIST OF FIGURES (CONT.)

LIST OF FIGURES (CONT.)

LIST OF TABLES

LIST OF SYMBOLS

a	endogenous respiration rate
A	abbreviation for coefficient of Equation 4.10
A_{ij}	amplitude of Fourier series component
b	estuary half-width
b_o	initial width of a dispersing patch
B	abbreviation for coefficient of Equation 4.10
C	concentration of dissolved constituent
D_{BOD}	concentration of biochemical oxygen demand
C_{DEF}	DO deficit, C_{DO} (saturation) - C_{DO}
C_{DO}	concentration of dissolved oxygen
C_h	Chezy coefficient
C_o	initial average concentration in a dispersing patch
C_{SBOD}	source concentration of BOD
C_{SDO}	source concentration of DO
C_{SNI}	concentration in the nitrogen system, where I = 1, 2, 3, 4, refers to organic, ammonia, nitrite, and nitrate nitrogen respectively
D/Dt	total derivative
D_z	component of longitudinal dispersion due to transverse velocity variations
D_v	component of longitudinal dispersion due to vertical velocity variations
D_w	base value diffusion coefficient
D_x, D_y, D_z	eddy diffusion or dispersion coefficients in the x-, y-, and z-directions, respectively

D_{zo}	D_z at neutral stability, $R_i = 0$
D_∞	dispersion coefficient for an infinitely long tidal cycle
e_x, e_y, e_z	turbulent diffusion coefficients in the x-, y-, and z-directions respectively
f_1	function relating D_x to U, C_h, and h
f_2	function relating D_y to V, C_h, and h
$f_n(t)$	function of lunar position
g	acceleration of gravity
h	mean sea level depth
h_t	vertical half-thickness of dye patch
h_z	hydraulic radius
H	sum of mean sea level depth and tide height
H_n	amplitude of tidal component
i	square root of -1
j	subscript indicating the number of a constituent
k	finite-difference index in the y-direction
k_d	dimensionless drag coefficient
K_h	epoch
k_p	half saturation constant for predators
k_s	coliform decay coefficient due to solar radiation
K_d	first order decay coefficient for coliforms
K_{ij}	component of reaction matrix
K_s	half saturation constant for nutrients
l	finite difference index in time
l(t)	solar radiation intensity
l_x	length scale in oceanic diffusion

L	length of estuary
m	finite difference index in the x direction
n	finite difference index in the η direction
N	the Manning factor
N_g^2	stratification number
N_s	stratification index
p	pressure
P	average concentration over a finite difference grid
$\vec{P}$	concentration vector
P_p	concentration of predators
q	horizontal velocity vector
q_n	tidal flowrate component
r	die-off rate due to physicochemical effects
R_i	Richardson number
S	source sink term
$\vec{S}$	source sink vector
S_n	concentration of nutrients
t	time
T	temperature
T_{100}	temperature of depth of 100 m
T_D	abbreviation for dispersive terms of mass transport equation
T'_H	dimensionless horizontal tidal variable
T'_v	dimensionless vertical tidal variable
T_t	tidal period
u	x-directed velocity
u'	velocity fluctuation
$\bar{u}$	time mean velocity

u^*	shear velocity
U	vertically averaged x-directed velocity
v	y-directed velocity
V	vertically averaged y-directed velocity
V_s	sedimentation velocity
w	z-directed velocity
WH	wave height
WL	wave length
WT	wave period
W_x	wind velocity in x-direction
W_y	wind velocity in y-direction
x	major horizontal axis
y	horizontal axis perpendicular to x-axis
y_{pc}	yield of predators on bacteria
z	vertical axis
Z	numerical error
α	dissipation parameter for diffusion
α_p	adjustable coefficient for calculating D_z
α_D	dimensional constant in velocity fluctuation relation
α_s	light attenuation coefficient in water
β	proportionality constant in R_i - D_z relations
β_p	adjustable coefficient for calculating D_z
β_s	accuracy criterion for tidal model
Δ	finite difference increment
∂	partial derivative in x-y-z coordinates

δ	partial derivative in x-y-η coordinates
Δ	partial derivative in x-y-z coordinates, in terms of x-y-η coordinates
ϵ	density gradient
ξ	tide height relative to mean sea level
η	dimensionless vertical axis
η_p	adjustable coefficient for calculating D_z
1	abbreviation for coefficient of Equation 4.9
2	abbreviation for coefficient of Equation 4.9
m	maximum predation rate
μ_m	maximum coliform growth rate
ρ	mass density of dissolved constitutent
ρ_a	density of air
σ	dispersion
σ_{rc}	dispersion measured radially
τ_{ij}	shear stress tensor
τ_k	time to first flood after high water
τ	propagation factor
ω	dimensionless vertical velocity
ω_s	angular speed of the earth

I. INTRODUCTION

Water Quality

"Water quality" generally refers to the ability of a body of water to support a healthy natural ecosystem, and additionally, to lend itself to the pleasures of man. The addition to the water of any substance that impairs this ability results in the degradation of water quality. Historically, it has been one of the "pleasures of man" to use bodies of water to dispose of various waste products. When the ocean or coastal waters were used for waste disposal, they were considered to be an ideal and limitless sink, capable of absorbing the wastes without reducing the water quality. Indicators of water quality (dissolved oxygen content, biochemical oxygen demand, fecal bacteria, heavy metal concentrations) were expected to be reduced to normal (ambient) levels due to the great assimilative or self-purifying capacity of the sea.

The growth of population and industrial production, especially close to the sea, in the past century has begun to strain the assimilative capacity of nearshore waters. Many harbors and confined bodies are so fouled that the natural aquatic populations are destroyed. Some areas that were thought to be in a natural state have revealed dangerously high levels of pollutants

(1)*. Some offshore areas close to population centers show marked degradation due to offshore dumping (2,3). Yet in other areas, similar quantities of waste have been dumped with minimal observed ill effects (4,5). It is clear that under some conditions, coastal waters are being taxed beyond their capacity; yet if conditions are suitable, the water can survive being used as a dump. Certainly, the need for waste disposal areas is pressing, and land disposal presents equally complex problems.

The critical question, then, is to what extent waste disposal in coastal waters can be permitted, without rendering the waters unfit for productive and pleasurable activity. Three aspects of this question must be dealt with: (1). What levels of which pollutants will produce what harmful effects? This question is the province of scientists, and the answers involve extensive and difficult laboratory and field testing, with results that to date are unsatisfactory. (2). What methods can be used to reduce harmful wastes to acceptable levels? Here the engineers join the scientists to develop or improve methods of waste treatment, outfall design, and environmental monitoring and modeling. (3). What are "acceptable levels" of pollution? This question can only be answered by the political process. The public must define, through

* Numbers in parentheses refer to listed references.

government, its economic priorities with regard to pollution. The usual practice is to classify waters according to their suitability for various activities under existing conditions, and to upgrade the waters whenever possible (6). As indicated by the recent defeat of sewer bond issues in Rhode Island (7), the public is likely to accept some reduction of water quality, rather than bear the cost of cleaning up.

Water Quality Models

Questions (1) and (2), above, form the realm in which water quality modeling can be of use. The term "model" has various levels of meaning. In a general sense, a model is "a conceptual idealization or simplified representation of a physical process" (8). This could include physical (hydraulic) models. A slight refinement is to define a model as the mathematical expression of the physical process; that is, the application of the principles of Newtonian fluid mechanics with approximations appropriate to an estuary or continental shelf (8). In the most specific sense, "model" refers to a mathematical formulation of the physical problem, along with an appropriate solution technique.

Water quality modeling has two purposes; diagnosis (identifying and isolating factors affecting water quality), and prediction of the effects of changes in

the system. A predictive model offers a technique widely useful in the design of waste disposal systems. The usual objective is to predict the distribution of a dissolved constituent or water quality indicator. Comparison of the distributions under different circumstances can aid in outfall location and design, setting water quality standards, choosing optimum levels of waste treatment, or anticipating the effects of special circumstances such as sewage plant overflow caused by storm runoff.

The mathematical model involves solution of the hydrodynamic equations and the parabolic, partial differential equation for transport of a dissolved constituent, by numerical techniques if necessary. Work began on this problem by using a one-dimensional approximation, a reasonable simplification for stream flow with a plane source of material. This was shown to be useful in rivers and in long, narrow estuaries (9,10,11). The more difficult two-dimensional computations have been applied to estuaries and lakes (12,13,14,15,16). In this case, either vertical averaging (13,14) or lateral averaging (15,16) was employed to eliminate the variation in whichever dimension was least important. There remained considerable uncertainty about the third dimension, which limited the applicability of these models to either shallow or narrow estuaries. The solution of the three-dimensional system presented a formidable task and

promised to consume large amounts of computer time and storage.

Many estuaries do not lend themselves well to a two-dimensional approximation. Estuaries with insignificant lateral currents and depth variation are rare. Although two-dimensional models can incorporate those variations, they can shed no light on the effect of outfalls at different depths, surface versus submerged discharges, or vertical stratification. A particular problem posed by stratification is the effect of seasonal variation in salinity structure. Also, due to the increasing use of relatively unconfined continental shelf waters for waste disposal, knowledge of the behavior of a dispersant in all three dimensions becomes essential. Information concerning vertical distributions is of particular importance in continental shelf waters; for instance, the settling patterns in barge disposal of sewage sludge-- a problem of increasing concern.

The Problem and the Method

The greatest obstacle to developing a three-dimensional model is that the vertical velocities are largely due to gravitational flow, which can be neglected in horizontal flow. Since gravity flow in estuaries and seas is mainly due to salinity gradients,

it would seem that the hydrodynamic and mass transport models must be coupled-- a serious complication (8). The hydrodynamic models used to obtain the current velocity input for the mass transport equation have used an approximation of constant density, which is useless in obtaining vertical velocities. The approach to be taken here, in the absence of a working three-dimensional hydrodynamic model, is to neglect all vertical velocities, and model the vertical transport of constituents by the diffusive mechanism only, which can incorporate salinity effects. This will be justified in Chapter III. The model has the capability to utilize vertical velocities, however. Models to generate the vertical velocity components, currently under development, will permit full realization of this capability.

A computer program to solve the three-dimensional mass transport equation by an alternating-direction-implicit (A.D.I.) finite difference method (17) has been written. A tidal current model has been developed for the Narragansett Bay area (18), based on Leendertse's long-wave propagation model (19). This has been employed to supply the required tide heights and horizontal current velocities.

Coliform bacteria concentration, the most widely-used indicator of sewage contamination, has been modeled only in a very sketchy manner, using a constant decay coefficient (20), or an oversimplified advection model,

with a constant, two-zone flow approximation (21). In addition, a well-distributed coliform data set exists for the Providence River estuary at the head of Narragansett Bay (22). This area is suitable for model development, due to its well-defined physical boundaries and sewage sources. This area is therefore chosen as the model area, with coliform bacteria as the quality indicator.

At this point, it is well to define the relationships of the physical and biochemical parameters which form the system to be modeled. The features being considered are shown in Figure 1.1, modified from Leendertse's model (14). The advection model will be discussed in Chapter V; the kinetic model in Chapter VI.

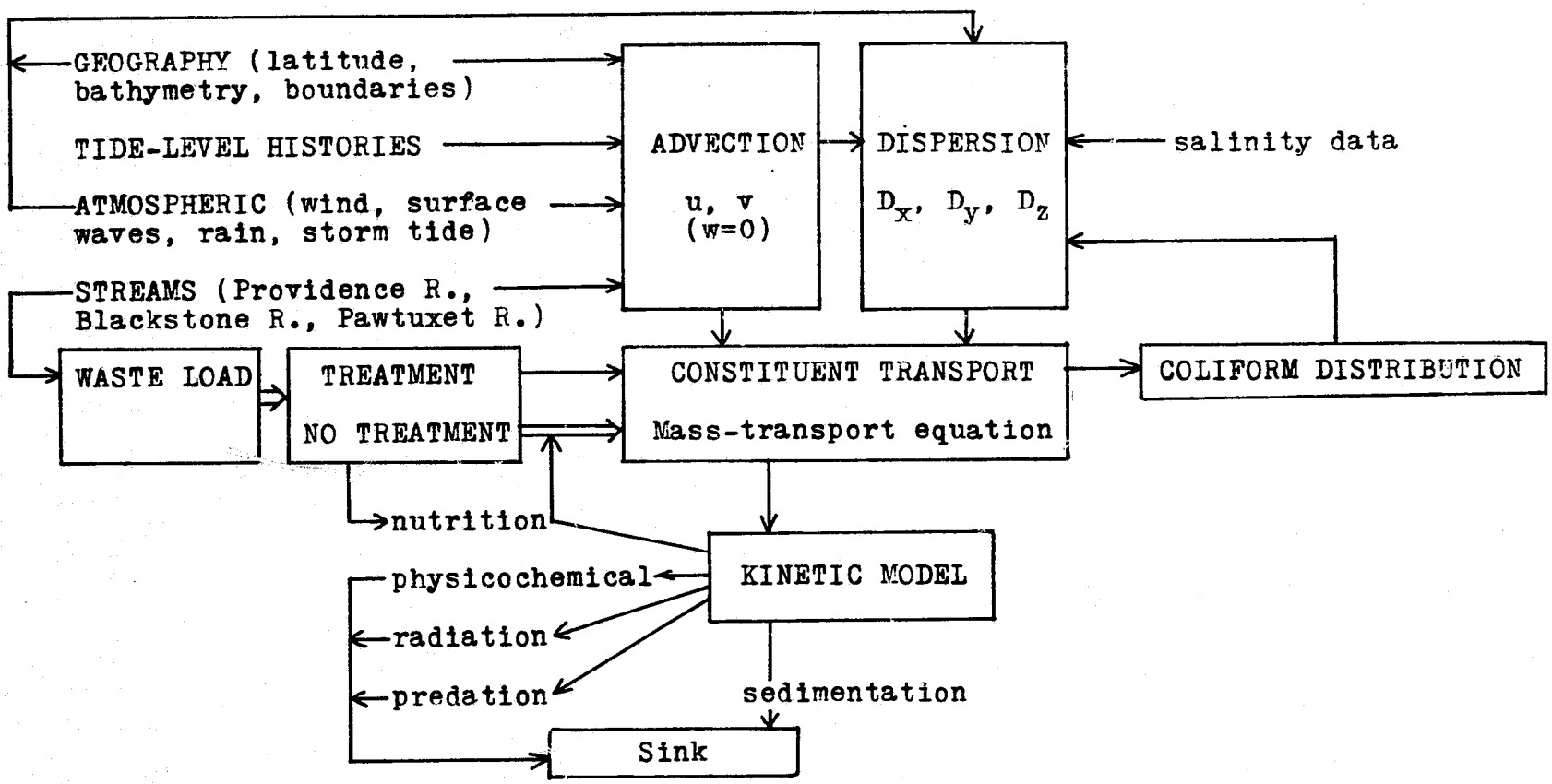

Figure 1.1. The environmental model

II. MASS TRANSPORT EQUATION AND SOLUTION

Basic Equation

The equation for transport of dissolved or suspended matter involves three mechanisms. Material is transported by advection due to the mean tidal velocity, and by dispersion due to turbulent mixing. Also, matter is transported into or out of the field at the boundaries, injected at sources, and removed or regenerated by reactions in the field. Using the familiar oceanographic coordinate system, in which the x- and y-directions are in the mean sea level plane, and z is directed downward from mean sea level, the mass transport equation is (23):

$$\frac{\partial \rho}{\partial t} + \frac{\partial \rho u}{\partial x} + \frac{\partial \rho v}{\partial y} + \frac{\partial \rho w}{\partial z} = \frac{\partial}{\partial x}\left(e_x \frac{\partial \rho}{\partial x}\right) + \frac{\partial}{\partial y}\left(e_y \frac{\partial \rho}{\partial y}\right) + \frac{\partial}{\partial z}\left(e_z \frac{\partial \rho}{\partial z}\right) + S \quad (2.1)$$

where ρ is the concentration of dissolved constituent

u, v, w are the x-, y-, z-directed velocities

e_x, e_y, e_z are the turbulent diffusion coefficients in the x, y, and z direction, respectively

S is the source-sink term.

The above includes approximations appropriate to estuaries and continental shelves. The diffusion terms

express the time-averaged turbulent flux terms $\overline{u'\rho'}$ as the product of an eddy diffusion coefficent and a mean concentration gradient. They do not include molecular diffusion, which for large bodies of water would be several orders of magnitude smaller than that due to turbulence. The velocities u, v, and w are time averages over a period much shorter than a tidal cycle, but longer than the turbulent fluctuations.

Spaulding (24) has found it helpful to non-dimensionalize the vertical axis. This eliminates complicated boundary conditions at the estuary bottom where depth variations are considerable, and also facilitates inclusion of the tidal variation in the overall depth. The parameter used to non-dimensionalize is the sum of the mean sea level depth, $h(x,y)$, and the tidal height, $\xi(x,y,t)$, at any time. The sum is called H. A dimensionless vertical scale, η, is defined:

$$\eta = \frac{z-\xi}{H} \quad \text{or} \quad z = \eta H + \xi \tag{2.2}$$

Thus η equals zero at the free surface and -1 at the bottom. A fairly complicated transformation is required to express Equation 2.1 in terms of the new vertical coordinate.

From Equation 2.2, since H and z are independent,

$$dz = H\, d\eta \tag{2.3}$$

Using the symbol δ to represent derivatives in the x-y-η

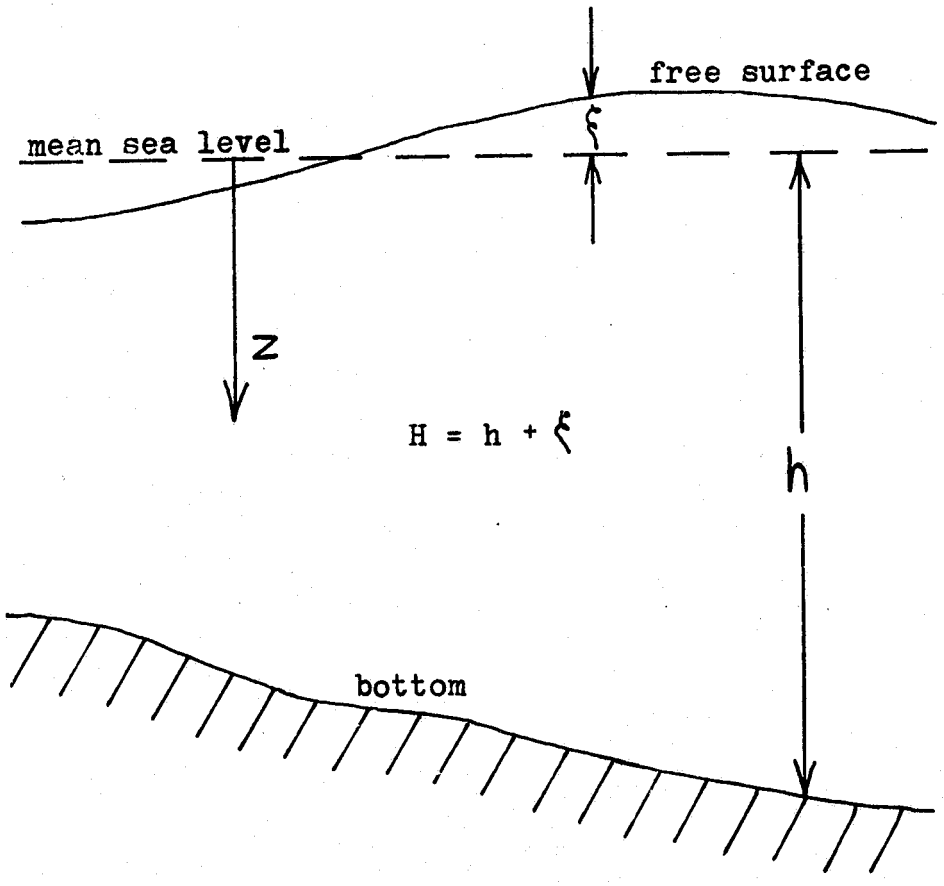

Figure 2.1. Definition of vertical coordinates

coordinates, the relationships between the partial derivatives in the x,y,z system and those in the x,y,η system are:

$$\frac{\partial}{\partial t} = \frac{\delta}{\delta t} - \frac{\delta z}{\delta t}\frac{\partial}{\partial z} = \frac{\delta}{\delta t} - \frac{\delta(\eta H + \xi)}{\delta t}\frac{\delta}{H\delta\eta} \qquad (2.4)$$

$$\frac{\partial}{\partial x} = \frac{\delta}{\delta x} - \frac{\delta(\eta H + \xi)}{\delta x}\frac{\delta}{H\delta\eta} \qquad (2.5)$$

$$\frac{\partial}{\partial y} = \frac{\delta}{\delta y} - \frac{\delta(\eta H + \xi)}{\delta y}\frac{\delta}{H\delta\eta} \qquad (2.6)$$

$$\frac{\partial}{\partial z} = \frac{\delta}{H\delta\eta} \qquad (2.7)$$

To find the relationship between the real velocity w and the dimensionless vertical velocity, ω, Equations 2.4 to 2.7 are substituted into the expression for the total derivative D / Dt. Since by definition, $D\eta / Dt = \omega$, the real vertical velocity is related to the dimensionless vertical velocity by:

$$w = \omega H + \frac{\delta(\eta H + \xi)}{\delta t} + u\frac{\delta(\eta H + \xi)}{\delta x} + v\frac{\delta(\eta H + \xi)}{\delta y} \qquad (2.8)$$

Substituting Equations 2.4 through 2.8 into the advective terms of Equation 2.1, rearranging, and multiplying by H, yields:

$$\frac{\delta H\rho}{\delta t} + \frac{\delta Hu\rho}{\delta x} + \frac{\delta Hv\rho}{\delta y} + \frac{\delta H\omega\rho}{\delta\eta} = HT_D \qquad (2.9)$$

where T_D represents the dispersive terms.

To express the dispersive terms compactly, let

$$\frac{\Delta}{\Delta x} = \frac{\delta}{\delta x} - \frac{\delta(\eta H + \xi)}{\delta x} \frac{\delta}{H \delta \eta} \qquad (2.10)$$

$$\frac{\Delta}{\Delta y} = \frac{\delta}{\delta x} - \frac{\delta(\eta H + \xi)}{\delta y} \frac{\delta}{H \delta \eta} \qquad (2.11)$$

Transforming the z-dispersive terms by Equation 2.3, and the x- and y-terms by Equations 2.10 and 2.11 respectively, the full equation for mass transport becomes:

$$\frac{\delta H\rho}{\delta t} + \frac{\delta Hu\rho}{\delta x} + \frac{\delta Hv\rho}{\delta y} + \frac{\delta H\omega\rho}{\delta \eta} = \qquad (2.12)$$
$$H \frac{\Delta}{\Delta}\left(e_x \frac{\Delta \rho}{\Delta x}\right) + H \frac{\Delta}{\Delta}\left(e_y \frac{\Delta \rho}{\Delta y}\right) + \frac{\delta}{\delta \eta}\left(\frac{e_z}{H} \frac{\delta \rho}{\delta \eta}\right) + HS$$

If one is willing to sacrifice some accuracy, the dispersive terms can be expanded and simplified by assuming the higher-order terms to be small. The simplified form is then:

$$HT_D = \frac{\delta}{\delta x}\left(H e_x \frac{\delta \rho}{\delta x}\right) + \frac{\delta}{\delta y}\left(H e_y \frac{\delta \rho}{\delta y}\right) + \frac{\delta}{\delta \eta}\left(\frac{e_z}{H} \frac{\delta \rho}{\delta \eta}\right) \qquad (2.13)$$

Reaction Model Concept

The source-sink term, S in Equation 2.12 above, includes the reaction kinetics, if any, of the water

quality parameter. The composition of the term will depend on whether the constituent is conservative, undergoes simple decay, two-stage, or multi-stage reactions. Examples of the source term formulations follow:

(1). Salinity (conservative) (24)

$$S = 0 \qquad (2.14a)$$

(2). Coliform bacteria (single-stage decay)

$$S = C_S + K_d C \qquad (2.14b)$$

(3). DO-BOD (two-stage consecutive reaction) (8)

$$\text{DO:} \quad S = C_{SDO} + K_{11} C_{DEF} - K_{12} C_{BOD}$$
$$\text{BOD:} \quad S = C_{SBOD} - K_{22} C_{BOD} \qquad (2.14c)$$

where K_{22} is the BOD decay rate

K_{11} is the reaeration rate

C_{DEF} is the DO deficit, $C_{DO}^{(sat.)} - C_{DO}$

C_{SDO} is sources and sinks of oxygen, i.e., at the boundaries,

C_{SBOD} is waste-load BOD.

(4). Nitrification (multi-stage consecutive) (8)

Organic matter: $S = C_{SN1} + K_{11} N_1$

Ammonia: $S = C_{SN2} + K_{22} N_2 + K_{12} N_1$

Nitrite: $S = C_{SN3} + K_{33} N_3 + K_{23} N_2$

Nitrate nitrogen: $S = C_{SN4} + K_{44} N_4 + K_{34} N_3$

where N_s is a concentration, and the subscripts 1, 2, 3, and 4 refer to organic, ammonia, nitrite, and nitrate nitrogen respectively.

As the examples above indicate, this problem lends itself to a matrix formulation. As suggested by Leendertse, this is expressed as:

$$S = [K] \vec{P} + \vec{S} \qquad (2.15)$$

where $\vec{S}$ is the source or sink vector

$[K]$ is the reaction matrix

$\vec{P}$ is the concentration vector.

For example, in the DO-BOD system, this becomes

$$S = [K]\vec{P} + \vec{S}$$

$$= \begin{bmatrix} -K_{11} & -K_{12} \\ 0 & -K_{22} \end{bmatrix} \begin{bmatrix} C_{DO} \\ C_{BOD} \end{bmatrix} + \begin{bmatrix} K_{11} C_{DO(sat.)} + C_{SDO} \\ C_{SBOD} \end{bmatrix}$$

Numerical Techniques

A basic approach to an initial-value problem expressed as a set of partial differential equations is the finite-difference approximation. This means that the differentials are expressed as a small but finite step in space, over which the valuables of the dependent variables are calculates repetitively at similarly small time steps. The following integer subscripts will be used to denote spatial increments and the time step in the corresponding directions:

m: x-direction

k: y-direction

n: η-direction

l: time

For parabolic, and also for elliptic, equations, the alternating direction method (17) has been effective. This involves splitting the equation into a different level for each direction, and advancing in fractions of time steps. The advantages are unconditional stability, suitability for an implicit solution, and the ability to solve by a tridiagonal matrix technique. This method was extended by Douglas (17) and Douglas and Gunn (25) for three-dimensional

computations, and will be employed in the present study. An additional refinement is to choose a space-staggered grid system, as shown in Figure 2.1 (17). The purpose of the staggered grid is to have each variable centered between the ones upon which its calculation most depends. The distances are expressed as the products of the aforementioned integers, m, k, n, and the spatial grid sizes Δx, Δy, $\Delta\eta$. The mass density, ρ, is now called P, to indicate that it is an average value over the grid volume, rather than a point function. The functional relation is now expressed as (24):

$$P(x,y,\eta,t) = P(m\Delta x, k\Delta y, n\Delta\eta, l\Delta t) = P^{l}_{m,k,n} \qquad (2.16)$$

The following difference operators are defined:

$$\delta_x P^{l}_{m,k,n} = P^{l}_{m+\frac{1}{2},k,n} - P^{l}_{m-\frac{1}{2},k,n}$$

$$\delta_y P^{l}_{m,k,n} = P^{l}_{m,k+\frac{1}{2},n} - P^{l}_{m,k-\frac{1}{2},n}$$

$$\delta_\eta P^{l}_{m,k,n} = P^{l}_{m,k,n+\frac{1}{2}} - P^{l}_{m,k,n-\frac{1}{2}}$$

The first equation below calculates the x-directed concentration variations from time-level l to $l+\frac{1}{3}$. These values are then used to calculate the y-directed variations from time-level $l+\frac{1}{3}$ to $l+\frac{2}{3}$. Finally, the η-variations are calculated from level $l+\frac{2}{3}$ to $l+1$, using the previously obtained values. This completes the time step. Using the approach of Douglas (1), the finite-difference form of Equation 2.12 is the following three-equation system (24):

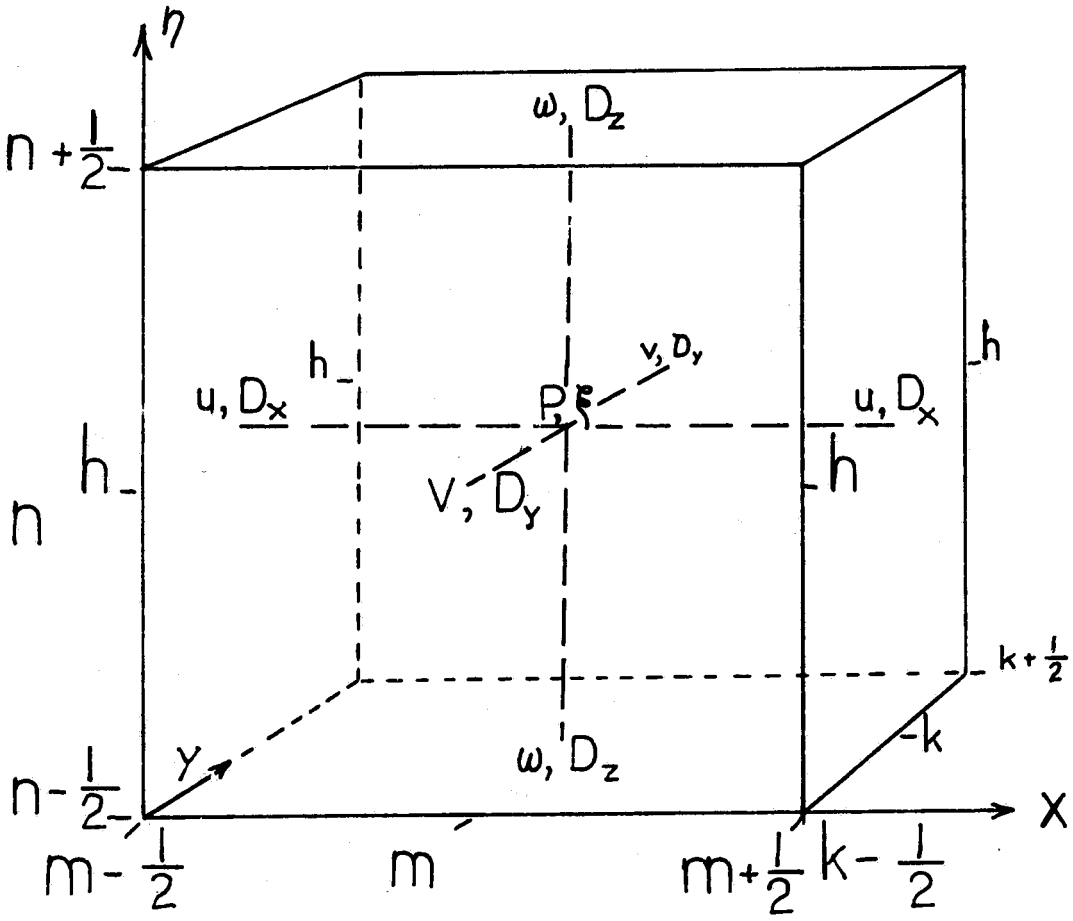

h- Mean sea level depth

ξ- tidal height

u, v, ω- velocities in x, y, η directions respectively

P- mass density

D_x, D_y, D_z- Dispersion coefficients

Figure 2.2. Three-dimensional space-staggered grid system

$$\frac{(HP)^{\ell+\frac{1}{3}} - (HP)^{\ell}}{\Delta t} = -\frac{1}{2}\delta_x(UHP)^{\ell+\frac{1}{3}} - \frac{1}{2}\delta_x(UHP)^{\ell} + \frac{1}{2}\delta_x\left(D_x H \delta_x(P)\right)^{\ell+\frac{1}{3}}$$
$$+\frac{1}{2}\delta_x\left(D_x H \delta_x(P)\right)^{\ell} - \delta_y(VHP)^{\ell} - \delta_\eta(\omega HP)^{\ell} + \delta_y\left(D_y H \delta_y(P)\right)^{\ell}$$
$$+\delta_\eta\left(\frac{D_z}{H}\delta_\eta(P)\right)^{\ell} + SH^{\ell} \qquad (2.17)$$

$$\frac{(HP)^{\ell+\frac{2}{3}} - (HP)^{\ell}}{\Delta t} = -\frac{1}{2}\delta_x(UHP)^{\ell+\frac{1}{3}} - \frac{1}{2}\delta_x(UHP)^{\ell} + \frac{1}{2}\delta_x\left(D_x H \delta_x(P)\right)^{\ell+\frac{1}{3}}$$
$$+\frac{1}{2}\delta_x\left(D_x H \delta_x(P)\right)^{\ell} - \frac{1}{2}\delta_y(VHP)^{\ell+\frac{2}{3}} - \frac{1}{2}\delta_y(VHP)^{\ell} + \frac{1}{2}\delta_y\left(D_y H \delta_y(P)\right)^{\ell+\frac{2}{3}}$$
$$+\frac{1}{2}\delta_y\left(D_y H \delta_y(P)\right)^{\ell} - \delta_\eta(\omega HP)^{\ell} + \delta_\eta\left(\frac{D_z}{H}\delta_\eta(P)\right)^{\ell} \qquad (2.18)$$

$$\frac{(HP)^{\ell+1} - (HP)^{\ell}}{} = -\frac{1}{2}\delta_x(UHP)^{\ell+\frac{1}{3}} - \frac{1}{2}\delta_x(UHP)^{\ell} + \frac{1}{2}\delta_x\left(D_x H \delta_x(P)\right)^{\ell+\frac{1}{3}}$$
$$+\frac{1}{2}\delta_x\left(D_x H \delta_x(P)\right)^{\ell} - \frac{1}{2}\delta_y(VHP)^{\ell+\frac{2}{3}} - \frac{1}{2}\delta_y(VHP)^{\ell} + \frac{1}{2}\delta_y\left(D_y H \delta_y(P)\right)^{\ell+\frac{2}{3}}$$
$$+\frac{1}{2}\delta_y\left(D_y H \delta_y(P)\right)^{\ell} - \frac{1}{2}\delta_\eta(\omega HP)^{\ell+1} - \frac{1}{2}\delta_\eta(\omega HP)^{\ell} + \frac{1}{2}\delta_\eta\left(\frac{D_z}{H}\delta_\eta(P)\right)^{\ell+1}$$
$$+\frac{1}{2}\delta_\eta\left(\frac{D_z}{H}\delta_\eta(P)\right)^{\ell} \qquad (2.19)$$

A simplification can be made by subtracting Equation 2.17 from 2.18, and 2.18 from 2.19. This yields (24):

$$\frac{2}{\Delta t}\left((HP)^{\ell+\frac{1}{3}} - (HP)^{\ell}\right) = -\delta_x(UHP)^{\ell+\frac{1}{3}} - \delta_x(UHP)^{\ell}$$
$$+\delta_x\left(D_x H \delta_x(P)\right)^{\ell+\frac{1}{3}} + \delta_x\left(D_x H \delta_x(P)\right)^{\ell} - 2\delta_y(VHP)^{\ell} - 2\delta_\eta(\omega HP)^{\ell}$$
$$+2\delta_y\left(D_y H \delta_y(P)\right)^{\ell} + 2\delta_\eta\left(\frac{D_z}{H}\delta_\eta(P)\right)^{\ell} - 2HS^{\ell+\frac{1}{3}} \qquad (2.20)$$

$$\frac{2}{\Delta t}\left((HP)^{\ell+\frac{2}{3}} - (HP)^{\ell+\frac{1}{3}}\right) = -\delta_y(VHP)^{\ell+\frac{2}{3}} - \delta_y(VHP)^{\ell}$$
$$+\delta_y\left(D_y H \delta_y(P)\right)^{\ell+\frac{2}{3}} - \delta_y\left(D_y H \delta_y(P)\right)^{\ell} \qquad (2.21)$$

$$\frac{2}{\Delta t}\left((HP)^{l+1}-(HP)^{l+\frac{2}{3}}\right) = -\delta_\eta\left(\omega HP\right)^{l+1} + \delta_\eta\left(\omega HP\right)^{l}$$
$$+\delta_\eta\left(\frac{D_z}{H}\delta_\eta(P)\right)^{l+1} - \delta_\eta\left(\frac{D_z}{H}\delta_\eta(P)\right)^{l} \qquad (2.22)$$

The source-sink term, (HS) in Equation 2.12, is approximated by the reaction matrix scheme. In finite difference notation, this term becomes

$$(HS_j)^{l+\frac{1}{2}} = \sum_{j=1}^{j_{max}} (HK_{ij}\, P_j)^{l+\frac{1}{2}} + (HS_j)^{l+\frac{1}{2}} \qquad (2.23)$$

where the subscripts i and j distinguish elements of the reaction matrix.

In the above, the value of $P_j^{l+\frac{1}{2}}$ is unknown. If the previous value of P is used, accuracy is lost. The alternative is to estimate a new value for $P_j^{l+\frac{1}{2}}$ from Equations 2.20, 2.21, and 2.22. Then the solution must be readvanced in time using the estimate. This restores the accuracy, but doubles the computational time. The additional accuracy gained by this estimation normally does not justify the additional computational time requirement, and is therefore not used in this study.

III. METHODS FOR CALCULATING DISPERSION COEFFICIENTS

Definitions

Qualitative definitions of diffusion and dispersion have been suggested by Holley (26): "let diffusion refer to transport in a given direction due to the difference between the true convection in that direction and the time average of the convection in that direction . . . Let dispersion refer to the transport in a given direction due to the difference between the true convection in that direction and the spatial average of the convection in that direction." Briefly, diffusion is due to molecular and turbulent motion, and dispersion is due to the variation of the mean velocity across a section.

A diffusion coefficient is given by

$$D_x = \frac{1}{2} \frac{d(\sigma_x^2)}{dt} \tag{3.1}$$

where σ_x is the mean square dispersion of particles (27); in other words, the standard deviation of the concentration distribution in the dye plume. This consists of a molecular and an eddy diffusion term. The former is negligible, especially in open waters, where the molecular effect is several orders of magnitude smaller than the eddy effect.

Prandtl expressed the diffusion coefficient in terms of fluid turbulence (27):

$$D_x = l_x \sqrt{\overline{u'^2}} \qquad (3.2)$$

where l_x is a mixing length, and $\overline{u'^2}$ is the mean square velocity fluctuation. The mixing length can be defined in several ways, and will be discussed in a later section. The velocity fluctuation is the difference between the velocity at any instant and the mean velocity:

$$u = \bar{u} + u' \qquad (3.3)$$

The mean square dispersion is given at any time by the concentration of the dispersant at a distance x (28):

$$\sigma_x = \frac{1}{c_o b_o} \int_{-\infty}^{\infty} x^2 c(x)\, dx \qquad (3.4)$$

where b_o is the initial width of the patch of dispersant, and c_o is the initial average concentration therein. Foxworthy found that as the time scale of the process increases, the value of σ is time-dependent (29). For small, intermediate, and large time scales, was found proportional to t^2, t^3, and t respectively. Thus the diffusivity is determined by different functions of time, until the time scale is such that the patch has become larger than the characteristic eddies. This is called the asymptotic phase.

Oceanic Diffusion-- Horizontal

The horizontal eddy diffusion coefficient, in the

absence of a stream flow, is generally taken as a function only of a length scale, which increases as the patch disperses. The simplest definition of the scale, l_x, is the width of the patch at a given time (27). As a mixing length, l_x is defined as the characteristic distance traveled by the eddies before losing their identity. This, however, is not a very useful definition. Taking the scale as the patch width, this is variously defined according to the dispersion σ. For lateral diffusion (27):

$$l_x = 4\sigma \tag{3.5}$$

or, for a line source, so that $l_x = b$ at $x = 0$:

$$l_x = 2\sqrt{3}\,\sigma \tag{3.6}$$

For radial diffusion, Okubo gives (30):

$$l_x = 3\sigma_{rc} \tag{3.7}$$

where the subscript rc signifies the radial distribution. The above all specify that 95% of the diffusant is contained within a distance of 4σ, $2\sqrt{3}\,\sigma$, or $3\sigma_{rc}$.

Oceanic turbulent diffusion is considered to consist of three phases, corresponding to the aforementioned time scales (29):

(a). eddies larger than the initial dye patch,

(b). eddies comparable in size to the dye patch,

(c). eddies smaller than the dye patch.

(c) is the asymptotic phase, and produces the greatest rate of mixing. In finite difference modeling, the requirement of an initial average concentration

throughout a large finite volume makes it reasonable to assume that the diffusion is in the asymptotic phase. If the model scale is such that eddies larger than a single grid exist, the eddies then appear as part of the velocity field. As the resolution of the hydrodynamic model is improved, the dispersion terms become less important.

The basic relation considered to hold for oceanic turbulent diffusion, in the asymptotic phase, comes from Richardson's law for atmospheric diffusion (31):

$$D_x = \alpha_D l_x^{4/3} \tag{3.8}$$

where D_x is the horizontal eddy diffusion coefficient, and α_D is the dissipation parameter. This is called the "four-thirds law". Many field measurements of the diffusion coefficient have been made. The general procedure is to use a fluorometer to measure the concentration of dye tracer at a known distance and time from its injection. The coefficient is calculated from (26):

$$D_x = \frac{1}{2} \frac{(\sigma_2^2 - \sigma_1^2)}{(t_2 - t_1)} \tag{3.9}$$

In the attempt to determine the validity of the four-thirds law for diffusion in ocean waters, and to determine the values of the coefficient, compilations of the field data have been made by Yudelson (32) and Okubo (30). Their diagrams look very much the same. But Okubo, in the more recent report, has the more

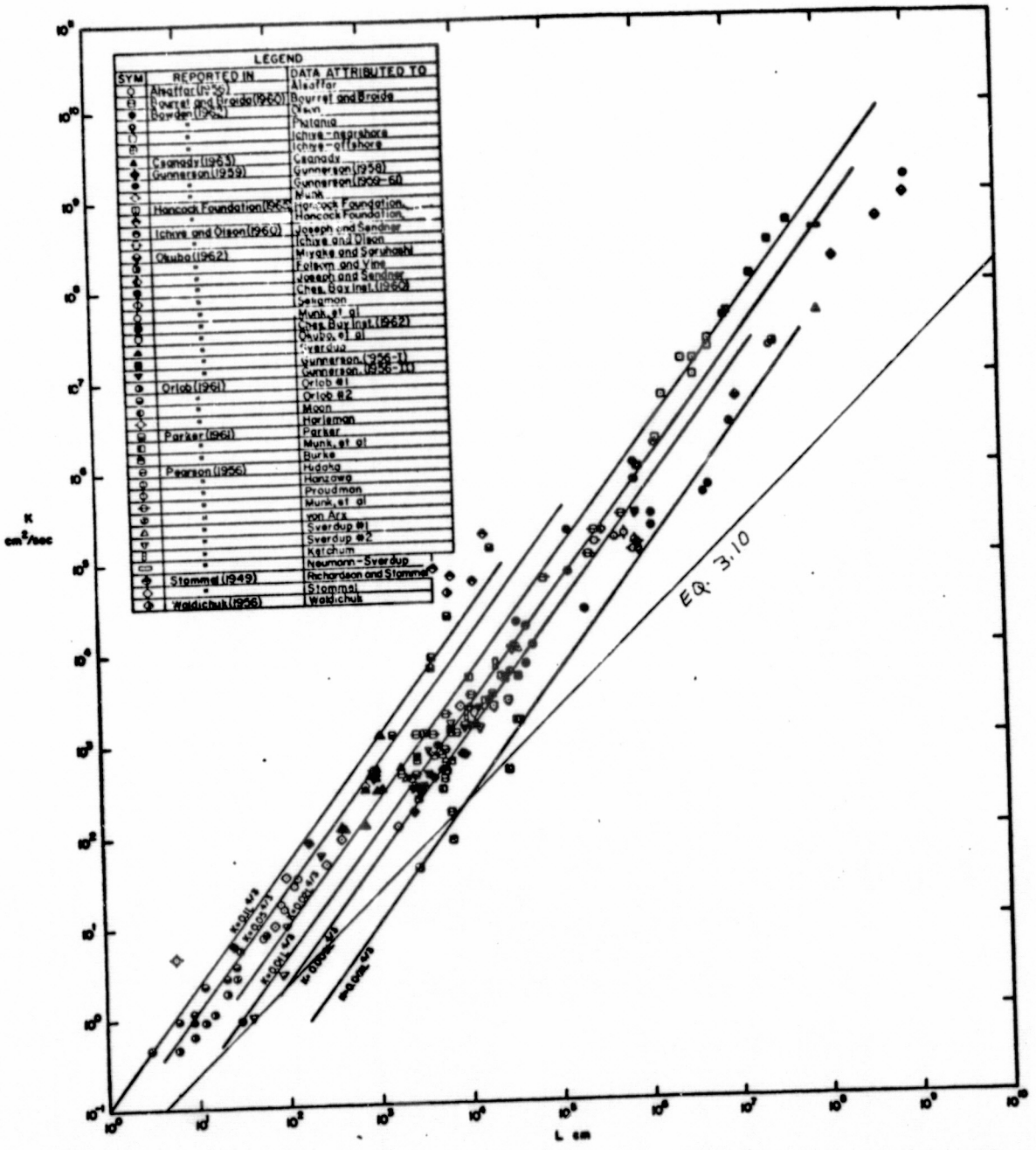

FIGURE 3.1. Diffusivity (cm^2/sec) vs. Length Scale (cm) Data Collected By Yudelson (32).

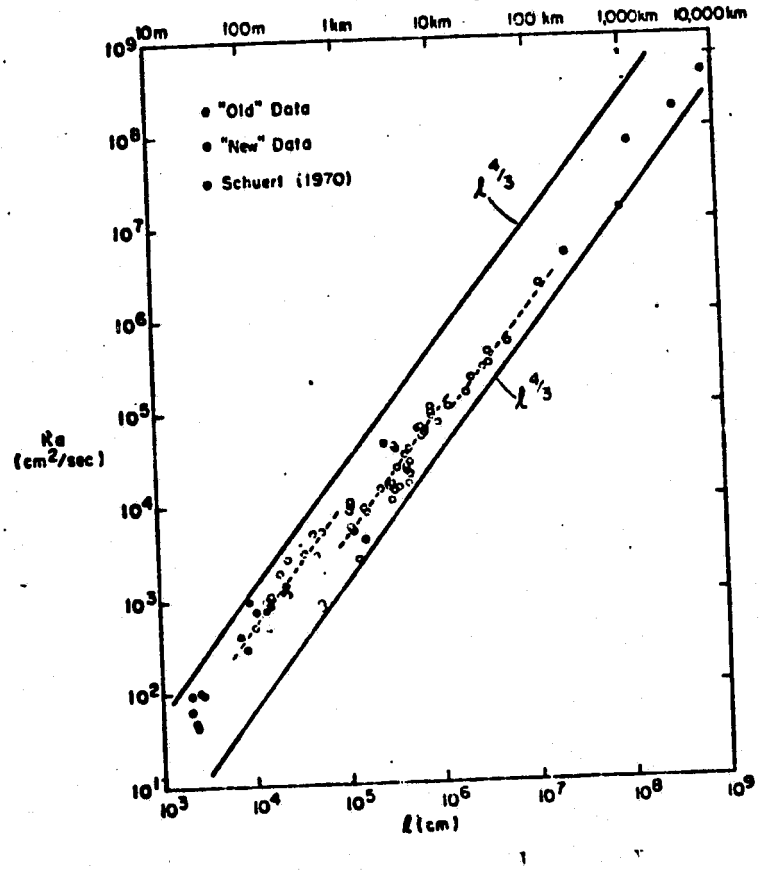

FIGURE 3.2. Diffusivity (cm^2/sec) vs. Length Scale (cm) Data Collected by Okubo (30).

enlightening conclusions.

Figure 3.1 shows diffusivity versus length scale for data obtained in 44 surveys (32). The locations include lakes, estuaries, bays, coastal waters, shallow seas, and deep ocean. The lines drawn are the four-thirds law for different values of the coefficient (0.1 to 0.001 cm^2/sec.). The scatter spans two orders of magnitude. This is not entirely surprising, considering the variety of locations. However, values for different ocean locations are as widely scattered as any. Yudelson notes that many points fall on the 4 /3 power lines for α_D's of 0.02, 0.01, and 0.005 $cm.^2$/sec. This happens in the middle range of l_x, from 10m. to 10km., which is the most useful range for modeling.

Okubo (30) shows a diagram, Figure 3.2, very similar in appearance to that of Yudelson. The data are from twenty investigations, all slightly more recent than those cited by Yudelson. Between the two lines delineating the four-thirds law, a shift from left to right with increasing scale is apparent, indicating that the overall exponent is less than four-thirds. This trend is also apparent, although not noted, in Yudelson's diagram.

Fitting a line to his points by eye, Okubo offers (30):

$$D_x = 0.0103\ l_x^{1.15} \qquad (3.10)$$

which has also been drawn in on Yudelson's diagram. Okubo suggests that the four-thirds power law is valid

only locally for some length scales. This is shown by dotted lines fitted by eye, where:

$\alpha_D \approx 0.008$ for the range 1.5×10^6 cm $< l_x < 2 \times 10^7$ cm.

$\alpha_D \approx 0.01$ for the range 10^5 cm. $< l_x < 1.5 \times 10^6$ cm.

$\alpha_D \approx 0.03$ for the range 10^4 cm. $< l_x < 10^5$ cm.

Obviously, the data sets used by Yudelson and Okubo do not coincide very well (Okubo's line, Equation 3.10, is to the right of almost all of Yudelson's points). In the interest of precise comparison, both data sets (ref. 32, pp.A-2 to A-8, and ref 30, pp.793 to 795) have been subjected to least-squares fitting, and are drawn in Figure 3.3. Also shown is a four-thirds law used by Koh and Chang (33) in a barge-dumping model, in which $\alpha_D = 0.00015$. For the data of Yudelson and Okubo, only the points in the useful range for modeling, 1 meter to 100 kilometers, were used. The equations obtained, and the standard deviations in orders of magnitude (since it was a logarithmic operation), are as follows:

Okubo:

$$D_x = 0.0366\ l_x^{1.0384},\ l_x \text{ in cm., standard deviation } 0.051$$
$$D_x = 0.00136\ l_x^{1.0384},\ l_x \text{ in feet} \qquad (3.11)$$

Yudelson:

$$D_x = 0.0655\ l_x^{1.1464},\ l_x \text{ in cm.}$$
$$D_x = 0.00333\ l_x^{1.1464},\ l_x \text{ in feet} \qquad (3.12)$$

standard deviation 0.3056, 143 data points

Composite:

$$D_x = 0.18\ l_x^{0.99833},\ l_x \text{ in cm.}$$

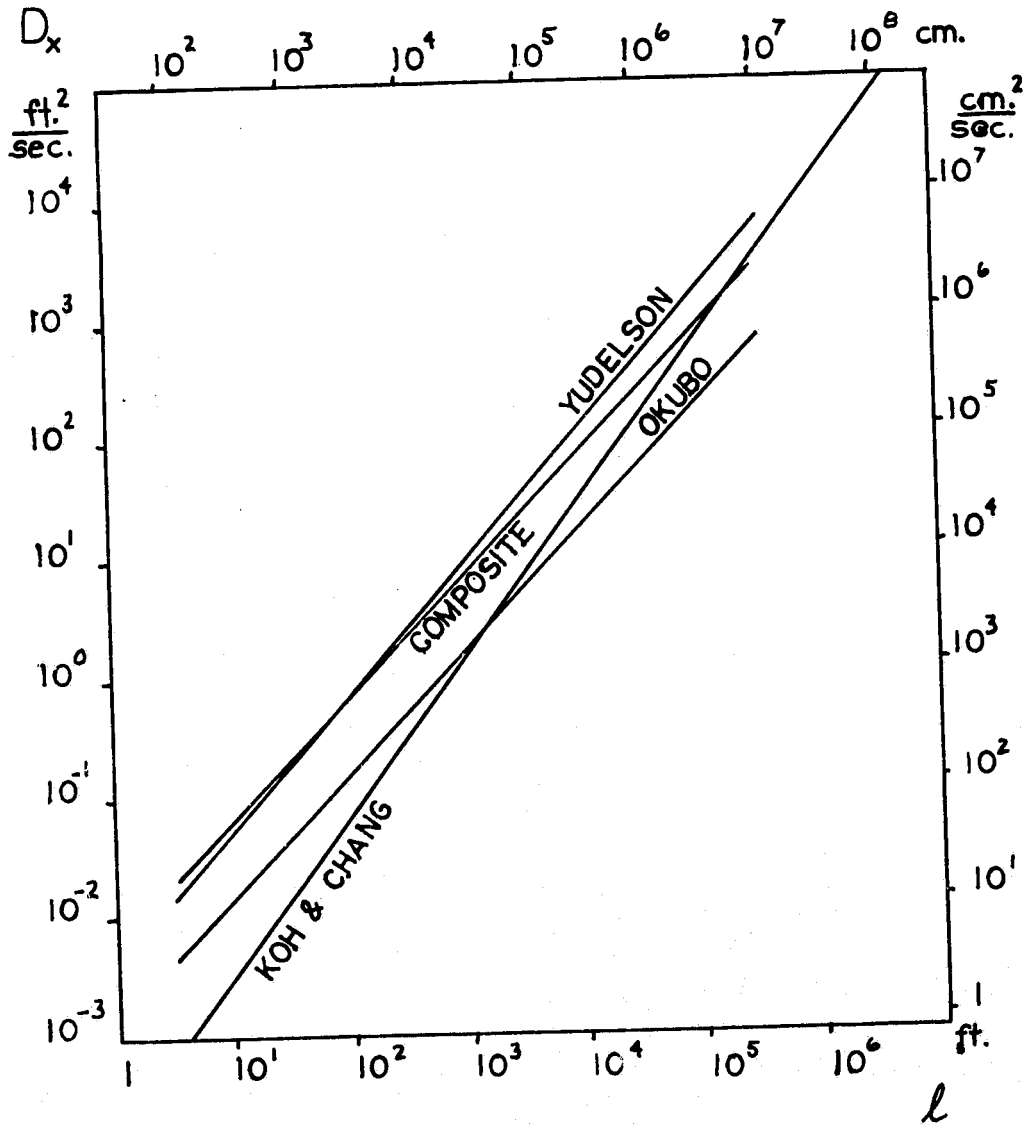

Figure 3.3. Offshore Diffusion Coefficient Relations.

D_x vs. l

$$D_x = 0.0059\ l_x^{0.99833}\ ,\ l_x \text{ in feet} \qquad (3.13)$$

standard deviation .3445, 198 data points

Equation 3.11 is slightly different from Equation 3.10, due to the dropping of data for l_x greater than 10^7 cm. The slope of the composite line is reduced because Yudelson's data included more points in the lower range of l_x than did that of Okubo. Perhaps because of this, Okubo's relation is preferable for offshore models.

Okubo was very demanding in his selection of data, requiring dye release to resemble a point source, and the distribution to be measured according to certain specifications. It is not likely, though, that this justifies ignoring Yudelson's data. The composite relation is probably most representative, although Okubo's is more attractive. If there were agreement about the localities in which the four-thirds power law holds for a certain value of α_D, this law might be useful. But that does not appear to be the case. Equation 3.13 indicates that D_x may actually be directly proportional to l_x.

Studies of dispersion in unconstrained waters indicate the variation of the dispersion coefficient only as a function of the scale. In rivers and estuaries, other factors are included: mean flow velocity, the bottom roughness as expressed by the Chezy coefficient, the depth of the water, wave action, hydraulic radius, and tidal period. An approach to modeling horizontal diffusion in open waters would be to

assign a value of D_x to each spatial grid by one of the equations 3.11, 3.12, or 3.13. The length scale would be twice the distance from the grid to the point of origin of the pollutant. This means that dispersants from several sources would have to be modeled as separate constituents, using a different set of dispersion coefficients for each source.

Vertical Diffusion Coefficients

Diffusion in the vertical direction is restrained by stability, by the bottom and the free surface, and by the magnitude of the vertical component of flow, which is normally very small relative to horizontal flow. Thus it has an effect several orders of magnitude smaller than that of horizontal dispersion. The latter, however, is still a small effect when dispersive transport is compared with advective transport (14). This is not likely to be the case in the vertical direction, since the vertical flow is also very small. Vertical diffusion and vertical advection are very closely related effects, since they are driven by the same force (instability). Since diffusion is also highly dependent on wave action, it is likely to be more important than advection. This indicates that ignorance of the actual vertical advection, or the inability to simplify it to finite-difference grids, may be partially overcome by using diffusion alone to model vertical

transport.

The simplest method of calculating the vertical diffusion coefficient, D , is correlation with the Richardson number :

$$R_i = \frac{g}{\rho}\frac{d\rho}{dz}\Big/0.7\left(\frac{u}{h}\right)^2 \qquad (3.14)$$

This incorporates stratification and the rate of lateral flow. However, since vertical diffusion is a sensitive process and difficult to measure, it has proved very difficult to define this relationship. All the correlations listed in Table 3.1 have been offered (33,34). Calculation from the Richardson number would require salinity and temperature, or density profiles from the region of interest.

The only general approach to determining D_z is to measure the vertical distribution of some constituent in the region of interest, and note the corresponding physical factors, such as surface waves, the salinity profile, depth, and currents. This has been done for heat and for suspended matter by Sastry and Okubo (35), and Ichiye et al. (36), respectively.

Ichiye et al. obtained an in-depth picture by measuring the distribution of suspended matter in deep waters, for nine widely separated stations in the Carribean. Yet not enough data were obtained to relate eddy diffusion to static stability conclusively. D_z was found to vary both horizontally and vertically. In the upper layer of the sea, to 150 m., D_z varied from 0.7 to

Table 3.1. Correlations of D with Richardson Number or Density Gradient ϵ

$D_{z0} = D_z$ at $R_i = 0$, the neutral case

β is a proportionality constant

Rossby & Montgomery, 1935 (33)	$D_z = D_{z0}(1+\beta R_i)^{-1}$	(3.15a)
Rossby & Montgomery, 1935 (33)	$D_z = D_{z0}(1+\beta R_i)^{-2}$	(3.15b)
Holzman, 1943 (33)	$D_z = D_{z0}(1-\beta R_i)$, $R_i \leq \frac{1}{\beta}$	(3.15c)
Yamamoto, 1959 (33)	$D_z = D_{z0}(1-\beta R_i)^{1/2}$, $R_i \leq \frac{1}{\beta}$	(3.15d)
Mamayev, 1958 (33)	$D_z = D_{z0}\, e^{-\beta R_i}$	(3.15e)
Munk & Anderson, 1948 (33)	$D_z = D_{z0}(1+\beta R_i)^{-\frac{3}{2}}$, $\beta = 3.33$	(3.15f)
Harremoes, 1968 (33)	$D_z = 5\times10^{-3}\epsilon^{-\frac{2}{3}}$ cm^2/sec., $5\times10^{-9} < \epsilon < 15\times10^{-5}$ cm^{-1}	(3.15g)
Kolesnikov, 1961 (33)	$D_z = D_{z0} + \beta/\epsilon$, cm^2/sec. $D_{z0}=12$ $\beta = 8.3\times10^{-5}$ $D_{z0}=2$ $\beta = 10.0\times10^{-5}$	(3.15h)
Koh and Fan, 1969 (33)	$D_z = 10^{-4}/\epsilon$, $4\times10^{-7} \leq \epsilon \leq 10^{-2}$	(3.15i)
Guttman and Huang (34)	$D_z = u L R_i^{-3/2}$; L, length scale; u, velocity scale of motion	(3.15j)

8 cm^2/sec. In intermediate depths it was between 5 and 13 cm^2/sec., and from 0.2 to 2 cm^2/sec. within 80 m. of the bottom.

Kullenberg (37) offers a definition of D_z and a simple relation based on measurements in shallow water, 14 to 30 meters. He finds that stratification and wind velocities have marked influence on vertical diffusion. The survey was based on the following definition:

$$D_z = \frac{4h_t}{\pi^2(t_2-t_1)} \ln\left(\frac{C_1}{C_2}\right) \qquad (3.16)$$

where h_t is the half-thickness of the dye layer, above or below the point of injection. Kullenberg derives the following relation from his experiments:

$$D_z = 8.9 \times 10^{-8} W^2 N_q^{-2} \frac{dq}{dz} \qquad (3.17)$$

where W is wind velocity, m /sec.

q is the horizontal velocity vector, m /sec.

N_q is the stratification number, $\frac{g\Delta\rho}{\rho\Delta z}$, $\frac{1}{sec^2}$

Some sort of vertical velocity profile must be obtained to estimate dq /dz. The obvious criticism of this relation is that it implies no vertical diffusion in the absence of wind, and infinite diffusion in unstratified waters. The variation of D_z with depth is dependent on the functions chosen for N_q and dq /dz.

Bastry and Okubo (35) suggest a method for obtaining heat diffusion coefficients, which could be

applied to concentration by analogy. The method requires knowledge of the temperature (or concentration) profile, and the absolute vertical velocity profile, in the waters of interest. The governing assumption is that the sum of vertical advection and vertical eddy diffusion is the same at any depth. A value of D_z is estimated for a certain depth, say 100 m. Then:

$$D_z = \left(\frac{\partial T}{\partial z}\right)^{-1} \left[wT - wT_{100} + \left(D_z \frac{\partial T}{\partial z}\right)_{100}\right] \qquad (3.18)$$

If the temperature T and the vertical velocity w are known at all depths, a profile of D_z can be obtained. The assumed value of $(D_z)_{100}$ must be chosen on whatever information is available, but values which would make D_z negative at some depth, or unreasonably high near the surface, compared to measurements found in the literature (33), can be eliminated.

The most flexible and most comprehensive method is that offered by Pritchard (38). Based on measurements in the James River, it calculates D from the Richardson number, wave parameters, horizontal flow, depth, and empirical coefficients. Although the coefficients have only been obtained for the James River, the formulation was designed for partially-mixed estuaries, and should be fairly general. Since field measurements of stratification are required for all methods, some diffusion measurements taken at the same time would permit adjustment of these coefficients. Pritchard's formulation is:

$$D_z = \frac{\eta_p u_z^2 (H-z)^2}{H^3}(1+\beta_p R_i)^{-2} + \alpha_p z \frac{(H-z)}{H}\frac{WH}{WT}\exp\left(\frac{-2\pi z}{WL}\right)(1+\beta_p R_i)^{-2} \quad (3.19)$$

where η_p, β_p, α_p are adjustable coefficients

z is distance downward from the surface

WH is wave height

WL is wave length

WT is wave period.

This formulation has been used by Spaulding (11) without changing Pritchard's coefficients. No matter which method is used to calculate D_z, some field information is necessary. In the open ocean case, if diffusion measurements cannot be made, values must be assumed based on the most similar cases in which measurements have been made (33).

Horizontal Dispersion in Estuaries

Mass transport in estuaries is usually dominated by currents caused by tides or river inflow, and the effect of bottom and shore is more pronounced than in offshore areas. For these reasons, a length scale is not considered sufficient for calculation of D_x and D_y. Methods that have been used for estuaries are based on the mean current velocity, and are therefore said to calculate dispersion coefficients rather than diffusion (14,39).

Holley, Harleman, and Fischer (39) present a rather complicated scheme for tidal estuaries. It appears to be applicable to wide coastal bays if the hydraulic

radius is taken as equal to the depth. New physical factors taken into account here are the oscillation of the tidal flow, the Chezy coefficient, and the width of the body of water.

The method begins with Elder's empirical relations for longitudinal, lateral, and vertical dispersion (40):

$$D_x = 5.93\, h_z u^* \tag{3.20}$$

$$D_y = 0.23\, h_z u^* \tag{3.21}$$

$$D_z = 0.067\, h_z u^* \tag{3.22}$$

where

$$u^* = \left| \frac{g}{C_h^2} \right|^{\frac{1}{2}} \bar{u}$$

C_h is the Chezy coefficient

h_z is the hydraulic radius, which is taken equal to the depth.

Two dimensionless variables incorporating the tidal period are introduced:

$$T_H' = T_t \Big/ \frac{b^2}{D_y} \tag{3.23}$$

$$T_V' = T_t \Big/ \frac{h^2}{D_z} \tag{3.24}$$

where b is the estuary half-width

h is the depth

T_t is the tidal period.

Holley et al. then produce a formula relating the diffusion coefficients in each direction to the coefficent for an infinitely long tidal cycle, D_∞. Fortunately, for vertical variations in the mean flow, this reduces to:

$$D_v = D_{\infty v} = 5.93\ hu^* \tag{3.25}$$

For transverse variations,

$$\frac{D_t}{D_{\infty t}} = 10\left(T_H'\right)^2 \tag{3.26}$$

and

$$D_{\infty t} = h_z u^* \left(0.30\ \overline{u''^2}\right) \tag{3.27}$$

33 where $\overline{u''^2}$ is the cross-sectional average of the squared velocity fluctuations, and

$$u'' = \alpha_D (z - \tfrac{1}{2}z) \sin\left(\frac{2\pi t}{T}\right) \tag{3.28}$$

Very little is actually known about the likely values of u'', and a value of the dimensional constant α_D must be assumed. In the above, D_v and D_t represent the longitudinal dispersion due to vertical and transverse velocity variations, respectively. If the velocity distribution is known, D_x can be taken equal to the larger of D_v or D_t. If not, it is recommended that D_x be taken equal to D_v.

Leendertse (14) offers the most appealing method for calculating dispersion in an estuary. He also starts from Elder's equations, 3.20 and 3.21. The trouble with these is that they indicate no dispersion in the absence of a mean flow. However, it is clear that dispersion in a natural body of water will still be considerable, due to turbulent motion and wind effects. Leendertse assumed the following functional relationships:

$$D_x = f_1 (U, C_h, H) + D_w \tag{3.29}$$

$$D_y = f_2(V, C_h, H) + D_w \qquad (3.30)$$

where D_y is a diffusion coefficient dependent on wave and wind conditions, and on the lateral diffusion.

For use in this development, which is to be applied to a partially-mixed estuary, Pritchard's method for the vertical diffusion coefficient will be used (Equation 3.19). The horizontal dispersion coefficients can best be calculated from Equations 3.29 and 3.30, using Equations 3.20 and 3.21 as the functions f_1 and f_2. The value D_w can be taken as a diffusion coefficient, as calculated from Equation 3.13, using a typical width of the estuary as a length scale. This would permit adaptation of the same method to offshore areas, whether or not the mean flow is dominant over turbulence.

Table 3.2 summarizes the aspects of the different methods presented. The information listed must either be gathered in the field, or assumed similar to data already available (if it is not self-evident, as would be values for the length scale).

TABLE 3.2. Computational methods for diffusion coefficients

Reference	Equations	Required Information
Horizontal:		
1. Power laws (27,26,27)	11, 12, 13	l_x
2. Elder (39)	20, 21	h, u, C_h
3. Holley et al. (39)	20-28	h, u, C_h, b, T, u'
4. Leendertse (14)	29, 30	h, u, C_h, D_w
Vertical:		
1. Kullenberg (37)	17	W, N^2, dq /dz
2. Sastry and Okubo (35)	18	vertical velocity concentrations D_z at some depth
3. Holley et al. (39)	25	h, u, C_h
4. Richardson no. (33,30)	15	R_i, D_{zo} , ϵ, β
5. Pritchard (38)	19	R_i, u, z, WH, WT, WL η_p, α_p, β_p

IV. INVESTIGATION OF COMPUTATIONAL ASPECTS

The finite-difference equations presented in Chapter II are, of course, only approximations to the mass transport equation. It is essential to know the effects of the approximations. In order for the model to be useful, the numerical and true solutions must converge as the grid size and time step are decreased. For simplified cases, analytical proofs of convergence and stability can be made. For the more complicated system under consideration, it is desirable to demonstrate the computational veracity with some simulations. This has not been done previously because of limitations in computer size and speed. However, the time was taken here to attempt verification of some predicted computational effects.

Convergence

In order to demonstrate convergence of the numerical solution with an analytical solution, a rectangular basin with a constant, unidirectional current and an instantaneous plane source of material was simulated. The solution for these conditions is given by Diachishin (41), as follows:

$$P = \frac{g^i_{pl} \exp\left[-\frac{(x-ut)^2}{4D_x t}\right]}{4\pi D_x t} \qquad (4.1)$$

where g^i_{pl} is the instantaneous plane source strength per unit area,

D_x is the longitudinal dispersion coefficient,

x is the downstream distance,

u is the constant stream velocity, and

t is the time elapsed after injection.

The plane source was simulated by a row one grid wide, across the entire width and depth of the basin. Into this row a relatively dilute constituent was injected over one time step, so that the total mass injected per cross-sectional square foot was equal to g^i_{pl}. The distribution was printed at chosen time steps as the constituent was advected and dispersed downstream. It is expected that as the time step and grid spacing are decreased, the finite-difference and analytical solutions will converge. Thus the simulation was performed for both large and small time steps and grid spacings.

The results of the simulation are shown in Figures 4.1 and 4.2. It is obvious that the simulation is very poor for the large values of Δt and Δx, and that the solutions are converging to an acceptable representation as the sizes are reduced. One may note that even in the better case, the simulation is still rather poor after the shorter simulation time. This is because the material is already distributed over one grid Δx in

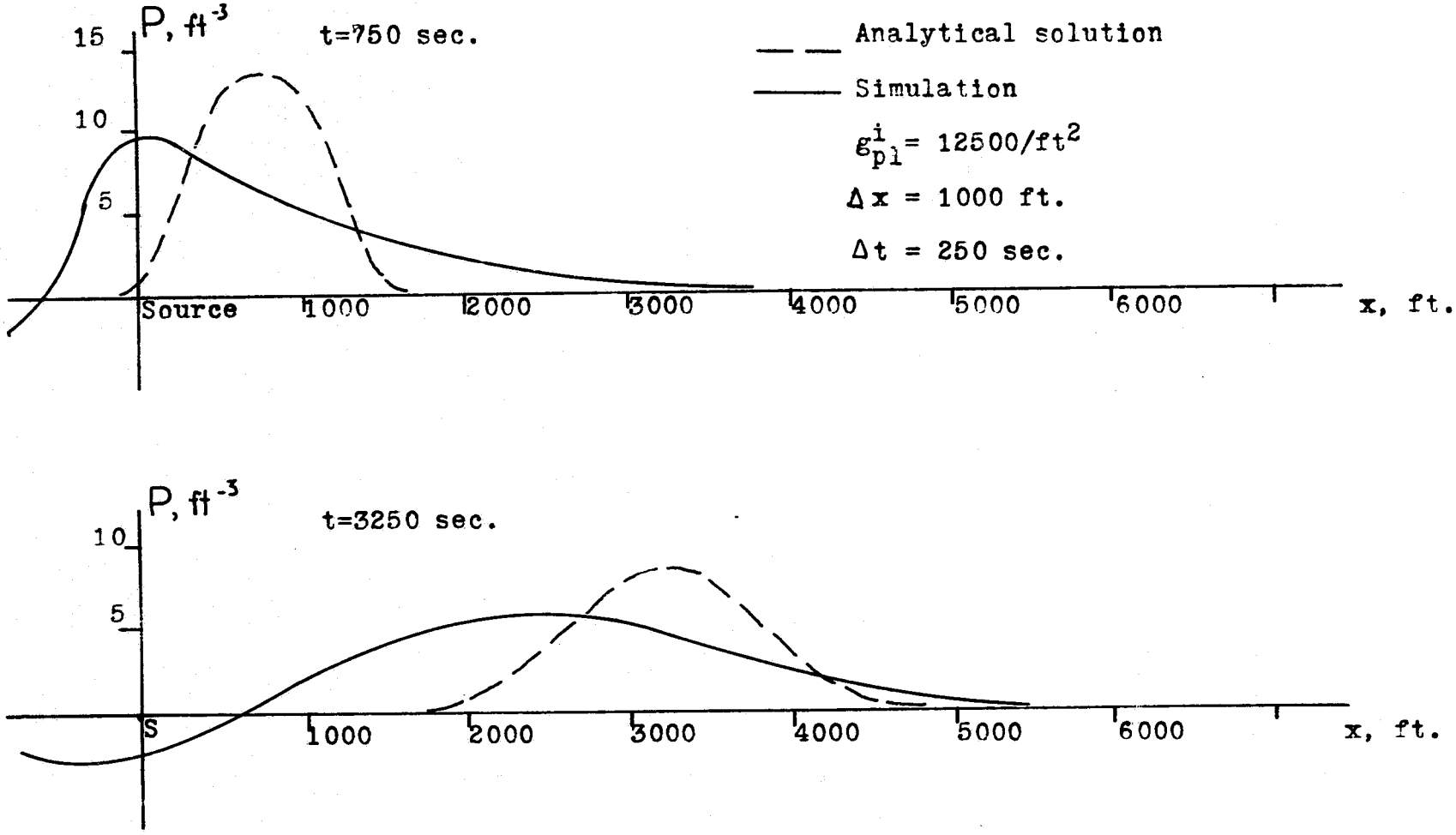

Figure 4.1. Plane-source Simulation. P(x,t) vs. x for large time, space increments

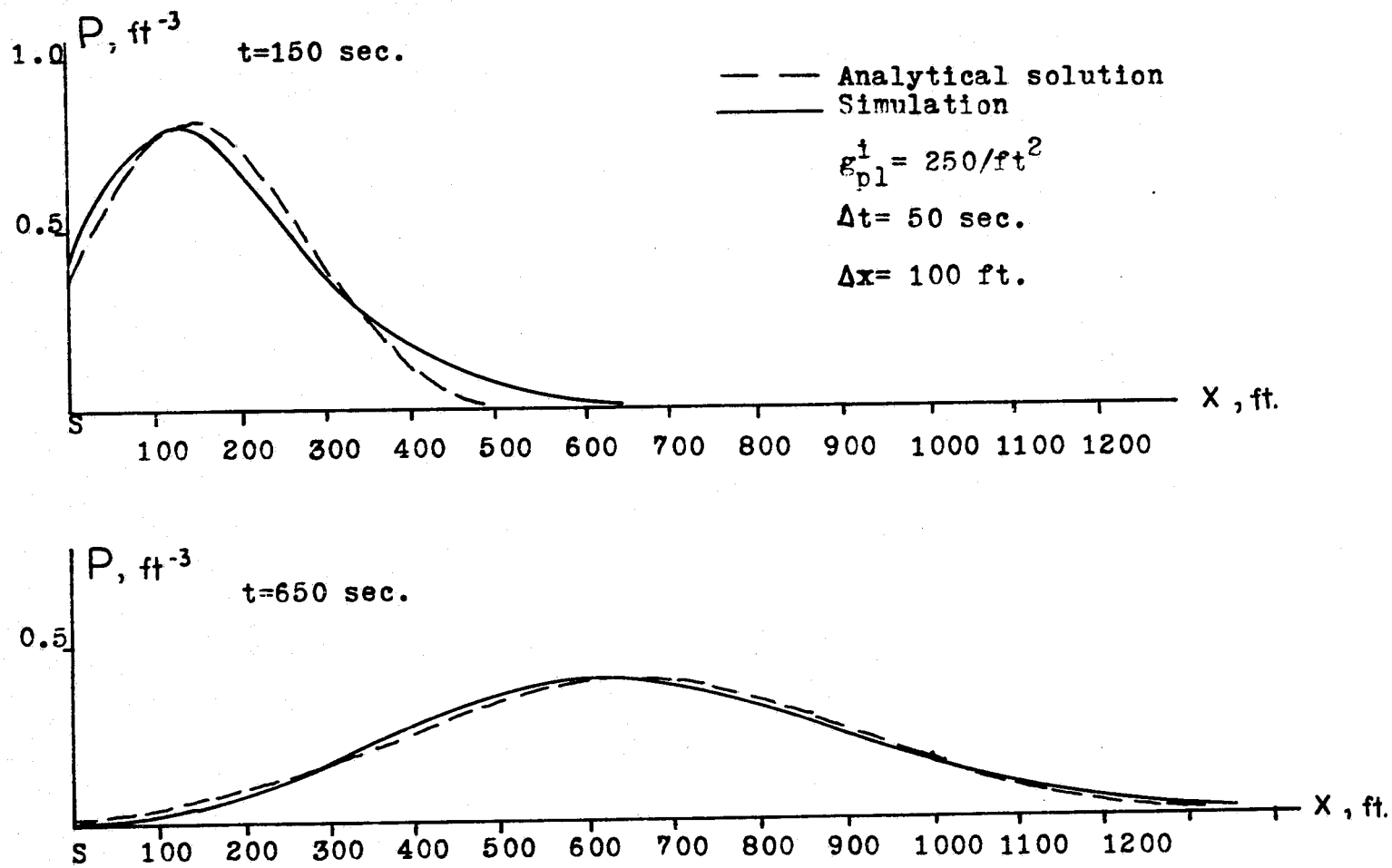

Figure 4.2. Plane-source Simulation. P(x,t) vs. x for small time, space increments

width, rather than being planar, at the source. As the constituent proceeds downstream, this error becomes less significant.

Stability and Accuracy

Stability is the requirement that errors introduced in the computational method do not amplify in an unlimited manner (19). A definition of stability is as follows (15):

> If $p^{\ell}_{m,k,n}$ is the theoretical solution of the finite difference equation, and $\tilde{p}^{\ell}_{m,k,n}$ is the numerical solution, then stability exists if the difference (error),
>
> $$Z^{\ell}_{m,k,n} = p^{\ell}_{m,k,n} - \tilde{p}^{\ell}_{m,k,n} \qquad (4.2)$$
>
> remains bounded as ℓ increases.

For a parabolic or elliptic linear equation with constant coefficients, the alternating-direction-implicit method has been shown to be unconditionally stable (17,42,43). Spaulding (15) has proved unconditional stability of his method for the two-dimensional laterally-averaged mass transport equation, with the restriction that the dispersion coefficients are constant.

According to the von Neumann method of analysis, the error $z^{\ell}_{m,k,n}$ (Equation 4.2) is harmonically decomposed into the error function

$$E(x) = \sum_j A_j e^{i\beta_j x} \qquad (4.3)$$

where the frequency β_j is arbitrary,

A_j is the amplitude,

i = square root of -1.

Only a single component, $j = s$, need be dealt with. To follow an error as time increases, the error being zero at time $t = 0$, the solution of the finite-difference equation is taken as

$$e^{\alpha_s t} e^{i\beta_s x}$$

The error $e^{i\beta_s x}$ will not grow with time if the criterion

$$\left| e^{\alpha_s t} \right| \leq 1 \qquad (4.4)$$

is met. For the restricted cases described, expressions for the parameter $e^{\alpha_s t}$ can be obtained, and can be computed to meet this criterion, thereby proving unconditional stability.

Although the equations of Chapter II do not meet the above restrictions, and stability has not been proved for this case, there is numerical evidence that stability arguments will remain valid (17,43). In the applications to be described in Chapter VII, the computational method exhibited stable behavior at all times, when correctly posed.

In a simpler sense, stability is also governed by the dimensionless parameter $\frac{u\Delta t}{\Delta x}$, which is considered a basic stability indicator of finite difference methods.

The criterion is:

$$\left| \frac{u \Delta t}{\Delta x} \right| \leq F \qquad (4.5)$$

where F depends on the type of differencing system employed, and is typically of the order of unity. This normally requires that a particle must not be advected across an entire grid during one time step, and thereby lost. A similar, but less demanding criterion involves the dispersion coefficient:

$$\left| \frac{D_x \Delta t}{(\Delta x)^2} \right| \leq F \; . \qquad (4.6)$$

which is less demanding because it is easier to meet for real bodies of water.

The accuracy of the alternating-direction implicit method has been calculated by Douglas (17) to be of the order of $(\Delta x^2 + \Delta t^2)$, where Δx is expressed as the fraction of the model length spanned by one grid, and Δt as the fraction of the simulated time spanned by one step. The desired accuracy, combined with the criteria of Equations 4.5 and 4.6, will give an idea of the time and grid increments required. However, the geometry of the water body may impose stricter limits, and, as described below, there are other numerical effects which require consideration.

Dispersive and Dissipative Effects

Stability and convergence alone are not sufficient conditions for a useable model. The additional numerical effects of concern are dispersive and

dissipative characteristics. These are defined in terms of a number of superimposed Fourier series, of different frequencies, which constitute the spatial variation of mass density. The dispersive effect is displayed when the components in the computational model propagate at a speed different from that of the analytical solution. The dissipative effect is evident when the components decay in amplitude without any physical reason. Since decay for physical reasons, such as dispersion and biochemical reactions, will exist in the real problem, it is essential that the dissipative error not be large enough to be confused with any real decay.

For this purpose, analytical investigations of these effects have been performed (14, 15). It was necessary to analyze a simple one-dimensional mass transport equation for a rectangular basin. Therefore, it is desirable to compare the performance of the proposed finite- difference equations to that predicted for the simpler case. This is done by simulating a concentration wave in a rectangular basin for a number of different values of the dimensionless parameters $\frac{u\Delta t}{\Delta x}$ and $\frac{D_x \Delta t}{(\Delta x)^2}$, sufficient to construct figures similar to those given by Spaulding (15) and Leendertse (14).

The mass transport equation that was analyzed is:

$$\frac{\partial P}{\partial t} + u \frac{\partial P}{\partial x} - D_x \frac{\partial^2 P}{\partial x^2} = 0 \qquad (4.7)$$

where u and D_x are constant. The analysis of Leendertse

(14), which is summarized here, uses a multi-operation method, obtaining equations for $P_m^{\ell+1}$ and $P_m^{\ell+2}$. The solution in terms of a Fourier series is:

$$P(x,t) = \sum_j P_j^* \exp\left[i\left(\sigma_j x + \omega_j t\right)\right] \tag{4.8}$$

where ω_j is the frequency of the jth component,

σ_j is the wave number, $2\pi/L$,

P_j^* is the complex amplitude.

The finite difference equations are abbreviated as:

$$P_m^{*\,\ell+1} = \lambda_1 P_m^{*\,\ell}$$

$$P_m^{*\,\ell+2} = \lambda_2 P_m^{*\,\ell+1} \tag{4.9}$$

where

$$\lambda_1 = \frac{1}{1 + iA + B}$$

$$\lambda_2 = \frac{1}{1 - iA - B} \tag{4.10}$$

and

$$A = \frac{u\Delta t}{\Delta x} \sin(\sigma \Delta x)$$

$$B = \frac{4 D_x \Delta t}{(\Delta x)^2} \sin^2\left(\frac{\sigma \Delta x}{2}\right) \tag{4.11}$$

obtained from the full set of difference equations.

The quantities needed to indicate dispersive and

dissipative effects are the modulus of the propagation factor and the phase shift. The propagation factor is:

$$T\left(\frac{L_w}{\Delta x}\right) = \frac{\exp\left[i(\omega' t + x)\right]}{\exp\left[i(\omega t + x)\right]} \qquad (4.12)$$

where ω' is the frequency of the computed wave, and ω is the frequency of the prototype wave, after the wave has propagated one wavelength. The rate of propagation of the real wave is $\sigma u \Delta t$; the computed speed is the real part of Equation 4.10. Thus for the two operations of the computation, the ratios of computed to theoretical wave speed are:

$$R_1 = \frac{\tan^{-1}\left(\frac{A}{1+B}\right)}{\sigma u \Delta t}$$

$$R_2 = \frac{\tan^{-1}\left(\frac{A}{1-B}\right)}{\sigma u \Delta t} \qquad (4.13)$$

and the total ratio is

$$R = \frac{1}{2}(R_1 + R_2) \qquad (4.14)$$

The analytical solution for the amplitude of the mass density fluctuation is

$$P(x,t) = \exp\left(-\sigma^2 D_x \Delta t\right) \tag{4.15}$$

The modulus of the propagation factor is found to be:

$$\left|T\left(\frac{Lw}{\Delta x}\right)\right| = \left| \frac{\sqrt{\left[(1-B)^2+A^2\right] / \left[(1+B)^2+A^2\right]}}{\exp\left(-\sigma^2 D_x \Delta t\right)^2} \right|^{\frac{n}{2}} \tag{4.16}$$

where n is the number of operations used while the wave propagates one wavelength.

To determine the dispersive and dissipative effects of the method of solution given in Chapter II, the initial mass field was set to a sine wave variation in the x-direction, which was renewed at the source as it propagated downstream. After it had propagated one wavelength, the amplitude and phase shift were noted. The modulus was calculated from Equation 4.15 and the observed amplitude. By close comparison of Figures 4.3, 4.4, and 4.5 with those prepared from the analysis (15, 14), it is evident that the full set of equations performs very much as predicted by the analysis of the simpler equations.

Leendertse's observation that there should be at least ten grid points per wavelength, to insure that dispersive and dissipative effects are negligible, is borne out by this study. When the wavelength of concern is the tidal wavelength, which is of the order of 200 nautical miles in Narragansett Bay (18), this condition

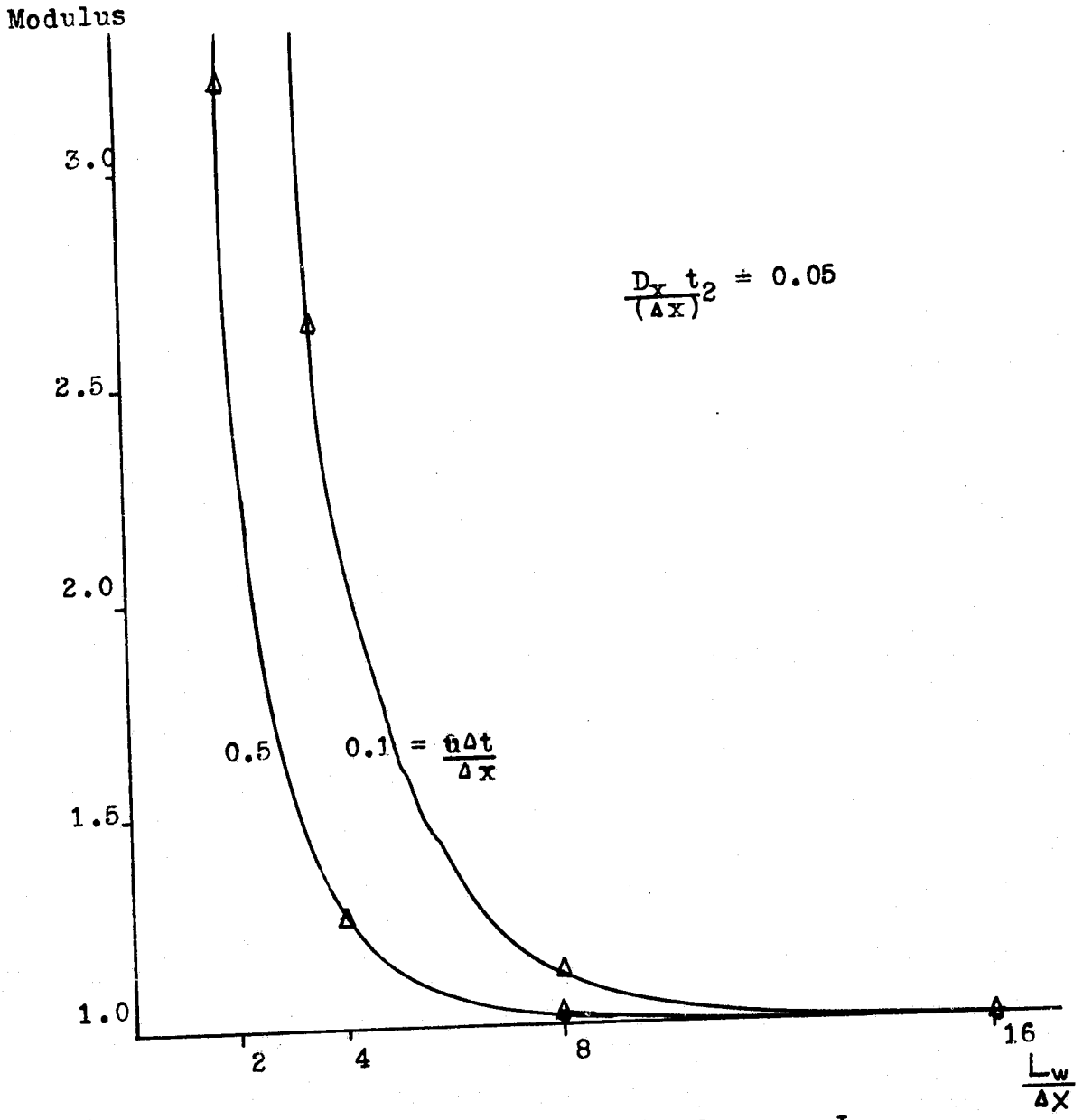

Figure 4.3. Dissipative Effect. Modulus vs. $\frac{L_w}{\Delta x}$

Modulus, $\left|T(\frac{L_w}{\Delta x})\right|$ = $\frac{\text{Amplitude, model}}{\text{Amplitude, analytical}}$

after one period $\frac{L_w}{u}$

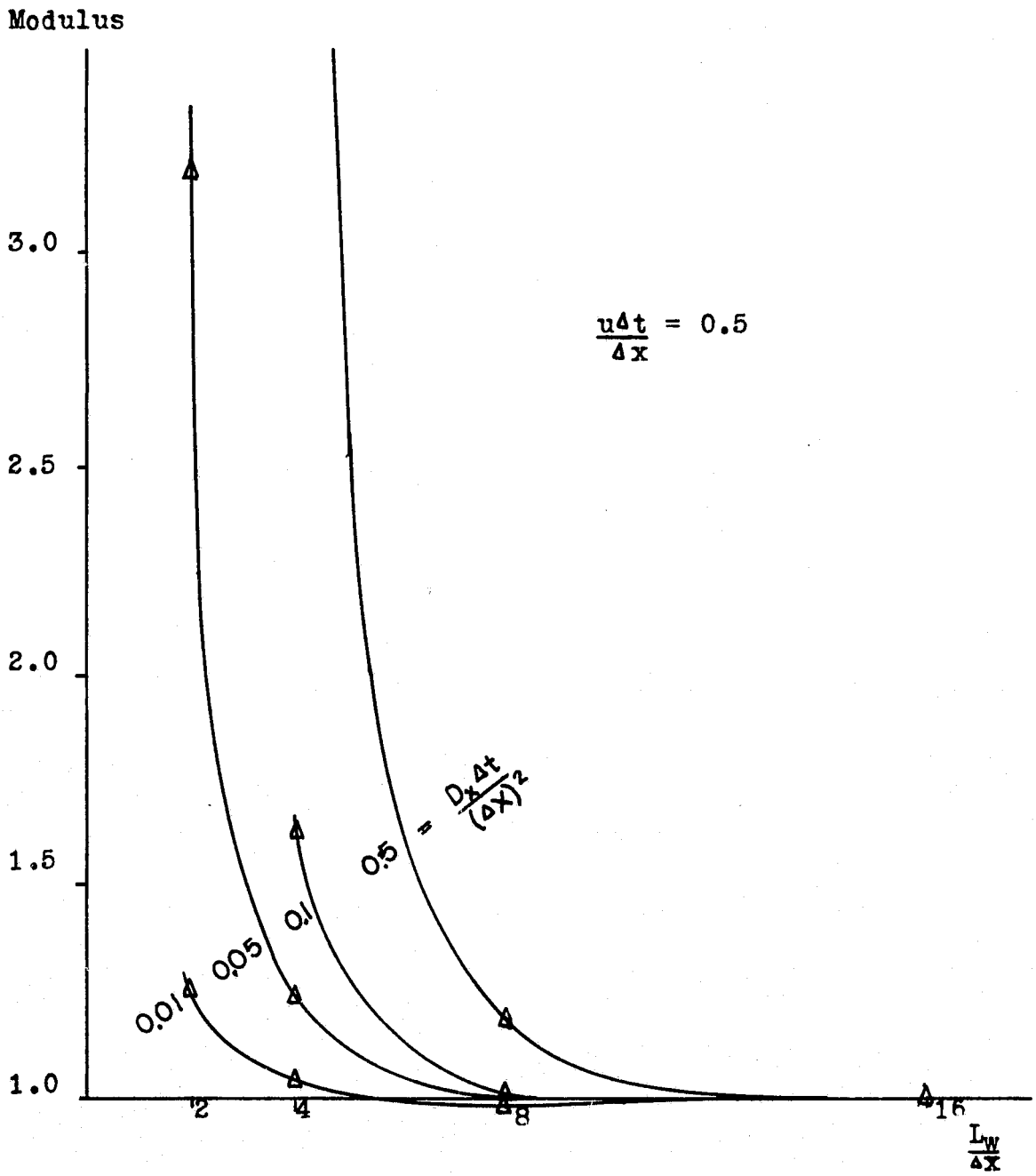

Figure 4.4. Dissipative Effect. Modulus vs. $\frac{L_w}{\Delta x}$

$$\text{Modulus}, \left| \mathcal{T}\left(\frac{L_w}{\Delta x}\right) \right| = \frac{\text{Amplitude, model}}{\text{Amplitude, analytical}}$$

after one period $\frac{L_w}{u}$

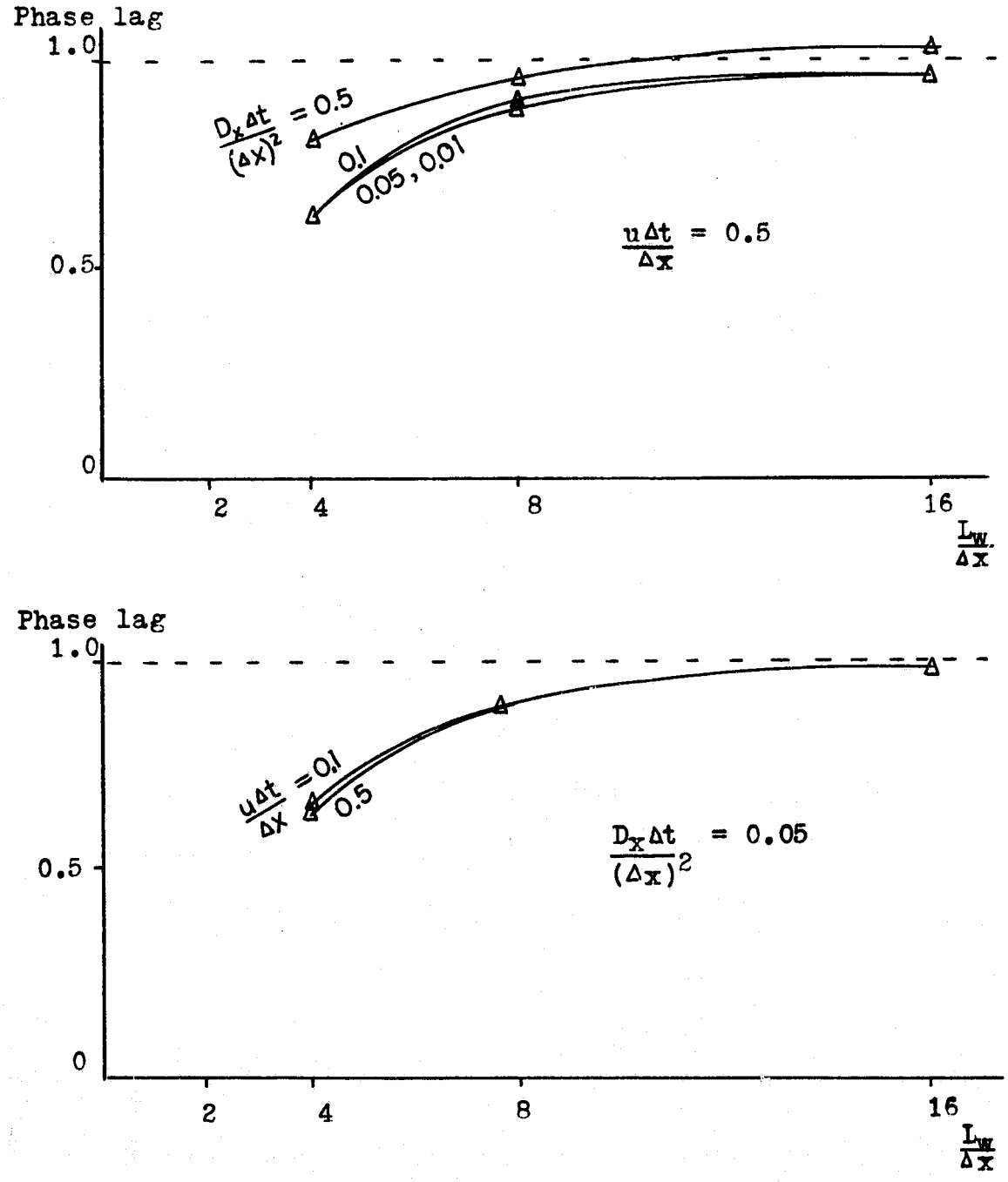

Figure 4.5. Dispersive Effect. Phase lag vs. $\frac{L_w}{\Delta x}$

$$\text{Phase lag} = \frac{\text{L (model, after one period)}}{L_w}$$

is easily met, for a total model length shorter than the wavelength. A couple of further observations are in order, with regard to the behavior of the computed wave. First, what has been called the dissipative effect turns out to be a divergence, that is, the failure of the amplitude to decay as fast as it should, according to Equation 4.15. This is in accordance with the behavior predicted by Equation 4.16. Second, the phase shift was observed to occur as the wave was generated at the head of the model basin. Only the wave at the head was shortened; waves downstream lagged in time but did not shorten or propagate more slowly than the current field. This is expected, as the number of waves must be conserved. These properties are illustrated in Figure 4.6.

Discontinuities

When a discharge occurs in a stream flow, a discontinuity of mass density occurs upstream from the source. Some matter should be taken upstream by dispersion, but the computational method is unable to properly represent the discontinuity. This is because its Fourier decomposition consists of waves which are too short to be encompassed in the grids, and thus a disturbance is generated at the source. The effect of this is to underestimate the influence of dispersion, and negative values of mass density may be produced, as

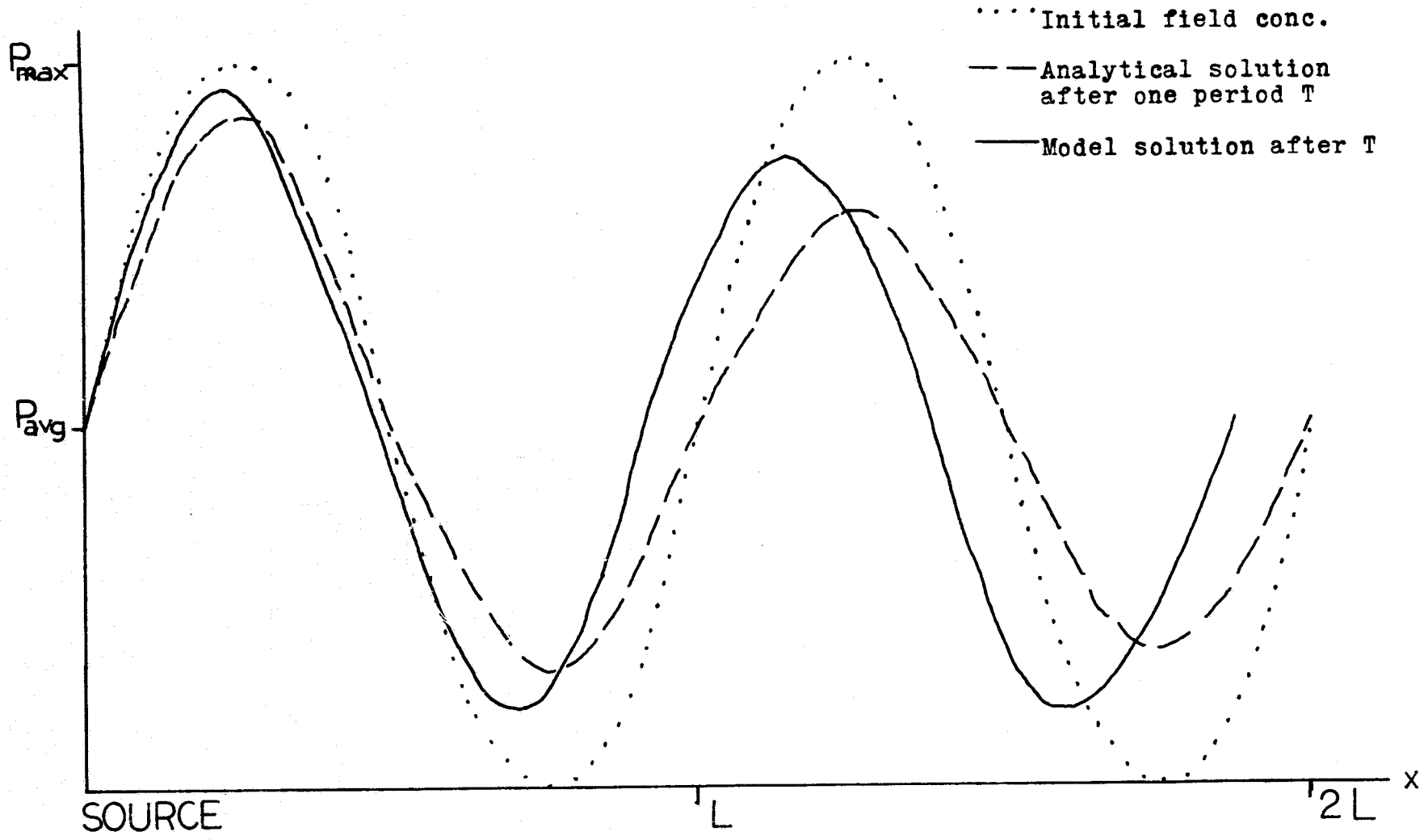

Figure 4.6. Dispersive and Dissipative Behavior for $\frac{L_w}{\Delta x} < 10$. P(x,t) vs. x

can be seen in Figure 4.1.

When the location of the discontinuity is known, upstream flux differencing, as described by Leendertse (14), can be used. This will increase the dispersion enough to supress the disturbance. However, for a three-dimensional problem, a more general approach is needed. There is the problem of a polluted stream entering a larger bay, which can produce a line of discontinuities. Also, reversal of the current field after slack tide can produce the same kind of disturbance. To handle these conditions, Leendertse's method of adding artificial dispersion at extreme concentration gradients can be applied in all three dimensions. The previously calculated dispersion coefficients are adjusted as follows:

$$D_{m+\frac{1}{2}} = D_{m+\frac{1}{2}} \left\{ 1 + e_1 \left[\frac{(P^{\ell}_{m+1} - P^{\ell}_{m})^2}{(P^{\ell}_{m+1} + P^{\ell}_{m})^2} \right] \right\} \qquad (4.17)$$

where e_1 is an empirical coefficient. Similar expressions are used in the other directions. It can be seen that the amount of dispersion added depends on the mass density difference between the two grids. The use of this method adds to the computational time, but reduces the generation of negative densities. If the scheme is not used carefully, though, it has the effect of flattening real peaks by adding too much dispersion. Therefore a numerical study was made to determine an

"optimum" value of the coefficient e_1. Again a plane source in a rectangular basin was simulated. The coefficient e_1 was varied while other parameters were held constant. The results are shown in Figure 4.7.

The optimum value of e_1 appears to be about 0.20. The effect of flattening the peak at large values of e_1, and the upstream negatives at smaller values, are clearly visible. In the real-world simulations described in Chapter VII, it was found that values larger than 0.20 could be used without flattening the peaks excessively. This is probably because, with dispersion acting in all three directions, the concentration gradients and hence the amount of adjustment made are reduced relative to the rectangular basin case.

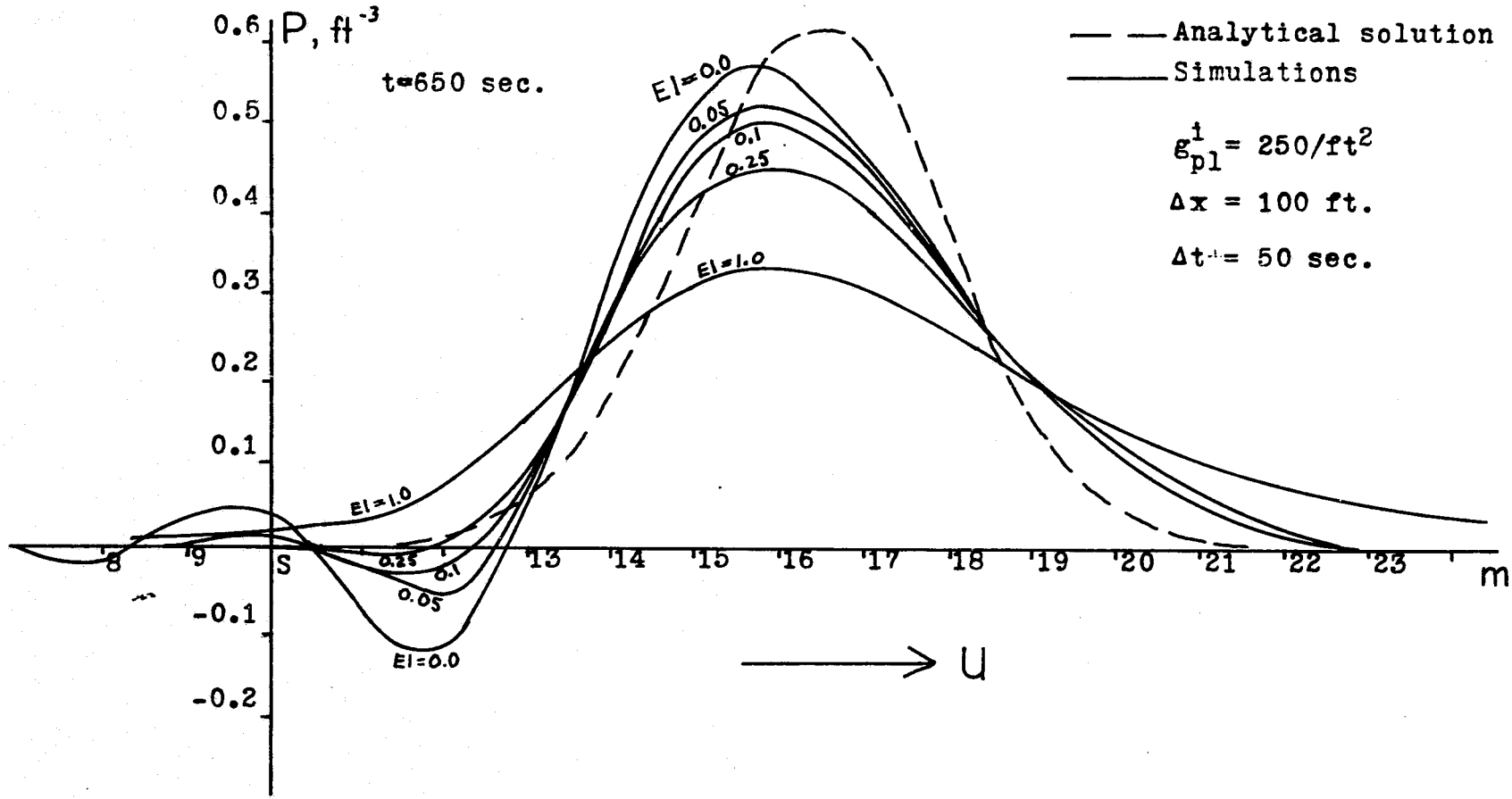

Figure 4.7. Plane-source Simulations with Adjusted Dispersion Coefficients at Discontinuity. P(x,t) vs. m, m=x/Δx

V. TWO-DIMENSIONAL VERTICALLY-AVERAGED TIDAL MODEL

The most useful method to date for the computation of hydrodynamic input for the water quality model is a two-dimensional, vertically-averaged tidal hydraulics model. The method was developed by Leendertse (19), and applied by Hess and White (18) to Narragansett Bay. The program was applied to the Providence River area to determine the circulation and the tide height information. The use of this kind of model requires that the actual vertical variations of the velocities be small (19).

Equations and Solution Method

The system of equations to be solved consists of the Eulerian Navier-Stokes momentum equations, and mass conservation for incompressible flow, as follows (18):

$$\frac{\partial u}{\partial t} + \frac{\partial uu}{\partial x} + \frac{\partial uv}{\partial y} + \frac{\partial uw}{\partial z} = -\frac{1}{\rho}\frac{\partial p}{\partial x} + fv + \frac{1}{\rho}\left(\frac{\partial \tau_{xx}}{\partial x} + \frac{\partial \tau_{xy}}{\partial y} + \frac{\partial \tau_{xz}}{\partial z}\right) \tag{5.1}$$

$$\frac{\partial v}{\partial t} + \frac{\partial uv}{\partial x} + \frac{\partial vv}{\partial y} + \frac{\partial wv}{\partial z} = -\frac{1}{\rho}\frac{\partial p}{\partial y} - fu + \frac{1}{\rho}\left(\frac{\partial \tau_{yx}}{\partial x} + \frac{\partial \tau_{yy}}{\partial y} + \frac{\partial \tau_{yz}}{\partial z}\right) \tag{5.2}$$

$$\frac{\partial w}{\partial t} + \frac{\partial uw}{\partial x} + \frac{\partial vw}{\partial y} + \frac{\partial ww}{\partial z} = -\frac{1}{\rho}\frac{\partial p}{\partial z} - g + \frac{1}{\rho}\left(\frac{\partial \tau_{zx}}{\partial x} + \frac{\partial \tau_{zy}}{\partial y} + \frac{\partial \tau_{zz}}{\partial z}\right) \tag{5.3}$$

$$\frac{\partial u}{\partial x} + \frac{\partial v}{\partial y} + \frac{\partial w}{\partial z} = 0 \tag{5.4}$$

The horizontal velocities are averaged by integrating in the z-direction, from -h at the bottom to ξ at the surface. The z-momentum equation is reduced to the hydrostatic equation, $\frac{\partial p}{\partial z} = -\rho g$, by making the Boussinesq assumption that pressure varies only with depth. The pressure at the surface is assumed constant.

Bottom stresses are approximated by the Chezy relationship:

$$\tau_x = \frac{\rho g u \left(u^2 + v^2\right)^{1/2}}{C_h^2} \tag{5.5}$$

where the Chezy coefficient, C_h, is given by

$$C_h = \frac{1.49}{N}\left(h + \xi\right)^{1/6} \tag{5.6}$$

where $(h + \xi)$ is in feet, and N is the Manning factor. Choice of a value for the Manning factor must be made experimentally. The surface stresses due to wind are approximated by the quadratic law for turbulent flow.

The final differential equations used (19) are the following:

$$\frac{\partial u}{\partial t} + \frac{\partial UU}{\partial x} + \frac{\partial UV}{\partial y} = -g\frac{\partial \xi}{\partial x} + fV + \frac{k_d \rho_a}{\rho}\frac{W_x|W_x|}{H} - \frac{gU(U^2+V^2)^{\frac{1}{2}}}{C_h^2 H} \qquad (5.7)$$

$$\frac{\partial V}{\partial t} + \frac{\partial UV}{\partial x} + \frac{\partial VV}{\partial y} = -g\frac{\partial \xi}{\partial y} - fU + \frac{k_d \rho_a}{\rho}\frac{W_y|W_y|}{H} - \frac{gV(U^2+V^2)^{1/2}}{C_h^2 H} \qquad (5.8)$$

$$\frac{\partial \xi}{\partial t} + \frac{\partial HU}{\partial x} + \frac{\partial HV}{\partial y} = 0 \qquad (5.9)$$

where capital U and V signify vertical averaging, as

$$U = \frac{1}{H}\int_{-h}^{\xi} u\,dz \quad \text{and} \quad V = \frac{1}{H}\int_{-h}^{\xi} v\,dz$$

ρ_a is the density of air,

k_d, a dimensionless drag coefficient, is taken to be 0.0025

W_x, W_y are wind velocities in the indicated directions,

$H = h + \xi$.

The solution approach used by Leendertse involves space- and time-staggering of U and V, and a multi-operation computation. A concise description of this method, given by Hess and White (18), is quoted here:

> The time step is split into two halves, and the time derivative taken over the half time step. . . . In the first half time step, values of U and ζ are computed implicitly along a grid row in the x-direction at the time $(t + \frac{1}{2})\Delta T$. Then V is computed at the same time level explicitly. In the second half time step, V and ζ are computed implicitly at $(t + 1)\Delta T$ along grid rows in the y-direction, after which U is calculated explicitly at $(t + 1)\Delta T$.
>
> "In the first half time step, the time derivative of U in the x-momentum equation is approximated by a backward difference: . . . In the second half time step, a forward difference is used: . . . Thus, over a full time step, the time derivative is a central difference . . .

The complete finite-difference equations (19), and details of the solution, are given in the appendices of the report by Hess and White (18).

Application to the Providence River

The model area is to be that part of Narragansett Bay called the Providence River. It is actually a partially- mixed estuary with its circulation dominated by tides, although wind and gravitational circulation may be important at times. The fresh-water inflow during one tidal cycle is about six per cent of the tidal prism. There are three water boundaries: the narrows at the mouth of the Seekonk River, at the north end; the mouth of the Pawtuxet River on the west shore; and the interface with the lower bay, which is a line between Conimicut and Nyatt Points. There are also two small rivers, the Moshassuc and the Woonasquatucket, which enter near the mouth of the Seekonk. The major

bathymetric feature is the forty-foot deep shipping channel which stretches the entire length of the model area. Figure 5.1 shows the location of the model area with respect to Narragansett Bay and Rhode Island Sound.

The x-direction for the finite-difference grid network is chosen to follow the east shore of the river, approximately the same direction as the expected mean flow. Since this shore is fairly straight, the matching of the shoreline by square grids is optimized. Thus the x-axis is a line directed S 22° E, the m-index increasing to the south. The y-axis is perpendicular with the k-index increasing to the east. The first computational field was taken as 32 by 12 grids, with a Δx of 1221 feet. This was increased to 51 by 18 ($\Delta x = \Delta y = 750$ feet), in an attempt to improve the resolution. The most difficult geometric location to model accurately is the narrow mouth of the Seekonk River, which spans about 750 feet where it merges with the model area, but is much narrower just to the east. An attempt to model the narrowest entrance with a smaller Δx would have increased the storage and time requirements greatly, without providing useful resolution in any other part of the model. Figure 5.2 is a map of the model area, showing the land and water boundaries.

The depth field was prepared from U.S. Coast and Geodetic Survey Chart No 278. The mean low-water soundings closest to the southeast corner of each grid $(m + \frac{1}{2}, k + \frac{1}{2})$ were placed in a matrix, adding the

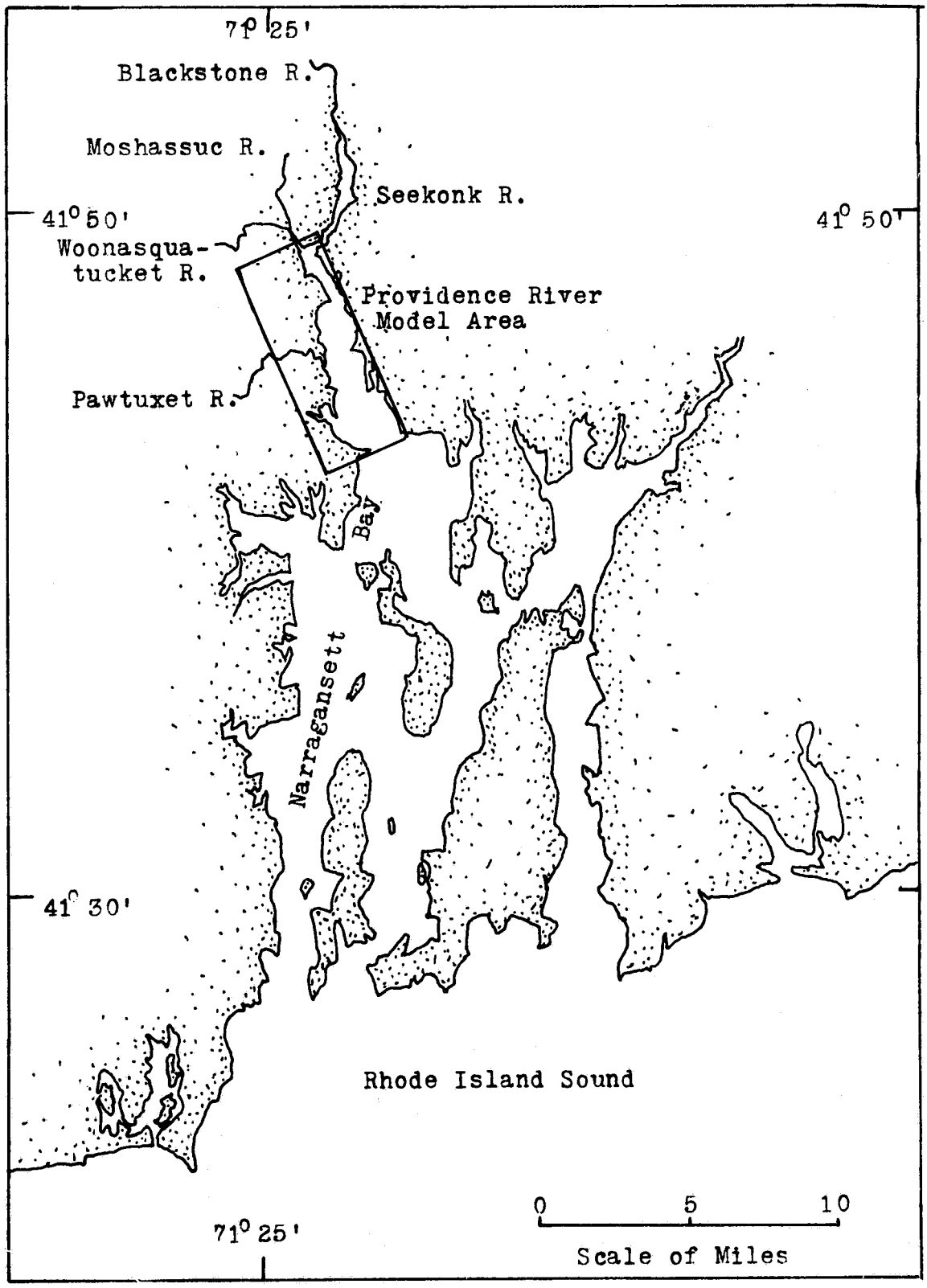

Figure 5.1. Location of model area

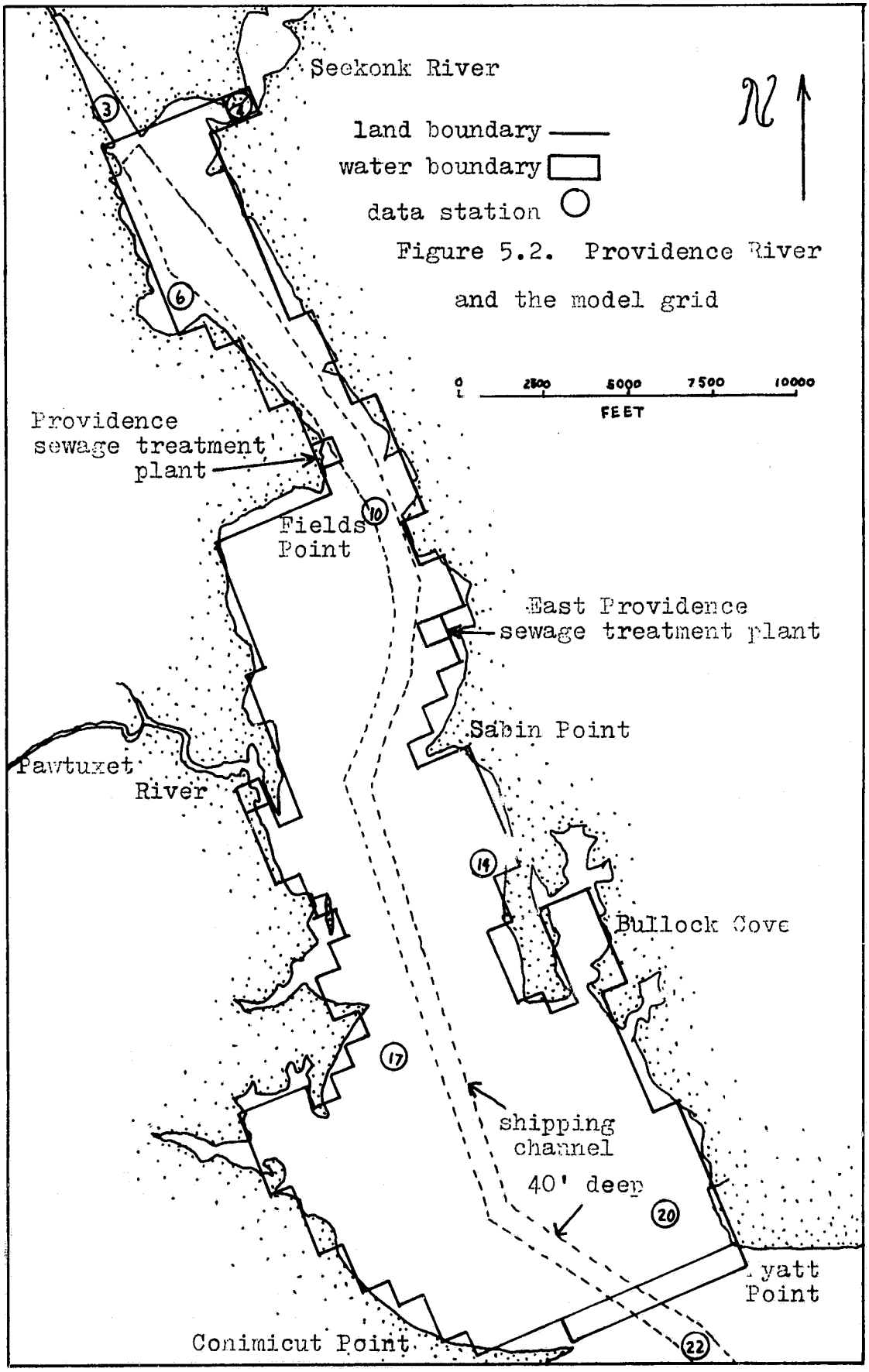

Figure 5.2. Providence River and the model grid

FIGURE 5.2 Providence River Showing Orientation of Grid System.

difference between mean sea level and mean low water. An exception to this procedure was made at the Seekonk River boundary where the depths were chosen arbitrarily, to ensure that the model represented the actual cross-sectional area of the interface.

The boundary condition at all land-water interfaces is that the velocity component normal to the boundary is zero. The water boundaries offer a choice of specifying either the tide height or the current velocity at every step. For a river boundary with an approximately constant flowrate, it is easiest to specify the velocity, which is the flowrate divided by the cross-sectional area, and which will vary inversely with the rise and fall of the tide. The Pawtuxet River boundary is handled in this manner.

Since the flowrates at the wide lower boundary are unknown, the tide height is specified. Good information is available. From tide-height histories taken by the Coast and Geodetic Survey at Newport, Bristol, and Providence Harbor, Hess and White obtained the amplitudes and phases of the main harmonic constituents of the astronomical tide. The tide height as a function of time (18) is:

$$\xi(t) = \sum_n f_n(t)\, H_n \cos\left(\omega_0 t + (V_0 + u)_n - k_n\right) \qquad (5.10)$$

where n is the number of the constituent,

$f_n(t)$ is a function of lunar position which

modifies the amplitude,

H_n is the amplitude,

ω_s is the angular speed in degrees per hour,

$V_o + U$ is the equilibrium argument at t=0,

k_n is the epoch, relative to Greenwich, England,

t is the time in hours after reference time.

The seventeen largest constituents are used. Their amplitudes at the lower boundary are obtained by interpolation from the known amplitudes for Newport, Bristol, and Providence Harbor.

The Seekonk River boundary presents problems, not only because it is narrow, but also because the flow is still tidally dominated. Since the flow through this boundary reverses direction with the tides, it is difficult to specify the velocity. In the Narragansett Bay model, Hess and White handle a similar problem by expressing the velocity as a function of the three lunar constituents of the tide. The three components of the flowrate are obtained by data analysis, and the total flowrate as a function of time is given by (18):

$$q = \sum_n q_n \cos\left[\frac{2\pi k}{12.42}(t - \tau_k)\right] \qquad (5.11)$$

where τ_k is the time to first flood after high water. Sufficient data was not available to apply this method to the Seekonk boundary, but assuming the lunar influence to be similar, the same constituents were used to calculate the flowrates there.

Specifying the tide height seems a more likely alternative, but would mask the actual river inflow. The most accurate method is apparently to add to the model grid an area representative of the area of the tidal Seekonk, and let it interact with the original model basin. This permits adding the inflow of the Blackstone River at a location removed from the narrow boundary. The computational time and storage are increased, but the requirement is minimized by fitting the extra grids as compactly as possible into extra space. Since the actual circulation in the Seekonk is not of interest, it is only necessary to represent the storage volume accurately, and the shape approximately. The result is that the tidal flow and the river flow are both modeled satisfactorily.

Two considerations determined the length of the time step. First, it must be compatible with the required time step of the mass transport model. The second consideration is Leendertse's parameter of accuracy (19):

$$\beta_s = \frac{\Delta t}{\Delta x}\sqrt{gh} \qquad (5.12)$$

where h is the maximum water depth. β_s must be of the order of five or less for a solution of acceptable accuracy. Thus,

$$\Delta t_{max} = \frac{\beta \Delta x}{\sqrt{gh}} = \frac{(5)(750)}{\sqrt{(32.2)(40)}} \simeq 105 \text{ sec.}$$

A 100-second time step turned out to be perfectly compatible with the requirements of the water quality model.

Verification of the Tidal Model

There is only one set of current data that has been taken in the model area. Haight, in 1930, made measurements at many stations in Narragansett Bay, at all stages of the tide (44). Six stations within the model area were occupied. The magnitude and direction of the current, the time relative to high tide at Newport, and the estimated component due to wind were presented.

To compare the model predictions with the existing data, runs of the model were made for a date on which the tidal range was the average, 4.6 feet at Providence. Initial conditions were established by a 24-hour simulation starting with zero tide height and velocities. This was found to be an adequate startup time to eliminate transients.

The velocities calculated are dependent upon the bottom roughness, and thus upon the value chosen for the Manning factor in Equation 5.6. Hess and White (18) recommend a value of 0.026 for the Providence River, based on their modeling. The data gathered by Haight presents an opportunity to adjust the Manning factor. Figure 5.3 shows the measured values at the narrowest

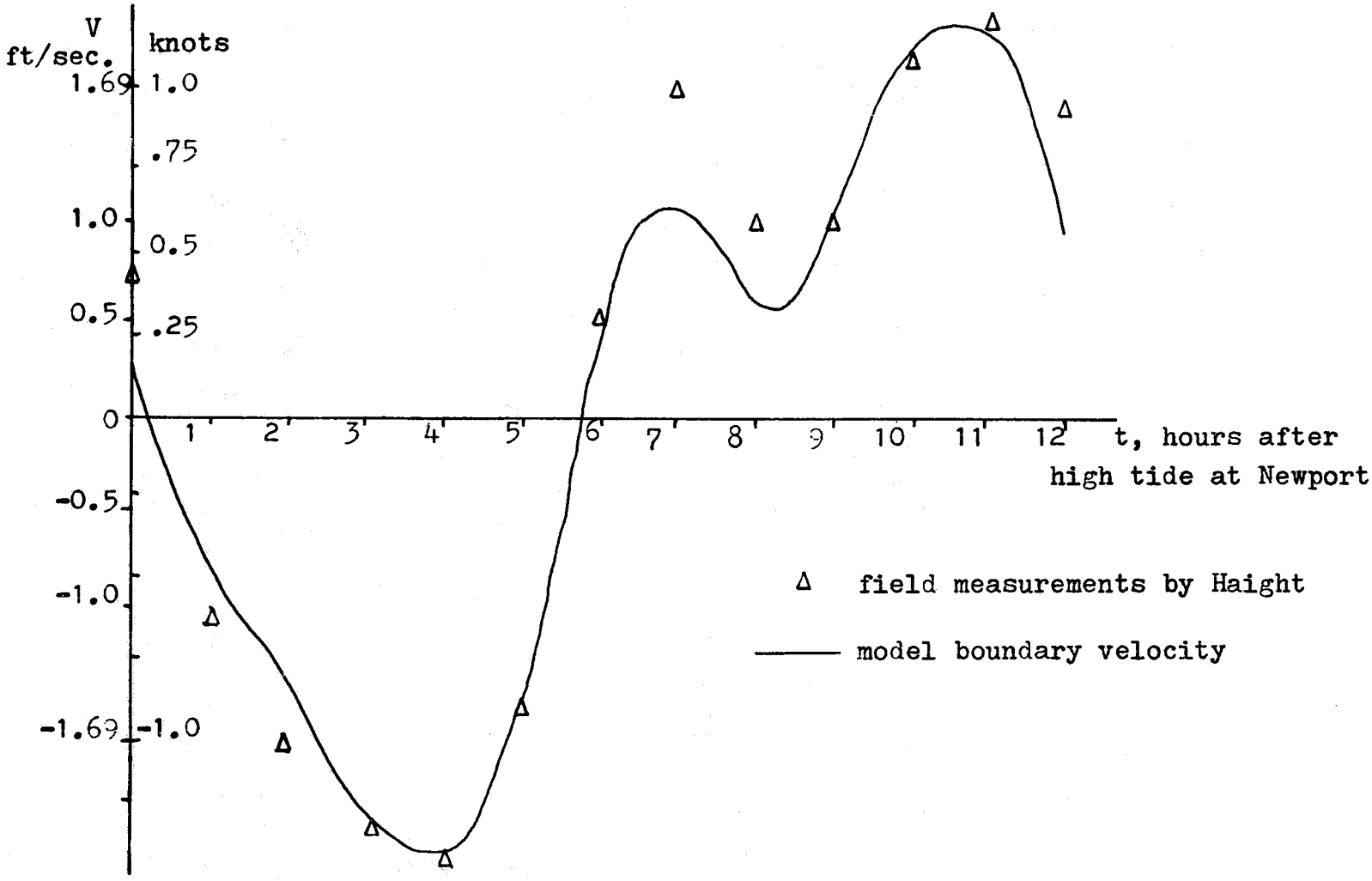

Figure 5.3. Seekonk River Velocity Boundary Condition. Velocity vs. time

part of the mouth of the Seekonk, at each hour of an average tidal cycle. (The estimated components due to wind were removed by Haight.) Using a single-grid boundary of the same cross-sectional area as the real channel at Haight's station, the Manning factor was adjusted until the best fit was found. This occurred for a Manning factor of 0.030.

Some distortion is expected at this location due to the fact that the model grid is about three times as wide and one-third as deep as the real channel. This is all right at mean tide, but at low tide, the cross-sectional area of the model is considerably less than that of the real channel, due to the lesser depth. However, since the greatest flow occurs when the tide level is near mean, this effect is not severe.

Figure 5.3 shows excellent agreement in phase and in amplitude with Haight's data. The first peak of the double flood (characteristic of Narragansett Bay) is not well-matched in amplitude, but failure to reproduce a single data point does not indicate a flaw in the equations or boundary conditions. Indeed, were Haight's points connected into a continuous curve, the area underneath would indicate that the volume of the flood tide is greater than that of the ebb, river inflow notwithstanding. The model is checked for mass conservation at all times, by summing the river and tidal inflows over time, and comparing this to the change in the water content of the entire model. The

greatest error found, which always returned to zero within the tidal cycle, was 0.7 per cent of the total mass.

In an effort to verify the model more broadly, current vector plots were obtained for the whole field, at each hour of a tidal cycle. Haight's normalized vectors were transferred to the plots for comparison. . These are presented in Figures 5.4 through 5.15. At slack tide the currents are variable and agreement is not good. However, the model appears to reproduce the data extremely well on the ebb tide, both in magnitude and in direction. Motion becomes random again at slack, but returns to fair, though clearly not as precise, agreement on the flood tide. This situation is complicated by the characteristic double flood, which in effect inserts an extra period of slack water between the two parts of the flood. On the whole, it appears that the model predicts the same kinds of motion-- eddies of the same size, duration, and location-- as are indicated by the field measurements. The one consistent difference is that the measured magnitudes are greater than those predicted. This is very likely to be the result of vertical averaging, since Haight's measurements were taken in the upper layers, mostly by floating spars.

Input for the Water Quality Model

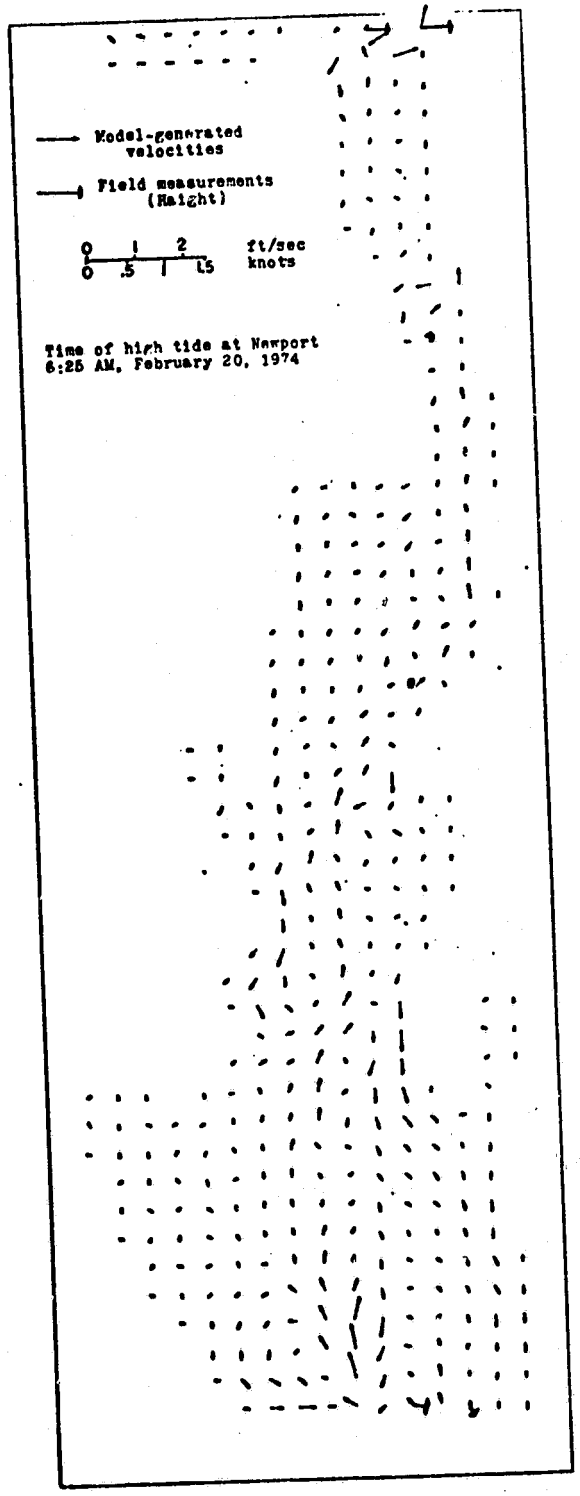

FIGURE 5.4 Comparison of Field Measurements and Model Predictions for Tidal Velocities, High Water at Newport, R. I.

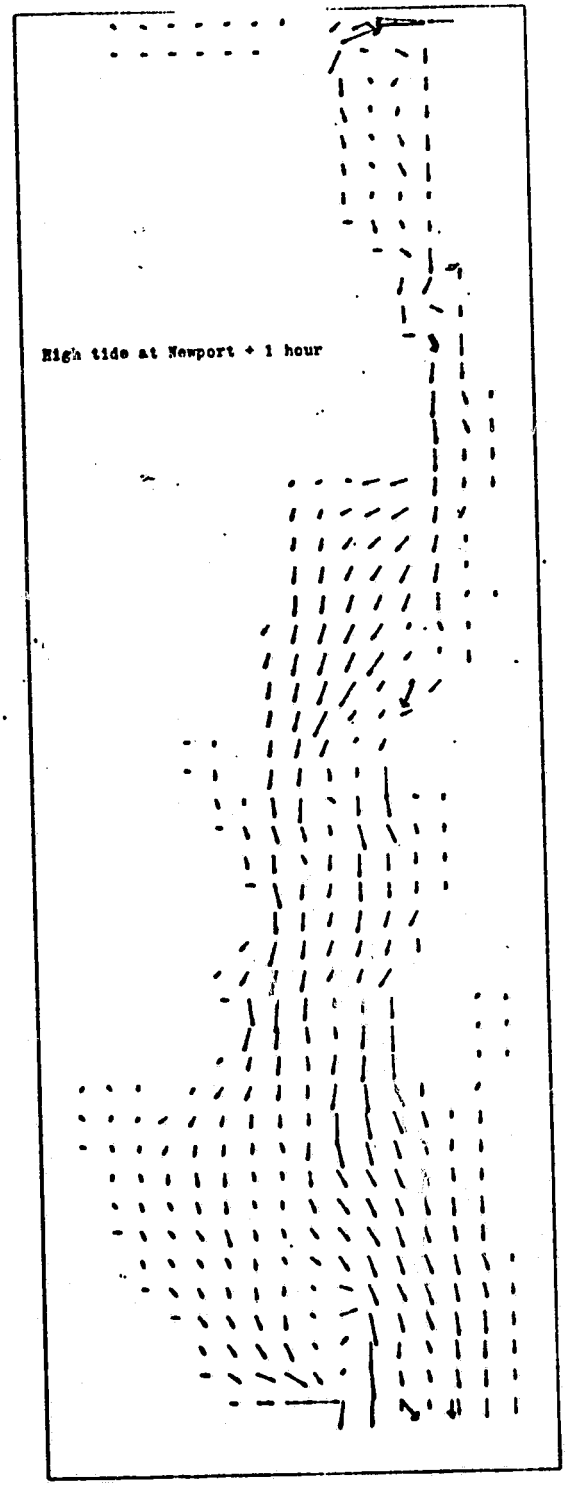

FIGURE 5.5 Comparison of Field Measurements and Model Predictions for Tidal Velocities, One Hour After High Water at Newport, R. I.

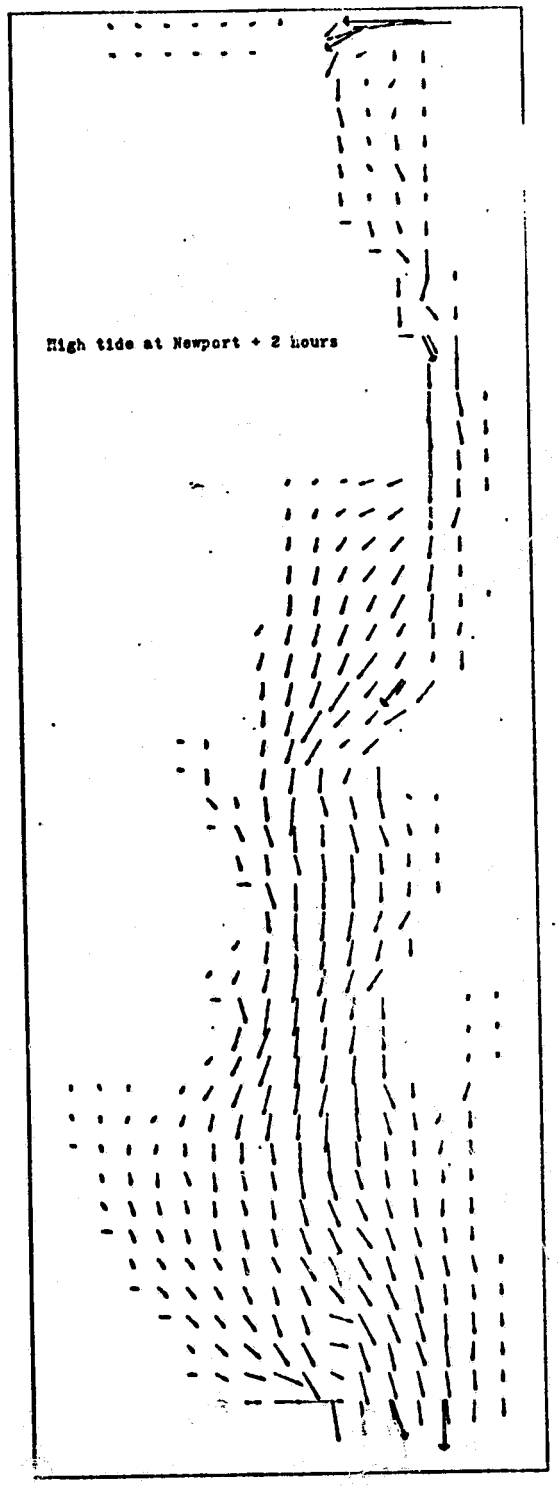

FIGURE 5.6 Comparison of Field Measurements and Model Predictions for Tidal Velocities, Two Hours After High Water at Newport, R. I.

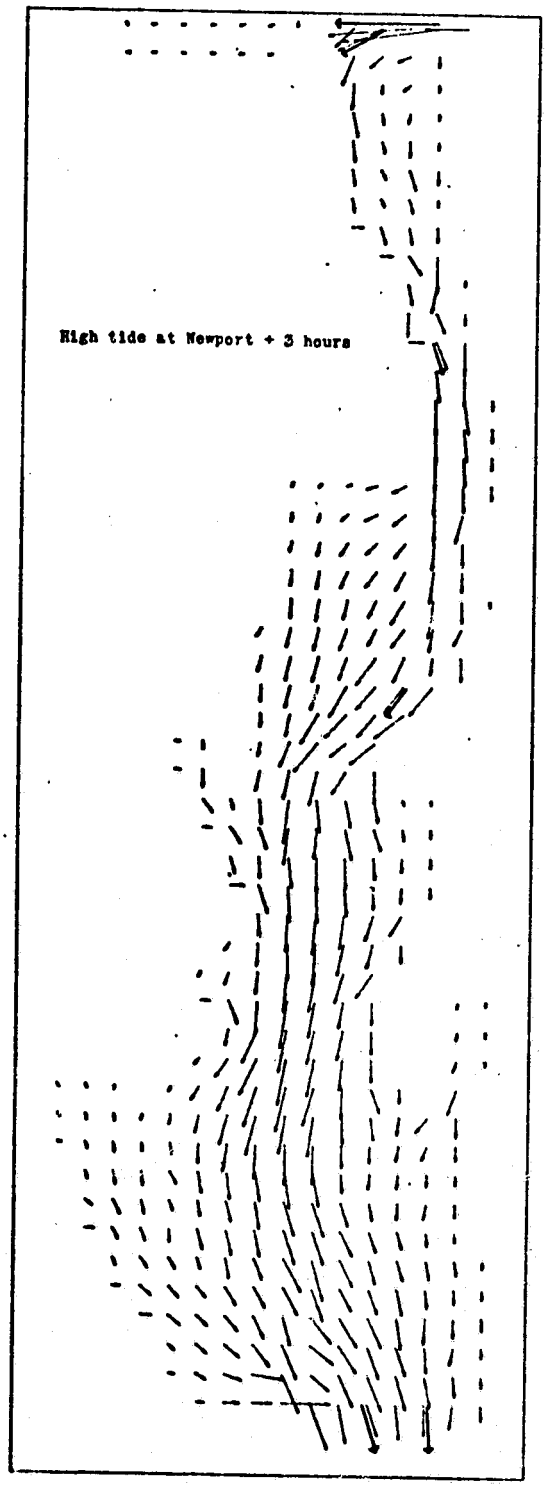

FIGURE 5.7 Comparison of Field Measurements and Model Predictions for Tidal Velocities, Three Hours After High Water at Newport, RI.

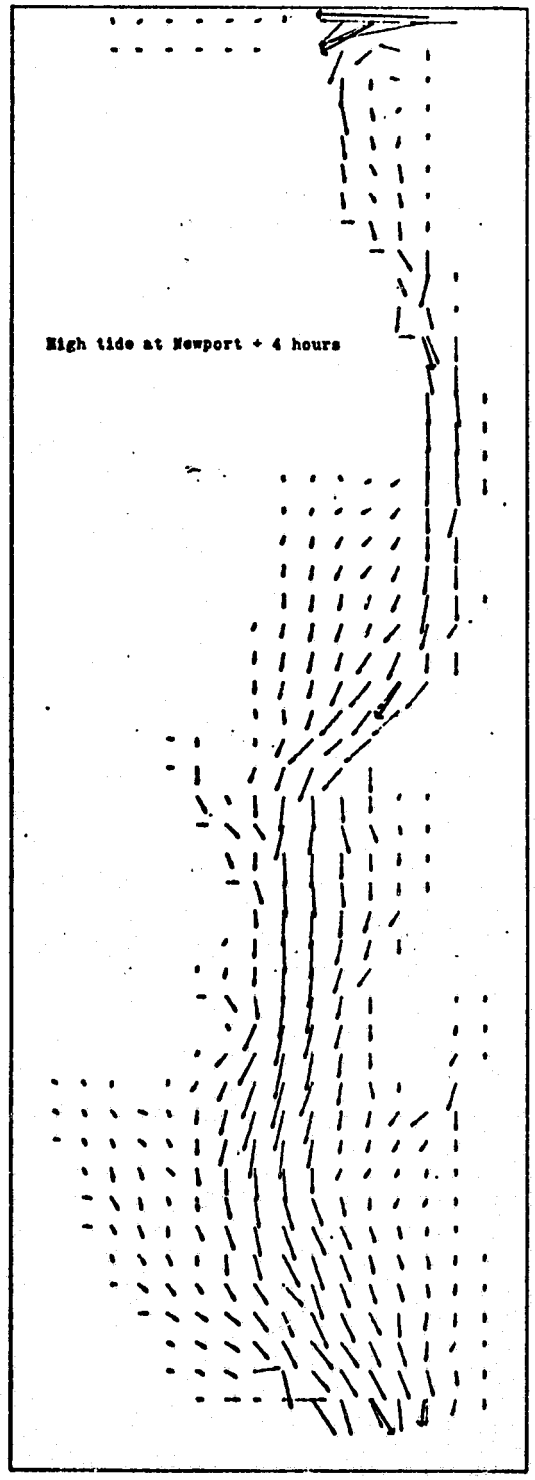

FIGURE 5.8 Comparison of Field Measurements and Model Predictions for Tidal Velocities, Four Hours after High Water at Newport, R. I.

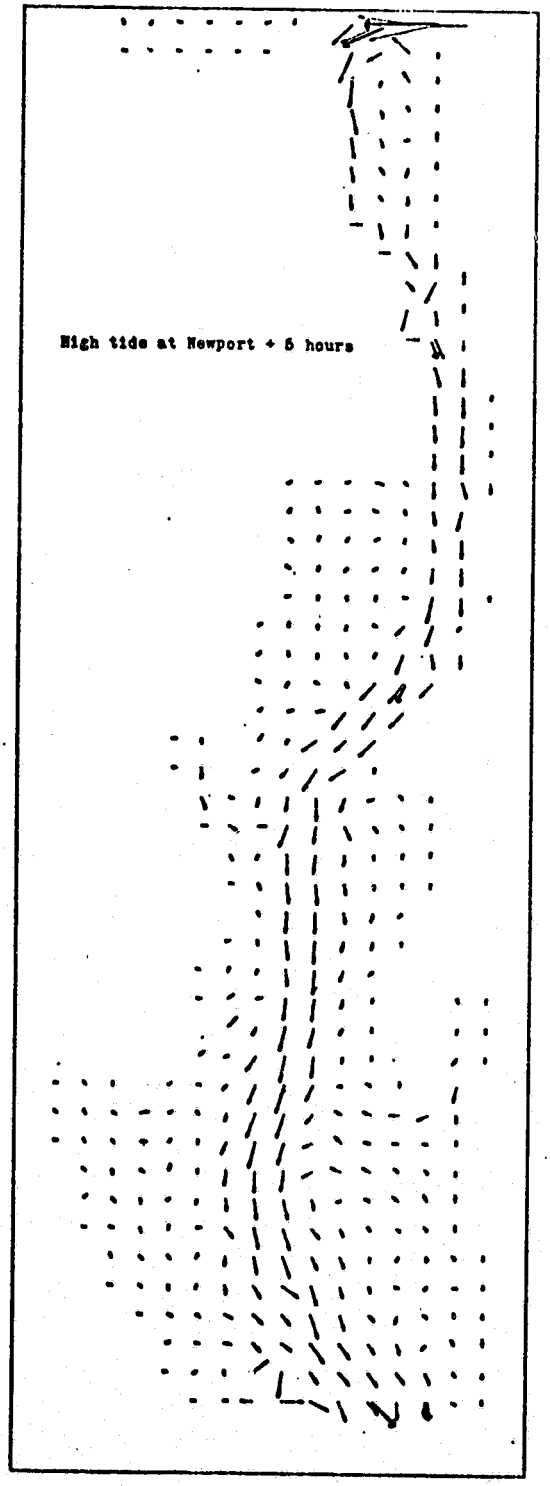

FIGURE 5.9 Comparison of Field Measurements and Model Predictions for Tidal Velocities, Five Hours after High Water at Newport, R. I.

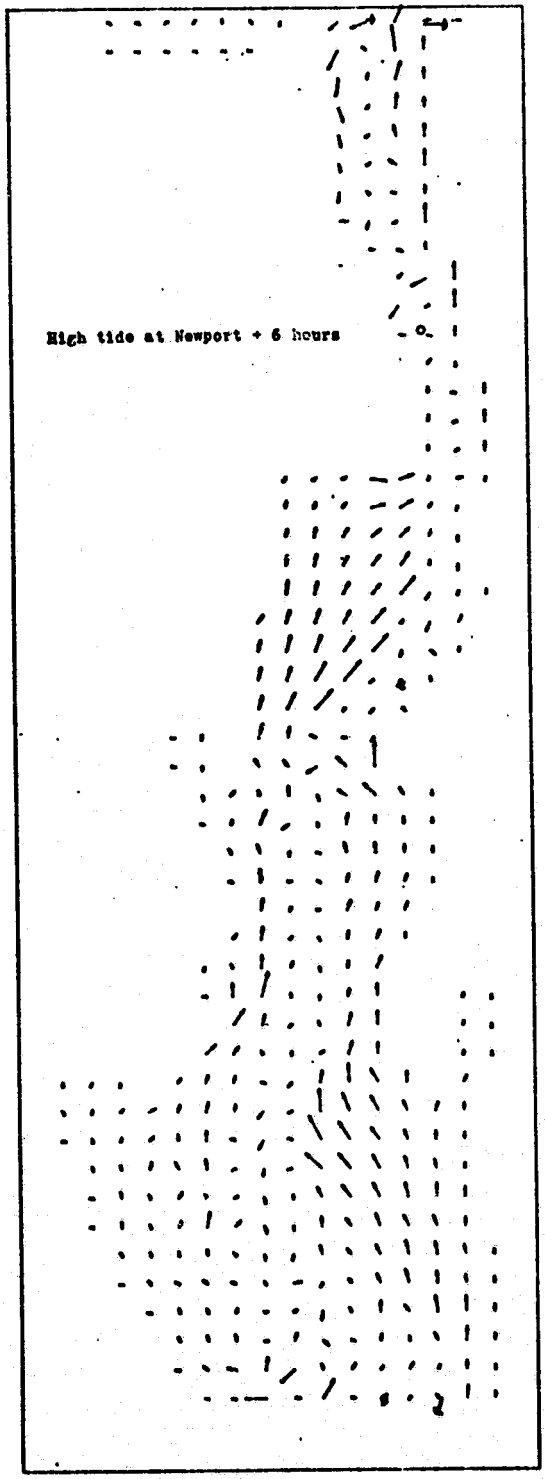

FIGURE 5.10 Comparison of Field Measurements and Model Predictions for Tidal Velocities, Six Hours after High Water at Newport, R. I.

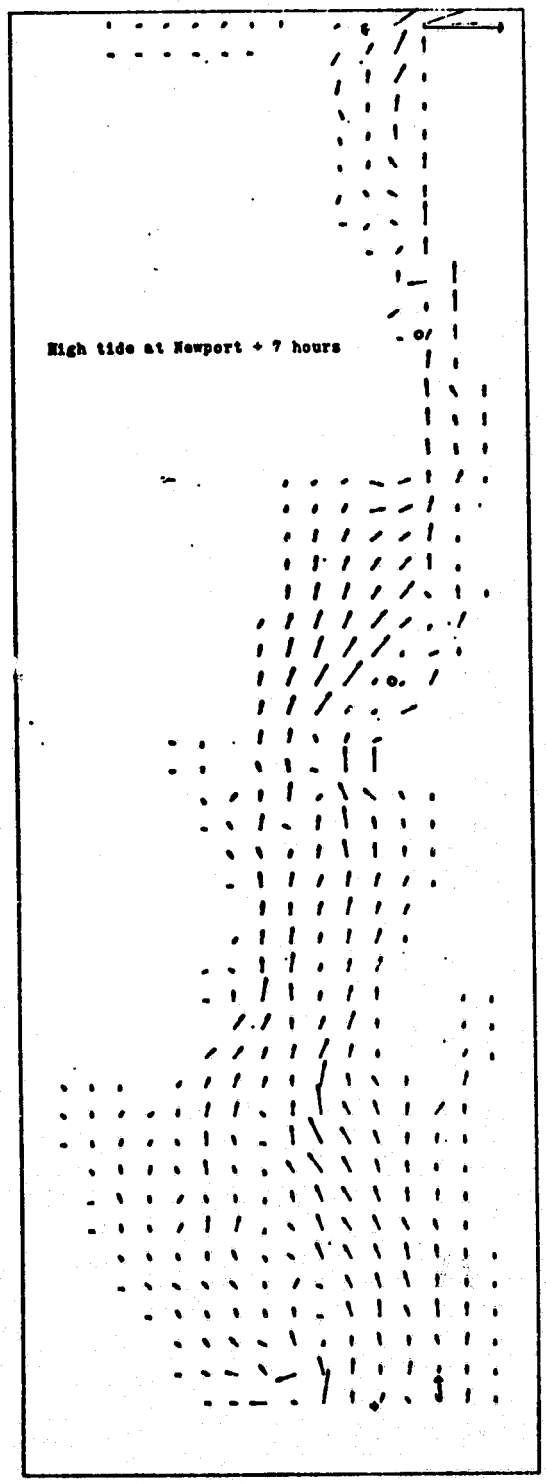

FIGURE 5.11 Comparison of Field Measurements and Model Predictions for Tidal Velocities, Seven Hours after High Water at Newport, R. I.

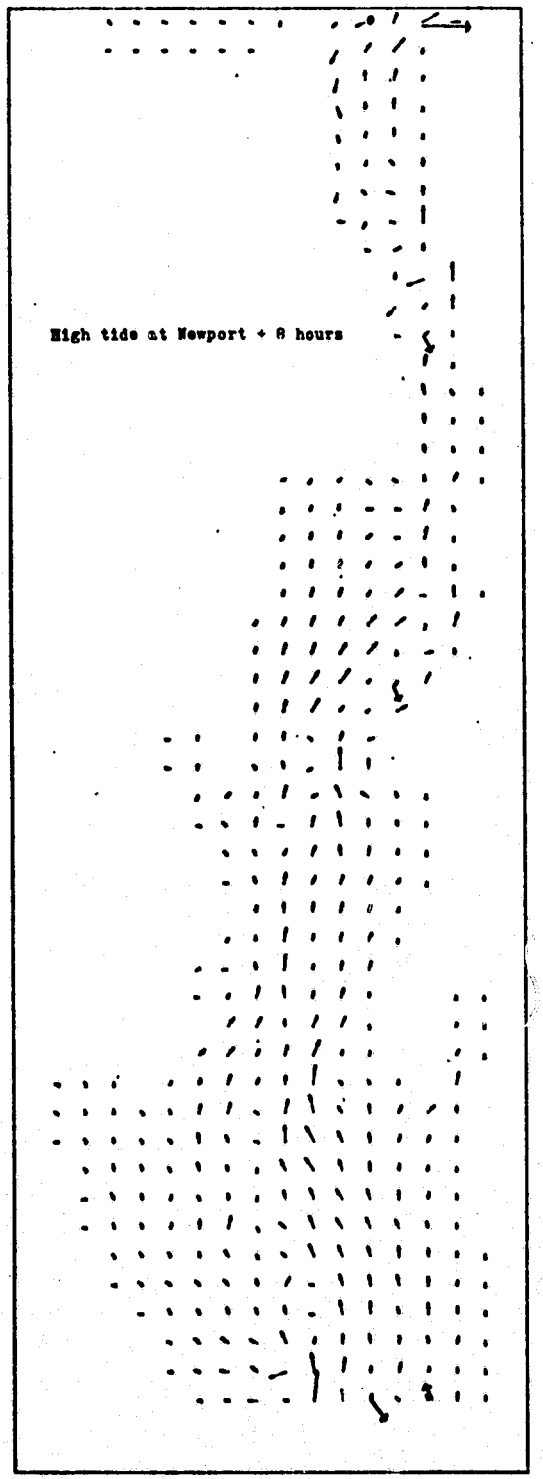

FIGURE 5.12 Comparison of Field Measurements and Model Predictions for Tidal Velocities, Eight Hours after High Water at Newport, R. I.

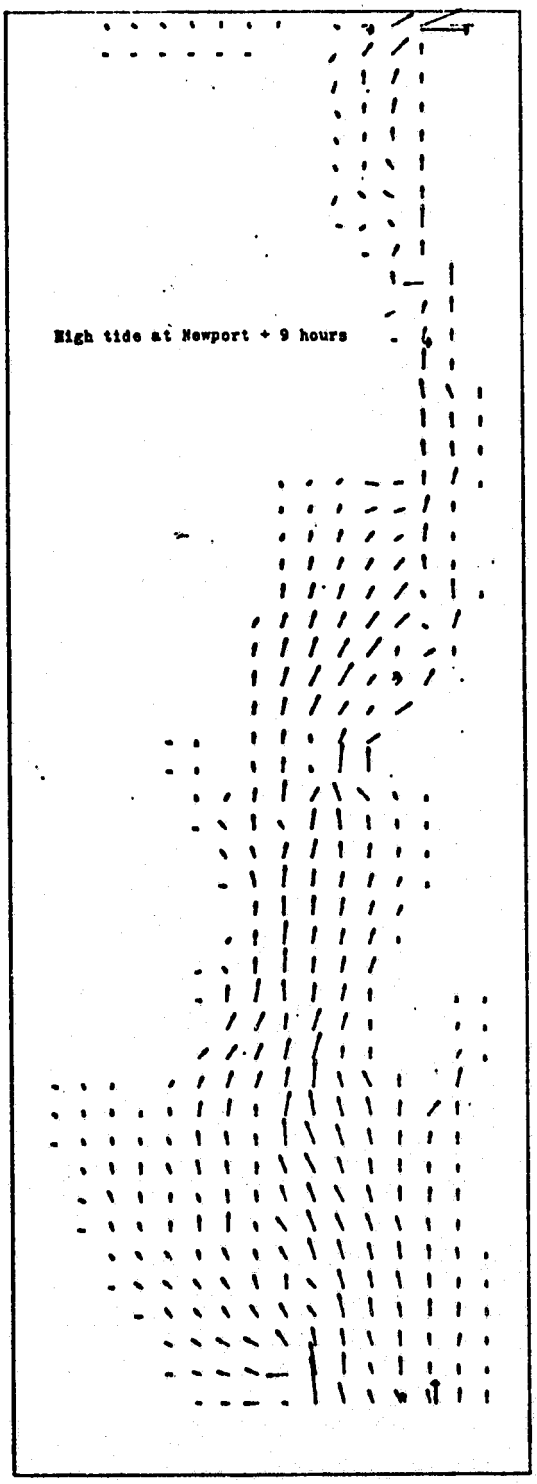

FIGURE 5.13 Comparison of Field Measurements and Model Predictions for Tidal Velocities, Nine Hours after High Water at Newport, R. I.

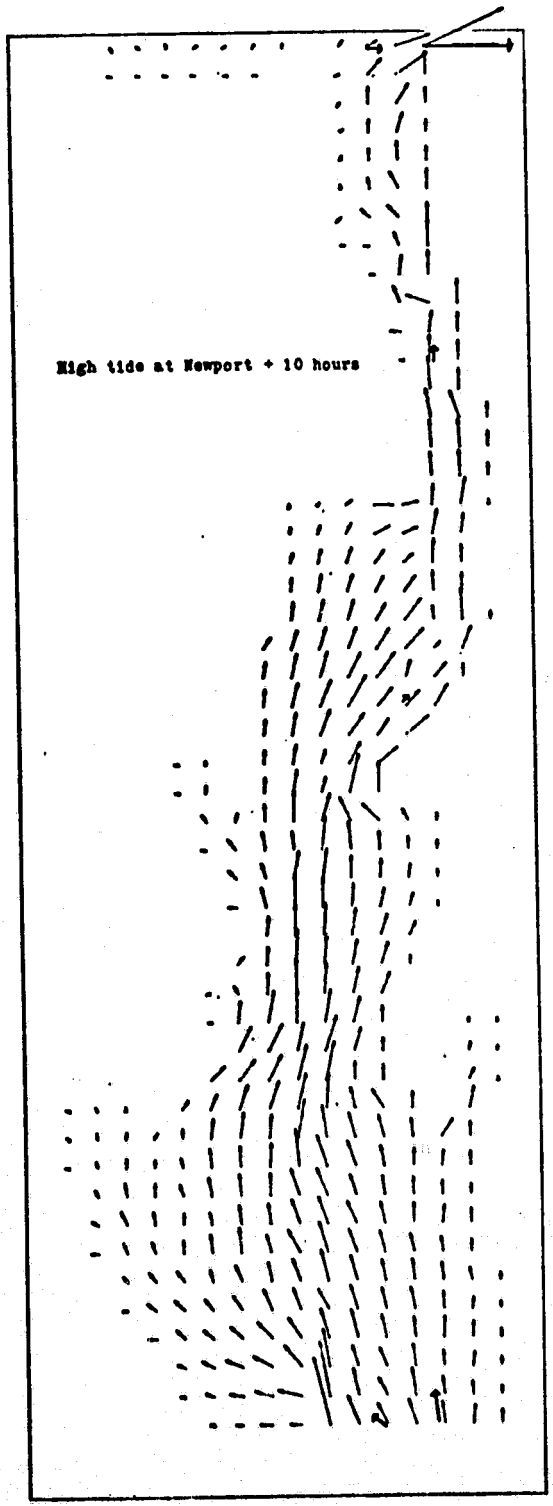

FIGURE 5.14 Comparison of Field Measurements and Model Predictions for Tidal Velocities, Ten Hours after High Water at Newport, R. I.

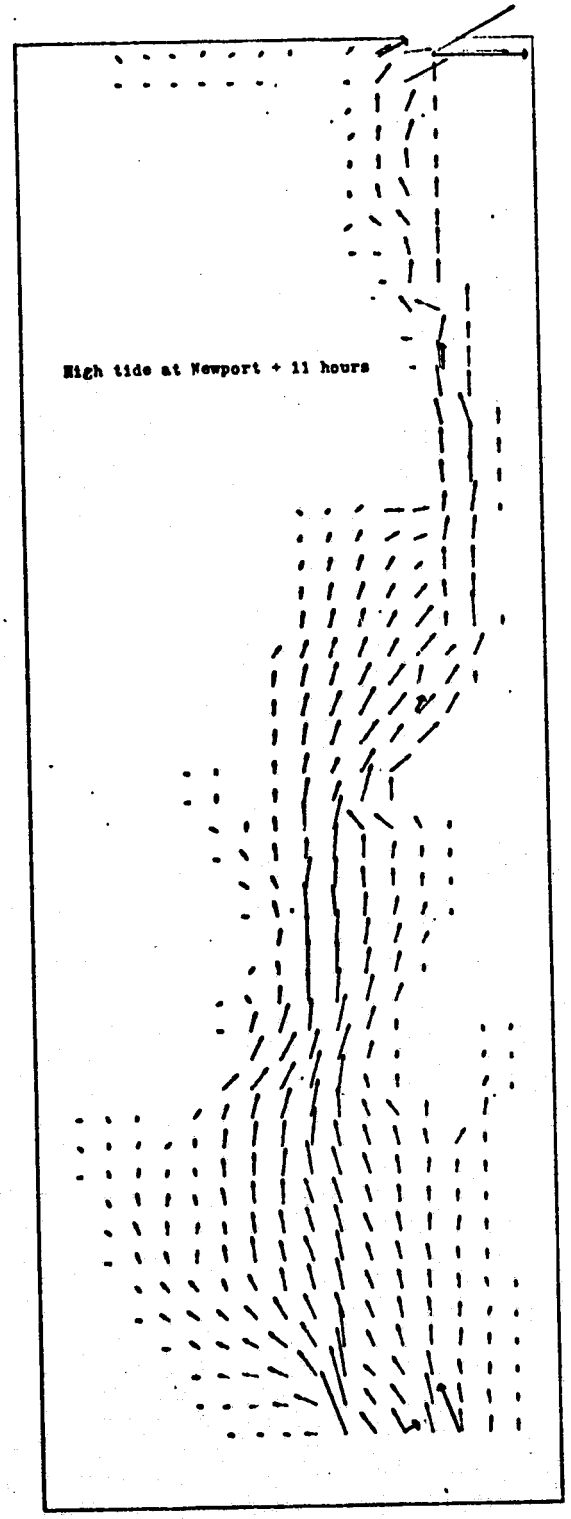

FIGURE 5.15 Comparison of Field Measurements and Model Predictions for Tidal Velocities, Eleven Hours after High Water at Newport, R. I.

Values of the u- and v-velocities, and the tide heights generated by the tidal model, are stored for each grid point and time step. The information is read as input to the water quality model at each time step. Care must be taken to supply the information correctly, since the two models are computationally incompatible.

The problem is mainly that the two-dimensional model has a time step divided into two levels, while the three- dimensional model has three levels. The information generated by the tidal model is u, v, and the tide height (called se) at each step. The information required by the water quality model is u and v at the beginning and end of each step (u, v, up, vp), and the tide height at each fraction of a step and at the end of the step (1, 1 +$\frac{1}{3}$, 1 +$\frac{2}{3}$, 1 +1: se, sep, seq, ser). The match-up is made by staggering the reading of v and u, reading the unwanted arrays into a dummy variable that is not used. The order of reading and dummying the velocities is reversed after each step, to prevent the models from building errors due to model matching. The values read at 1 +1 are carried over to the values of 1 at the start of the next step. This sequence is illustrated in Figure 5.16. The values read and used are circled; the values read into the dummy are crossed off. The time levels assigned to each variable are indicated by the subscripts. The method imposes the requirement that the water quality model have a time step three times as long as that of the tidal model.

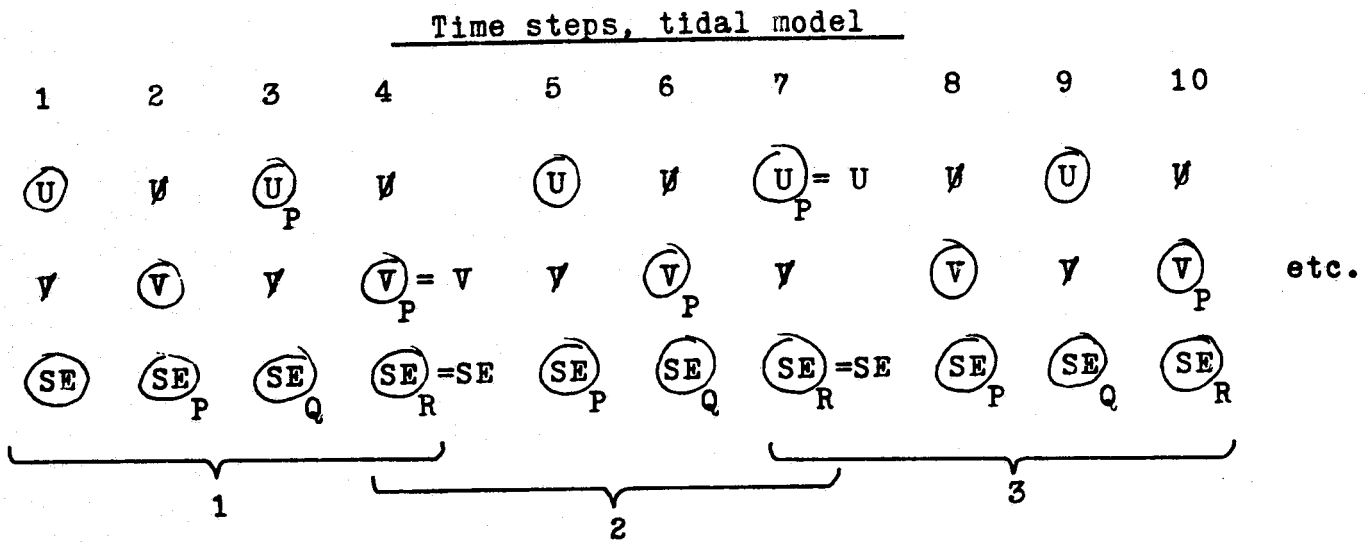

Figure 5.16. Reading sequence for hydrodynamic input to water quality model

Fortunately, for this body of water, it is possible to use the optimum time step for both models.

All of this is accomplished by a subroutine in the water quality model which is called at each time step. The velocities, read into a horizontal matrix, are then extended to all the vertical levels. This method has been checked for mass conservation, as described in Chapter VII, and found to be excellent in this regard.

VI. SIGNIFICANCE AND BEHAVIOR OF COLIFORM BACTERIA IN SEA WATER

Value as an Indicator of Sewage Contamination

Due to the difficulty of isolating pathogenic bacteria and enteric viruses from water and sewage, it has long been the practice to infer the quality of water, or the potential hazards of wastes, from the concentrations of the more abundant and easily detectable coliform bacteria group. The groundwork for this practice was laid by Escherich in 1885, who determined Baccilus coli to be characteristic of the feces of warm-blooded animals. Although the total coliform count is still the commonly used indicator and is the basis of water quality standards, its use as an indicator has recently come under heavy attack from microbiologists.

Concern over the presence of disease organisms in natural waters falls into three areas: transmission of disease through drinking water (not a concern of this paper), contamination of shellfish, and infection of swimmers. Coliform standards have long been in effect for the first two considerations (45,46). There is clear evidence linking consumption of contaminated shellfish or drinking water to outbreaks of typhoid

fever or infectious hepatitis (47,48).

The danger of bathing in contaminated sea water is not at all clear. There is almost no evidence conclusively linking polluted beaches to disease outbreaks. On this basis, some have gone so far as to state that bathing in sewage-polluted sea water carries negligible risks to health, even if the water is aesthically unpleasant (48). However, it is extremely difficult to detect disease contracted by swimming, due to such problems as the transience of swimming populations, the long incubation periods (49) of diseases such as hepatitis (a month or more), and the scarcity of enteric diseases in the populations of the United States and the United Kingdom, where most of the studies have been attempted (49). This difficulty has been used as an argument both for and against the imposition of microbial standards for beaches (49,50).

The argument against classifying bathing waters by coliform levels centers upon, first, the absence of evidence of disease transmission, and second, the large observed variations in coliform counts with time at a given beach, which would seem to preclude assigning a beach to a certain class. Shuval (49), however, concludes from a mathematical estimate of the probability of contracting disease, that standards are needed. Although enteric disease has not been linked to contaminated bathing waters recent studies point conclusively to the danger of skin and upper respiratory

tract infections (51,52). It may be safe to conclude that when going swimming, one would wish to know whether the water is polluted.

The presumption that the total coliform level can indicate how polluted the water is, and with what harmful organisms, is increasingly in doubt. Although the occurrence of pathogens such as Salmonella and Streptococcus is generally found to be related to the coliform count (47,53), this is not always the case. Disease outbreaks due to Salmonella and Shigella have occurred in instances where the drinking water met the coliform standard (less than 2.2 per 100 ml.), and the ratio of Salmonellae to coliforms, usually very small, was greater than one (52). Another problem is that coliform levels can increase enormously in the presence of organic nutrients, while this effect is not observed for pathogens or viruses (51,52). Furthermore, and perhaps the most damaging to their indicator status, coliforms are more susceptible to disinfection than enteric pathogens (52,54,55). This would mean that the coliform test overestimates the effectiveness of sewage treatment, and the quality of the receiving waters. The nature of the coliform group itself presents some problems. Not all members of the group are of fecal origin; some occur on plants and in soil, and would be present in large numbers in runoff that was not necessarily contaminated with sewage. The different members Escherichia coli, Klebsiella, Citrobacter, and

Enterobacter have been found to have different die-off rates and different responses to nutrients (56). The various methods used to obtain coliform counts do not even detect all of the same organisms (52).

Dutka (52) specifies four criteria a good indicator should meet. They are:

1. Occurring in much greater numbers than the pathogens;

2. Not proliferating relative to the pathogens;

3. Being more persistant through disinfection and in the environment than pathogens;

4. Yielding an unambiguous identification.

Dutka concludes that the coliform group fails all these tests. He recommends that fecal coliforms, together with fecal streptococci, be used as an indicator instead. It has been found that enterococci are not subject to the growth phase, and the death rate is smaller and less sensitive to the environment than that of coliforms (55). Others have recommended Escherichia coli, which is of unquestionable fecal origin and has been studied individually to determine its die-off rate (51,53).

Despite the availability of this information, it will probably take years for regulatory agencies to adopt better indicators and acquire the new techniques. Meanwhile, the deterministic water quality model comes into its own. Any constituent can be modeled, including pathogens and viruses as well as indicators, providing

source levels and die-off rates can be estimated. Some good information is available on, for example, Salmonella (53). The use of a model can eliminate problems such as the uncertainty in the widely-used MPN (most probable number) test, and the presence of coliforms of non-fecal origin. Field data may be used to verify the model under known conditions, and the model will describe the effects of variations in the conditions.

Perhaps it is fortunate that total coliform data is the kind most likely to be available for verification purposes. Since much literature on coliform kinetics is available, this permits the best possible formulation of the kinetics in the model.

Reaction Kinetics of Coliforms in Sea Water

It is questionable whether the disappearance of coliforms in sea water is correctly called either "die-off" or "mortality". Inactivation and sedimentation are likely to be mechanisms of disappearance. It is clear from many studies (51,54, 55,57,58,59) that the disappearance is much more rapid in sea water than in fresh water. Many studies attempting to estimate the decay (disappearance, die-off) coefficients have been made, and many differing results have been obtained. At this point, it is still uncertain which mechanisms prevail, and under what

conditions.

The behavior of coliforms in sea water consists of up to three phases. Figure 6.1 illustrates the different kinds of behavior that may be found. The first, which is not always observed, is a lag phase, in which the population does not decrease, and may increase if nutrients are present. Lag periods of the order of 0.4 day (57), one day (56), and three weeks (51) have been reported. This phase is followed by an exponential decay. Many investigations have attempted to determine the coefficient of this decay, and the conditions upon which it depends. Finally there is a resistant phase, in which a certain portion of the population will persist long past the rest, due to an inherent ability to resist the pressures of the environment (56). This phase has not been well characterized.

The exponential decay coefficient, K_d, is defined in terms of the ratio of the coliform count at any time t to the initial count (59):

$$\frac{C}{C_o} = e^{-K_d t} \qquad (6.1)$$

Values of K_d are standardized by using the time, t_{90}, required for ninety per cent of the coliforms to disappear, so that

$$0.1 = e^{-K_d t_{90}}$$

Thus,

$$K_d = \frac{2.303}{t_{90}} \qquad (6.2)$$

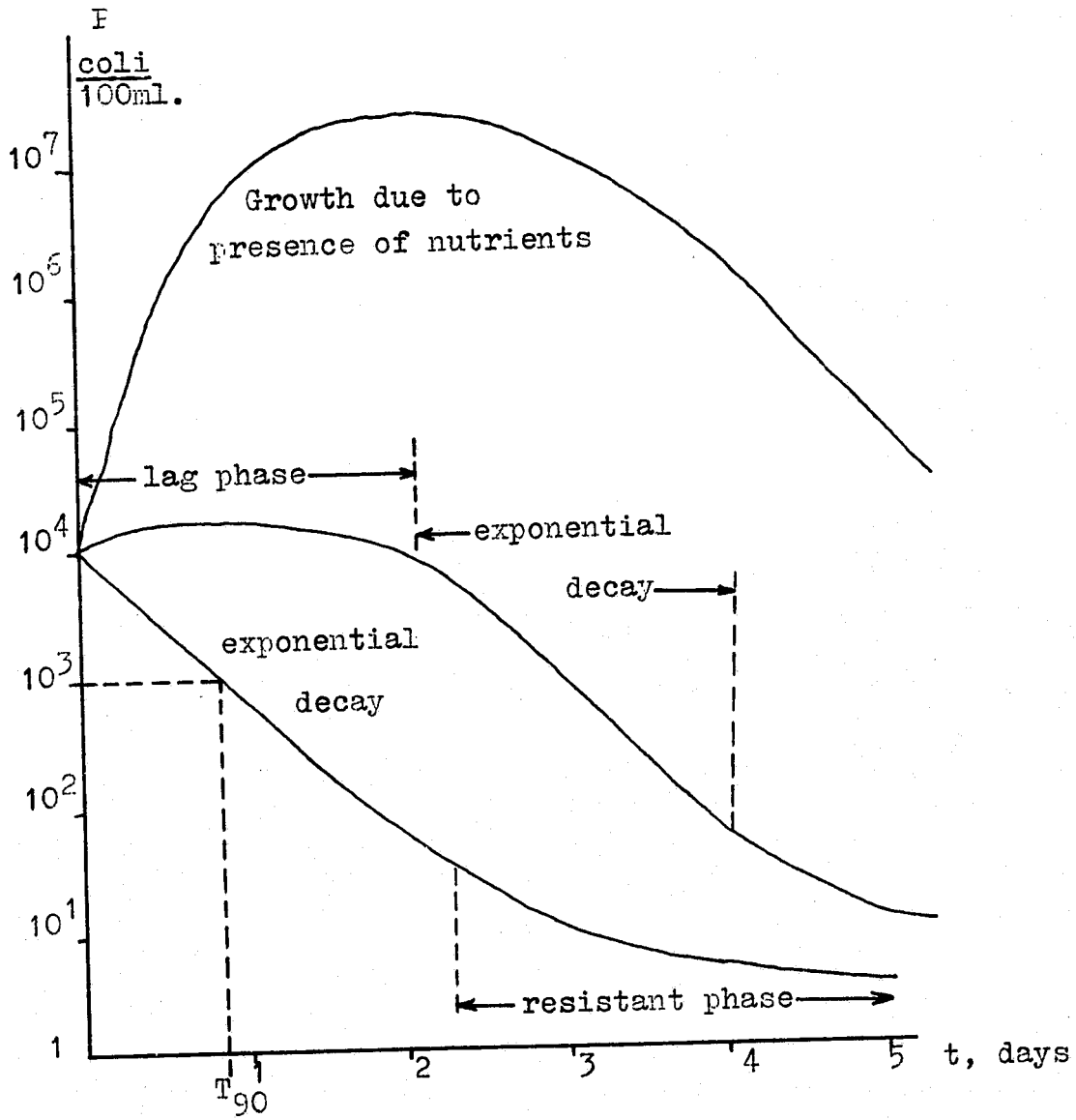

Figure 6.1. Types of coliform growth and decay

Log_{10} of concentration vs. time

The quantity t_{90} is of great interest because it gives a quick indication of the degree of self-purification of which the water is capable. Values for sea water can be as small as 20 minutes, or nearly 200 hours (60).

Studies of the decay rate have yielded widely varying results depending upon the location, whether samples were stored in the lab or in situ, upon the counting method, and on whether artificial or natural sea water was used. To obtain numerical values of the decay coefficients, and a model of the processes, reviews of the past findings must be made. Fortunately, two recent reviews offer an opportunity to neatly resolve part of the coliform kinetics problem.

Mitchell and Chamberlin (61) have formulated a model incorporating the major known, or generally accepted contributors to coliform disappearance and growth. Disappearance is due to sedimentation, solar radiation, predation, and physicochemical effects (osmotic effect, pH, specific ion toxicity). Growth is due to the presence of nutrients in the plume (carbon, nitrogen, phosphorus). The mass transport equation is given for one-dimensional flow:

$$u\frac{dC}{dx} - V_s\frac{dC}{dz} = e_x\frac{\partial^2 C}{\partial y^2} + e_z\frac{\partial^2 C}{\partial z^2} + \left[\frac{\mu_m S_n}{K_s + S_n} - a\right]C$$

$$-\left[\frac{\lambda_m P_p}{(k_p + C)Y_{pc}}\right]C - (k_s\, l(t)\, e^{-\alpha_s z})C - rC \qquad (6.3)$$

where V_s = sedimentation velocity;

C = coliform concentration;

μ_m = maximum coliform growth rate;

K_s = half-saturation constant for:

S, the concentration of nutrients;

a = endogenous respiration rate;

λ_m = maximum predation rate;

P_p = concentration of predators;

k_p = half-saturation constant for P ;

Y_{pc} = yield of predators on bacteria;

k_s =die-off rate due to solar radiation;

I(t) = solar radiation intensity;

α_s = attenuation of light in water;

r = physicochemical die-off rate.

The trouble with this model is that most of the above parameters are unknown. Not only are there no general values, but there aren't even good estimates or field measurements of, for example, the concentrations of predators. The model is presented in a more useful form in the following table, which gives estimated maximum die-off rates due to each component (61).

Table 6.1. Components of the Mitchell-Chamberlin Kinetic Model

Factor	Sensitivity	K (max)
Sedimentation	degree of treatment	0.6 /hr.
	turbulence	
Sunlight	season	4.0 /hr.
	latitude	
	turbidity	
Predation	temperature	0.3 /hr.
Nutrients	temperature	-0.6 /hr.
	degree of treatment	
	organic pollutants	
Physicochemical	temperature	0.15 /hr.

Still, it is not possible to make good estimates of the components of K_d, within the given maxima, without extensive measurements. However, from the literature, it is clear that three factors dominate the behavior of coliforms in sea water: temperature, sunlight, and the presence of nutrients.

The temperature dependence has been observed as early as 1956 (57). The familiar rule of thumb for biochemical processes, that the rate doubled for a temperature increase of 10°C, has been verified by

Gameson and Gould (60) for coliform decay; in fact, they found the factor to be 1.97. From a combination of earlier results and their own investigations in which light was excluded, Gameson and Gould proposed a relation for t_{90} as a function of temperature, in the absence of solar radiation:

$$\log_{10} t_{90}(\text{dark}) = 2.292 - 0.0295\ T \qquad (6.4)$$

where T in in degrees Centigrade.

The effect of sunlight, when clear beakers of sea water were exposed to it, was to reduce t_{90} to as little as 20 minutes (60). Many investigators have observed that the effect of solar radiation is pronounced. Adding the effect of sunlight to Equation 6.4, then, should incorporate two of the three important variables. Mitchell and Chamberlin obtained their estimated maximum K_d due to sunlight of 4 /hr. from an estimated minimum t_{90} of 30 minutes; using Gameson and Gould's 20 minutes, the maximum K_d becomes 6.9 /hr.

In using a finite difference model, it becomes practical to recalculate the decay coefficient at each time step, as the altitude of the sun varies. Assuming the maximum K of 6.9 to occur at the surface, with the sun directly overhead, the reduction in radiation intensity at the surface and at all depths, at other times, can be calculated. Relations giving radiation intensity

at the surface as a function of latitude, time of day, time of year, surface reflection, turbidity, atmospheric transmission, and cloudiness have been set forth by Ryan and Stolzenbach (62). As light is attenuated by the water, K_d now varies with depth, and a value must be calculated for each model grid point. Values for the attenuation coefficient have been obtained for the Providence River (63).

Modeling the lag or growth phase is more difficult. The lag phase is usually characterized by a time period, on the order of a day, during which no decay occurs. This would be very difficult to incorporate into an Eulerian calculation, since the time a particle has been in the field is not known. Equation 6.3 suggests that nutrients could be modeled as a second constituent, which would make good use of the model's capabilities as described in Chapter II. The concentration of nutrients, and the coefficients of interaction with coliforms, are not known for the Providence River, and would be difficult to obtain. However, if in any problem, modeling the growth phase was of particular interest, it might be worthwhile to attempt to obtain such data. This project will only attempt to demonstrate that the model has this capability.

VII. ESTUARY APPLICATION OF THE MODEL

Water Quality in the Providence River

The Providence River is surrounded by areas of high population density. It receives, either directly or indirectly, the effluent from sewage plants serving a population of about 373,000 (64), plus untreated waste. The Providence and East Providence sewage treatment plants discharge directly into the model area. The other significant quantities of waste enter by the Pawtuxet and Seekonk Rivers.

The levels of pollution are such that the entire model area is permanently closed to shellfishing. Field measurements of the coliform levels were made in 1966 at about eight stations in the model area, and at the mouths of the Pawtuxet and the Seekonk, by the MPN method. Since then, the quality has been improved, mainly by the addition of secondary treatment at the Blackstone Valley sewage plant on the Seekonk River. The main source of sewage pollution now is the Providence sewage treatment plant at Fields Point. Since the storm and sanitary sewers in the Providence, Pawtucket, and Central Falls area are combined, heavy rainfall causes the flow to exceed the plant's capacity. Untreated waste is then discharged directly into the

river. The official policy is to close nearly 10,000 additional acres south of the model area to shellfishing, for seven days after one-half inch of rainfall, and for ten days after an inch or more of rainfall (65). The Pawtuxet River also remains a large source of sewage pollution.

Figure 7.1 shows the field measurements of total coliform MPN made in 1966. Concentrations are plotted on a log scale, against the distance from the mouth of the Seekonk, along an approximately central axis of the model. Surface samples were taken at four different stages of the tide at each station: high tide on August 31, low tide plus three hours on September 8, high tide plus three hours on September 28, and low tide on November 21. All samples were taken in the mornings. The different dates make it difficult to distinguish seasonal from tidal variations. However, since the Most Probable Number is only a statistical estimate, and not a count of the coliform population, the uncertainty in the data itself may be greater than the seasonal variation.

The coliform levels for the four sources to be modeled (Seekonk River, Pawtuxet River, Providence sewage treatment plant, East Providence sewage treatment plant) are obtained from data kept by the Rhode Island Division of Water Supply and Pollution Control (64). Figure 7.1 shows four counts at the mouth of the Seekonk. (The other, higher counts shown at L =0 are in

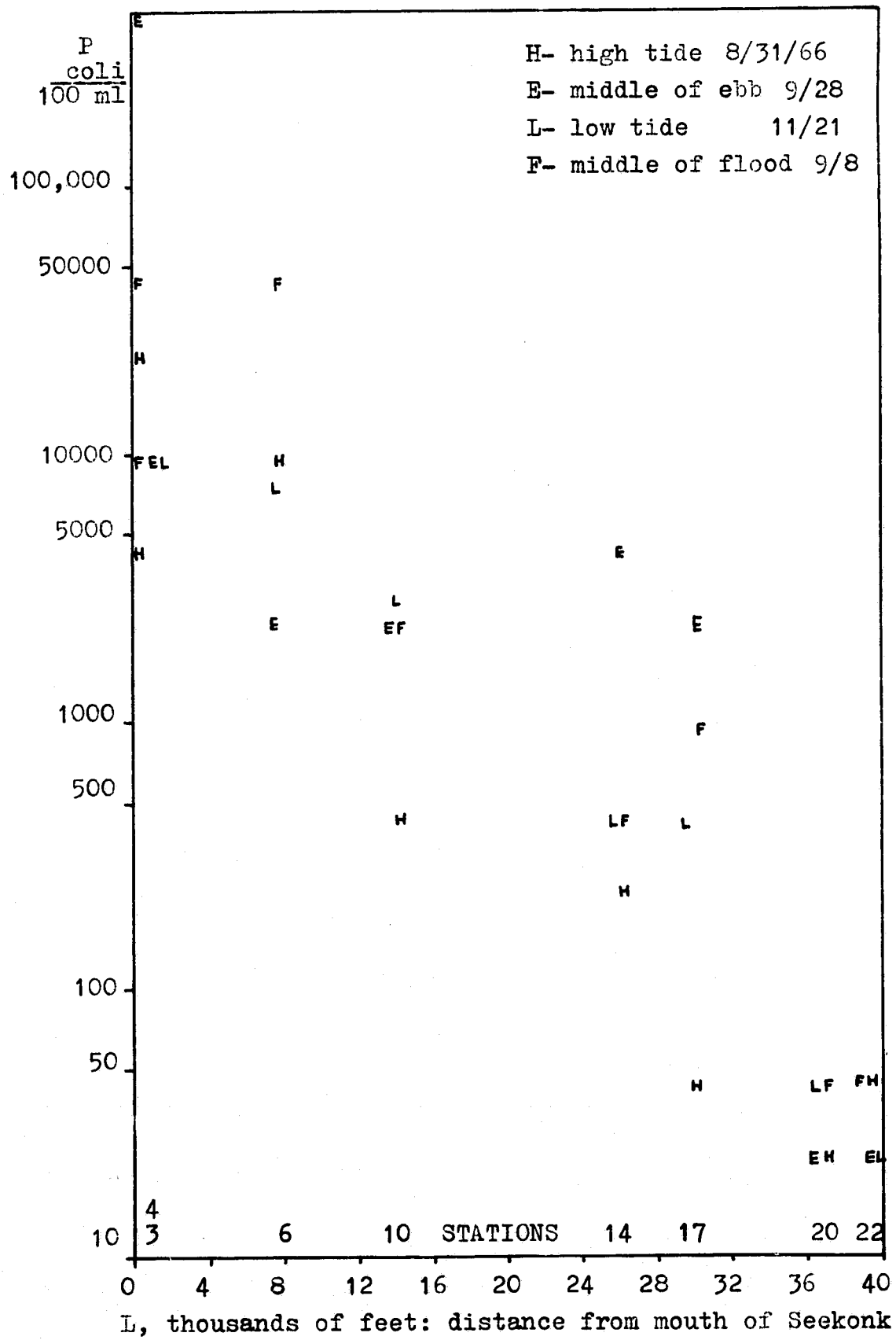

Figure 7.1. Field measurements of total coliform MPN

the mouth of the very small, non-tidal Providence River, whose coliform contribution is neglected.) At low tide, ebb, and flood, the value is 9300 coli /100 ml.; at high tide it is 4300. Extensive discussion of the modeling of this boundary follows. The Pawtuxet River, being non-tidal, will be modeled by a constant coliform level. From several measurements made at different times, the value 4300 /100 ml. is the most often repeated, and is selected as the most representative. Counts for the treated effluent of both sewage plants average 2300 /100 ml. Using these as source levels, verification of the model will be attempted for the conditions of 1966.

Modeling of a Conservative Constituent

The mass transport model is now used to model the distribution of a constituent equivalent in source levels to coliforms, but with no decay specified yet. The model grid and depth field are, of course, identical to those of the tidal model already developed, except for the additional area used by the tidal model for the Seekonk River. The horizontal dispersion coefficients are calculated from Equations 3.29 and 3.30. The value of D_w is taken as a turbulent diffusion coefficient, for a length scale equal to a typical width of the estuary. From Equation 3.13, a value of D_w=30 ft^2/sec. is obtained for l =3000 feet.

A salinity field is needed to calculate the

vertical diffusion coefficients. The Providence River has been found to be highly stratified. Rather than doubling the computational time by modeling salt dispersion, a constant salinity field is obtained by averaging field measurements (66) over a tidal cycle, and estimating a linear salinity increase from the inshore to the open end of the model. A different equation is used for each level. Thus the salinity varies from 14 ppt. at the north end to 22.5 at the south end in the top level, and from 27.0 to 32.9 ppt. in the bottom level.

The effect of the stratification is to suppress the effects of turbulence and small waves. A base value, similar in purpose to D_W, was set at 0.001 ft^2/sec. based on the order of magnitude of the smallest measured values of D_Z found in the literature (33). As calculated by Equation 3.19, D_Z exceeds this value only when waves such as would be generated by a sustained 20-knot wind are specified, and then only in surface waters. The stratification of the Providence River is thus seen to be a very important factor in suppressing vertical exchange.

It is desired to use a time step three times as long as that of the tidal model, or 300 seconds. Checking the velocity and dispersion criteria, the maximum velocity which occurs is 2.3 ft /sec, but velocities greater than 1.0 are rare. The largest dispersion coefficients obtained, prior to the use of

the subroutine for discontinuities, are about 80 ft^2 /sec. Thus,

$$\frac{u\,\Delta t(max)}{\Delta x} = \frac{2.3 \times 300}{750} = 0.92 \quad or \quad \frac{1.0 \times 300}{750} = 0.4$$

and $$\frac{D_x\,\Delta t(max)}{(\Delta x)^2} = \frac{80 \times 300}{(750)^2} = 0.043$$

A 300-second time step is acceptable, although it strains the limit at the Seekonk River boundary. It is not deemed profitable to double the computational time just to increase the accuracy at this location.

It is essential that the model conserve the mass of all constituents to within a few per cent, and that errors in mass conservation do not increase with time. The computer program checks for such errors at all times. Another method of checking the model for mass conservation and stability is to model a uniform field of an arbitrary conservative constituent, with constant and equal boundary concentrations. This also indicates how well the method used to link the tidal and mass

transport models, as described in Chapter V, conserves mass. This has been done for a field and boundaries of 5.0, simulating 24 hours with complete hydrodynamic input. Any deviation from the value 5.0 indicates computational error. The greatest deviation observed at any point was 0.073 (1.46 %), and the maximum total mass conservation error was less than one-tenth of one per cent. This test indicates very satisfactory performance by the model.

The point sources at the two sewage treatment plants are modeled by a source term existing in one grid or one column of the model. Due to the stratification present, and the fact that both outfalls are in shallow water (5 to 10 feet), it is expected that the effluent will rise to the surface. Therefore, the sources are placed in the surface level, N =2. The source levels are estimated by multiplying the coliform concentration by the discharge per second, and dividing by the volume of the grid. A flowrate of 53×10^6 gallons per day (Providence), with a coliform count of 2300 /100 ml., becomes a source of 0.1 ml. per second throughout the grid. For the East Providence plant, with a discharge of 4.99×10^6 and the same concentration, the source strength is 0.01 /100 ml.

Figure 7.2 shows contour maps of a simulation with the Providence plant as a point source. The constituent, with no decay specified for observation purposes, was injected into an empty initial field at

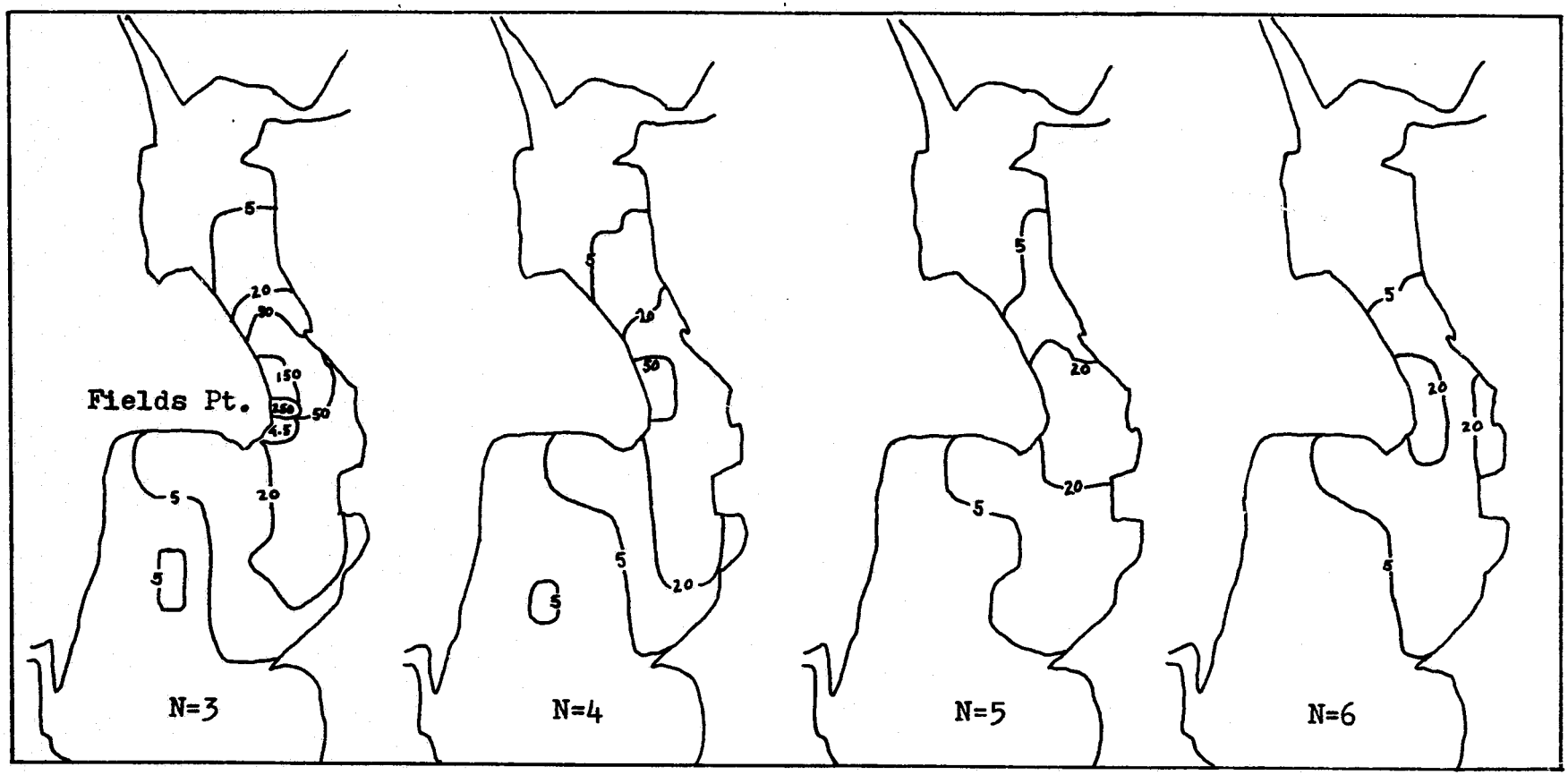

Figure 7.2. Simulation of Providence sewage plant as point source.
21 hours, no decay, source strength 0.1 coli/100 ml-sec.

the second level (N =3), starting at high tide. Figure 7.2 shows the distribution after 21 hours, which was the middle of the flood tide. The upstream discontinuity problem is evident in the pronounced dip just below (south of) the source grid. (The flood tide is flowing up the page.) The variation in the vertical direction indicates the magnitude of diffusion for D =0.001 ft^2 /sec.. The persistent 5-contour south of Fields Point, and the 20-contour opposite the source, are in shallow areas. This indicates that the coliforms become uniformly distributed in the column, by diffusion, when the depth is of the order of six feet or less. It can also be seen that the sewage treatment plant is a small source of fecal contamination under normal operation. It appears that its contribution will be negligible compared to the river sources.

Under the assumption that the sewage-contaminated fresh-water inflows will be buoyant, the source levels at the river boundaries are taken as maximum at the top level, decreasing linearly to one-third maximum at the bottom. Whether this distribution persists downstream will be an interesting facet of the three-dimensional model. Adding the river sources reveals several difficulties, due to the fact that the flow reverses at the mouth of the tidal Seekonk. First, specifying a constant boundary concentration of 9300 results in the upstream discontinuity problem again during flood tide. The concentration just inside the boundary takes a dip,

with the result that a large mass conservation error, up to 35 per cent, is produced. This is because the transport out of the model is calculated with the concentration just inside the boundary, which is too low. It is therefore necessary to extrapolate the boundary concentration. The first-order extrapolation is given by

$$P_K^{l+1} = P_K^l - \frac{V_{K-1}(P_K - P_{K-1})\Delta t}{\Delta y} - \frac{D_y (P_{K-1} - P_K)\Delta t}{(\Delta y)^2} \qquad (7.1)$$

This is used to calculate the boundary concentration during flood tide (whenever V at the boundary is positive). When the tide reverses, the concentration reverts to the constant 9300 level.

This still leaves a mass error of as much as nine per cent, due to the abrupt change in concentration upon returning to ebb. This is unrealistic, because the Blackstone Valley sewage plant is about three miles up the Seekonk. The flood tide would push the polluted waters back from the mouth, and the coliform level would

gradually return to maximum as the ebb progressed. It is necessary to use a ramp function to bring the boundary concentration back up. Since no field information is available to indicate how long this should take, the length of the ramp is taken to be 30 time steps, i.e., the first 2.5 hours of the ebb tide.

When all this refinement is made, there remains a mass conservation error between +3.5 and -1.5 %. (A positive error is an excess of the mass in the field over the sum of the initial field plus the net influx; a negative error is the opposite.) The error is found to follow the boundary velocity in phase, as shown in Figure 7.3. This indicates that the error is due to the degree of approximation in the extrapolation. Using more than one inside grid to extrapolate might reduce the error, but was not attempted. Since the error is roughly proportional to the velocity, the error might also be due in part to the aforementioned stability limit. Again, the error is not severe enough to demand a shorter time step. The fact that the negative error, on the ebb tide, is only half as large as the error on the flood, indicates that both factors induce error--the extrapolation error being added to the high-velocity error on the flood, and having no effect on the ebb.

Figure 7.3 also shows the boundary concentration as a function of time and velocity. The concentrations marked by the letters E, L, F, and H are the field measurements (22) at ebb, low, flood, and high tides

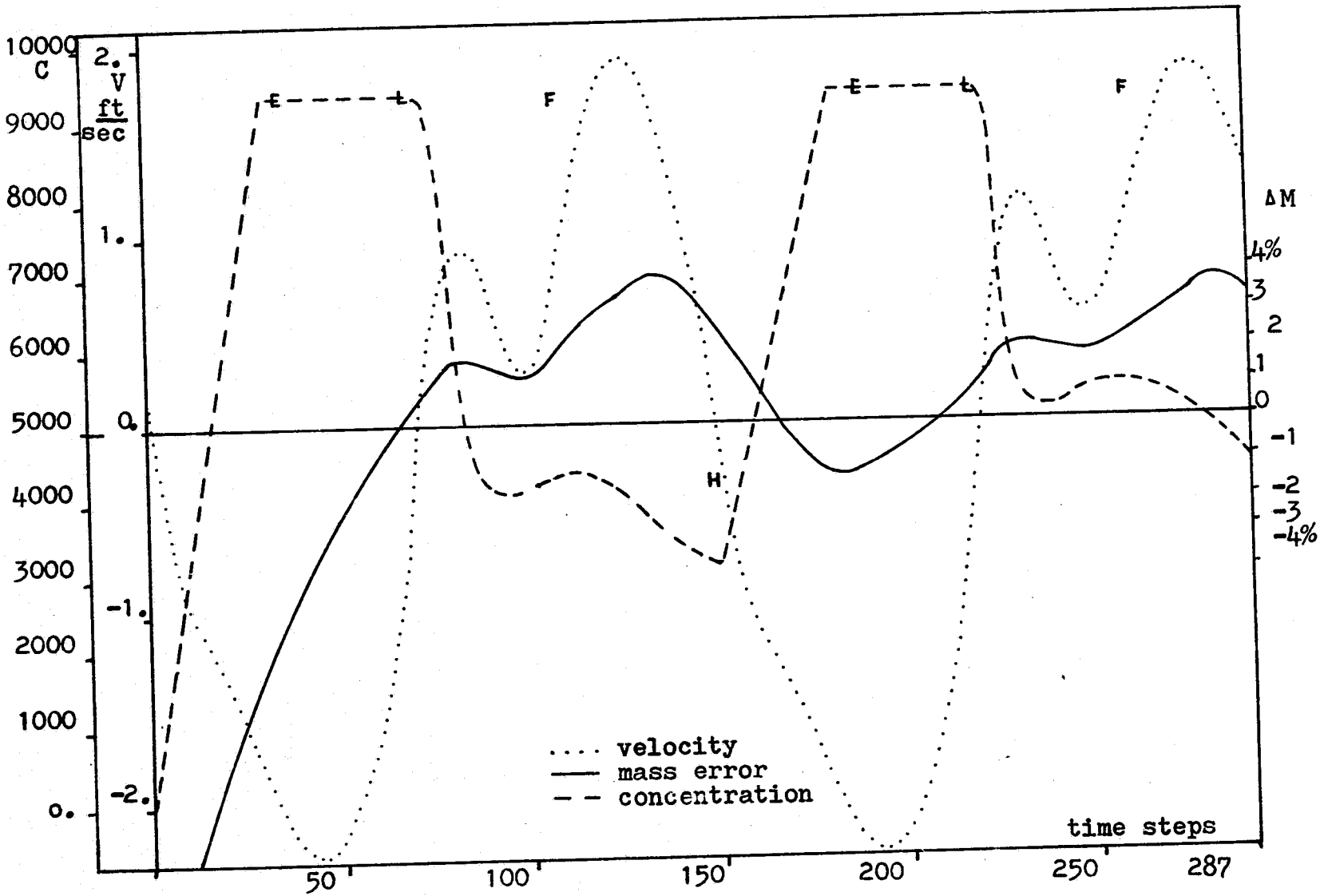

Figure 7.3. Boundary conditions at Seekonk R. V, C, and ΔM vs. time

respectively. The large mass conservation error at the start is the result of the empty initial field.

Extended runs of the model, to bring the model up to steady-state concentrations, revealed a peculiar and damaging effect of the method of adjusting dispersion coefficients at discontinuities. Occasionally, large errors would appear in the concentration field, at apparently random locations and times. Usually these errors were damped out, but in several cases the error continued to grow, with both positive and negative concentrations five or six orders of magnitude too large.

Upon closer inspection, it was found that this error began at a point where the dispersion coefficients were being adjusted by the subroutine, at a minor discontinuity. The method appears to destroy the stability of the overall solution technique. Although the mass transport computation tends to damp out the error, the subroutine overcompensates by continuing to increase the dispersion coefficients as the error increases, causing the error to spread.

The empirical coefficients, described in Chapter IV and Figure 4.7, were set at the rather high value of 0.5 at this time. Although reducing this value might have solved the problem, it was decided to bypass the subroutine, to remove all possibility of another such error. The capacity to reduce generation of negative concentrations was lost, but since the discontinuities

in the field were not important at this point in the computation, the adjustment was not greatly needed. It is recommended that the subroutine be used whenever discontinuities are expected to occur, preferably with a smaller value of the coefficients, such as 0.2. If the concentration field reveals an error at any time, the subroutine can then be bypassed, or suitably modified to account for the peculiarities of the flow system.

Continuing with the simulation of the conservative constituent, some concentration contour maps are shown to illustrate the pattern of river influx. Figures 7.4 through 7.6 show the coliform distribution (conservative) 18 hours from initial conditions, at low tide. The surface, middle, and bottom levels are shown in separate plots. Logarithmic contour intervals are used for clarity and to show the far field better. The most striking fact revealed here is that the vertical variation at the shallow mouth of the Pawtuxet River, from 4300 /100 ml. at the surface to 1430 at the bottom, is quickly eliminated by diffusion. Vertical variations at the deeper and more rapid Seekonk persist far downfield.

Figures 7.7 through 7.9 show the distribution at 23.92 hours, approaching high tide. The pollutant has been driven back up the estuary by the flood tide. The uniformity at the Pawtuxet has disappeared, indicating that for a diffusion coefficient of 0.001 ft /sec., complete vertical mixing takes place over a column 4

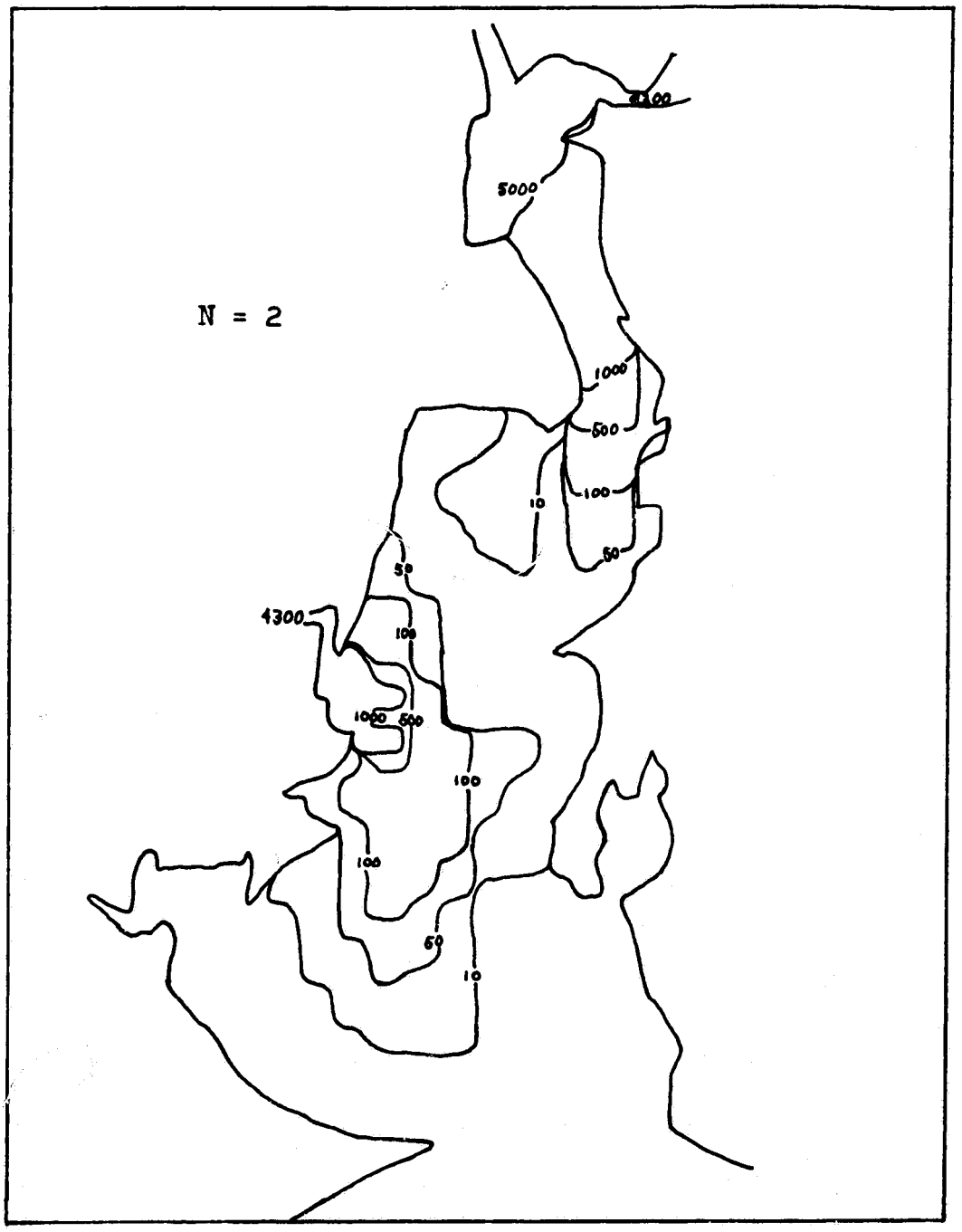

Figure 7.4. River influx, low tide.
Surface level, 18 simulated hours

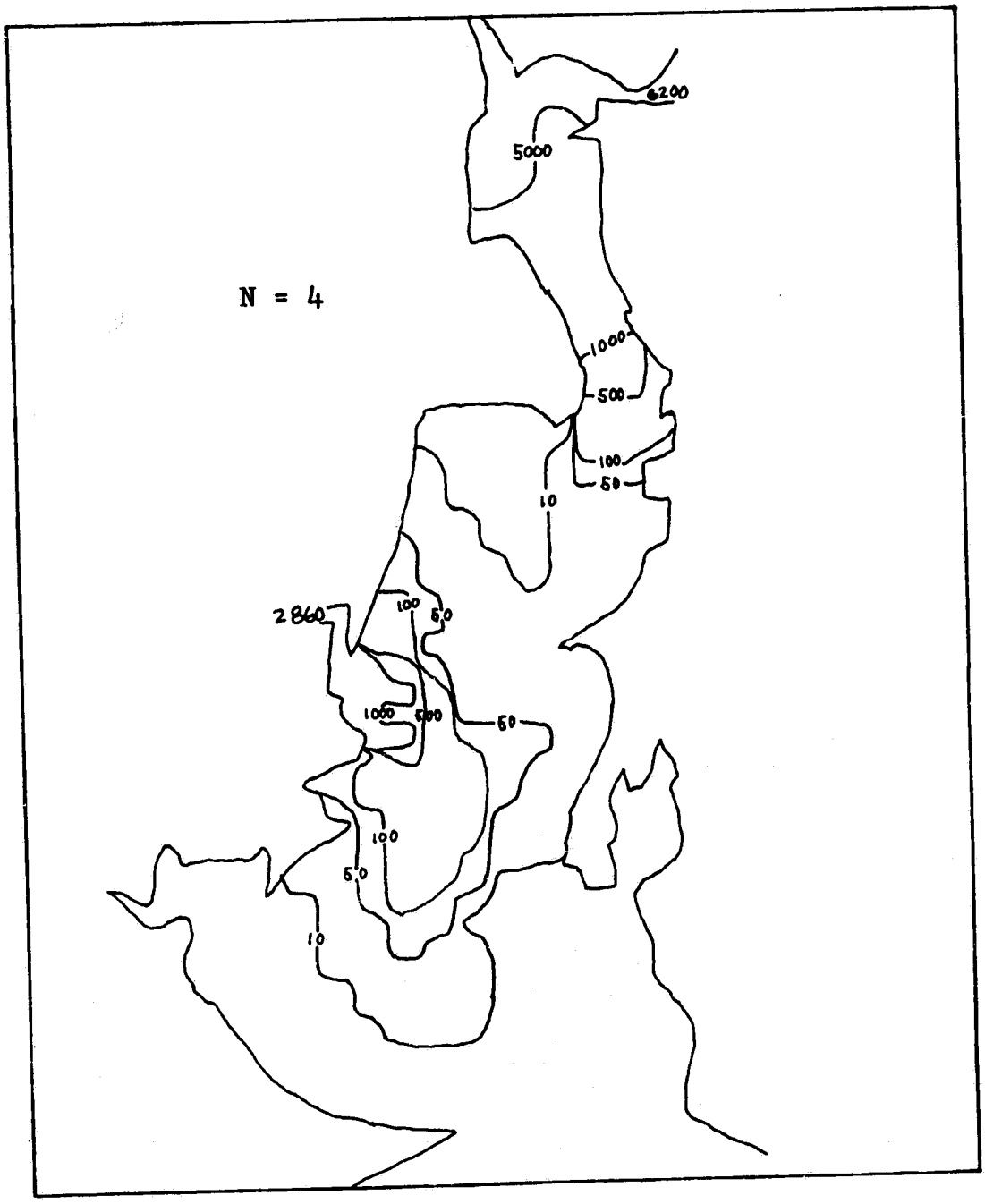

Figure 7.5. River influx, low tide.
Middle level, 18 simulated hours

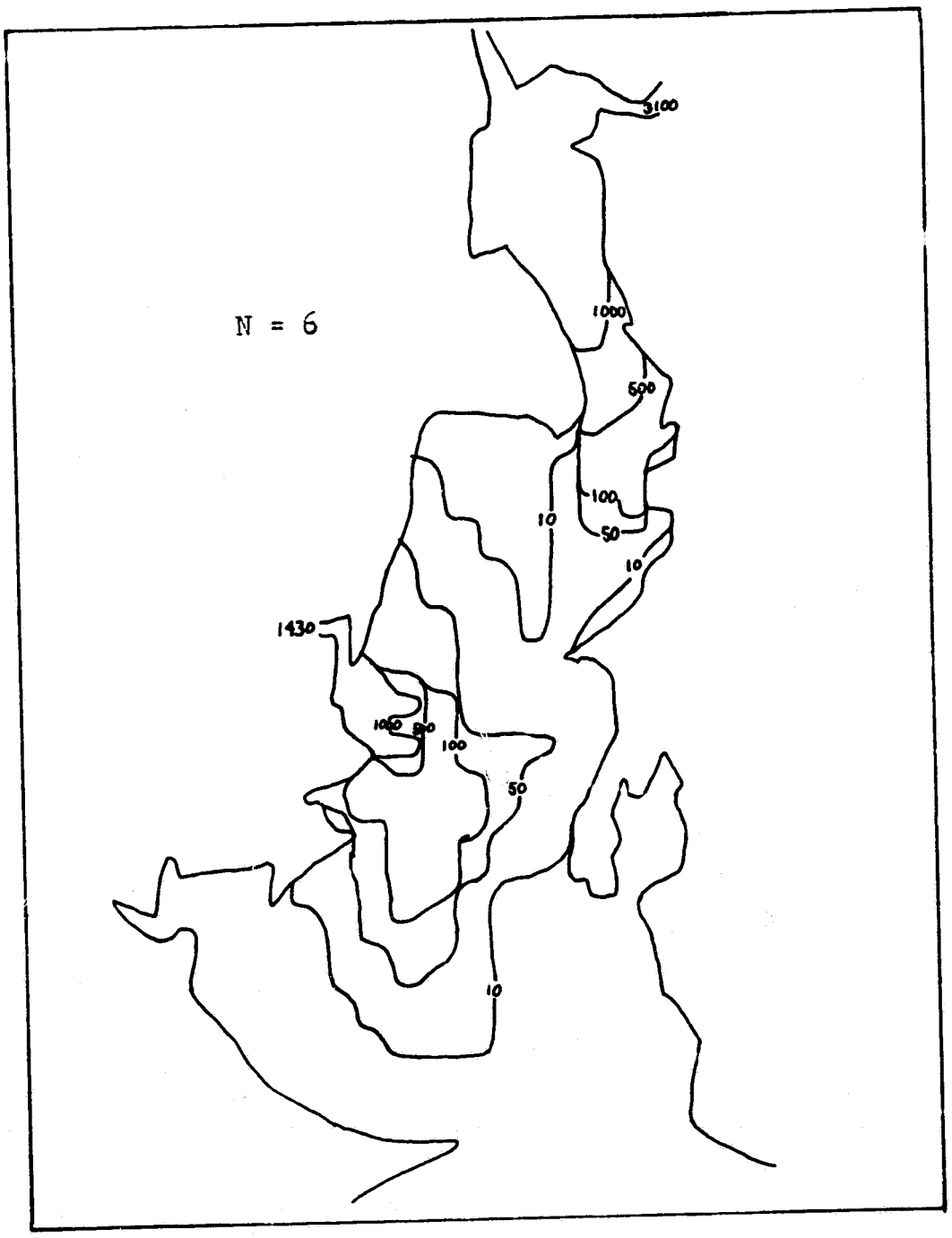

Figure 7.6. River influx, low tide.
Bottom level, 18 simulated hours

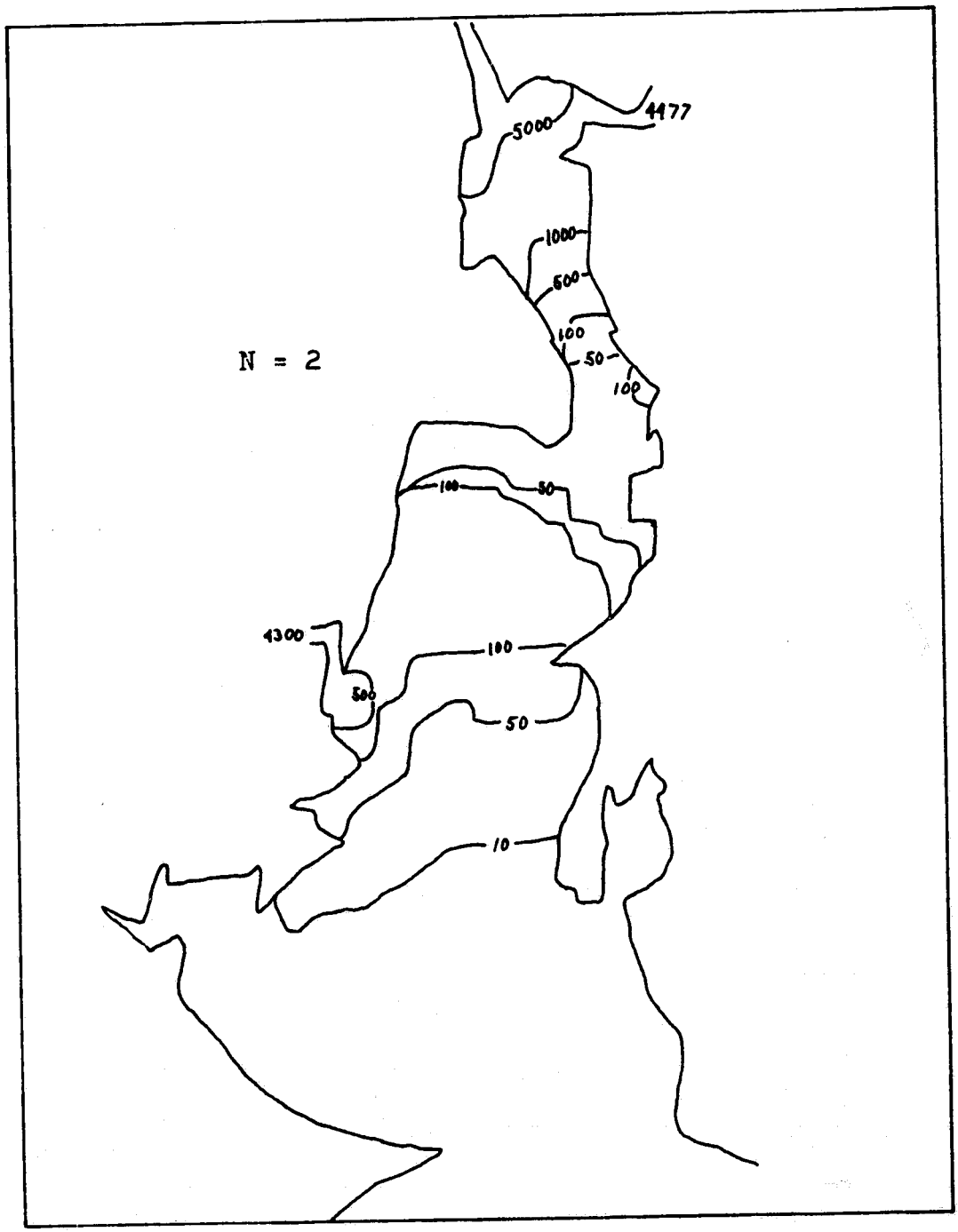

Figure 7.7. River influx, high tide.
Surface level, 23.9 simulated hours

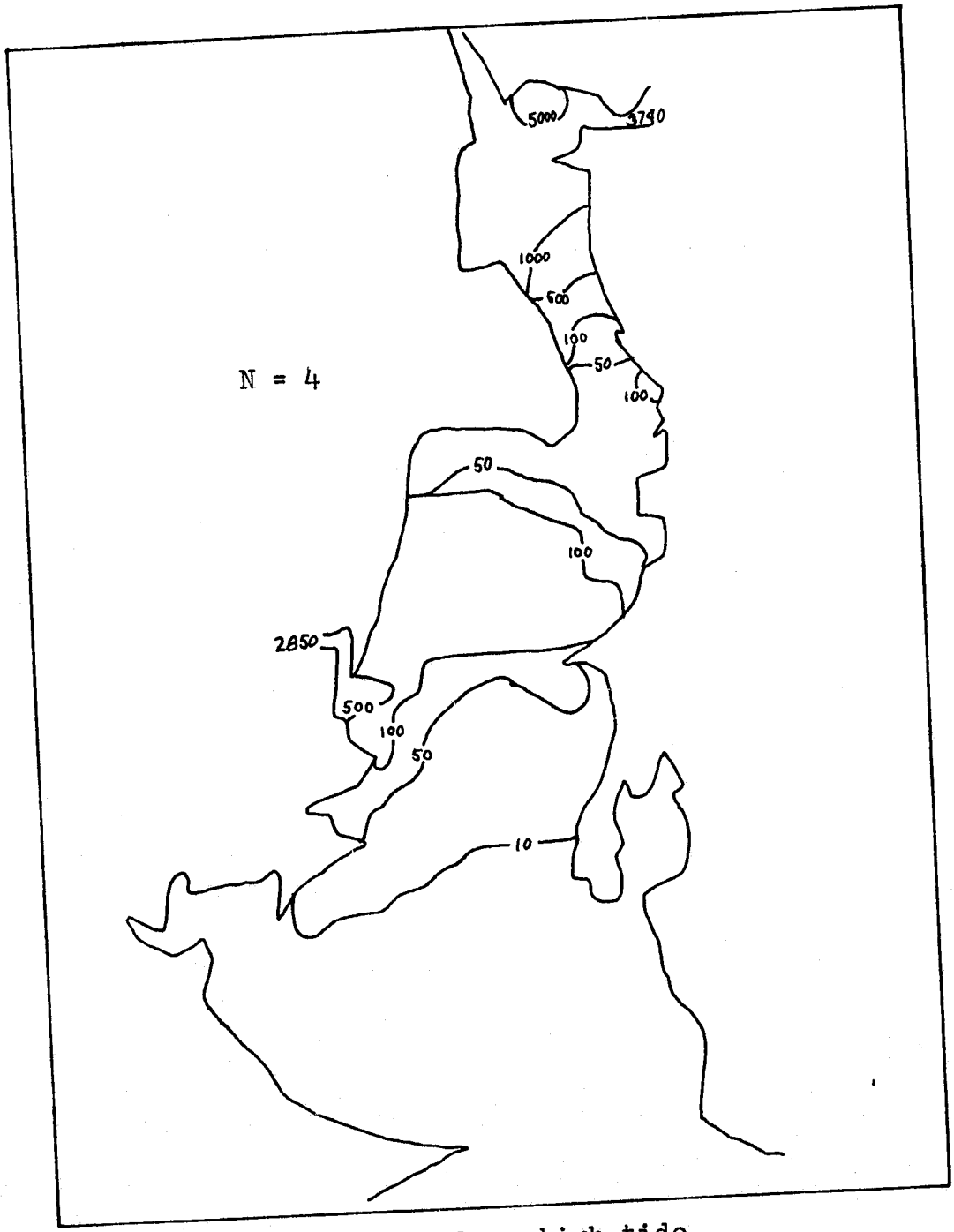

Figure 7.8. River influx, high tide
Middle level, 23,9 simulated hours

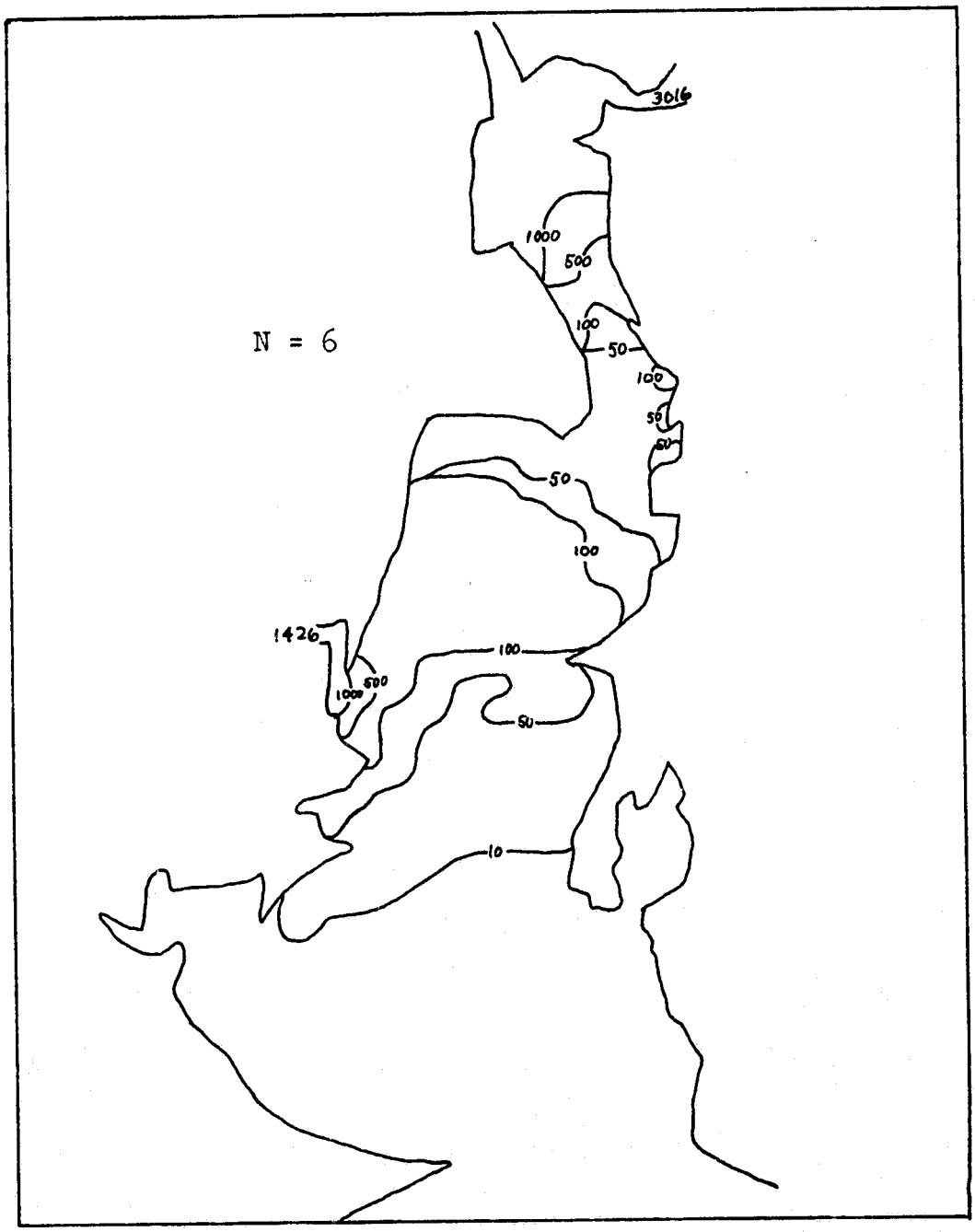

Figure 7.9. River influx, high tide
Bottom level, 23.9 simulated hours

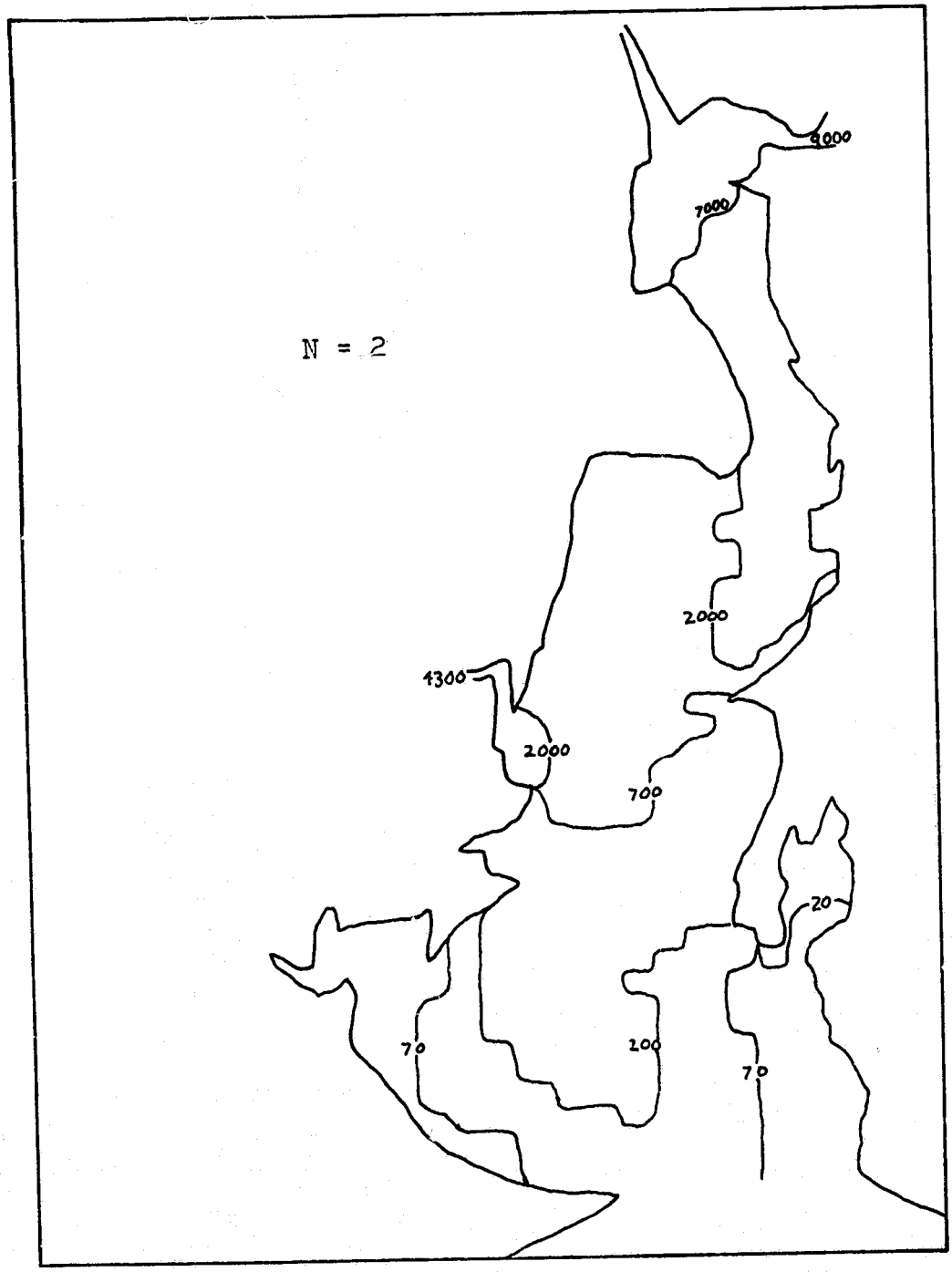

Figure 7.10. Steady state conservative distribution, low tide. Surface level, 92.25 hours

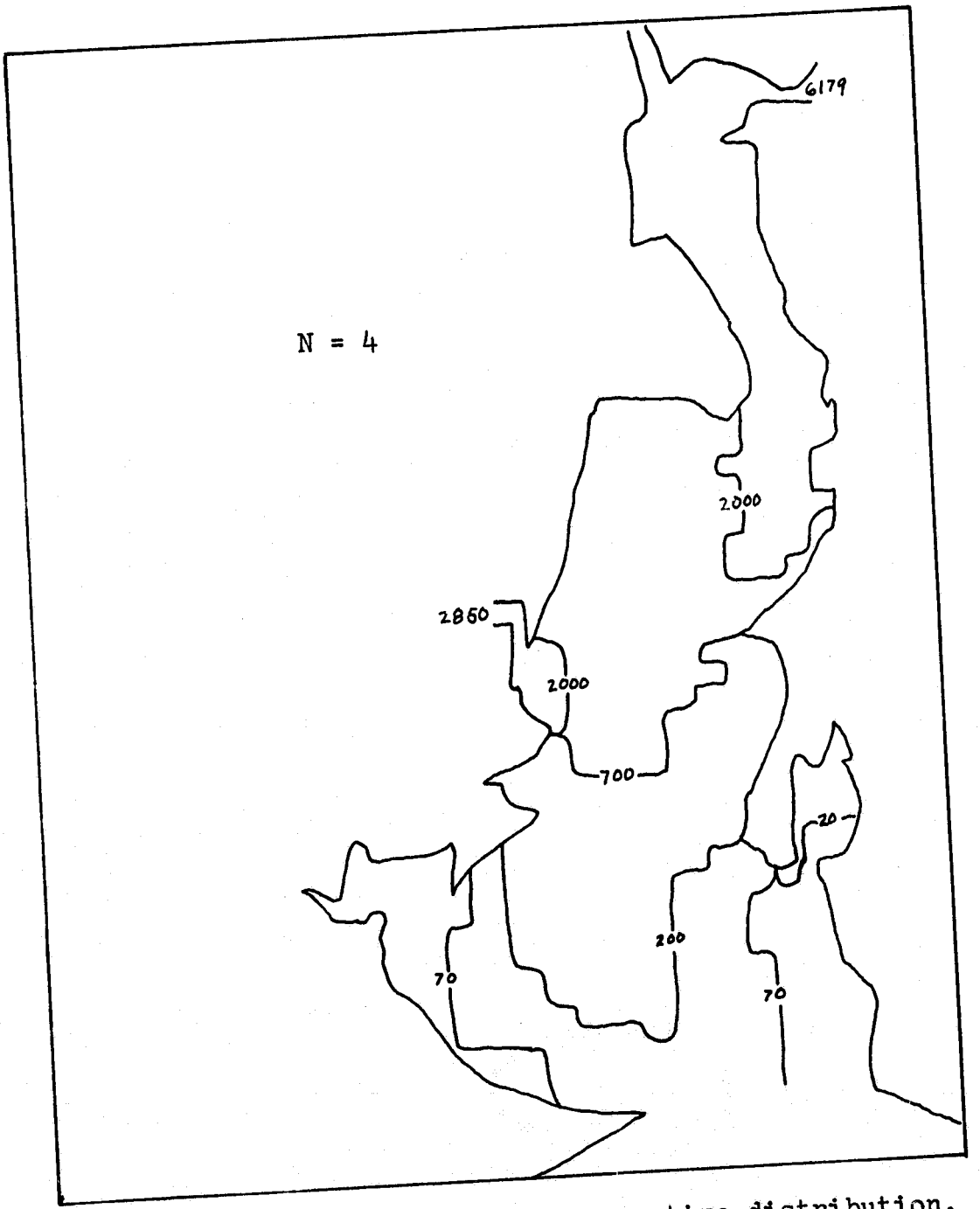

Figure 7.11. Steady state conservative distribution, low tide. Middle level, 92.25 hours, $D_z = 0.001 \frac{ft^2}{sec}$.

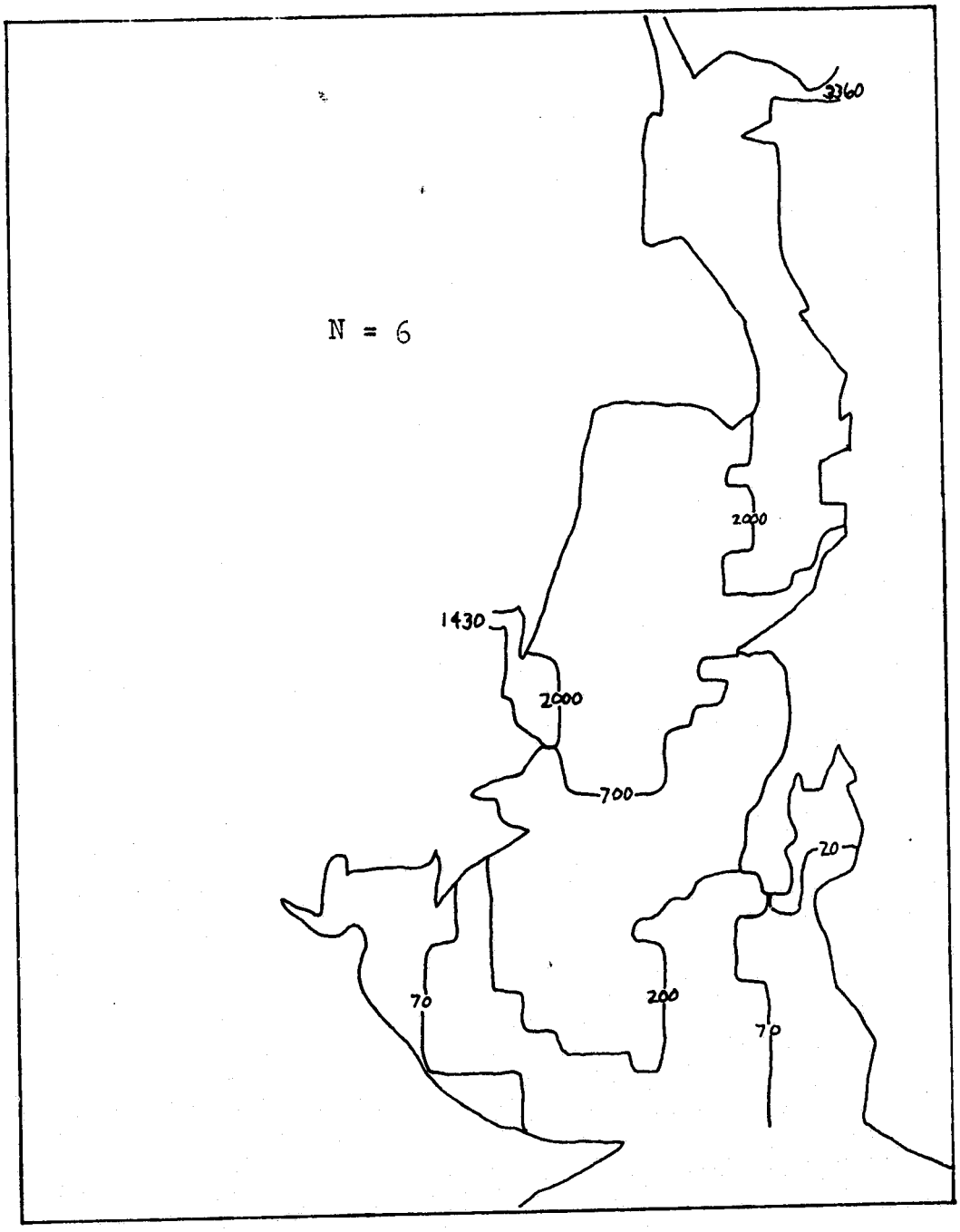

Figure 7.12. Steady state conservative distribution, low tide. Bottom level, 92.25 hours

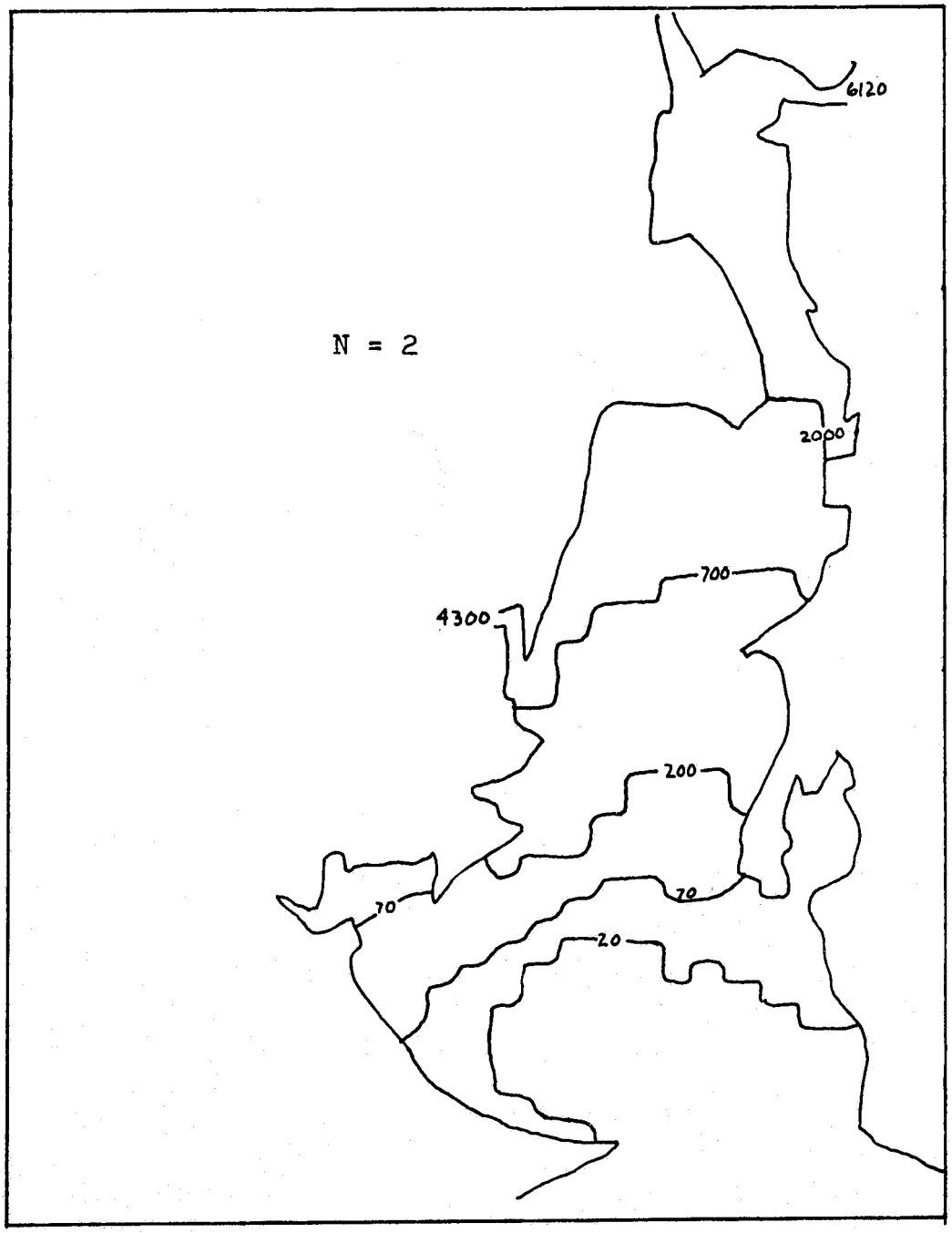

Figure 7.13. Steady state conservative distribution, high tide. Surface level, 98.17 hours

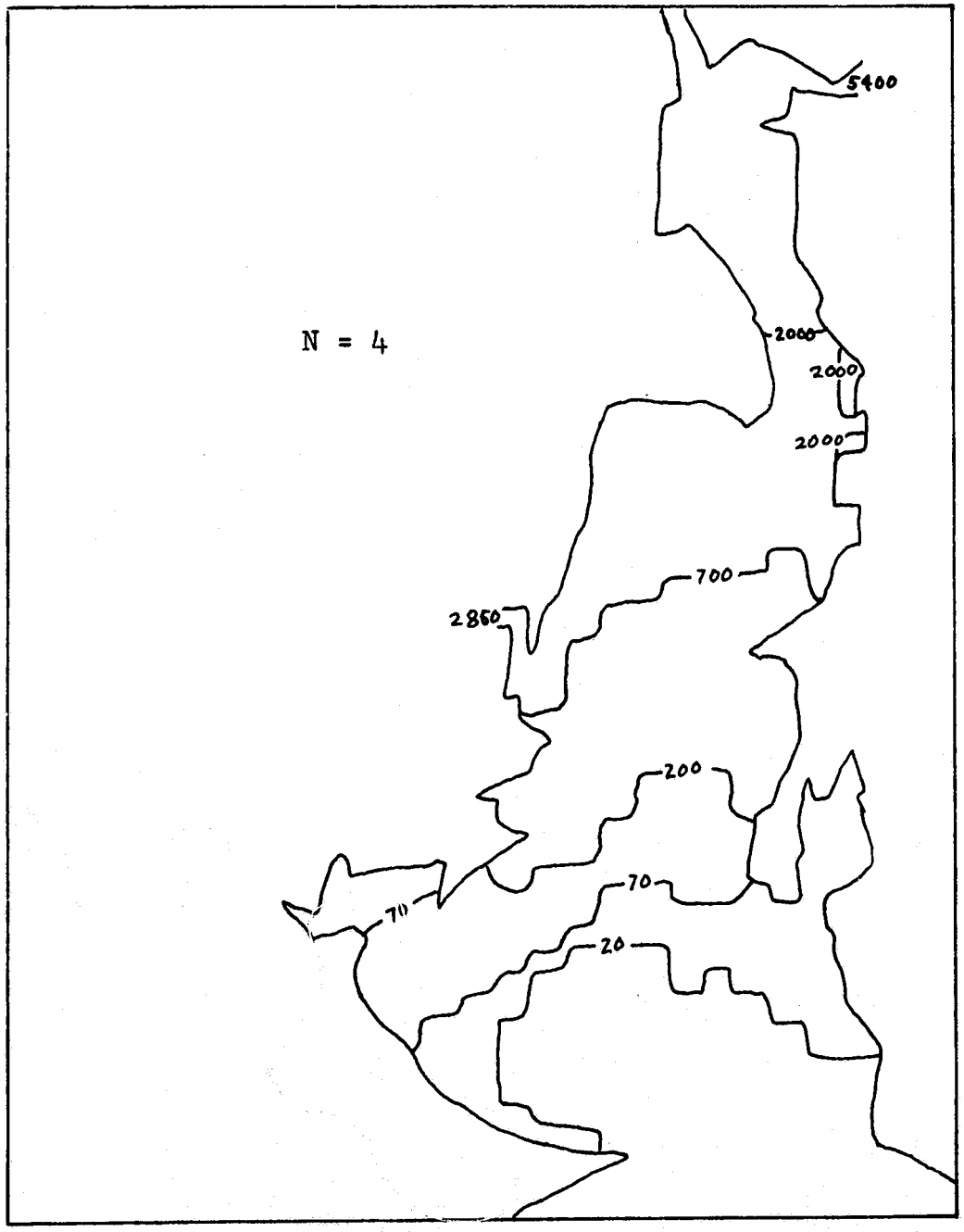

Figure 7.14. Steady state conservative distribution, high tide. Middle level, 98.17 hours, $D_z = 0.001 \frac{ft^2}{sec.}$

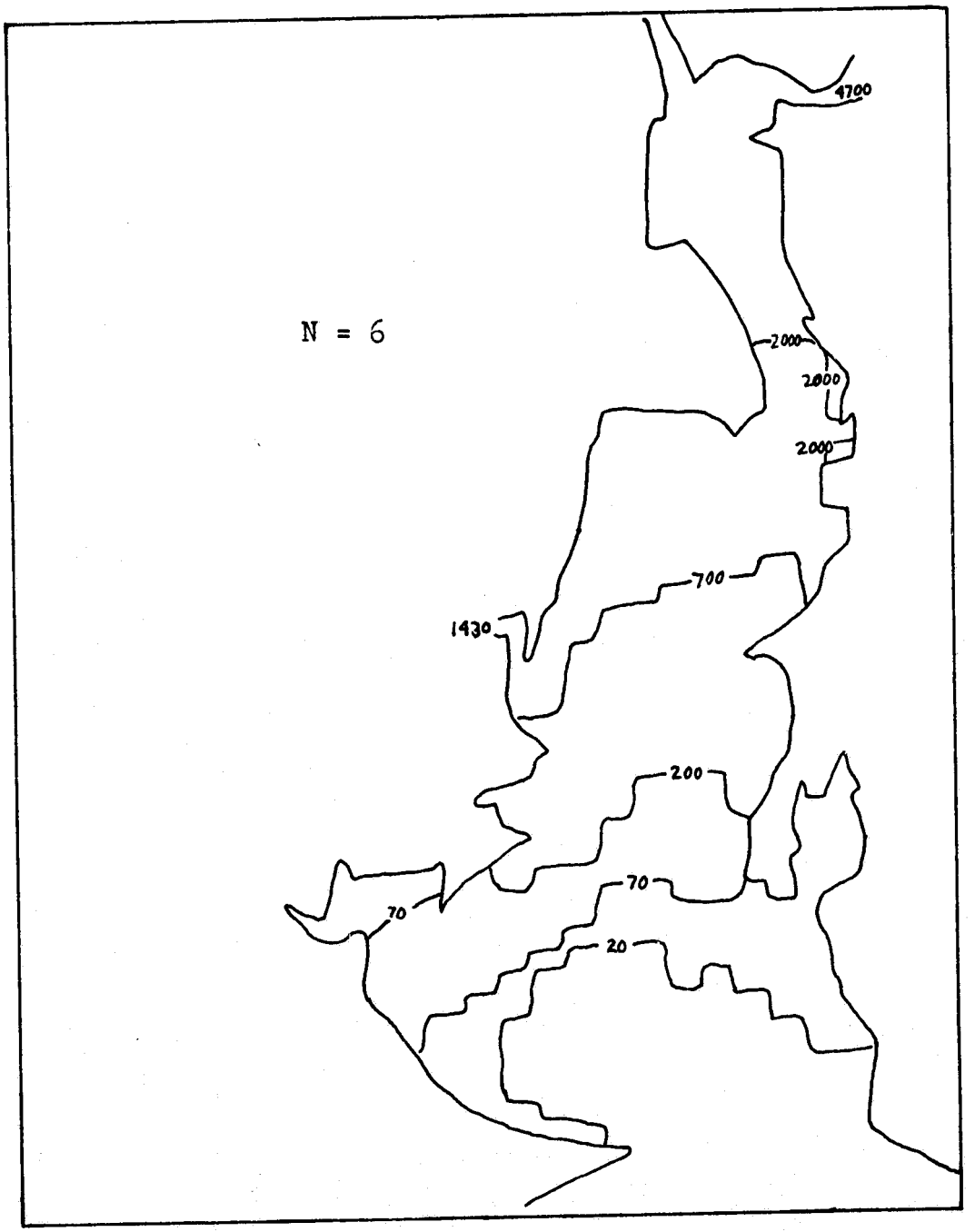

Figure 7.15. Steady state conservative distribution, high tide. Bottom level, 98.17 hours

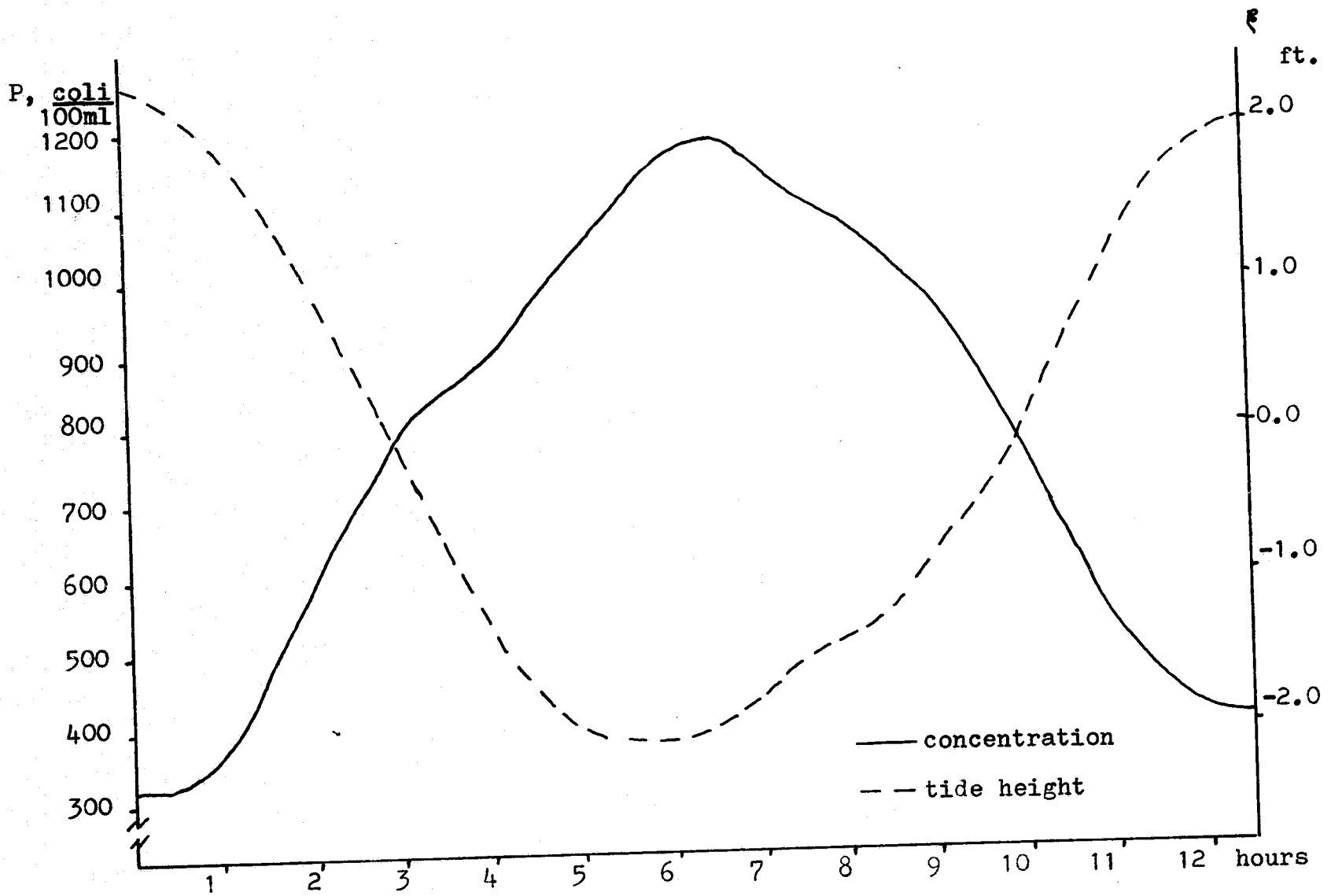

Figure 7.16. Typical plot of concentration vs. tide height. Grid 30,10,2; from 49th hr.

feet deep, but not over the high-tide depth of 8 feet. Curiously, the concentrations closest to the river increase slightly with depth. Some pockets of higher concentration, in shallows and in coves, are left behind by the reversing tide, as are particularly notable in the lower level.

Simulation continues, now adding the two sewage plant sources, which are quickly swallowed up by the much greater Seekonk influx. After 98 hours, nearly 8 tidal cycles, material is distributed throughout the model area, which appears to be approaching steady state. Figures 7.10 through 7.12 show the low tide conditions at 92.25 hours, and Figures 7.13 through 7.15 show the late flood tide at 98.17 hours. It is evident that the vertical variations are much reduced, and are scarcely revealed at all by the chosen contour intervals. Figure 7.16 shows a plot of concentration and tide height versus time, and their clearly inverse relationship. As the tide ebbs, the more polluted waters upstream are swept past the point, increasing the coliform concentration. As the tide reverses and cleaner water is swept back upstream, the concentration drops. Bullock Cove, a very shallow, narrow-necked inlet on the lower right, has finally filled with material, particularly after the flood tide.

The vertical variation that remains is greatest close to the river boundaries. To show this more clearly, Figures 7.18 and 7.19 show concentration-depth

profiles on lines extending away from the two river mouths, as shown by Figure 7.17. The rapid mixing at the Pawtuxet is obvious, particularly in the low tide case (Figure 7.18). Much of the vertical variation at the Seekonk is eliminated by passage through the very deep channel, which spreads the material vertically. The presence of the Providence sewage source, which is located in the last grid plotted for the Seekonk influx, is just visible as a slight increase in concentration at the surface.

Since the base value of D_z = 0.001 ft /sec. may be unrealistically high, the conservative constituent run was repeated for a base value of D_z = 0.00001 ft /sec. The profiles are shown again in Figures 7.20 and 7.21, revealing that the vertical structure persists much longer. Knowing which value is more nearly correct would require field information on the vertical variation of coliform densities.

Modeling of Coliform Decay

In order to observe the capabilities of the reaction matrix method, a uniform field of 50 coli /100 ml. throughout the Providence River was simulated with all velocities set to zero. The computation of depth- and time-varying decay coefficients, depending on the intensity of solar radiation, was programmed. The decay of the uniform field was allowed to proceed, with no

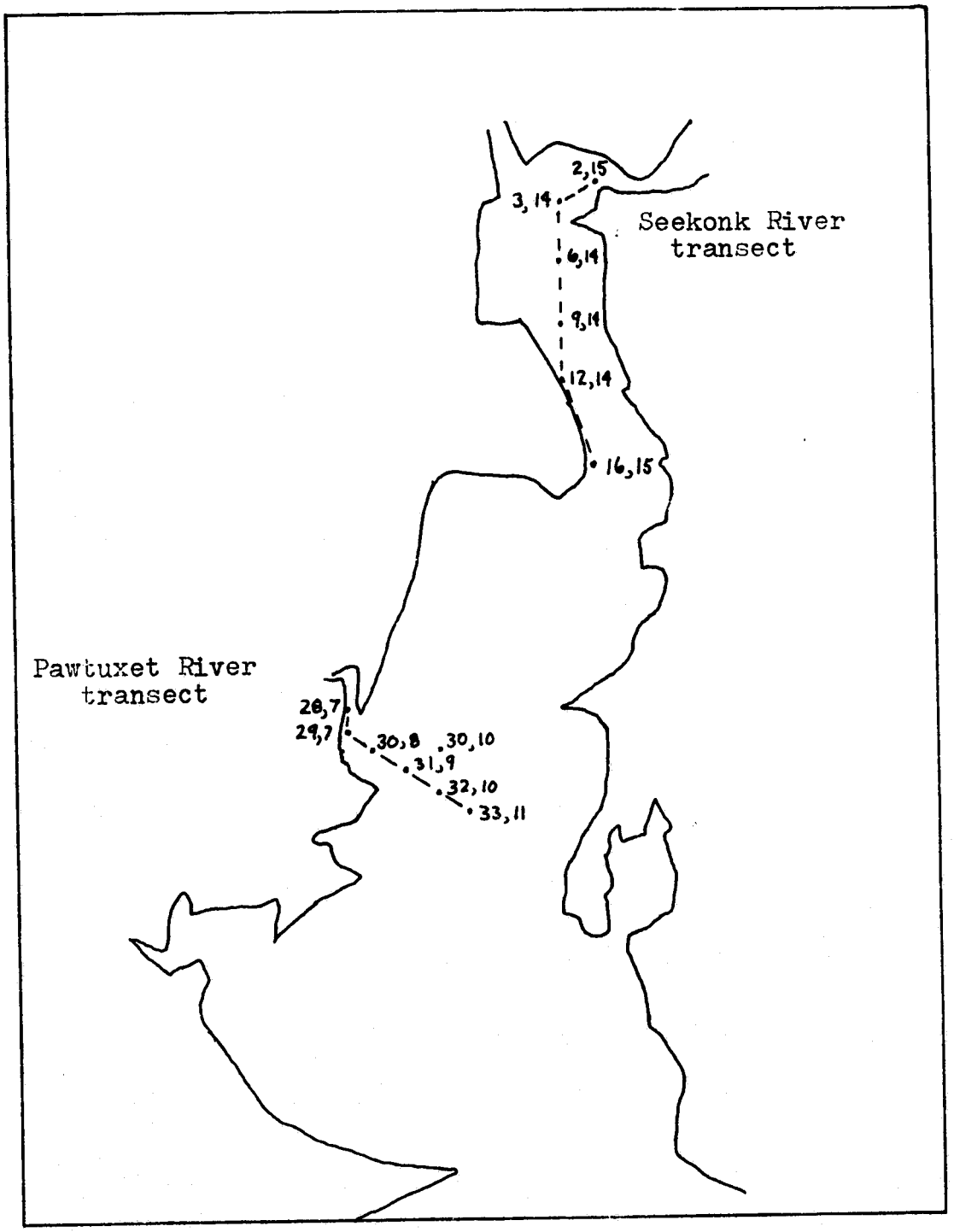

Figure 7.17. Locations of finite-difference grids having profile plots

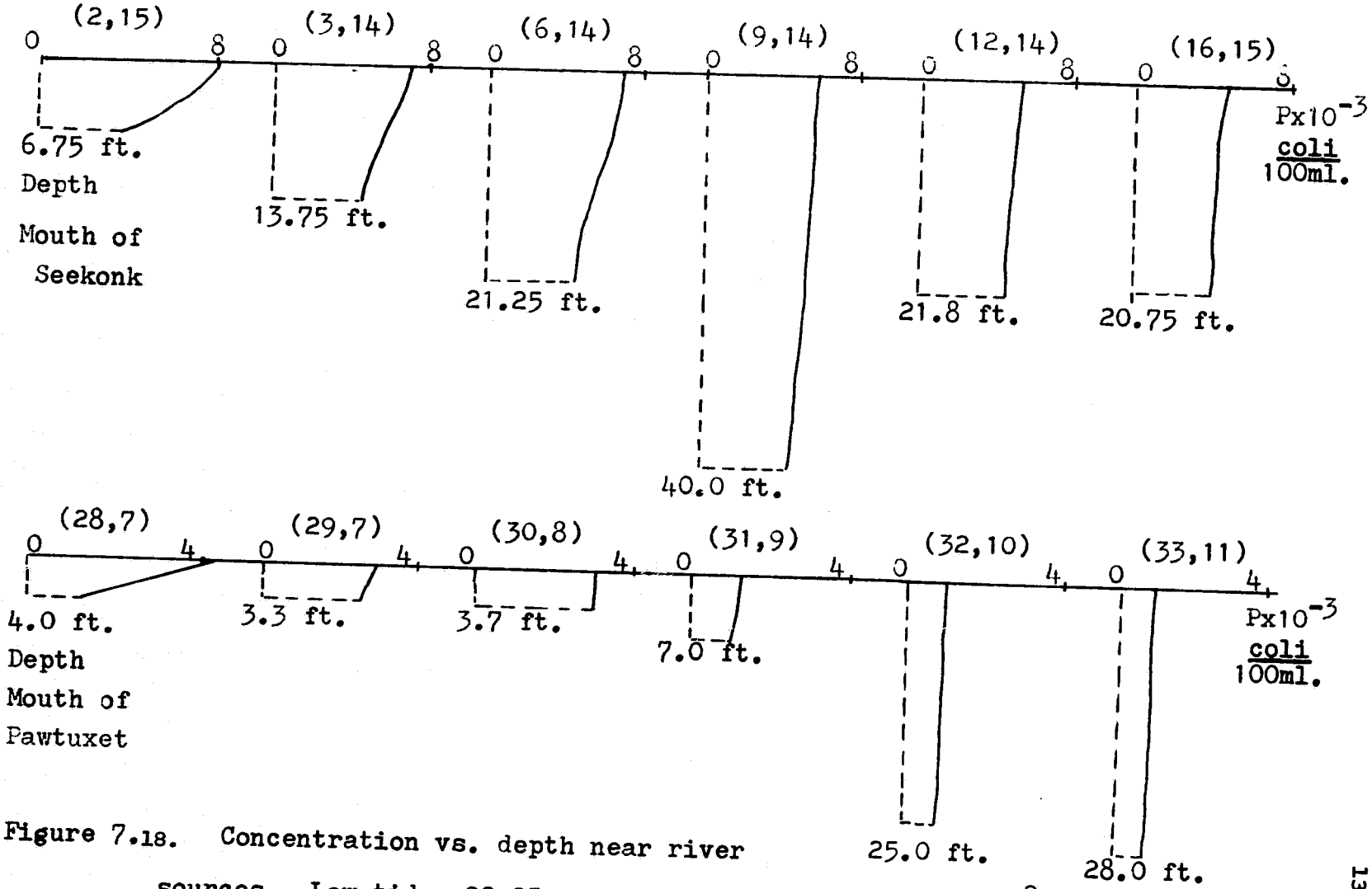

Figure 7.18. Concentration vs. depth near river sources. Low tide, 92.25 simulated hours. D_z= 0.001 ft^2/sec.

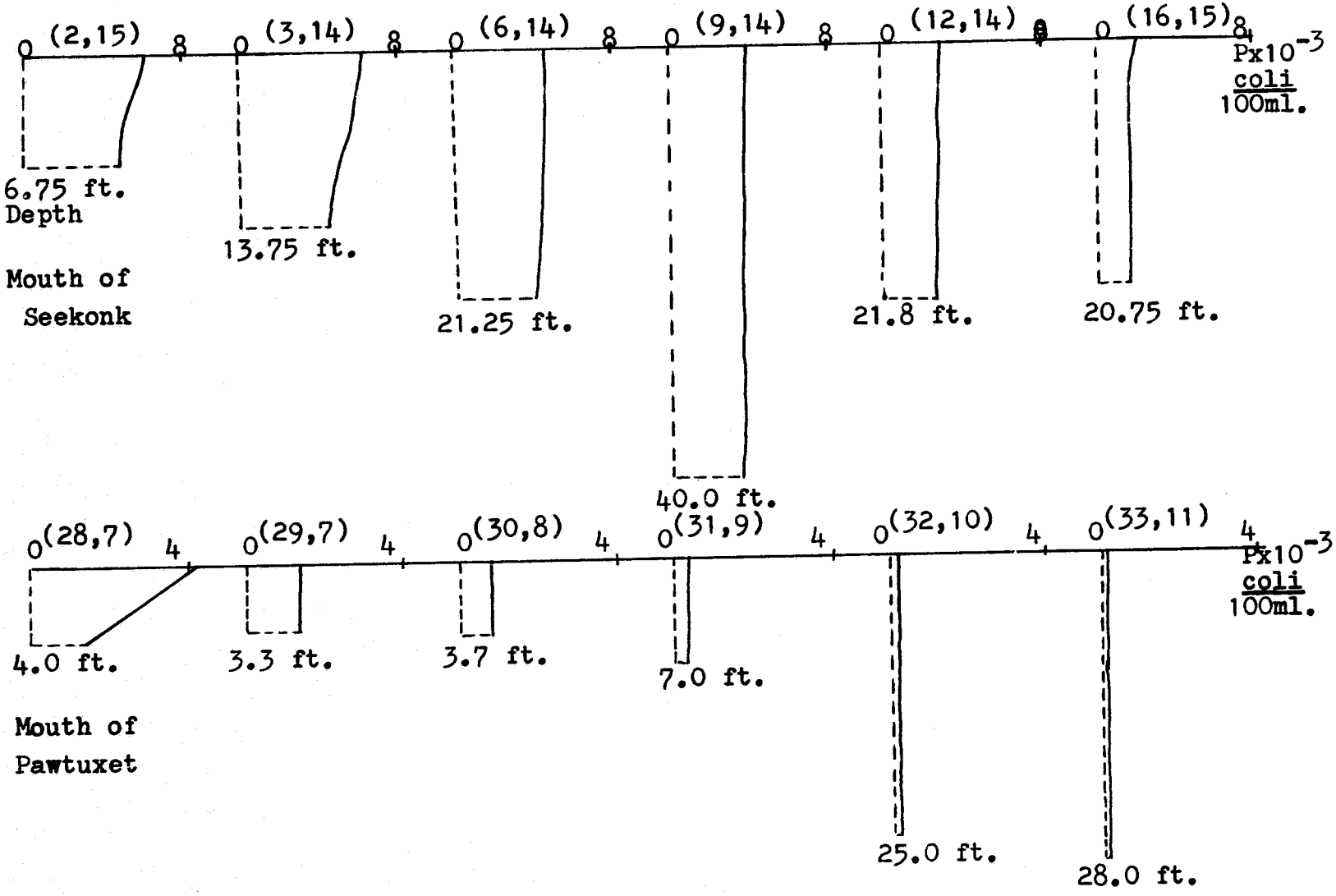

Figure 7.19. Concentration vs. depth near river sources.

High tide, 98.17 simulated hours. D_z= 0.001 ft^2/sec.

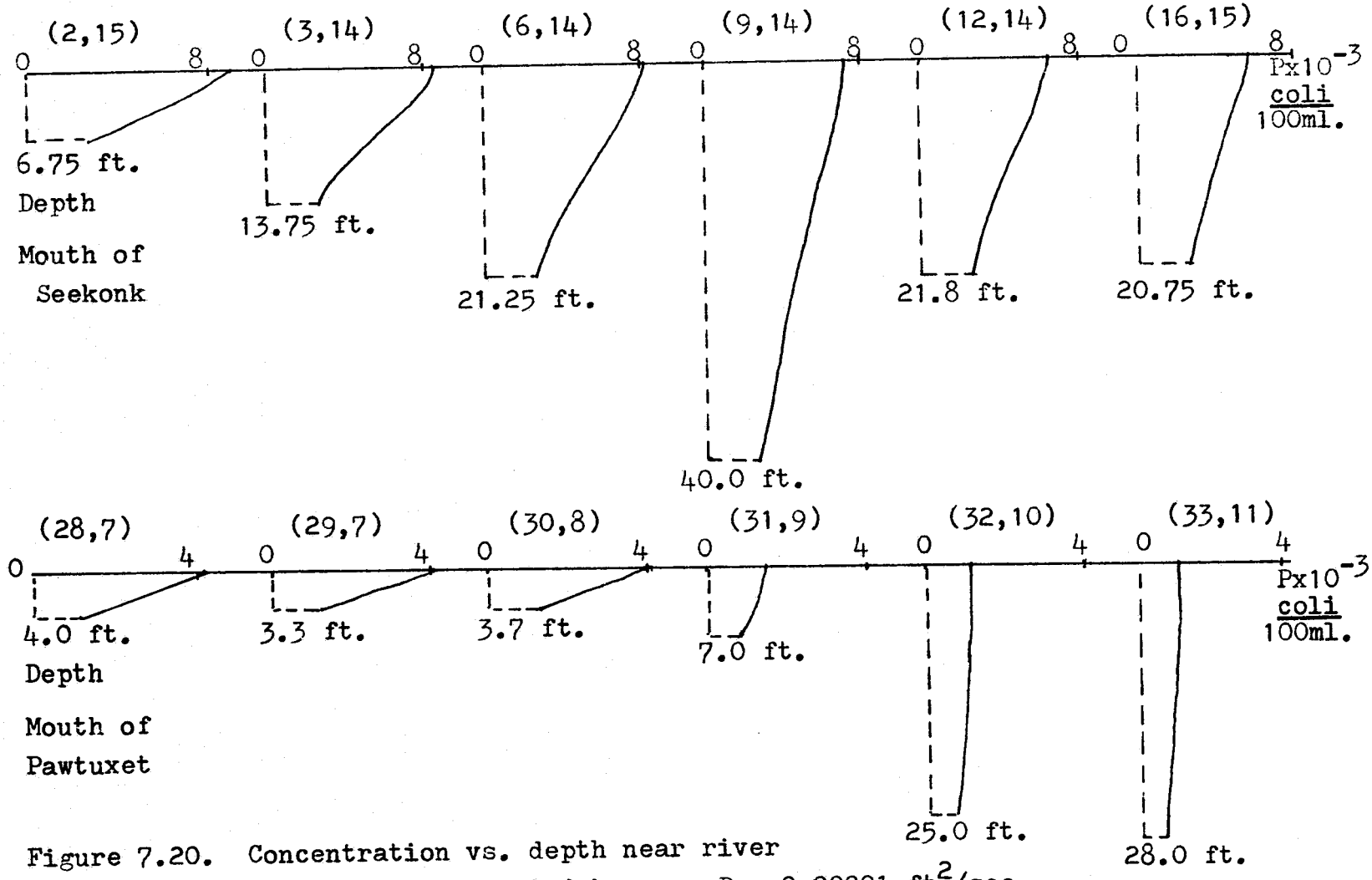

Figure 7.20. Concentration vs. depth near river sources. Low tide, 92.25 simulated hours. D_z= 0.00001 ft^2/sec.

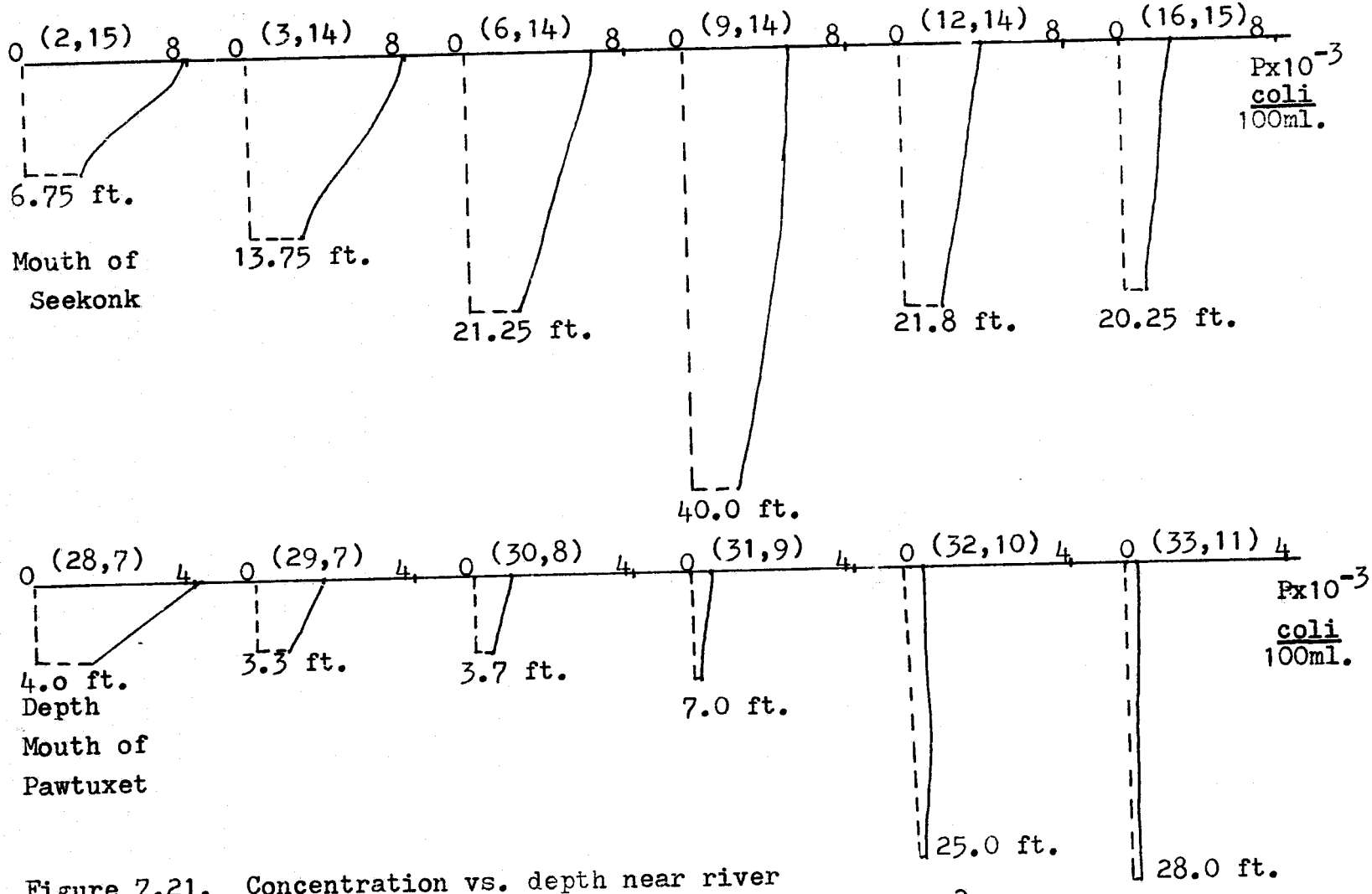

Figure 7.21. Concentration vs. depth near river sources. High tide, 98.17 simulated hours. D_z= 0.00001 ft^2/sec.

addition of material, beginning at 6:00 A.M. on the longest day of the year.

Figure 7.22 shows the concentrations at the surface and bottom, after 12 hours of decay, with the depth field presented for comparison. The decay is seen to be rapid in the shallow water, and apparently no more rapid than decay in the dark in the deepest water. It is evident that this rate of decay will quickly eliminate the coliform population in shallow water, on the order of 90 % in a day, although they may persist in deep water.

The same approach was used to determine what sort of a reaction matrix would effectively simulate a lag or growth phase, taking a nutrient of undetermined nature as a second constituent. Figure 7.23 shows the type of behavior produced, and the reaction matrices used. The values have the following meaning:

K_{11} - natural decay of coliforms in the dark

K_{12} - growth of coliforms due to the presence of a nutrient

K_{21} - disappearence of the nutrient due to use by the coliforms

K_{22} -natural decay of the nutrients, taken as zero because it is unknown.

The first simulation shows a slight lag phase and a rapid decay of the nutrients; the second reaction matrix, with a larger K_{12} and a smaller K_{21}, shows a growth phase. It can be seen that as the population of

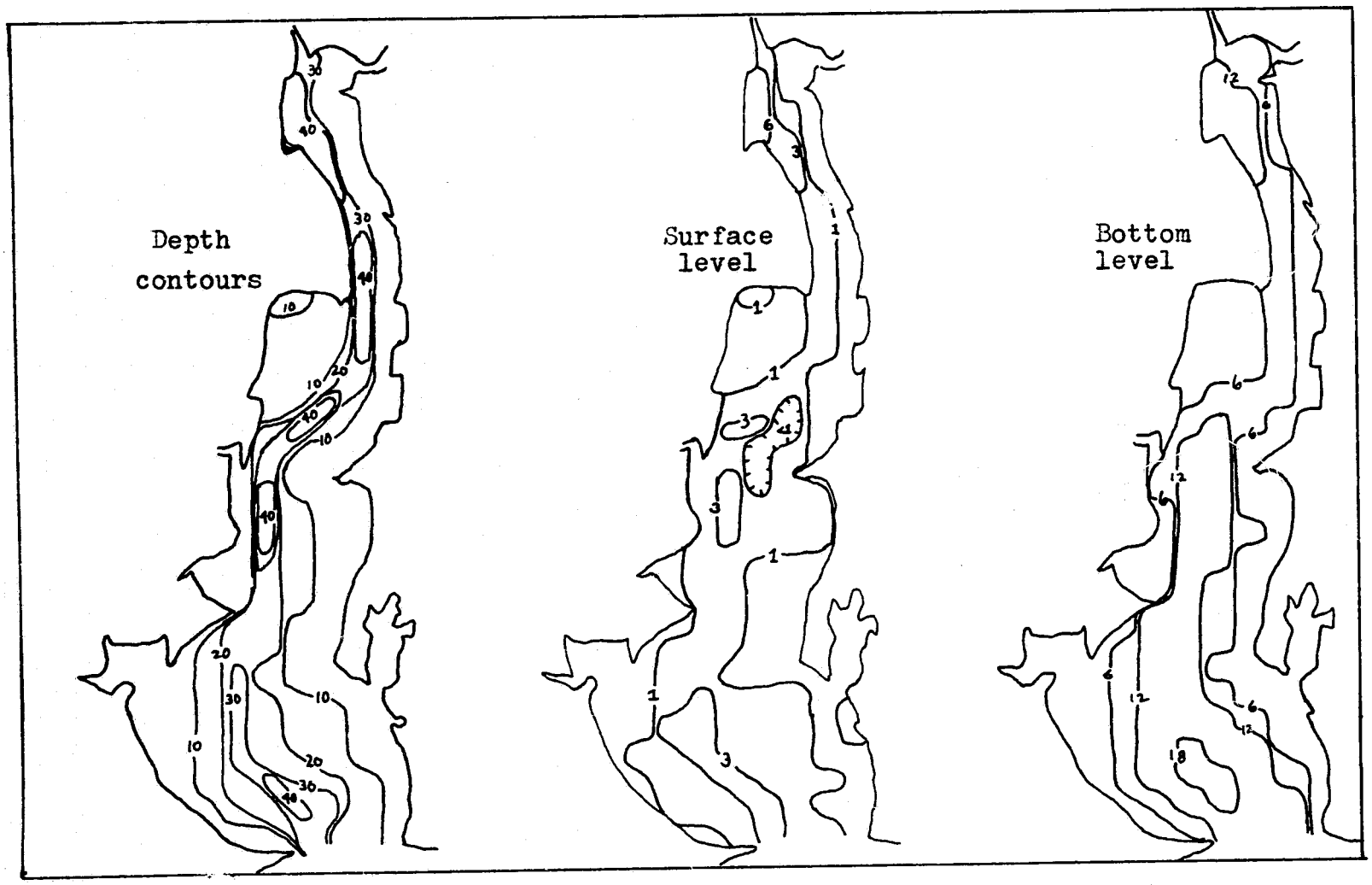

Figure 7. 22. Coliform decay due to solar radiation. Initial field strength 50, 6:00 A.M.; decay shown at 6:00 P.M.

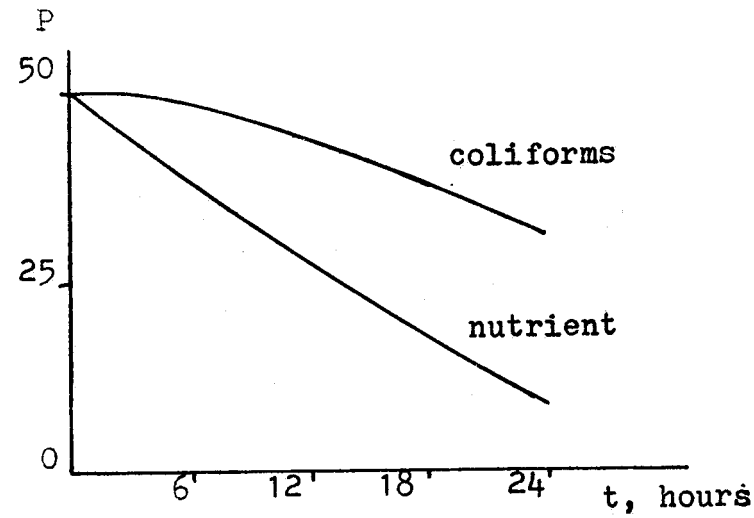

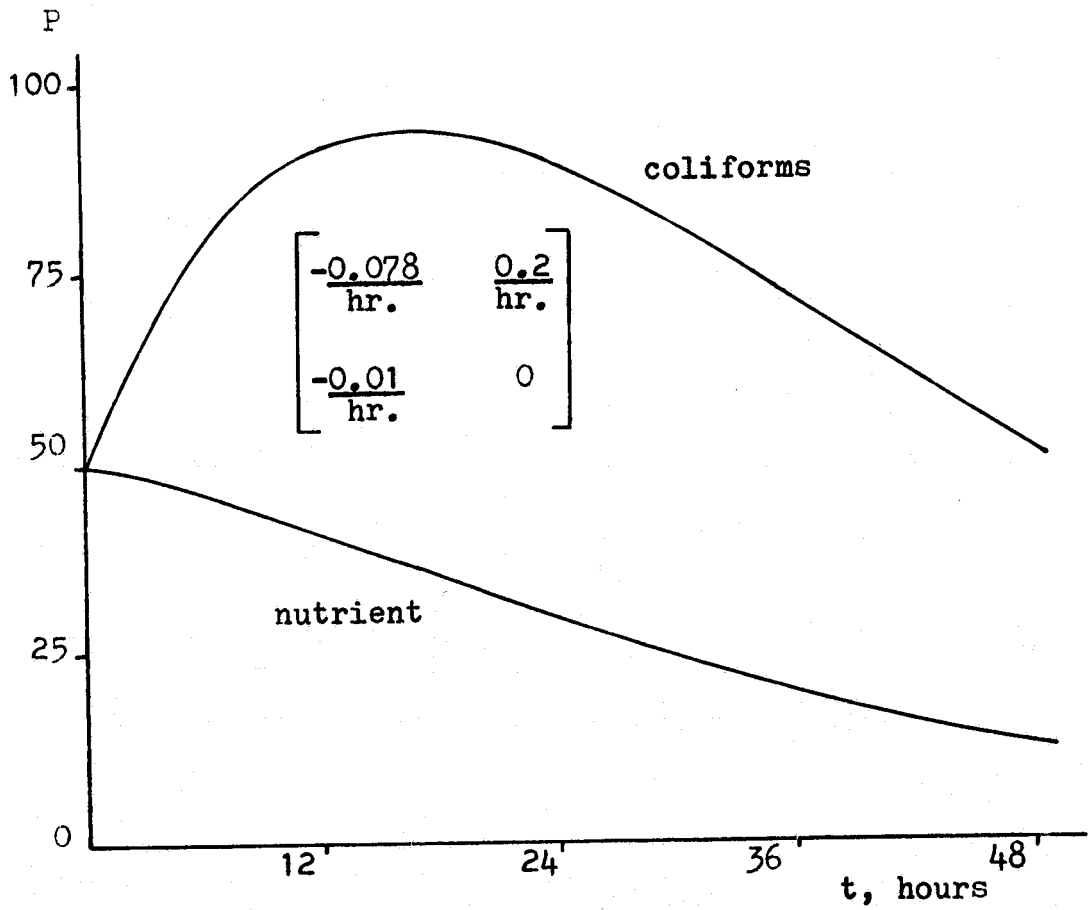

Figure 7.23. Effect of reaction matrices.

P vs. t for coliforms and an unspecified nutrient

coliforms drops off, the rate of consumption of the nutrient decreases.

The point of this demonstration is to show that the reaction matrix can be used to model more complex behavior than simple decay. Some careful field or laboratory measurements would be needed to obtain the proper reaction matrix for a problem in which a lag or growth is expected. It should be kept in mind that the coliform and nutrient concentrations will probably be expressed in different terms, and the reaction matrix values must account for this. For example, if the arbitrary 50-concentration used for the initial level of the nutrient represented 50 % sewage effluent present, the coefficient for coliform growth, K_{12}, would probably be much higher. A simple simulation, such as that just performed, would be very helpful to check the reaction matrix before applying it to a real-world problem.

Figures 7.24 and 7.25 show the comparison of the field data with the predicted concentrations of the conservative constituent at the same stations (the surface values). They appear to agree remarkably well. This could mean either that there is no decay or that it is only of the order of the difference between the near-steady state prevailing here and true steady state. Clearly, the field data indicate no such rate of decay as would be produced by solar radiation. For a final run, a decay coefficient equal to the rate for decay in the dark at a water temperature of 75°F (Equation 6.4)

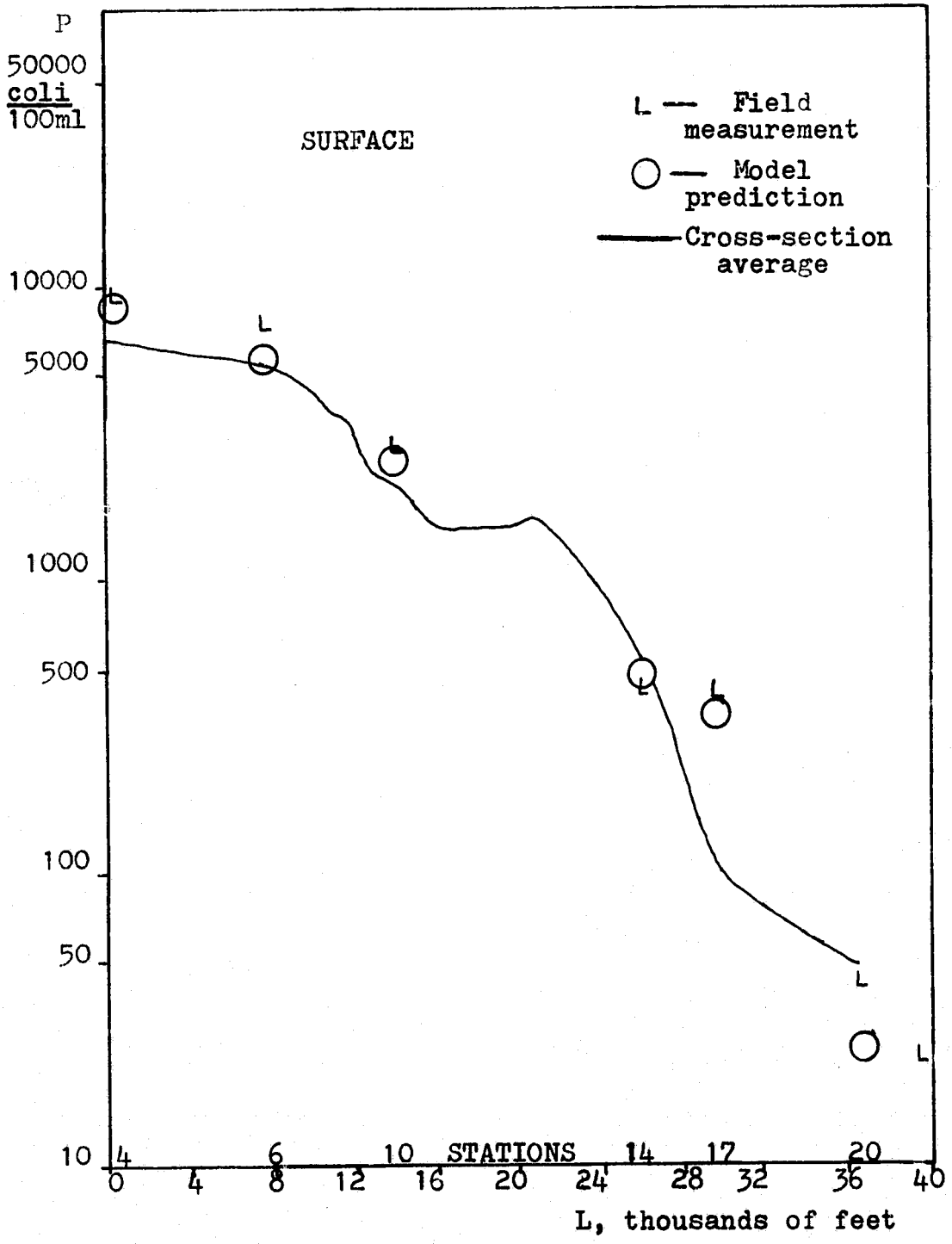

Figure 7.24. Model predictions and field data.
No decay, low tide, 92.25 hours

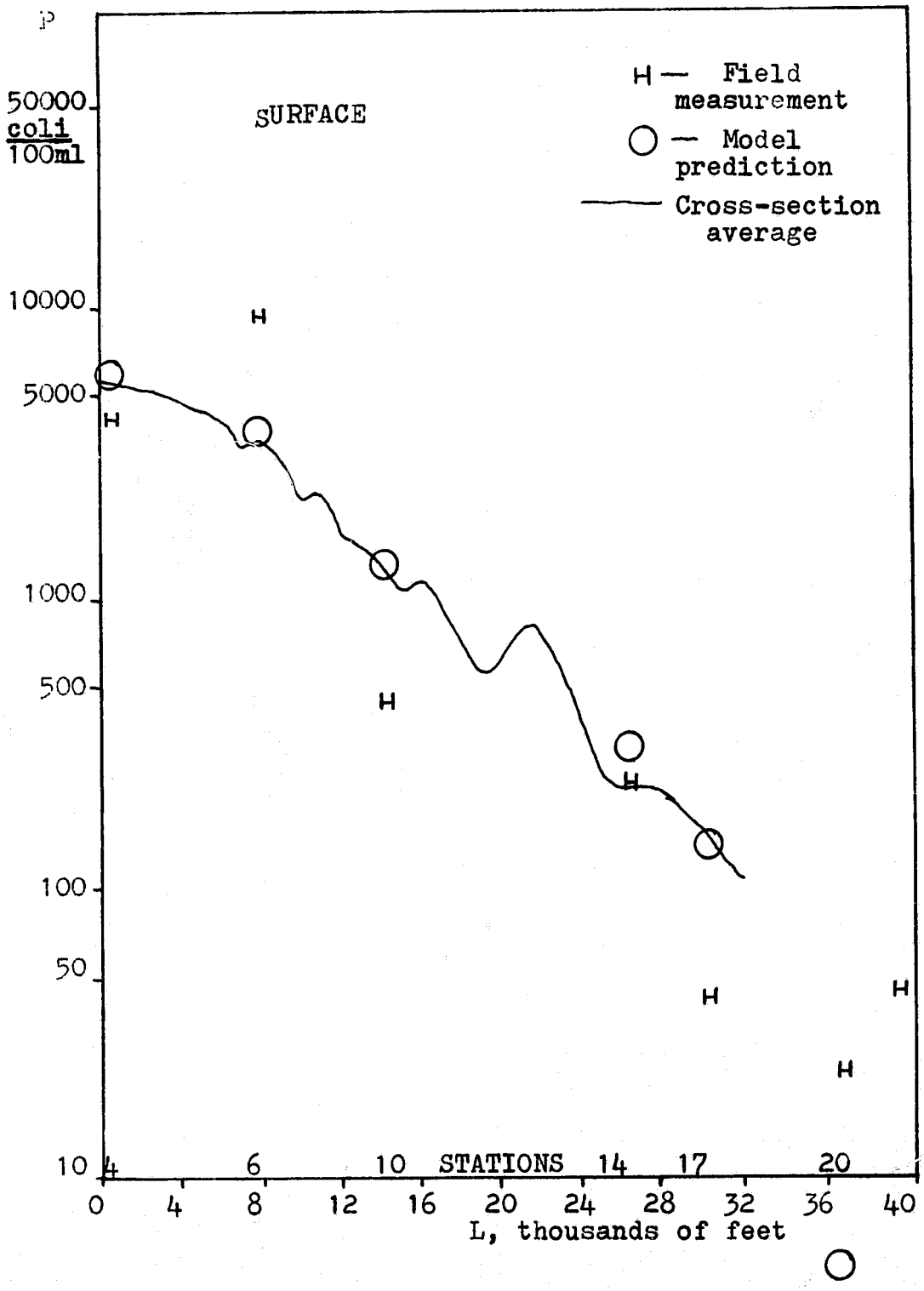

Figure 7.25. Model predictions and field data.
No decay, high tide, 98.17 hours

was specified. This was run starting from the conservative concentration field at the end of 98.17 hours, for another 18 hours. Figures 7.26 and 7.27 show the data and predictions after 12.0 and 18.0 additional hours. The predicted values have now dropped consistently below the field measurements.

Since the conservative values agree so well with the data, it is most likely that little decay actually takes place under the conditions prevailing, except in the southernmost part of the model area, most distant from the sources. This appears to indicate that nutrients are present throughout the area, causing the coliforms to persist. In 1966, the Blackstone Valley sewage plant on the Seekonk River was a very large source of organic matter, and the Pawtuxet River is thought to be a source of a variety of nutrients (56). This is the likely explanation for the apparent lack of decay.

It can be seen that in order to model coliforms faithfully, a good idea of the processes prevailing is needed. This can only be obtained from field measurements in the area to be modeled, or in a very similar area.

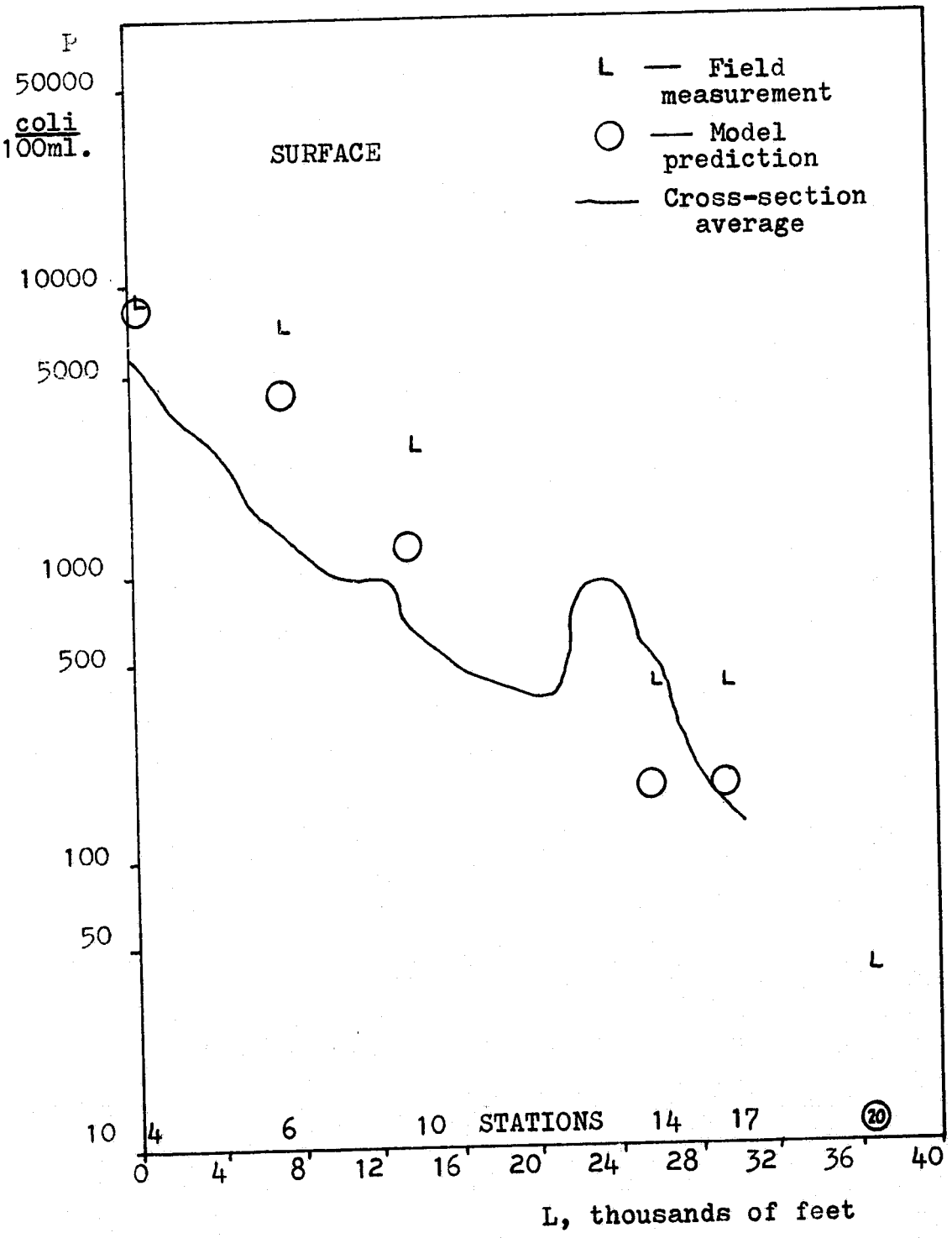

Figure 7.26. Model predictions and field data.
K_d = 0.078/hr, low tide, 98.17 + 18 hours

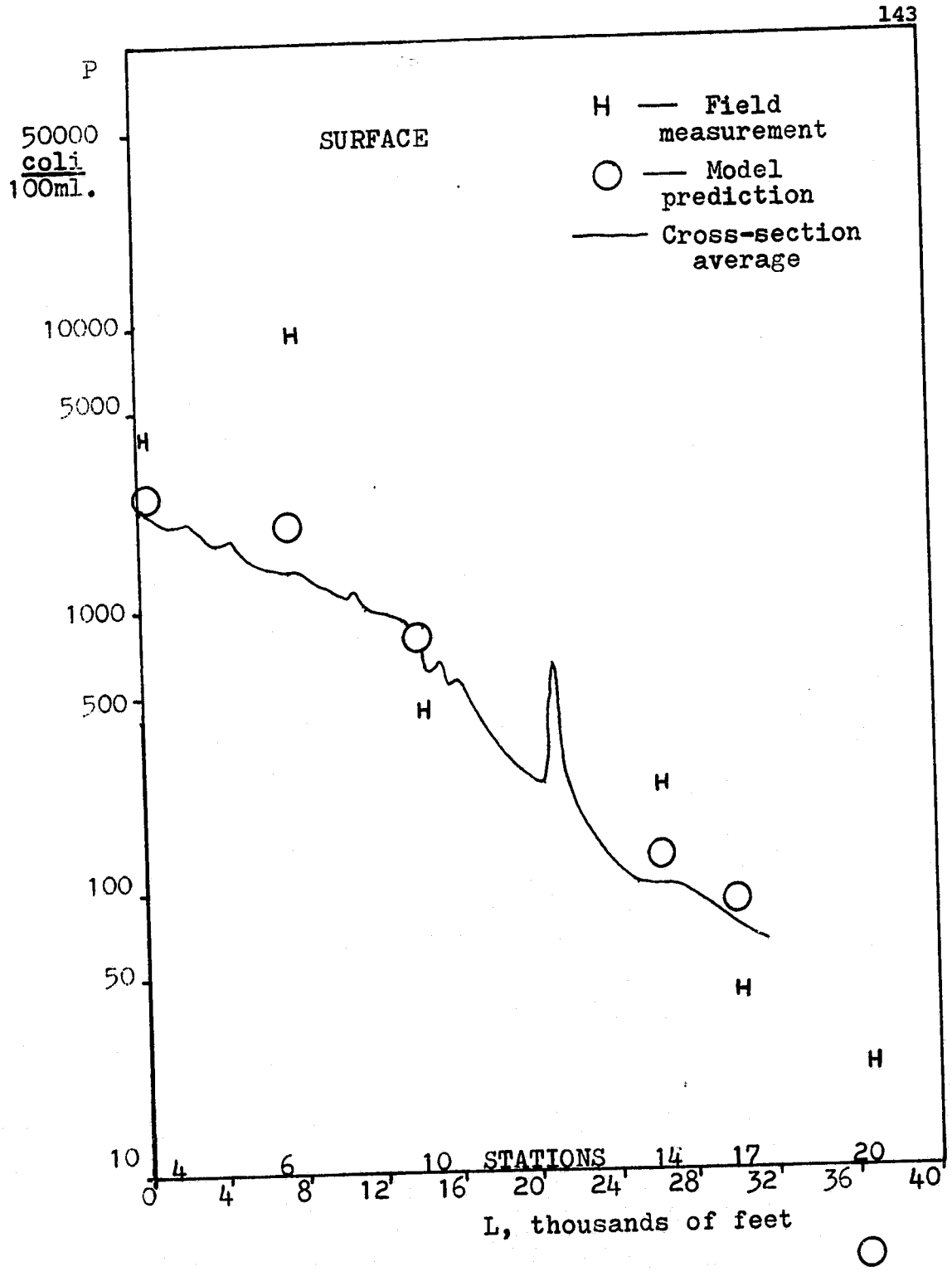

Figure 7.27. Model predictions and field data

K = 0.078/hr, high tide, 98.17 + 12 hours

VIII. STEADY STATE MODEL

Since there are many situations when the steady state solution of the mass transport equation is of particular interest in an area under study, it would be desirable to determine necessary modifications to the existing numerical procedure to handle this situation. Following the work of Douglas (17) and Wachpress (67), the time step increment Δt in Equations 2.20, 2.21, and 2.22 can be replaced by a positive number iteration parameter or sequence of iteration parameters and by iteration with these parameters a steady state solution obtained.

After convergence of the solution is assumed, the problem then becomes the determination of a sequence of iteration parameters which, when applied in some cyclic pattern, will cause the rate of convergence to be maximized. Since the literature (17,25,67) provides only an indication of possible iteration parameters for a simple heat diffusion problem with constant dispersion coefficients, an optimum sequence of parameters is not available for the general mass transport equation and normally has to be determined through numerical experiments. Indications of possible parameter selection have been made in the work of Aziz and Hellums (43), Gordon and Spaulding (68), and Anasoulis and

McDonald (69) but are not directly applicable to this case.

Spaulding (24), in earlier work on the three-dimensional convective dispersion model, has used a cyclic iteration sequence given by

5×10^{-6}
25×10^{-5}
1.25×10^{-4}
6.25×10^{-4}
3.125×10^{-3}

for relatively simple channel flow cases. There appears no reason to consider this an optimum sequence, but the solution converges quickly with reasonable error levels, so this sequence will be used in the work that follows.

Using the iteration sequence outlined above, the steady state model has been compared to appropriate analytical solutions for conservative waste discharges in open channels with and without decay as well as the simple dissolved oxygen-biochemical oxygen demand coupled reaction mechanism. With an iteration convergence criteria of 5×10^{-4}, the maximum error level in any solution was of the order of 0.5-1 %.

To further test the steady state model, a comparison between an analytical solution for a continous point release in a three-dimensional uniform channel flow and the numerical solution were compared. Table 8.1 gives the details on the model parameters employed.

Figure 8.1 shows a comparison between the analytical solution of Cleary and Adrian (70) for concentration and the present model along a line passing through the point

TABLE 8.1

CONTINUOUS POINT SOURCE RELEASE IN A UNIFORM CHANNEL FLOW

MODEL PARAMETERS

FLOW	UNIFORM CHANNEL FLOW U = 1 FT/SEC
DISPERSION	$D_x = D_y = 500$ FT^2/SEC $D_z = .01$ FT^2/SEC
SOURCE	.03 UNITS/FT^3 SEC AT X = 5000 FT, Y = 4500 FT AND Z = 12.5 FT
GRID SPACING	$\Delta X = 1000$ FT, $\Delta Y = 1000$ FT $\Delta \eta = \Delta Z = 5$ FT
CHANNEL GEOMETRY	CHANNEL DIMENSIONS, LENGTH - (DIRECTION OF FLOW) 30,000 FT WIDTH - 10,000 FT DEPTH - 25 FT
ITERATION CONVERGENCE CRITERIA	5×10^{-4}
BOUNDARY CONDITION	UPSTREAM - FIXED AT ZERO DOWNSTREAM - EXTRAPOLATED FROM INSIDE THE FIELD

source in the downstream direction. Figure 8.2 shows comparisons for two stations on the outside edge of the channel at the same Z height as the point source. It is to be noted that the concentrations on the left-hand side of the channel (facing downstream) are higher than those on the right. This is a result of the off-centered position of the point source (y = 4500 feet instead of y = 5000 feet).

Figures 8.1 and 8.2 clearly show that the steady state numerical model accurately predicts the concentration distribution for the case under consideration. The one area where model solutions deviate significantly from the analytical solution is near the point source. This difference is easily understood since the grid spacing of the numerical scheme is not refined enough to represent the steep concentration gradients near the point source.

Verification of the steady state model for these analytical solutions gives preliminary indication of the numerical behavior and the validity of the computational scheme. It remains, however, to extend the model to cases for which analytical solutions are not available.

In this light, the three-dimensional mass transport model was coupled to a steady state river hydrodynamics model to predict the motion of pollutants injected into separate streams for the case of river confluence. Employing Leendertse's (19) two-dimensional vertically-averaged hydrodynamics model with the input as specified

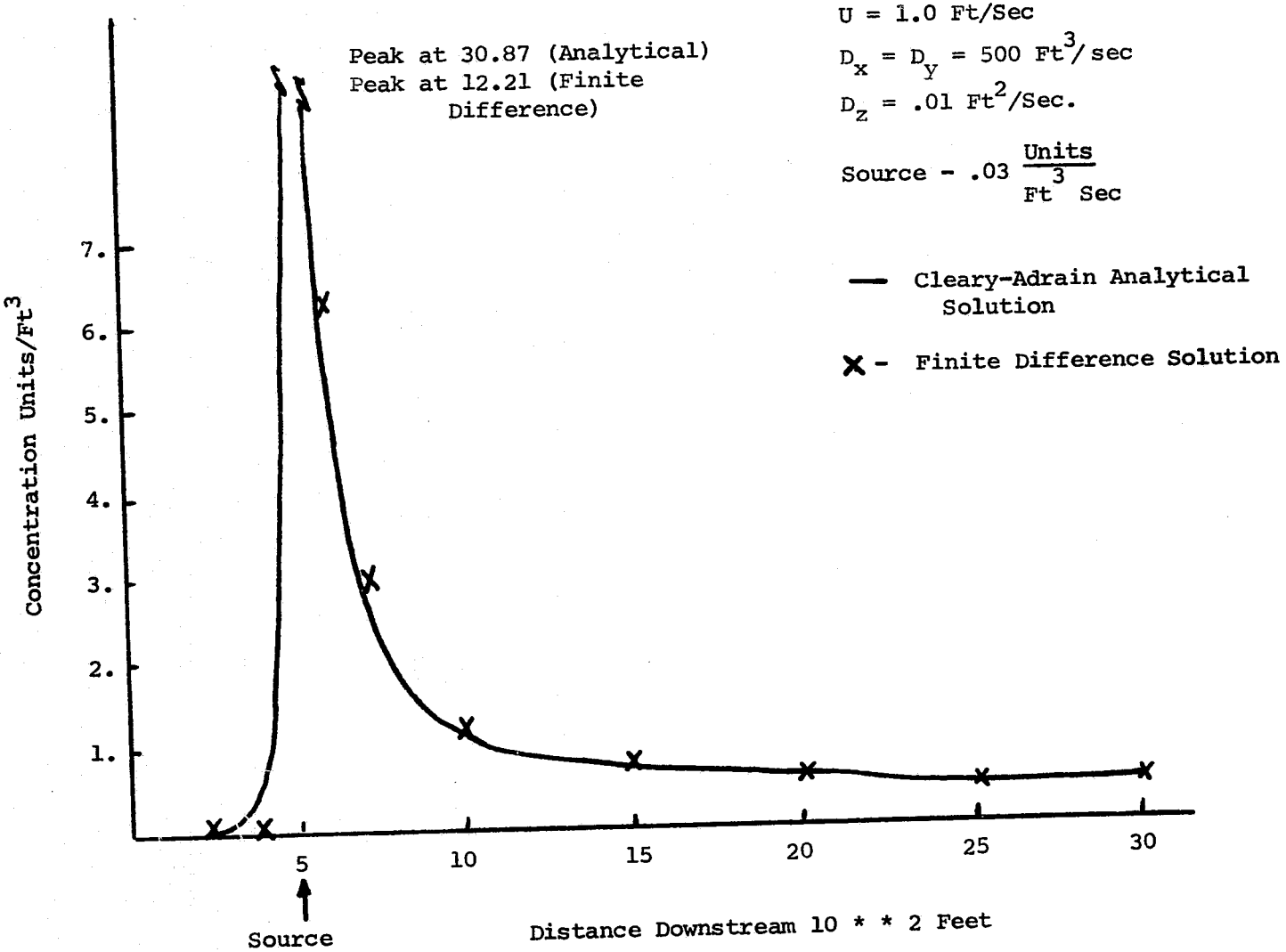

FIGURE 8.1. Comparison of numerical model prediction and analytic solution for a steady-state point release in a uniform channel flow for Y = 4500 ft., Z = 12.5 ft.

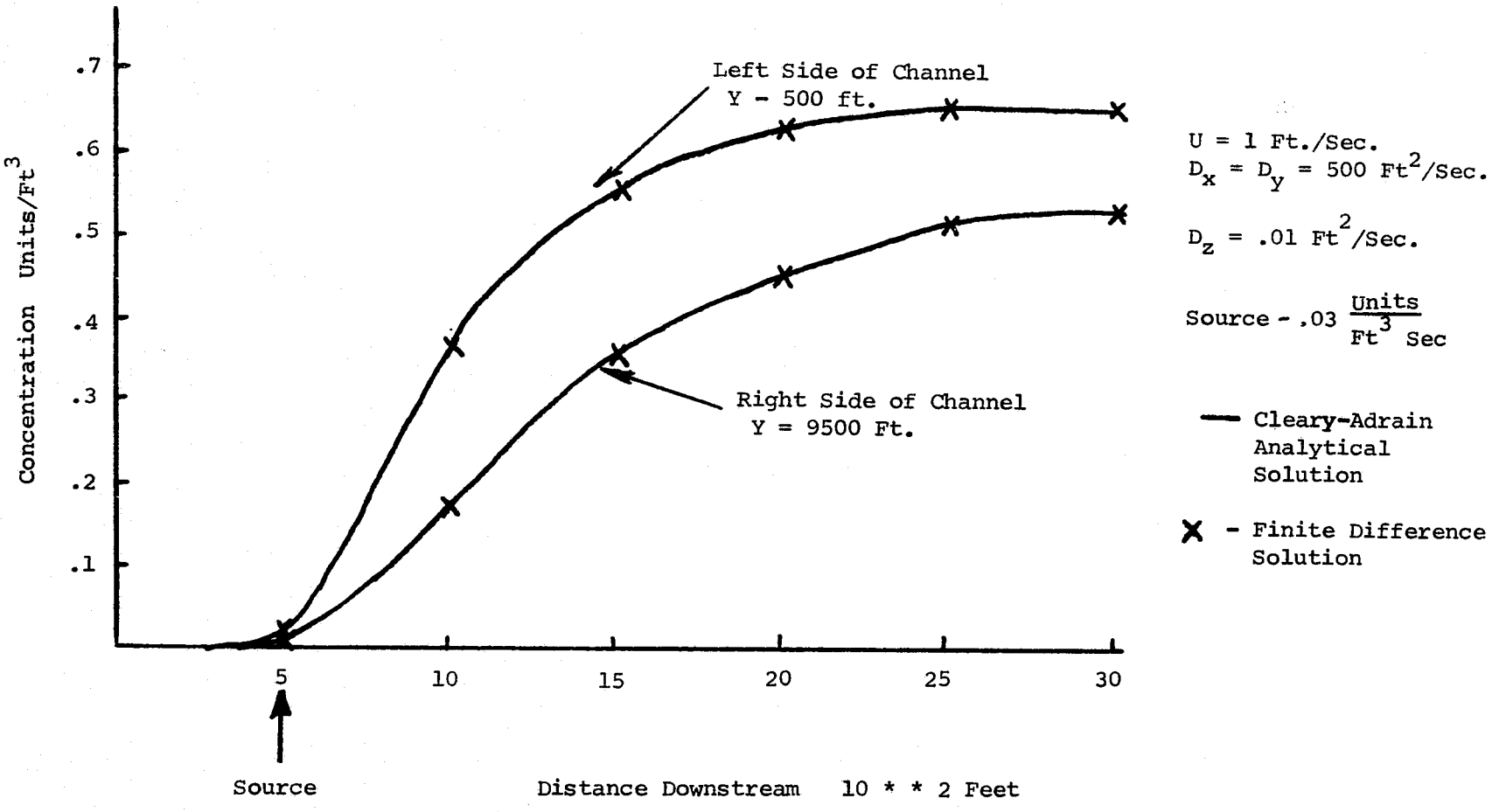

FIGURE 8.2. Comparison of numerical model prediction and analytic solution for a steady state point release in a uniform channel flow, Z = 12.5 Ft., Y = 500 Ft., and Y = 9500 Ft.

in Table 8.2 and the depth field as shown in Figure 8.3, the computational scheme was run until the flowrates for all river cross-sections achieved a steady state. Figure 8.4 shows the resulting steady-state velocity vector plot for the vertically-averaged circulation in the river confluence.

Employing the input conditions specified in Table 8.2, the mass transport model was run for a point source release in each stream. The results of the numerical solution are shown in Figures 8.5 through 8.9 for each of the nondimensional levels. (Level 2 at the river stream bottom through level 6 at the stream surface with a source input at level 4.) A well-defined vertical distribution of concentration is readily noted near the source input points. As one preceeds downstream the mixing of the two streams can be seen over the lateral as well as the vertical direction.

Figures 8.10 through 8.14 show the exact same case previously described but incorporate a first-order decay process with a decay coefficient of 0.00001 sec. The reduction of the concentrations at all levels is noted, but the structure of the concentration distribution remains fundamentally the same.

In each of the simulation cases described above, the outflow boundaries were allowed to seek a level appropriate with the internal solution by use of a simple continuative boundary extrapolation approach. From a numerical viewpoint this adjustment of boundaries

TABLE 8.2

MODEL INPUTS FOR STEADY STATE RIVER CONFLUENCE

RIVER MODEL

BOUNDARY CONDITIONS - CONSTANT INPUT FLOW RATES OF 100 FT^3/SEC AND 200 FT^3/SEC TO THE LEFT HAND AND RIGHT HAND STREAMS RESPECTIVELY, ZERO TIDAL HEIGHT AT LOWER BOUNDARY

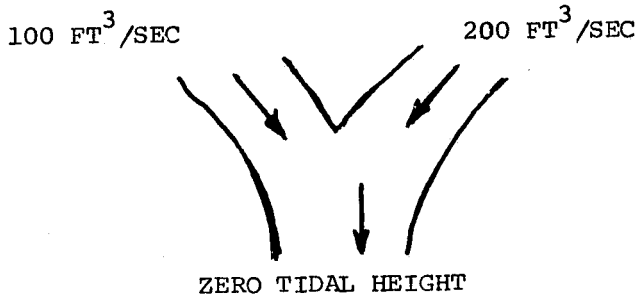

BOTTOM TOPOGRAPHY (SEE FIGURE 8.3)

GRID SPACING - $\Delta X = \Delta Y = 1000$ FT

TIME STEP - 40 SEC

SIMULATION TIME 8 HRS (ASSURE STEADY STATE FLOW CONDITIONS)

CONSTITUENT TRANSPORT MODEL

DISPERSION COEFFICIENTS

X & Y DIRECTIONS - 12 FT^2/SEC

Z DIRECTION - .01 FT^2/SEC

POINT SOURCES

GRIDS 13, 6, 4 and 9, 10, 4 - .03 $\frac{MG}{L\ SEC}$

VELOCITY - STEADY STATE FIELD FROM RIVER MODEL, TO INCLUDE THE SLOPE OF THE RIVER SURFACE AND ZERO VERTICAL VELOCITY ($\omega = 0$)

DECAY - (WHEN EMPLOYED) FIRST ORDER DECAY WITH K = .00001 SEC^{-1}

BOUNDARY CONDITIONS - ZERO CONCENTRATION BOUNDARIES SPECIFIED ON INFLOW AND A CONTINUATIVE SPECIFICATION ON OUTFLOW

GRID SPACING - $\Delta X = \Delta Y = 1000$ FT

INITIAL DEPTH FIELD IN FEET

	1	2	3	4	5	6	7	8	9	10	11	12
1	2.00	2.00	2.00	2.00	0.0	0.0	0.0	2.00	2.00	2.00	2.00	0.0
2	0.0	1.80	2.50	1.60	0.0	0.0	0.0	0.0	1.60	3.00	1.50	0.0
3	0.0	1.70	2.60	1.80	0.0	0.0	0.0	0.70	1.40	3.50	1.10	0.0
4	0.0	0.90	3.00	2.00	0.0	0.0	0.0	1.00	1.40	3.70	0.90	0.0
5	0.0	0.0	2.90	2.0	0.0	0.0	0.0	0.0	1.50	3.80	0.60	0.0
6	0.0	0.0	3.30	1.90	0.0	0.0	0.0	0.0	1.60	4.00	0.0	0.0
7	0.0	0.0	2.80	3.10	0.90	0.0	0.0	0.0	1.30	4.50	0.0	0.0
8	0.0	0.0	1.70	3.00	1.00	0.0	0.0	0.0	1.00	5.00	0.0	0.0
9	0.0	0.0	0.0	2.70	1.30	0.0	0.0	0.0	1.20	5.10	1.50	0.0
10	0.0	0.0	0.0	2.10	2.20	0.0	0.0	0.0	0.0	4.90	2.00	0.0
11	0.0	0.0	0.0	1.80	2.60	1.20	0.70	0.0	0.0	4.50	1.30	0.0
12	0.0	0.0	0.0	0.60	2.00	2.70	1.10	0.0	1.80	4.50	1.20	0.0
13	0.0	0.0	0.0	0.0	1.60	2.60	1.30	0.0	2.20	4.70	0.0	0.0
14	0.0	0.0	0.0	0.0	0.80	3.00	1.50	1.70	3.90	1.50	0.0	0.0
15	0.0	0.0	0.0	0.0	0.0	2.30	3.20	1.80	4.30	0.0	0.0	0.0
16	0.0	0.0	0.0	0.0	0.0	2.10	3.50	1.70	5.00	0.0	0.0	0.0
17	0.0	0.0	0.0	0.0	0.0	1.10	4.10	3.50	4.70	0.0	0.0	0.0
18	0.0	0.0	0.0	0.0	0.0	0.0	5.00	5.50	2.10	0.0	0.0	0.0
19	0.0	0.0	0.0	0.0	0.0	0.0	5.20	6.00	1.00	0.0	0.0	0.0
20	0.0	0.0	0.0	0.0	0.0	1.00	4.70	5.40	0.0	0.0	0.0	0.0
21	0.0	0.0	0.0	0.0	0.0	1.80	4.00	4.80	0.0	0.0	0.0	0.0
22	0.0	0.0	0.0	0.0	1.00	1.90	3.90	4.60	0.0	0.0	0.0	0.0
23	0.0	0.0	0.0	0.0	1.30	2.20	4.50	3.70	1.30	0.0	0.0	0.0
24	0.0	0.0	0.0	0.0	2.20	2.70	4.10	3.10	1.90	0.0	0.0	0.0
25	0.0	0.0	0.0	0.0	1.00	2.20	3.80	3.50	2.30	0.0	0.0	0.0
26	0.0	0.0	0.0	0.0	0.0	1.30	3.40	3.80	2.70	0.0	0.0	0.0
27	0.0	0.0	0.0	0.0	0.0	0.0	3.00	3.30	3.00	0.0	0.0	0.0
28	0.0	0.0	0.0	0.0	0.0	0.0	2.30	4.00	2.10	0.0	0.0	0.0
29	0.0	0.0	0.0	0.0	0.0	0.0	1.60	4.90	1.50	0.0	0.0	0.0
30	0.0	0.0	0.0	0.0	0.0	0.0	1.50	5.00	1.50	0.0	0.0	0.0
31	0.0	0.0	0.0	0.0	0.0	0.0	1.50	5.00	1.50	0.0	0.0	0.0
32	0.0	0.0	0.0	0.0	0.0	0.0	1.50	5.00	1.50	0.0	0.0	0.0

FIGURE 8.3. Depth field for river confluence study in grid system notation.

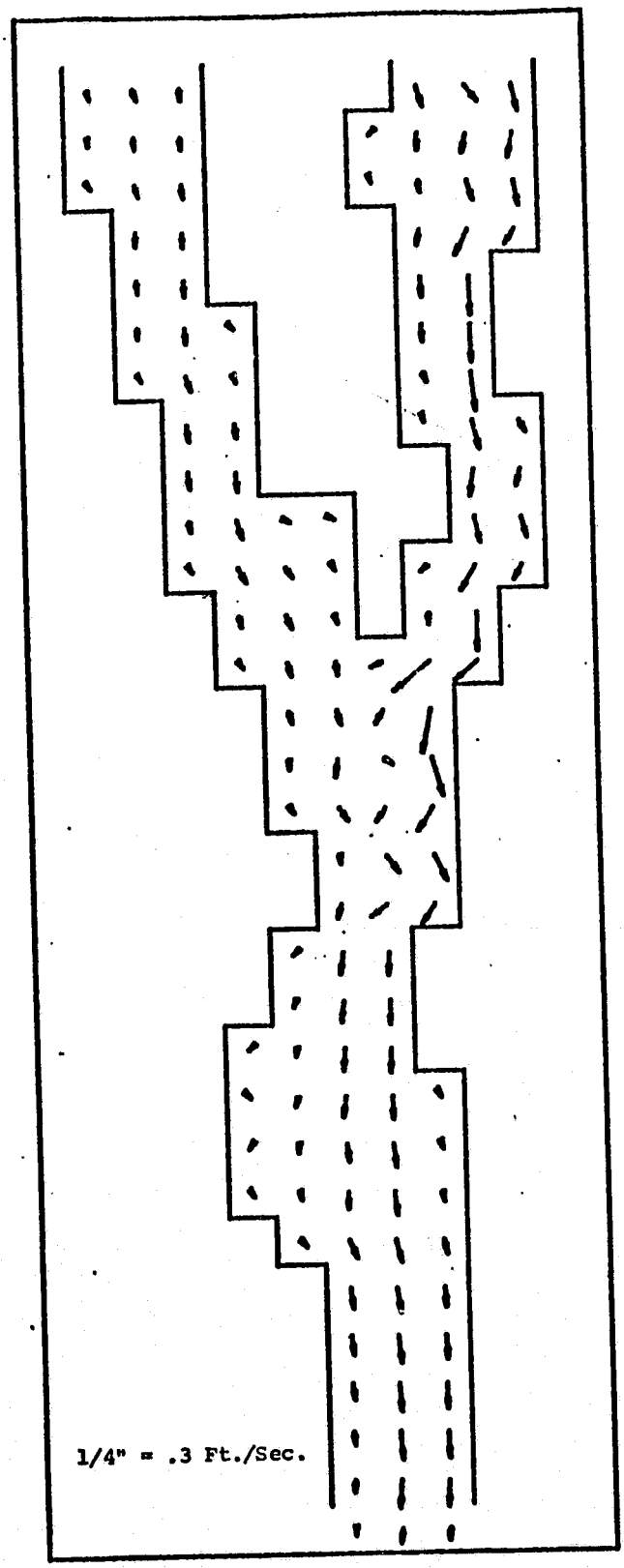

FIGURE 8.4. Velocity vector plot of river confluence under steady state flow conditions (see Table 8.2 for details).

CONCENTRATION OF CONSTITUTENT (MG/L) FOR LEVEL - 2
IN THE X AND Y PLANE

	1	2	3	4	5	6	7	8	9	10	11	12
1	0.0	0.0	0.0	0.0	0.0	0.0	0.0	0.0	0.0	0.0	0.0	0.0
2	0.0	0.000	0.000	0.000	0.0	0.0	0.0	0.0	0.000	0.000	0.000	0.0
3	0.0	0.000	0.000	0.000	0.0	0.0	0.0	0.000	0.000	0.000	0.000	0.0
4	0.0	0.000	0.000	0.000	0.0	0.0	0.0	0.000	0.000	0.000	0.000	0.0
5	0.0	0.0	0.000	0.000	0.0	0.0	0.0	0.0	0.003	0.005	0.002	0.0
6	0.0	0.0	0.000	0.000	0.0	0.0	0.0	0.0	0.003	0.020	0.0	0.0
7	0.0	0.0	0.000	0.000	0.000	0.0	0.0	0.0	0.010	0.068	0.0	0.0
8	0.0	0.0	0.000	0.000	0.000	0.0	0.0	0.0	0.014	0.230	0.0	0.0
9	0.0	0.0	0.0	0.000	0.000	0.0	0.0	0.0	0.192	0.647	0.831	0.0
10	0.0	0.0	0.0	0.000	0.000	0.0	0.0	0.0	0.0	0.825	0.842	0.0
11	0.0	0.0	0.0	0.001	0.004	0.041	0.094	0.0	0.0	0.842	0.843	0.0
12	0.0	0.0	0.0	0.003	0.024	0.108	0.205	0.0	0.843	0.843	0.843	0.0
13	0.0	0.0	0.0	0.0	0.232	1.386	0.834	0.0	0.843	0.843	0.0	0.0
14	0.0	0.0	0.0	0.0	0.282	1.001	0.890	0.856	0.843	0.843	0.0	0.0
15	0.0	0.0	0.0	0.0	0.0	0.991	0.915	0.861	0.844	0.0	0.0	0.0
16	0.0	0.0	0.0	0.0	0.0	0.969	0.920	0.875	0.853	0.0	0.0	0.0
17	0.0	0.0	0.0	0.0	0.0	0.971	0.928	0.880	0.858	0.0	0.0	0.0
18	0.0	0.0	0.0	0.0	0.0	0.0	0.922	0.893	0.876	0.0	0.0	0.0
19	0.0	0.0	0.0	0.0	0.0	0.0	0.906	0.885	0.872	0.0	0.0	0.0
20	0.0	0.0	0.0	0.0	0.0	0.900	0.900	0.888	0.0	0.0	0.0	0.0
21	0.0	0.0	0.0	0.0	0.0	0.898	0.897	0.890	0.0	0.0	0.0	0.0
22	0.0	0.0	0.0	0.0	0.898	0.897	0.896	0.891	0.0	0.0	0.0	0.0
23	0.0	0.0	0.0	0.0	0.898	0.897	0.895	0.892	0.892	0.0	0.0	0.0
24	0.0	0.0	0.0	0.0	0.898	0.897	0.895	0.893	0.893	0.0	0.0	0.0
25	0.0	0.0	0.0	0.0	0.898	0.897	0.895	0.894	0.893	0.0	0.0	0.0
26	0.0	0.0	0.0	0.0	0.0	0.898	0.896	0.894	0.894	0.0	0.0	0.0
27	0.0	0.0	0.0	0.0	0.0	0.0	0.896	0.895	0.894	0.0	0.0	0.0
28	0.0	0.0	0.0	0.0	0.0	0.0	0.897	0.896	0.895	0.0	0.0	0.0
29	0.0	0.0	0.0	0.0	0.0	0.0	0.897	0.896	0.895	0.0	0.0	0.0
30	0.0	0.0	0.0	0.0	0.0	0.0	0.898	0.897	0.896	0.0	0.0	0.0
31	0.0	0.0	0.0	0.0	0.0	0.0	0.898	0.897	0.896	0.0	0.0	0.0
32	0.0	0.0	0.0	0.0	0.0	0.0	0.0	0.0	0.0	0.0	0.0	0.0

FIGURE 8.5. Concentration of pollutant (Mg/l) for level -2

CONCENTRATION OF CONSTITUTENT (MG/L) FOR Z LEVEL - 3
IN THE X AND Y PLANE

	1	2	3	4	5	6	7	8	9	10	11	12
1	0.0	0.0	0.0	0.0	0.0	0.0	0.0	0.0	0.0	0.0	0.0	0.0
2	0.0	0.000	0.000	0.000	0.0	0.0	0.0	0.0	0.000	0.000	0.000	0.0
3	0.0	0.000	0.000	0.000	0.0	0.0	0.0	0.000	0.000	0.000	0.000	0.0
4	0.0	0.000	0.000	0.000	0.000	0.000	0.000	0.000	0.000	0.000	0.000	0.0
5	0.0	0.0	0.000	0.000	0.0	0.0	0.0	0.0	0.003	0.005	0.002	0.0
6	0.0	0.0	0.000	0.000	0.0	0.0	0.0	0.0	0.003	0.020	0.0	0.0
7	0.0	0.0	0.000	0.000	0.000	0.0	0.0	0.0	0.010	0.068	0.0	0.0
8	0.0	0.0	0.000	0.000	0.000	0.0	0.0	0.0	0.014	0.240	0.0	0.0
9	0.0	0.0	0.0	0.000	0.000	0.0	0.0	0.0	0.193	0.835	0.846	0.0
10	0.0	0.0	0.0	0.000	0.000	0.0	0.0	0.0	0.0	0.846	9.843	0.0
11	0.0	0.0	0.0	0.001	0.004	0.041	0.094	0.0	0.0	0.843	0.843	0.0
12	0.0	0.0	0.0	0.003	0.024	0.109	0.205	0.0	0.843	0.043	0.843	0.0
13	0.0	0.0	0.0	0.0	0.232	1.495	0.837	0.0	0.843	0.843	0.0	0.0
14	0.0	0.0	0.0	0.0	0.282	1.006	0.890	0.856	0.843	0.843	0.0	0.0
15	0.0	0.0	0.0	0.0	0.0	0.991	0.915	0.861	0.844	0.0	0.0	0.0
16	0.0	0.0	0.0	0.0	0.0	0.969	0.920	0.875	0.853	0.0	0.0	0.0
17	0.0	0.0	0.0	0.0	0.0	01971	0.928	0.880	0.858	0.0	0.0	0.0
18	0.0	0.0	0.0	0.0	0.0	0.0	0.922	0.893	0.876	0.0	0.0	0.0
19	0.0	0.0	0.0	0.0	0.0	0.0	0.906	0.885	0.872	0.0	0.0	0.0
20	0.0	0.0	0.0	0.0	0.0	0.900	0.900	0.888	0.0	0.0	0.0	0.0
21	0.0	0.0	0.0	0.0	0.0	0.898	0.897	0.890	0.0	0.0	0.0	0.0
22	0.0	0.0	0.0	0.0	0.898	0.897	0.896	0.891	0.0	0.0	0.0	0.0
23	0.0	0.0	0.0	0.0	0.898	0.897	0.895	0.892	0.892	0.0	0.0	0.0
24	0.0	0.0	0.0	0.0	0.898	0.897	0.895	0.893	0.893	0.0	0.0	0.0
25	0.0	0.0	0.0	0.0	0.898	0.897	0.895	0.894	0.893	0.0	0.0	0.0
26	0.0	0.0	0.0	0.0	0.0	0.898	0.896	0.894	0.894	0.0	0.0	0.0
27	0.0	0.0	0.0	0.0	0.0	0.0	0.896	0.895	0.894	0.0	0.0	0.0
28	0.0	0.0	0.0	0.0	0.0	0.0	0.897	0.896	0.895	0.0	0.0	0.0
29	0.0	0.0	0.0	0.0	0.0	0.0	0.897	0.896	0.895	0.0	0.0	0.0
30	0.0	0.0	0.0	0.0	0.0	0.0	0.898	0.897	0.896	0.0	0.0	0.0
31	0.0	0.0	0.0	0.0	0.0	0.0	0.898	0.897	0.896	0.0	0.0	0.0
32	0.0	0.0	0.0	0.0	0.0	0.0	0.0	0.0	0.0	0.0	0.0	0.0

FIGURE 8.6. Concentration of pollutant (Mg/l) for level - 3

CONCENTRATION OF CONSTITUENT (MG/L) - 1 FOR Z LEVEL - 4
IN THE X AND Y PLANE

	1	2	3	4	5	6	7	8	9	10	11	12
1	0.0	0.0	0.0	0.0	0.0	0.0	0.0	0.0	0.0	0.0	0.0	0.0
2	0.0	0.000	0.000	0.000	0.0	0.0	0.0	0.0	0.000	0.000	0.000	0.0
3	0.0	0.000	0.000	0.000	0.0	0.0	0.0	0.000	0.000	0.000	0.000	0.0
4	0.0	0.000	0.000	0.000	0.0	0.0	0.0	0.000	0.000	0.000	0.000	0.0
5	0.0	0.0	0.000	0.000	0.0	0.0	0.0	0.0	0.003	0.005	0.002	0.0
6	0.0	0.0	0.000	0.000	0.0	0.0	0.0	0.0	0.003	0.020	0.0	0.0
7	0.0	0.0	0.000	0.000	0.000	0.0	0.0	0.0	0.010	0.069	0.0	0.0
8	0.0	0.0	0.000	0.000	0.000	0.0	0.0	0.0	0.014	0.251	0.0	0.0
9	0.0	0.0	0.0	0.000	0.000	0.0	0.0	0.0	0.193	1.252	0.862	0.0
10	0.0	0.0	0.0	0.000	0.000	0.0	0.0	0.0	0.0	0.870	0.845	0.0
11	0.0	0.0	0.0	0.001	0.004	0.041	0.094	0.0	0.0	0.845	0.843	0.0
12	0.0	0.0	0.0	0.003	0.024	0.109	0.205	0.0	0.843	0.843	0.843	0.0
13	0.0	0.0	0.0	0.0	0.233	1.725	0.840	0.0	0.843	0.843	0.0	0.0
14	0.0	0.0	0.0	0.0	0.282	1.010	0.890	0.856	0.843	0.843	0.0	0.0
15	0.0	0.0	0.0	0.0	0.0	0.991	0.915	0.861	0.844	0.0	0.0	0.0
16	0.0	0.0	0.0	0.0	0.0	0.969	0.920	0.875	0.853	0.0	0.0	0.0
17	0.0	0.0	0.0	0.0	0.0	0.971	0.928	0.880	0.858	0.0	0.0	0.0
18	0.0	0.0	0.0	0.0	0.0	0.0	0.922	0.893	0.876	0.0	0.0	0.0
19	0.0	0.0	0.0	0.0	0.0	0.0	0.906	0.885	0.872	0.0	0.0	0.0
20	0.0	0.0	0.0	0.0	0.0	0.90	0.900	0.888	0.0	0.0	0.0	0.0
21	0.0	0.0	0.0	0.0	0.0	0.898	0.897	0.890	0.0	0.0	0.0	0.0
22	0.0	0.0	0.0	0.0	0.898	0.897	0.896	0.891	0.0	0.0	0.0	0.0
23	0.0	0.0	0.0	0.0	0.898	0.897	0.895	0.892	0.892	0.0	0.0	0.0
24	0.0	0.0	0.0	0.0	0.898	0.897	0.895	0.893	0.893	0.0	0.0	0.0
25	0.0	0.0	0.0	0.0	0.898	0.897	0.895	0.894	0.893	0.0	0.0	0.0
26	0.0	0.0	0.0	0.0	0.0	0.898	0.896	0.894	0.894	0.0	0.0	0.0
27	0.0	0.0	0.0	0.0	0.0	0.0	0.896	0.895	0.894	0.0	0.0	0.0
28	0.0	0.0	0.0	0.0	0.0	0.0	0.897	0.896	0.895	0.0	0.0	0.0
29	0.0	0.0	0.0	0.0	0.0	0.0	0.897	0.896	0.895	0.0	0.0	0.0
30	0.0	0.0	0.0	0.0	0.0	0.0	0.898	0.897	0.896	0.0	0.0	0.0
31	0.0	0.0	0.0	0.0	0.0	0.0	0.898	0.897	0.896	0.0	0.0	0.0
32	0.0	0.0	0.0	0.0	0.0	0.0	0.0	0.0	0.0	0.0	0.0	0.0

FIGURE 8.7. Concentration of pollutant (Mg/l) for level - 4

CONCENTRATION OF CONSTITUENT (MG/L) - 1 FOR Z LEVEL - 5
IN THE X AND Y PLANE

	1	2	3	4	5	6	7	8	9	10	11	12
1	0.0	0.0	0.0	0.0	0.0	0.0	0.0	0.0	0.0	0.0	0.0	0.0
2	0.0	0.000	0.000	0.000	0.0	0.0	0.0	0.0	0.000	0.000	0.000	0.0
3	0.0	0.000	0.000	0.000	0.0	0.0	0.0	0.000	0.000	0.000	0.000	0.0
4	0.0	0.000	0.000	0.000	0.0	0.0	0.0	0.000	0.000	0.000	0.000	0.0
5	0.0	0.0	0.000	0.000	0.0	0.0	0.0	0.0	0.003	0.005	0.002	0.0
6	0.0	0.0	0.000	0.000	0.0	0.0	0.0	0.0	0.003	0.020	0.0	0.0
7	00.	0.0	0.000	0.000	0.000	0.0	0.0	0.0	0.10	0.06	0.0	0.0
8	0.0	0.0	0.000	0.000	0.000	0.0	0.0	0.0	0.014	0.240	0.0	0.0
9	0.0	0.0	0.0	0.000	0.000	0.0	0.0	0.0	0.193	0.835	0.846	0.0
10	0.0	0.0	0.0	0.000	0.000	0.0	0.0	0.0	0.0	0.847	0.843	0.0
11	0.0	0.0	0.0	0.001	0.004	0.041	0.094	0.0	0.0	0.843	0.843	0.0
12	0.0	0.0	0.0	0.003	0.024	0.109	0.020	0.0	0.843	0.843	0.843	0.0
13	0.0	0.0	0.0	0.0	0.232	1.495	0.837	0.0	0.843	0.843	0.0	0.0
14	0.0	0.0	0.0	0.0	0.282	1.006	0.890	0.856	0.843	0.843	0.0	0.0
15	0.0	0.0	0.0	0.0	0.0	0.991	0.915	0.861	0.844	0.0	0.0	0.0
16	0.0	0.0	0.0	0.0	0.0	0.969	0.920	0.875	0.853	0.0	0.0	0.0
17	0.0	0.0	0.0	0.0	0.0	0.971	0.928	0.880	0.858	0.0	0.0	0.0
18	0.0	0.0	0.0	0.0	0.0	0.0	0.922	0.893	0.976	0.0	0.0	0.0
19	0.0	0.0	0.0	0.0	0.0	0.0	0.906	0.885	0.872	0.0	0.0	0.0
20	0.0	0.0	0.0	0.0	0.0	0.900	0.900	0.888	0.0	0.0	0.0	0.0
21	0.0	0.0	0.0	0.0	0.0	0.898	0.897	0.890	0.0	0.0	0.0	0.0
22	0.0	0.0	0.0	0.0	0.898	0.897	0.896	0.891	0.0	0.0	0.0	0.0
23	0.0	0.0	0.0	0.0	0.898	0.897	0.895	0.892	0.892	0.0	0.0	0.0
24	0.0	0.0	0.0	0.0	0.898	0.897	0.895	0.893	0.893	0.0	0.0	0.0
25	0.0	0.0	0.0	0.0	0.898	0.897	0.895	0.894	0.893	0.0	0.0	0.0
26	0.0	0.0	0.0	0.0	0.0	0.898	0.896	0.894	0.894	0.0	0.0	0.0
27	0.0	0.0	0.0	0.0	0.0	0.0	0.896	0.895	0.894	0.0	0.0	0.0
28	0.0	0.0	0.0	0.0	0.0	0.0	0.897	0.896	0.895	0.0	0.0	0.0
29	0.0	0.0	0.0	0.0	0.0	0.0	0.897	0.896	0.895	0.0	0.0	0.0
30	0.0	0.0	0.0	0.0	0.0	0.0	0.898	0.897	0.896	0.0	0.0	0.0
31	0.0	0.0	0.0	0.0	0.0	0.0	0.898	0.897	0.896	0.0	0.0	0.0
32	0.0	0.0	0.0	0.0	0.0	0.0	0.0	0.0	0.0	0.0	0.0	0.0

FIGURE 8.8. Concentration of pollutant (Mg/l) for level - 5

CONCENTRATION OF CONSTITUENT (MG/L) FOR Z LEVEL - 6
IN THE X AND Y PLANE

	1	2	3	4	5	6	7	8	9	10	11	12
1	0.0	0.0	0.0	0.0	0.0	0.0	0.0	0.0	0.0	0.0	0.0	0.0
2	0.0	0.000	0.000	0.000	0.0	0.0	0.0	0.0	0.000	0.000	0.000	0.0
3	0.0	0.000	0.000	0.000	0.0	0.0	0.0	0.000	0.000	0.000	0.000	0.0
4	0.0	0.000	0.000	0.000	0.0	0.0	0.0	0.000	0.000	0.000	0.000	0.0
5	0.0	0.0	0.000	0.000	0.0	0.0	0.0	0.0	0.00	0.00	0.00	0.0
6	0.0	0.0	0.000	0.000	0.0	0.0	0.0	0.0	0.00	0.02	0.0	0.0
7	0.0	0.0	0.000	0.000	0.000	0.0	0.0	0.0	0.010	0.068	0.0	0.0
8	0.0	0.0	0.000	0.000	0.000	0.0	0.0	0.0	0.014	0.230	0.0	0.0
9	0.0	0.0	0.0	0.000	0.000	0.0	0.0	0.0	0.192	0.647	0.831	0.0
10	0.0	0.0	0.0	0.000	0.000	0.0	0.0	0.0	0.0	0.825	0.842	0.0
11	0.0	0.0	0.0	0.001	0.004	0.041	0.094	0.0	0.0	0.842	0.843	0.0
12	0.0	0.0	0.0	0.003	0.024	0.108	0.205	0.0	0.843	0.843	0.843	0.0
13	0.0	0.0	0.0	0.0	0.232	1.386	0.834	0.0	0.843	0.843	0.0	0.0
14	0.0	0.0	0.0	0.0	0.282	1.001	0.890	0.856	0.843	0.843	0.0	0.0
15	0.0	0.0	0.0	0.0	0.0	0.991	0.915	0.861	0.844	0.0	0.0	0.0
16	0.0	0.0	0.0	0.0	0.0	0.969	0.920	0.875	0.853	0.0	0.0	0.0
17	0.0	0.0	0.0	0.0	0.0	0.971	0.928	0.880	0.858	0.0	0.0	0.0
18	0.0	0.0	0.0	0.0	0.0	0.0	0.922	0.893	0.876	0.0	0.0	0.0
19	0.0	0.0	0.0	0.0	0.0	0.0	0.906	0.885	0.872	0.0	0.0	0.0
20	0.0	0.0	0.0	0.0	0.0	0.900	0.900	0.888	0.0	0.0	0.0	0.0
21	0.0	0.0	0.0	0.0	0.0	0.898	0.897	0.890	0.0	0.0	0.0	0.0
22	0.0	0.0	0.0	0.0	0.898	0.897	0.896	0.891	0.0	0.0	0.0	0.0
23	0.0	0.0	0.0	0.0	0.898	0.897	0.895	0.892	0.892	0.0	0.0	0.0
24	0.0	0.0	0.0	0.0	0.898	0.897	0.895	0.893	0.893	0.0	0.0	0.0
25	0.0	0.0	0.0	0.0	0.898	0.897	0.895	0.894	0.893	0.0	0.0	0.0
26	0.0	0.0	0.0	0.0	0.0	0.898	0.896	0.894	0.894	0.0	0.0	0.0
27	0.0	0.0	0.0	0.0	0.0	0.0	0.896	0.895	0.894	0.0	0.0	0.0
28	0.0	0.0	0.0	0.0	0.0	0.0	0.897	0.896	0.895	0.0	0.0	0.0
29	0.0	0.0	0.0	0.0	0.0	0.0	0.897	0.896	0.895	0.0	0.0	0.0
30	0.0	0.0	0.0	0.0	0.0	0.0	0.898	0.897	0.896	0.0	0.0	0.0
31	0.0	0.0	0.0	0.0	0.0	0.0	0.898	0.897	0.896	0.0	0.0	0.0
32	0.0	0.0	0.0	0.0	0.0	0.0	0.0	0.0	0.0	0.0	0.0	0.0

FIGURE 8.9. Concentration of pollutant (Mg/l) for level - 6

CONCENTRATION OF CONSTITUENT (MG/L) FOR Z LEVEL - 2

IN THE X AND Y PLANE, DECAY COEFFICIENT K = .00001 (1/SEC)

	1	2	3	4	5	6	7	8	9	10	11	12
1	0.0	0.0	0.0	0.0	0.0	0.0	0.0	0.0	0.0	0.0	0.0	0.0
2	0.0	0.00000	0.00000	0.00000	0.0	0.0	0.0	0.0	0.00000	0.00000	0.00000	0.0
3	0.0	0.00000	0.00000	0.00000	0.0	0.0	0.0	0.00009	0.00001	0.00007	0.00004	0.0
4	0.0	0.00000	0.00000	0.00000	0.0	0.0	0.0	0.00024	0.00042	0.00039	0.00084	0.0
5	0.0	0.0	0.00000	0.00000	0.0	0.0	0.0	0.0	0.00308	0.00572	0.00209	0.0
6	0.0	0.0	0.00000	0.00000	0.0	0.0	0.0	0.0	0.00347	0.02017	0.0	0.0
7	0.0	0.0	0.00000	0.00000	0.00000	0.0	0.0	0.0	0.01062	0.06814	0.0	0.0
8	0.0	0.0	0.00000	0.00000	0.00001	0.0	0.0	0.0	0.01437	0.22957	0.0	0.0
9	0.0	0.0	0.0	0.00001	0.00002	0.0	0.0	0.0	0.19174	0.64640	0.82661	0.0
10	0.0	0.0	0.0	0.00002	0.00041	0.0	0.0	0.0	0.0	0.82203	0.83507	0.0
11	0.0	0.0	0.0	0.00121	0.00417	0.04107	0.09315	0.0	0.0	0.83681	0.83563	0.0
12	0.0	0.0	0.0	0.00362	0.02460	0.10747	0.20265	0.0	0.83343	0.83434	0.83327	0.0
13	0.0	0.0	0.0	0.0	0.23057	1.38058	0.82813	0.0	0.83066	0.83238	0.0	0.0
14	0.0	0.0	0.0	0.0	0.27855	0.99387	0.87946	0.84141	0.83041	0.83066	0.0	0.0
15	0.0	0.0	0.0	0.0	0.0	0.97890	0.90102	0.84548	0.82905	0.0	0.0	0.0
16	0.0	0.0	0.0	0.0	0.0	0.95298	0.90291	0.85768	0.83639	0.0	0.0	0.0
17	0.0	0.0	0.0	0.0	0.0	0.95091	0.90827	0.85989	0.83777	0.0	0.0	0.0
18	0.0	0.0	0.0	0.0	0.0	0.0	0.89887	0.86977	0.85259	0.0	0.0	0.0
19	0.0	0.0	0.0	0.0	0.0	0.0	0.87951	0.85919	0.84717	0.0	0.0	0.0
20	0.0	0.0	0.0	0.0	0.0	0.86542	0.87011	0.85990	0.0	0.0	0.0	0.0
21	0.0	0.0	0.0	0.0	0.0	0.86227	0.86472	0.85937	0.0	0.0	0.0	0.0
22	0.0	0.0	0.0	0.0	0.85523	0.85828	0.86090	0.85836	0.0	0.0	0.0	0.0
23	0.0	0.0	0.0	0.0	0.85388	0.85563	0.85760	0.85608	0.85205	0.0	0.0	0.0
24	0.0	0.0	0.0	0.0	0.85284	0.85366	0.85486	0.85403	0.85124	0.0	0.0	0.0
25	0.0	0.0	0.0	0.0	0.85246	0.85241	0.85296	0.85228	0.85029	0.0	0.0	0.0
26	0.0	0.0	0.0	0.0	0.0	0.85208	0.85193	0.85111	0.84956	0.0	0.0	0.0
27	0.0	0.0	0.0	0.0	0.0	0.0	0.85136	0.85044	0.84916	0.0	0.0	0.0
28	0.0	0.0	0.0	0.0	0.0	0.0	0.85079	0.84999	0.84893	0.0	0.0	0.0
29	0.0	0.0	0.0	0.0	0.0	0.0	0.85043	0.84966	0.84883	0.0	0.0	0.0
30	0.0	0.0	0.0	0.0	0.0	0.0	0.85039	0.84970	0.84894	0.0	0.0	0.0
31	0.0	0.0	0.0	0.0	0.0	0.0	0.85039	0.84970	0.84894	0.0	0.0	0.0
32	0 .0	0.0	0.0	0.0	0.0	0.0	0.0	0.0	0.0	0.0	0.0	0.0

FIGURE 8.10. Concentration of pollutant (Mg/l) for Level -2, decay coefficient K = .00001 sec - 1

CONCENTRATION OF CONSTITUTENT (MG/L) FOR Z LEVEL - 3

IN THE X AND Y PLANE, DECAY COEFFICIENT K = .00001 (1/SEC)

	1	2	3	4	5	6	7	8	9	10	11	12
1	0.0	0.0	0.0	0.0	0.0	0.0	0.0	0.0	0.0	0.0	0.0	0.0
2	0.0	0.00000	0.00000	0.00000	0.0	0.0	0.0	0.0	0.00000	0.00000	0.00000	0.0
3	0.0	0.00000	0.00000	0.00000	0.0	0.0	0.0	0.00009	0.00001	0.00007	0.00004	0.0
4	0.0	0.00000	0.00000	0.00000	0.0	0.0	0.0	0.00024	0.00042	0.00039	0.00084	0.0
5	0.0	0.0	0.00000	0.00000	0.0	0.0	0.0	0.0	0.00308	0.00572	0.00209	0.0
6	0.0	0.0	0.00000	0.00000	0.0	0.0	0.0	0.0	0.00347	0.02019	0.0	0.0
7	0.0	0.0	0.00000	0.00000	0.00000	0.0	0.0	0.0	0.01063	0.06854	0.0	0.0
8	0.0	0.0	0.00000	0.00000	0.00001	0.0	0.0	0.0	0.01436	0.23973	0.0	0.0
9	0.0	0.0	0.0	0.00001	0.00002	0.0	0.0	0.0	0.19188	0.83412	0.84175	0.0
10	0.0	0.0	0.0	0.00002	0.00041	0.0	0.0	0.0	0.0	0.84361	0.83699	0.0
11	0.0	0.0	0.0	0.00121	0.00417	0.04107	0.09315	0.0	0.0	0.83851	0.83586	0.0
12	0.0	0.0	0.0	0.00362	0.02460	0.10779	0.20266	0.0	0.83343	0.83443	0.83328	0.0
13	0.0	0.0	0.0	0.0	0.23077	1.48998	0.83090	0.0	0.83066	0.83240	0.0	0.0
14	0.0	0.0	0.0	0.0	0.27855	0.99806	0.87963	0.84141	0.83041	0.83067	0.0	0.0
15	0.0	0.0	0.0	0.0	0.0	0.97899	0.90103	0.84548	0.82905	0.0	0.0	0.0
16	0.0	0.0	0.0	0.0	0.0	0.95298	0.90291	0.85768	0.83639	0.0	0.0	0.0
17	0.0	0.0	0.0	0.0	0.0	0.95091	0.90827	0.85989	0.83777	0.0	0.0	0.0
18	0.0	0.0	0.0	0.0	0.0	0.0	0.89887	0.86977	0.85259	0.0	0.0	0.0
19	0.0	0.0	0.0	0.0	0.0	0.0	0.87951	0.85919	0.84717	0.0	0.0	0.0
20	0.0	0.0	0.0	0.0	0.0	0.86542	0.87011	0.85989	0.0	0.0	0.0	0.0
21	0.0	0.0	0.0	0.0	0.0	0.86227	0.86472	0.85937	0.0	0.0	0.0	0.0
22	0.0	0.0	0.0	0.0	0.85523	0.85828	0.86090	0.85836	0.0	0.0	0.0	0.0
23	0.0	0.0	0.0	0.0	0.85388	0.85563	0.85760	0.85608	0.85205	0.0	0.0	0.0
24	0.0	0.0	0.0	0.0	0.85284	0.85366	0.85486	0.85403	0.85124	0.0	0.0	0.0
25	0.0	0.0	0.0	0.0	0.85246	0.85241	0.85296	0.85228	0.85029	0.0	0.0	0.0
26	0.0	0.0	0.0	0.0	0.0	0.85208	0.85193	0.85111	0.84956	0.0	0.0	0.0
27	0.0	0.0	0.0	0.0	0.0	0.0	0.85136	0.85044	0.84916	0.0	0.0	0.0
28	0.0	0.0	0.0	0.0	0.0	0.0	0.85079	0.84999	0.84893	0.0	0.0	0.0
29	0.0	0.0	0.0	0.0	0.0	0.0	0.85043	0.84966	0.84883	0.0	0.0	0.0
30	0.0	0.0	0.0	0.0	0.0	0.0	0;85039	0.84970	0.84894	0.0	0.0	0.0
31	0.0	0.0	0.0	0.0	0.0	0.0	0.85039	0.84970	0.84894	0.0	0.0	0.0
32	0.0	0.0	0.0	0.0	0.0	0.0	0.0	0.0	0.0	0.0	0.0	0.0

FIGURE 8.11. Concentration of pollutant (Mg/l) for level -3, decay coefficient K = .00001 sec - 1

CONCENTRATION OF CONSTITUTENT (MG/L) FOR Z LEVEL - 4

IN THE X AND Y PLANE, DECAY COEFFICIENT K - .00001 (1/SEC)

	1	2	3	4	5	6	7	8	9	10	11	12
1	0.0	0.0	0.0	0.0	0.0	0.0	0.0	0.0	0.0	0.0	0.0	0.0
2	0.0	0.00000	0.00000	0.00000	0.0	0.0	0.0	0.0	0.00000	0.00000	0.00000	0.0
3	0.0	0.00000	0.00000	0.00000	0.0	0.0	0.0	0.00009	0.00001	0.00007	0.00004	0.0
4	0.0	0.00000	0.00000	0.00000	0.0	0.0	0.0	0.00024	0.00042	0.00039	0.00084	0.0
5	0.0	0.0	0.00000	0.00000	0.0	0.0	0.0	0.0	0.00308	0.00572	0.00209	0.0
6	0.0	0.0	0.00000	0.00000	0.0	0.0	0.0	0.0	0.00347	0.02019	0.0	0.0
7	0.0	0.0	0.00000	0.00000	0.00000	0.0	0.0	0.0	0.01063	0.06885	0.0	0.0
8	0.0	0.0	0.00000	0.00000	0.00001	0.0	0.0	0.0	0.01436	0.25070	0.0	0.0
9	0.0	0.0	0.0	0.00001	0.00002	0.0	0.0	0.0	0.19202	1.25177	0.85783	0.0
10	0.0	0.0	0.0	0.00002	0.00041	0.0	0.0	0.0	0.0	0.86675	0.83849	0.0
11	0.0	0.0	0.0	0.00121	0.00417	0.04107	0.09315	0.0	0.0	0.83984	0.93601	0.0
12	0.0	0.0	0.0	0.00362	0.02460	0.10812	0.20267	0.0	0.83343	0.83450	0.83330	0.0
13	0.0	0.0	0.0	0.0	0.23099	1.71978	0.83375	0.0	0.83066	0.83240	0.0	0.0
14	0.0	0.0	0.0	0.0	0.27855	1.00240	0.87976	0.84141	0.83041	0.83067	0.0	0.0
15	0.0	0.0	0.0	0.0	0.0	0.97906	0.90103	0.84548	0.82905	0.0	0.0	0.0
16	0.0	0.0	0.0	0.0	0.0	0.95298	0.90291	0.85768	0.83639	0.0	0.0	0.0
17	0.0	0.0	0.0	0.0	0.0	0.95091	0.90827	0.85990	0.83778	0.0	0.0	0.0
18	0.0	0.0	0.0	0.0	0.0	0.0	0.89887	0.86977	0.85259	0.0	0.0	0.0
19	0.0	0.0	0.0	0.0	0.0	0.0	0.87951	0.85919	0.84717	0.0	0.0	0.0
20.	0.0	0.0	0.0	0.0	0.0	0.86542	0.87011	0.85989	0.0	0.0	0.0	0.0
21	0.0	0.0	0.0	0.0	0.0	0.86227	9.86472	0.85937	0.0	0.0	0.0	0.0
22	0.0	0.0	0.0	0.0	0.85523	0.85828	0.86090	0.85836	0.0	0.0	0.0	0.0
23	0.0	0.0	0.0	0.0	0.85388	0.85563	0.85760	0.85607	0.85205	0.0	0.0	0.0
24	0.0	0.0	0.0	0.0	0.85284	0.85366	0.85486	0.85403	0.85124	0.0	0.0	0.0
25	0.0	0.0	0.0	0.0	0.85246	0.85241	0.85296	0.85228	0.85029	0.0	0.0	0.0
26	0.0	0.0	0.0	0.0	0.0	0.85208	0.85193	0.85111	0.84956	0.0	0.0	0.0
27	0.0	0.0	0.0	0.0	0.0	0.0	0.85136	0.85044	0.84916	0.0	0.0	0.0
28	0.0	0.0	0.0	0.0	0.0	0.0	0.85079	0.84999	0.84893	0.0	0.0	0.0
29	0.0	0.0	0.0	0.0	0.0	0.0	0.85043	0.84966	0.84883	0.0	0.0	0.0
30	0.0	0.0	0.0	0.0	0.0	0.0	0.85039	0.84970	0.84894	0.0	0.0	0.0
31	0.0	0.0	0.0	0.0	0.0	0.0	0.85039	0.84970	0.84894	0.0	0.0	0.0
32	0.0	0.0	0.0	0.0	0.0	0.0	0.0	0.0	0.0	0.0	0.0	0.0

FIGURE 8.12. Concentration of pollutant (Mg/l) for level - 3, decay coefficient, K = .00001 sec -1

CONCENTRATION OF CONSTITUTENT (MG/L) FOR Z LEVEL - 5

IN THE X AND Y PLANE, DECAY COEFFICIENT K = .00001 (1/SEC)

	1	2	3	4	5	6	7	8	9	10	11	12
1	0.0	0.0	0.0	0.0	0.0	0.0	0.0	0.0	0.0	0.0	0.0	0.0
2	0.0	0.00000	0.00000	0.00000	0.0	0.0	0.0	0.0	0.00000	0.00000	0.00000	0.0
3	0.0	0.00000	0.00000	0.00000	0.0	0.0	0.0	0.00009	0.00001	0.00007	0.00004	0.0
4	0.0	0.00000	0.00000	0.00000	0.0	0.0	0.0	0.00024	0.00042	0.00039	0.00084	0.0
5	0.0	0.0	0.00000	0.00000	0.0	0.0	0.0	0.0	0.00308	0.00572	0.00209	0.0
6	0.0	0.0	0.00000	0.00000	0.0	0.0	0.0	0.0	0.00347	0.02019	0.0	0.0
7	0.0	0.0	0.00000	0.00000	0.00000	0.0	0.0	0.0	0.01063	0.06854	0.0	0.0
8	0.0	0.0	0.00000	0.00000	0.00001	0.0	0.0	0.0	0.01436	0.23973	0.0	0.0
9	0.0	0.0	0.0	0.00001	0.00002	0.0	0.0	0.0	0.19188	0.83413	0.84175	0.0
10	0.0	0.0	0.0	0.00002	0.00041	0.0	0.0	0.0	0.0	0.84361	0.83699	0.0
11	0.0	0.0	0.0	0.00121	0.00417	0.04107	0.09315	0.0	0.0	0.83851	0.83586	0.0
12	0.0	0.0	0.0	0.00362	0.02560	0.10779	0.20266	0.0	0.83343	0.83443	0.83328	0.0
13	0.0	0.0	0.0	0.0	0.23077	1.48998	0.83090	0.0	0.83066	0.83240	0.0	0.0
14	0.0	0.0	0.0	0.0	0.27855	0.99806	0.87963	0.84141	0.83041	0.83067	0.0	0.0
15	0.0	0.0	0.0	0.0	0.0	0.97899	0.90103	0.84548	0.82905	0.0	0.0	0.0
16	0.0	0.0	0.0	0.0	0.0	0.95298	0.90291	0.85768	0.83639	0.0	0.0	0.0
17	0.0	0.0	0.0	0.0	0.0	0.95091	0.90827	0.85990	0.83778	0.0	0.0	0.0
18	0.0	0.0	0.0	0.0	0.0	0.0	0.89887	0.86977	0.85259	0.0	0.0	0.0
19	0.0	0.0	0.0	0.0	0.0	0.0	0.87951	0.85919	0.84717	0.0	0.0	0.0
20	0.0	0.0	0.0	0.0	0.0	0.86542	0.87011	0.85989	0.0	0.0	0.0	0.0
21	0.0	0.0	0.0	0.0	0.0	0.86227	0.86472	0.85937	0.0	0.0	0.0	0.0
22	0.0	0.0	0.0	0.0	0.85523	0.85828	0.86090	0.85836	0.0	0.0	0.0	0.0
23	0.0	0.0	0.0	0.0	0.85388	0.85563	0.85760	0.85607	0.85205	0.0	0.0	0.0
24	0.0	0.0	0.0	0.0	0.85284	0.85366	0.85486	0.85403	0.85124	0.0	0.0	0.0
25	0.0	0.0	0.0	0.0	0.85246	0.86240	0.85296	0.85228	0.85029	0.0	0.0	0.0
26	0.0	0.0	0.0	0.0	0.0	0.85208	0.85193	0.85111	0.84957	0.0	0.0	0.0
27	0.0	0.0	0.0	0.0	0.0	0.0	0.85136	0.95044	0.84916	0.0	0.0	0.0
28	0.0	0.0	0.0	0.0	0.0	0.0	0.85079	0.84999	0.84893	0.0	0.0	0.0
29	0.0	0.0	0.0	0.0	0.0	0.0	0.85043	0.84966	0.84883	0.0	0.0	0.0
30	0.0	0.0	0.0	0.0	0.0	0.0	0.85039	0.84970	0.84894	0.0	0.0	0.0
31	0.0	0.0	0.0	0.0	0.0	0.0	0.85039	0.84970	0.84894	0.0	0.0	0.0
32	0.0	0.0	0.0	0.0	0.0	0.0	0.0	0.0	0.0	0.0	0.0	0.0

FIGURE 8.13. Concentration of pollutant (Mg/l) for level - 5, decay coefficient K = .00001 sec - 1

CONCENTRATION OF CONSTITUENT (MG/L) FOR Z LEVEL - 6

IN THE X AND Y PLANE, DECAY COEFFICIENT K = .00001 (1/SEC)

	1	2	3	4	5	6	7	8	9	10	11	12
1	0.0	0.0	0.0	0.0	0.0	0.0	0.0	0.0	0.0	0.0	0.0	0.0
2	0.0	0.00000	0.00000	0.00000	0.0	0.0	0.0	0.0	0.00000	0.00000	0.00000	0.0
3	0.0	0.00000	0.00000	0.00000	0.0	0.0	0.0	0.00009	0.00001	0.00007	0.00004	0.0
4	0.0	0.00000	0.00000	0.00000	0.0	0.0	0.0	0.00024	0.00042	0.00039	0.00084	0.0
5	0.0	0.0	0.00000	0.00000	0.0	0.0	0.0	0.0	0.00308	0.00572	0.00209	0.0
6	0.0	0.0	0.00000	0.00000	0.0	0.0	0.0	0.0	0.00347	0.02017	0.0	0.0
7	0.0	0.0	0.00000	0.00000	0.00000	0.0	0.0	0.0	0.01063	0.06814	0.0	0.0
8	0.0	0.0	0.00000	0.00000	0.00001	0.0	0.0	0.0	0.01437	0.22957	0.0	0.0
9	0.0	0.0	0.0	0.00001	0.00002	0.0	0.0	0.0	0.19174	0.64640	0.82661	0.0
10	0.0	0.0	0.0	0.00002	0.00041	0.0	0.0	0.0	0.0	0.82203	0.83507	0.0
11	0.0	0.0	0.0	0.00121	0.00417	0.04107	0.09315	0.0	0.0	0.83681	0.83568	0.0
12	0.0	0.0	0.0	0.00362	0.02460	0.10740	0.20265	0.0	0.83343	0.83434	0.83327	0.0
13	0.0	0.0	0.0	0.0	0.23057	1.38058	0.82813	0.0	0.83066	0.83238	0.0	0.0
14	0.0	0.0	0.0	0.0	0.27855	0.99387	0.87946	0.84141	0.83041	0.83066	0.0	0.0
15	0.0	0.0	0.0	0.0	0.0	0.97890	0.90102	0.84548	0.8290[illegible]	0.0	0.0	0.0
16	0.0	0.0	0.0	0.0	0.0	0.95298	0.90291	0.85768	0.83039	0.0	0.0	0.0
17	0.0	0.0	0.0	0.0	0.0	0.95091	0.90827	0.85990	0.83778	0.0	0.0	0.0
18	0.0	0.0	0.0	0.0	0.0	0.0	0.89887	0.86977	0.85259	0.0	0.0	0.0
19	0.0	0.0	0.0	0.0	0.0	0.0	0.87951	0.85919	0.84717	0.0	0.0	0.0
20	0.0	0.0	0.0	0.0	0.0	0.86542	0.87011	0.85989	0.0	0.0	0.0	0.0
21	0.0	0.0	0.0	0.0	0.0	0.86227	0.86472	0.85937	0.0	0.0	0.0	0.0
22	0.0	0.0	0.0	0.0	0.85523	0.85828	0.86090	0.85836	0.0	0.0	0.0	0.0
23	0.0	0.0	0.0	0.0	0.85388	0.85563	0.85760	0.85607	0.85205	0.0	0.0	0.0
24	0.0	0.0	0.0	0.0	0.85284	0.85366	0.85486	0.85403	0.85124	0.0	0.0	0.0
25	0.0	0.0	0.0	0.0	0.85246	0.85241	0.85296	0.85228	0.85029	0.0	0.0	0.0
26	0.0	0.0	0.0	0.0	0.0	0.85208	0.85193	0.85111	0.84957	0.0	0.0	0.0
27	0.0	0.0	0.0	0.0	0.0	0.0	0.85136	0.85044	0.84916	0.0	0.0	0.0
28	0.0	0.0	0.0	0.0	0.0	0.0	0.85079	0.84999	0.84893	0.0	0.0	0.0
29	0.0	0.0	0.0	0.0	0.0	0.0	0.85043	0.84966	0.84883	0.0	0.0	0.0
30	0.0	0.0	0.0	0.0	0.0	0.0	0.85039	0.84970	0.84984	0.0	0.0	0.0
31	0.0	0.0	0.0	0.0	0.0	0.0	0.85039	0.84970	0.84894	0.0	0.0	0.0
32	0.0	0.0	0.0	0.0	0.0	0.0	0.0	0.0	0.0	0.0	0.0	0.0

FIGURE 8.14. Concentration of pollutant (Mg/l) for level - 6, decay coefficient K = .00001 sec - 1

to interior solution is extremely difficult to obtain in a steady state model. The primary difficulty is that the unsteady boundaries tend to cause the solution to become non-convergent. To overcome this problem, the present study held the boundaries fixed until the the numerical predictions had nearly converged, and then the boundary was adjusted. This process was repeated until neither the boundary nor the internal mass distribution changed significantly, i.e. within the convergence criteria.

Although there exists no data to compare the river confluence situations, the results indicate that the model is capable of giving reasonable quantitative predictions for complicated river geometries, flow conditions, and a variety of point loading situations. Extension of the model to a variety of species interactions is simply obtained through the reaction matrix- source-sink vector approach as previously outlined and demonstrated.

IX. APPLICATION TO BLOCK ISLAND SOUND

As a final application, the three-dimensional mass transport model has been coupled to a two-dimensional vertically-averaged tidal model for the Block Island Sound area (figure 9.1) and employed to simulate a continuous point release. The emphasis in performing this work is to show the feasibility of applying the computational system to a realistic coastal zone area.

Employing the depth contours shown in Figure 9.2 and the information contained in the first half of Table 9.1, a two-dimensional vertically-averaged tidal model employing the method of Leendertse (19) has been developed for the study area. Figures 9.3 through 9.15 show the model predictions for zero hours through twelve hours after high water at Newport, Rhode Island as well as the tidal heights for the area (note insert at the top of each figure). These predictions have been compared to existing National Ocean Survey tidal charts (71), and the general flow directions show good qualitative agreement.

To obtain a preliminary indication of the transport of material in the study area, a simple continuous point release of waste was simulated by a two-dimensional vertically-averaged concentration model (72) from a proposed discharge site in Charlestown, Rhode Island.

TABLE 9.1

TIDAL HYDRODYNAMIC AND MASS TRANSPORT MODEL INPUTS FOR BLOCK ISLAND SOUND

HYDRODYNAMICS	
GRID SPACING	$\Delta X = \Delta Y = 6076$ FT
TIME STEP	$\Delta t = 124.2$ SEC
MANNING ROUGHNESS	.025
BOUNDARY CONDITIONS	INPUT TIDAL HEIGHTS ON OPEN BOUNDARIES
DEPTH	SEE FIGURE 9.2
MASS TRANSPORT	
GRID SPACING	$\Delta X = \Delta Y = 6076$ FT
TIME STEP	$\Delta t = 496.8$ (TWO DIMENSIONAL VERTICALLY AVERAGED MODEL)
	$\Delta t = 1863.0$ (THREE DIMENSIONAL MODEL)
DISPERSION COEFFICIENT	$D_x = D_y = 35$ FT^2/SEC
	$D_z = .002 - .01$ (PARABOLIC PROFILE) FT.^{2}/SEC.
POINT SOURCE	4,685,776 LBS/DAY AT MID DEPTH (THREE DIMENSIONAL)
VELOCITY	FROM HYDRODYNAMICS MODEL WITH CYCLE USE OF THE PREDICTED TIDAL CYCLE

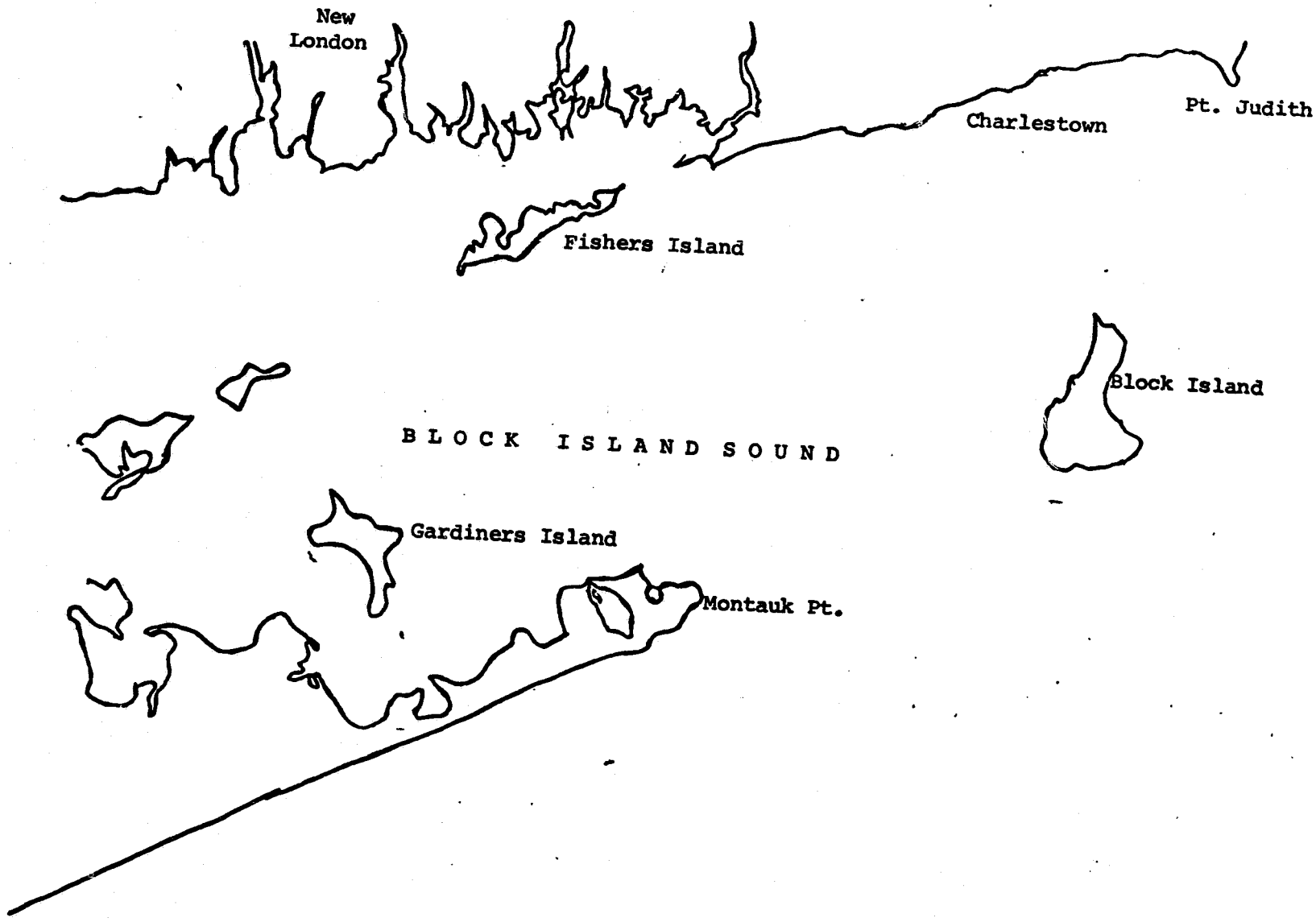

FIGURE 9.1 Block Island Sound Study Area

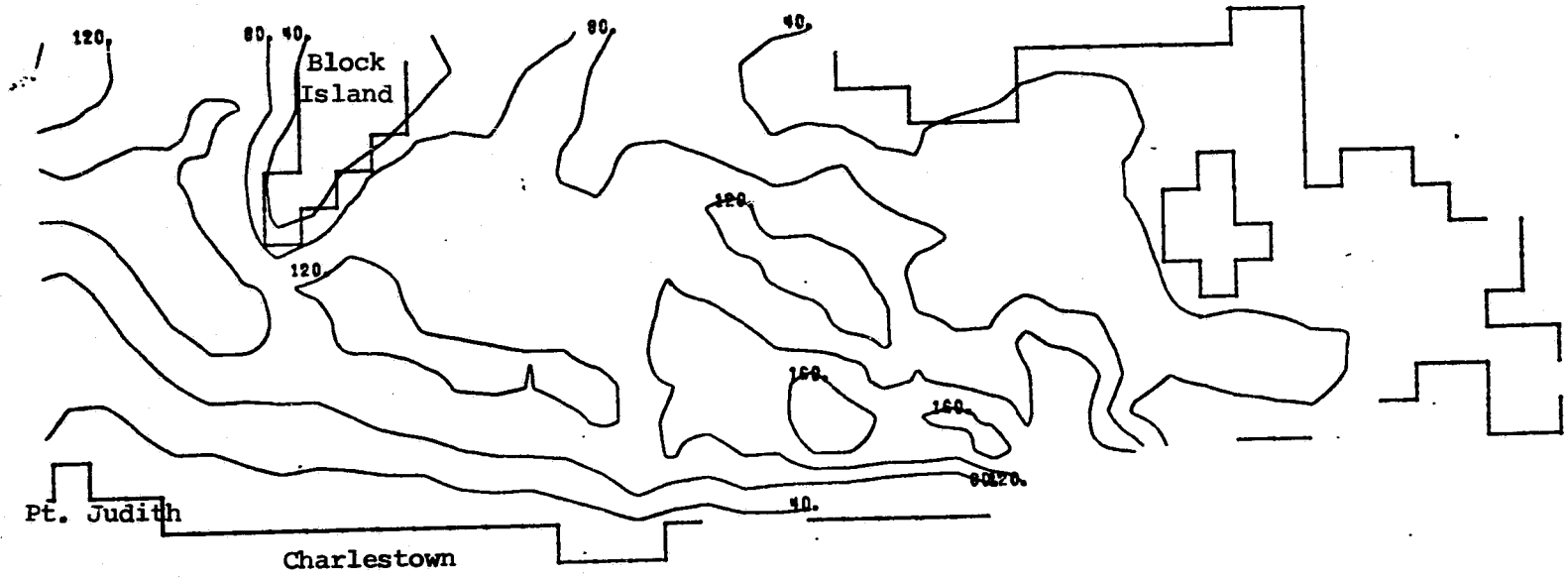

FIGURE 9.2. Depth Contours for Block Island Sound (40 Ft. Intervals)

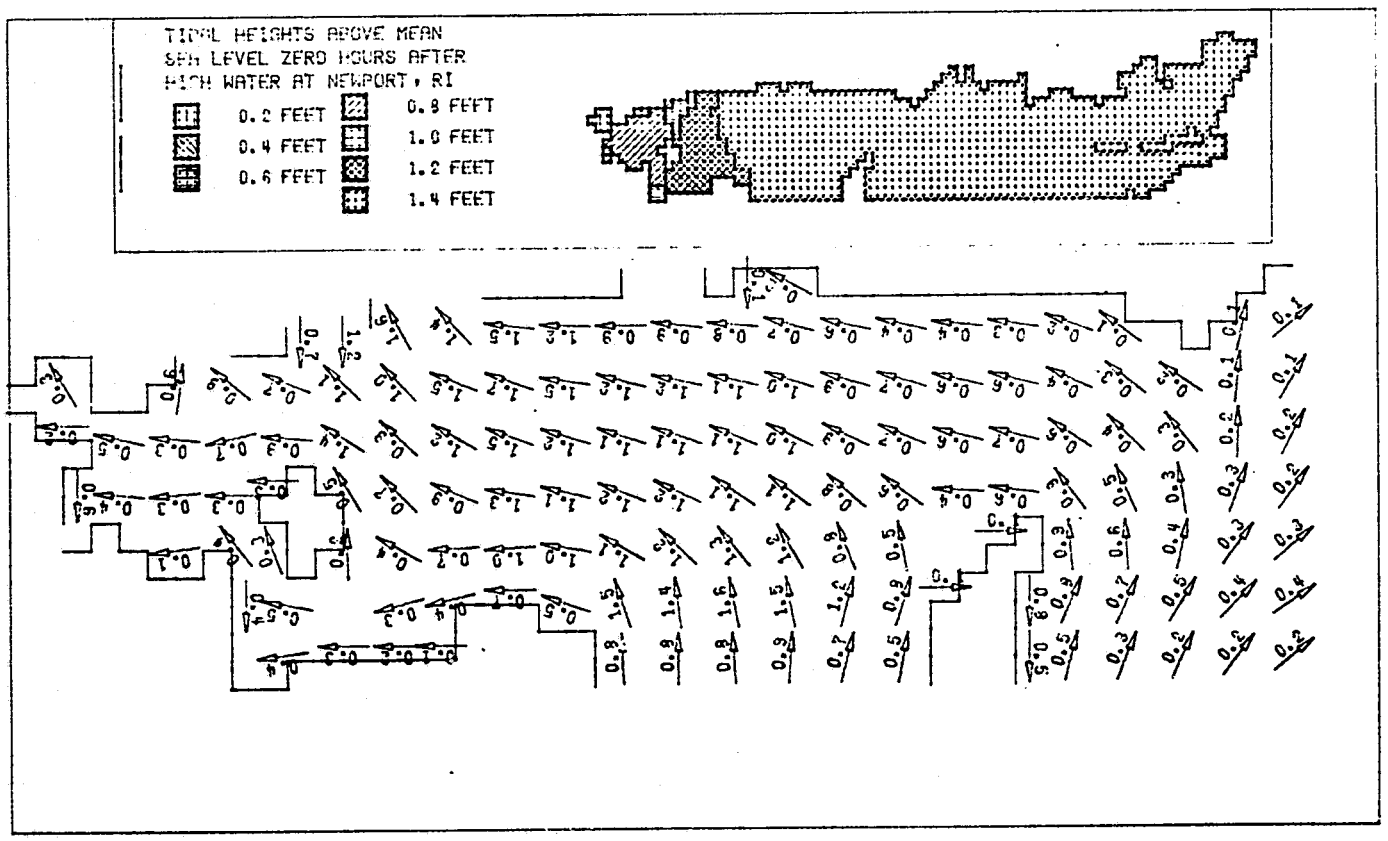

FIGURE 9.3 **Tidal Currents for Block Island Sound in Knots Zero Hours After High Water at Newport, RI.**

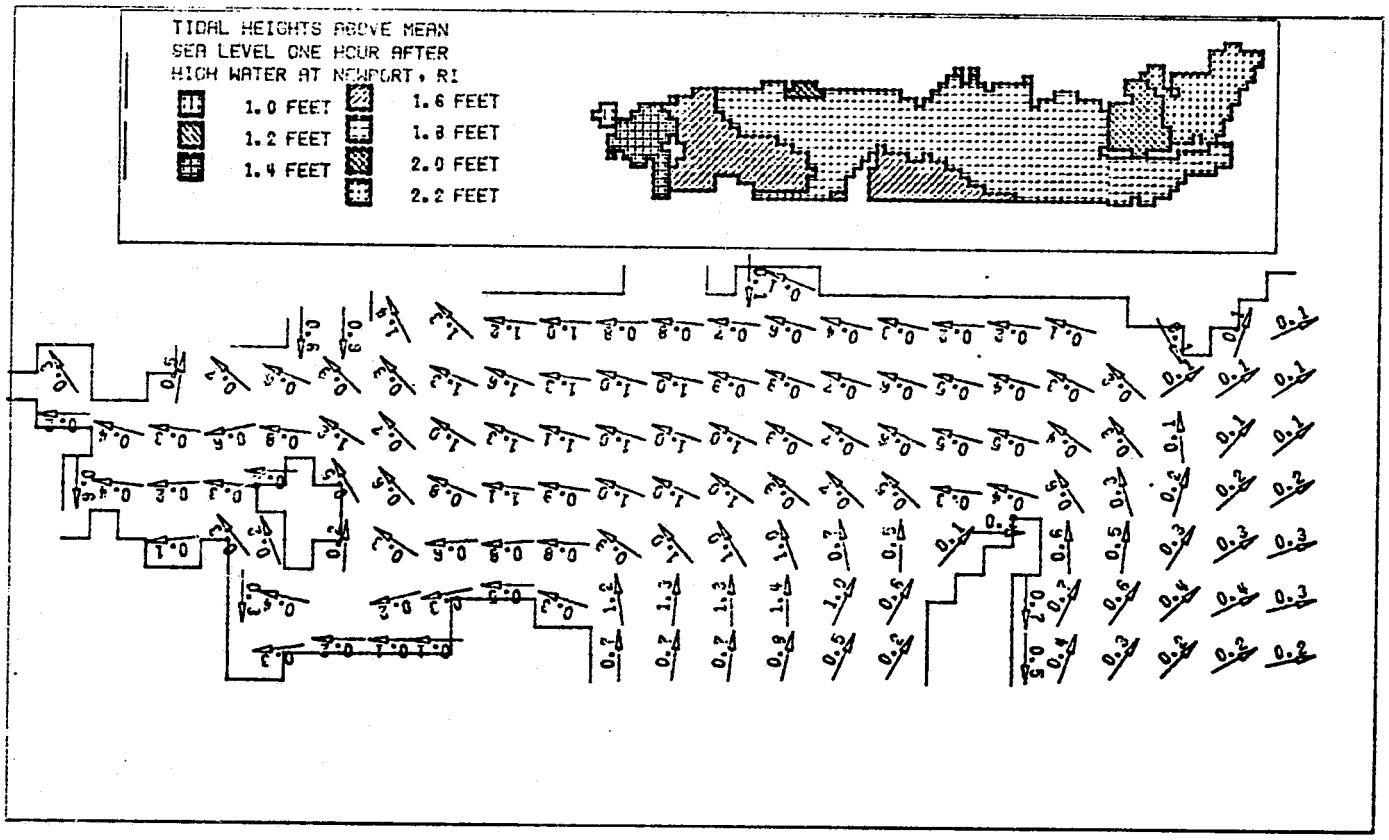

FIGURE 9.4 **Tidal Currents for Block Island Sound in Knots One Hour After High Water at Newport, RI**

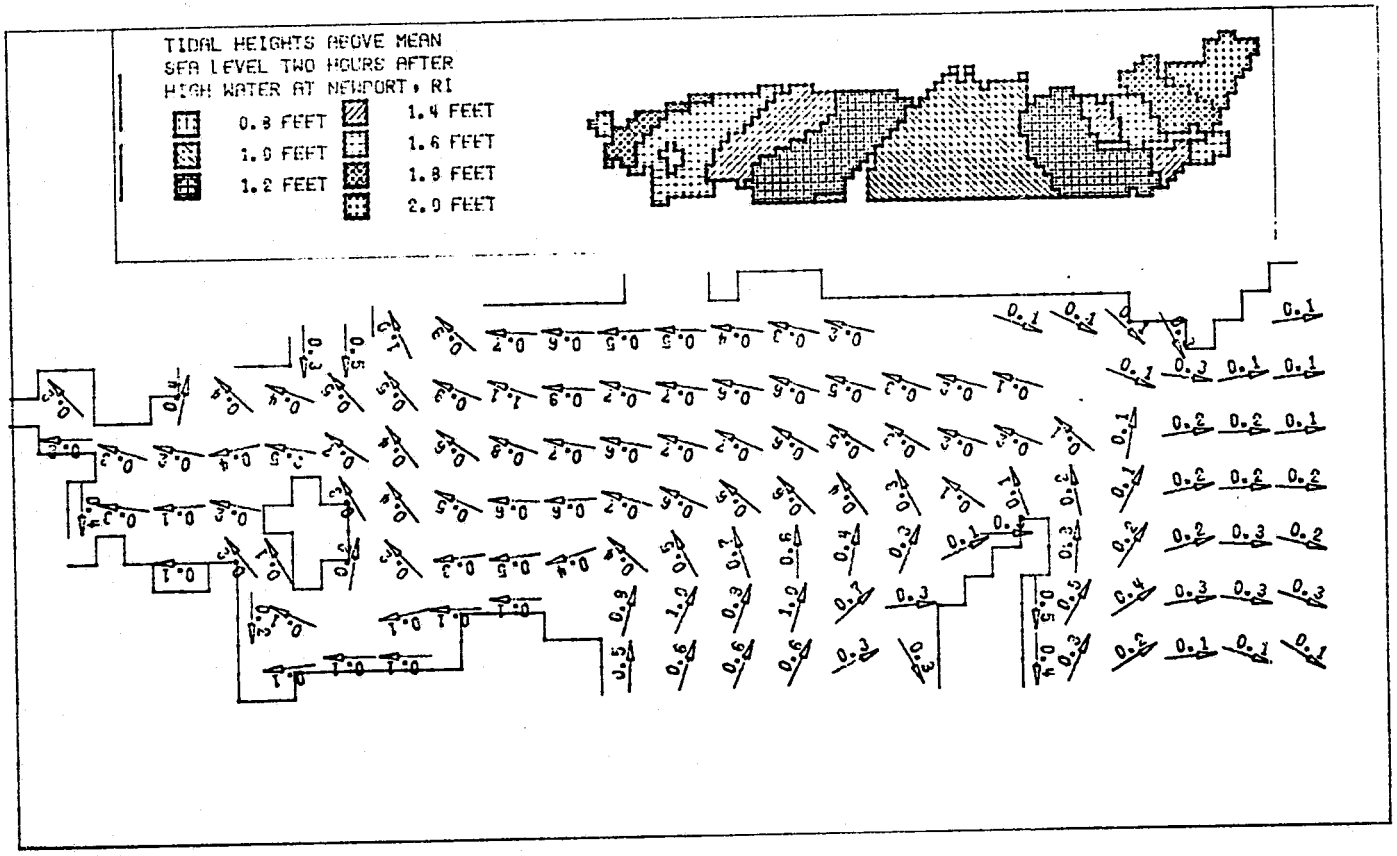

FIGURE 9.5 Tidal Currents for Block Island Sound in Knots Two Hours After High Water at Newport, RI.

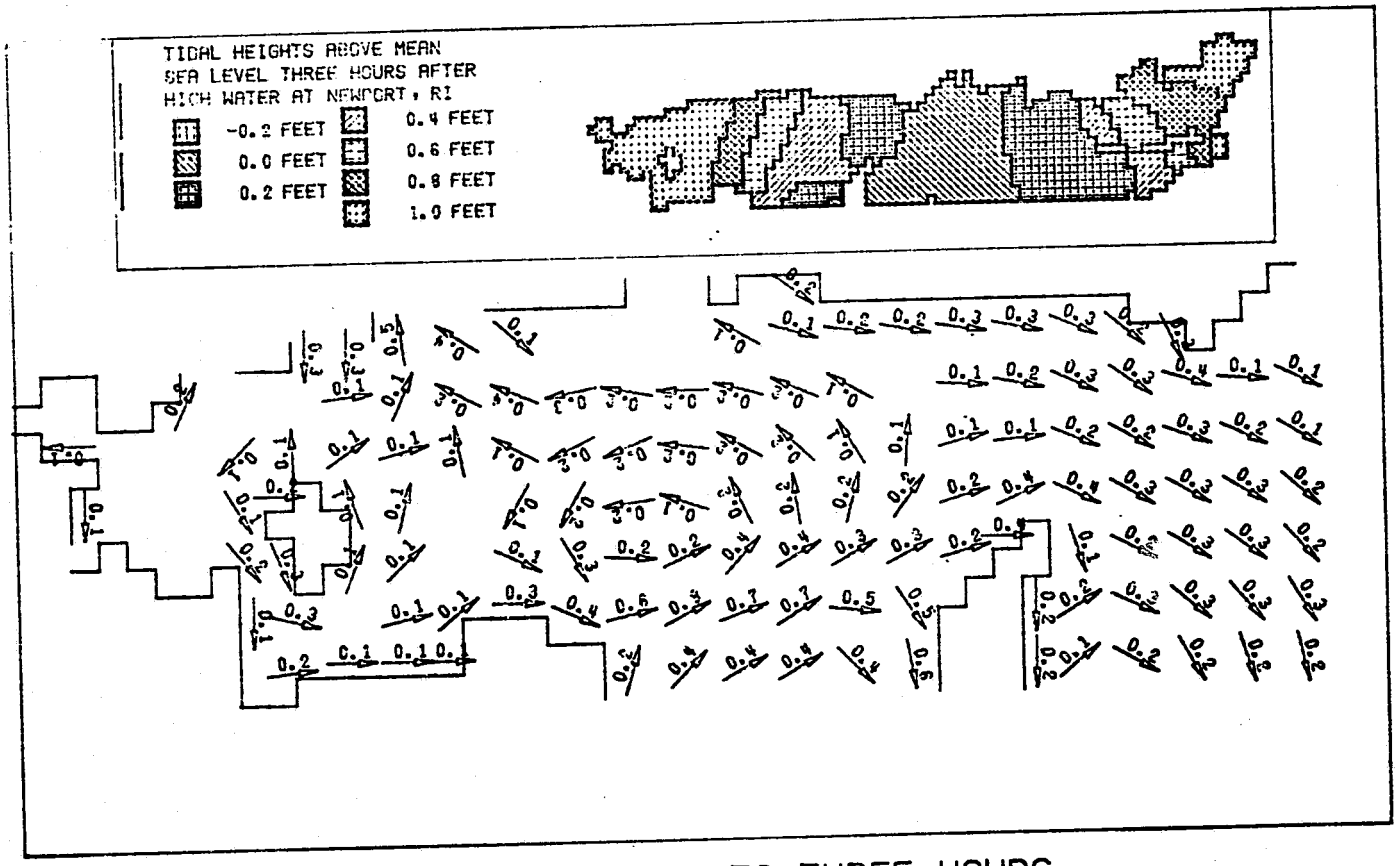

FIGURE 9.6 Tidal Currents for Block Island Sound in Knots Three Hours After High Water at Newport, RI

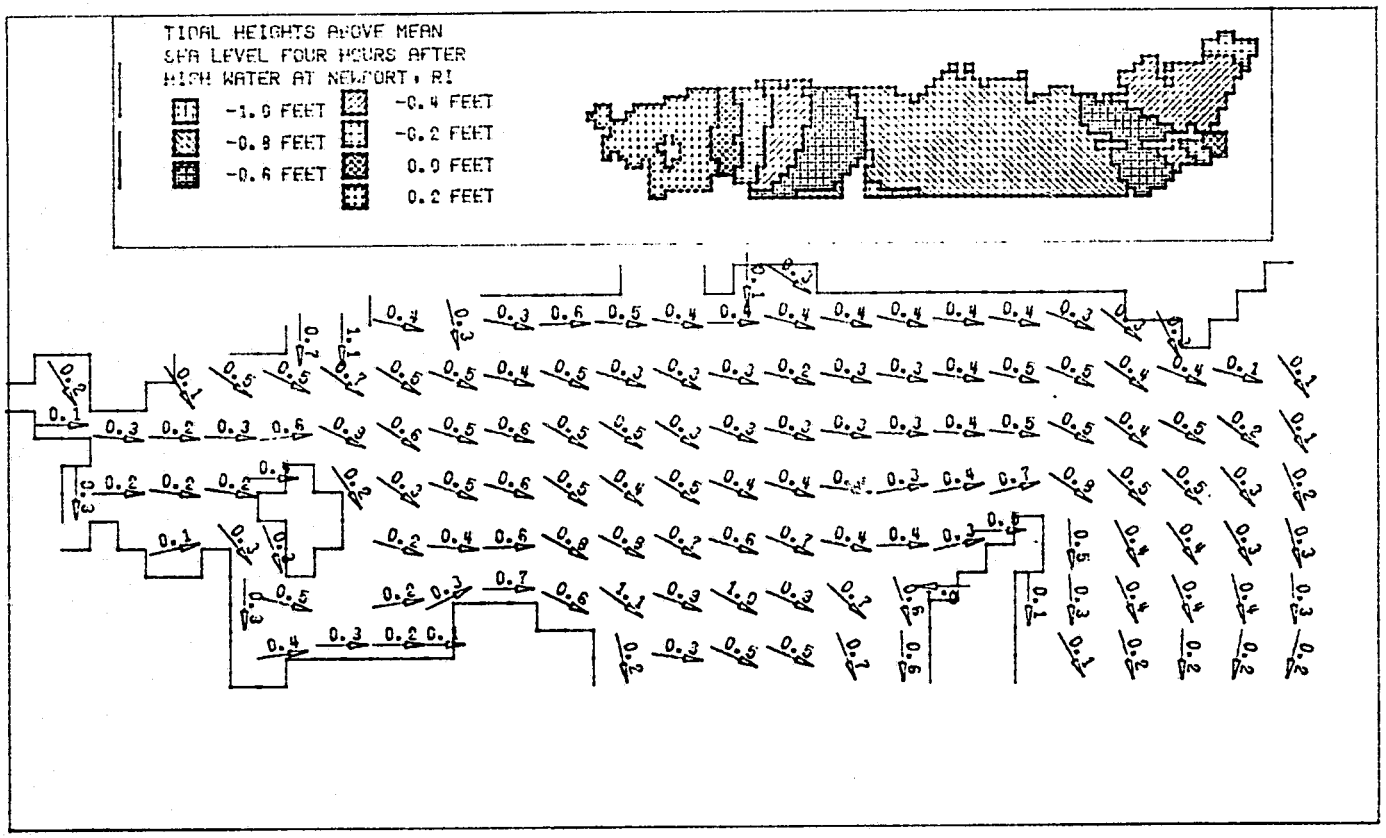

FIGURE 9.7 Tidal Currents for Block Island Sound in Knots Four Hours After High Water at Newport, RI

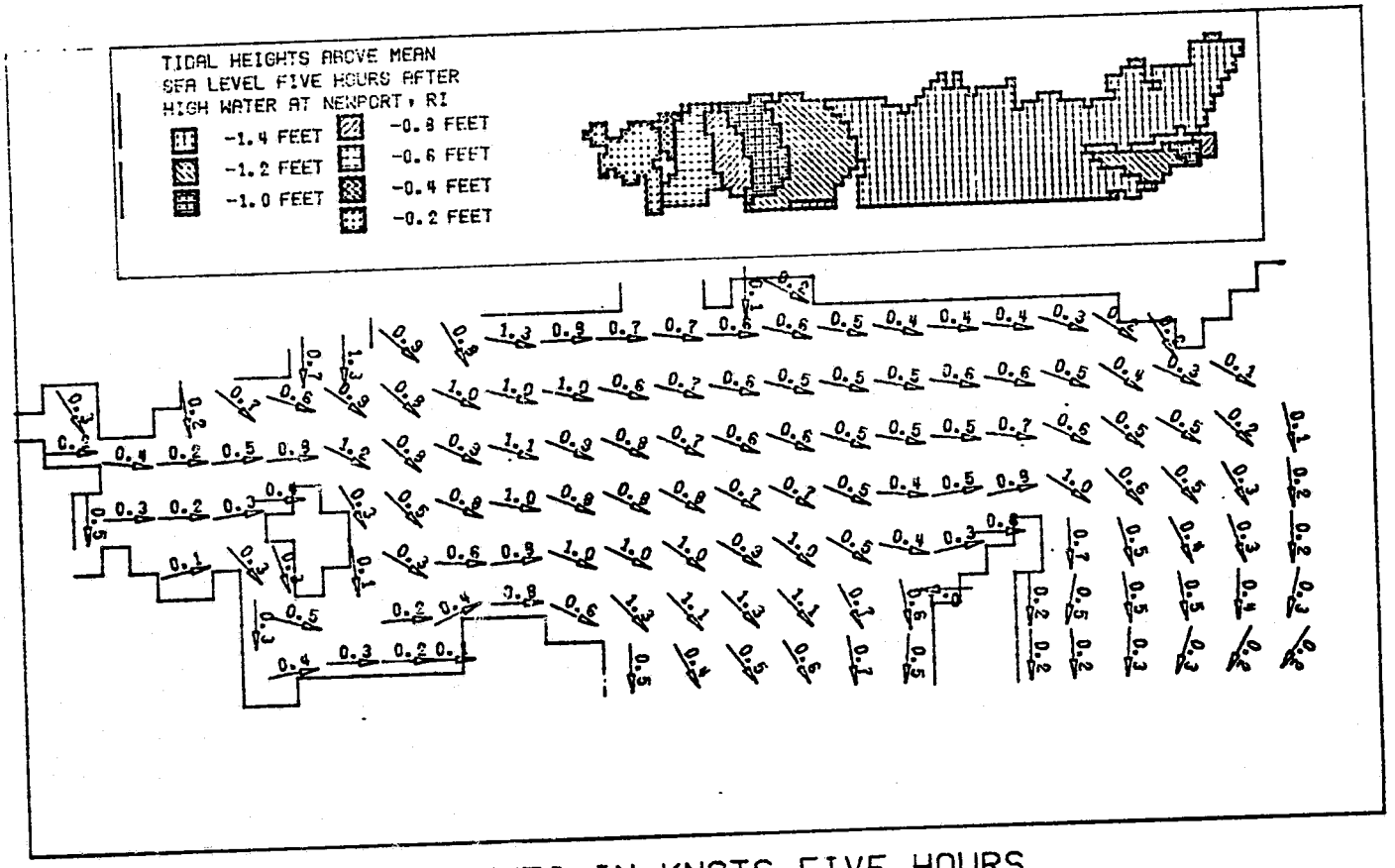

FIGURE 9.8 Tidal Currents for Block Island Sound in Knots Five Hours After High Water at Newport, RI

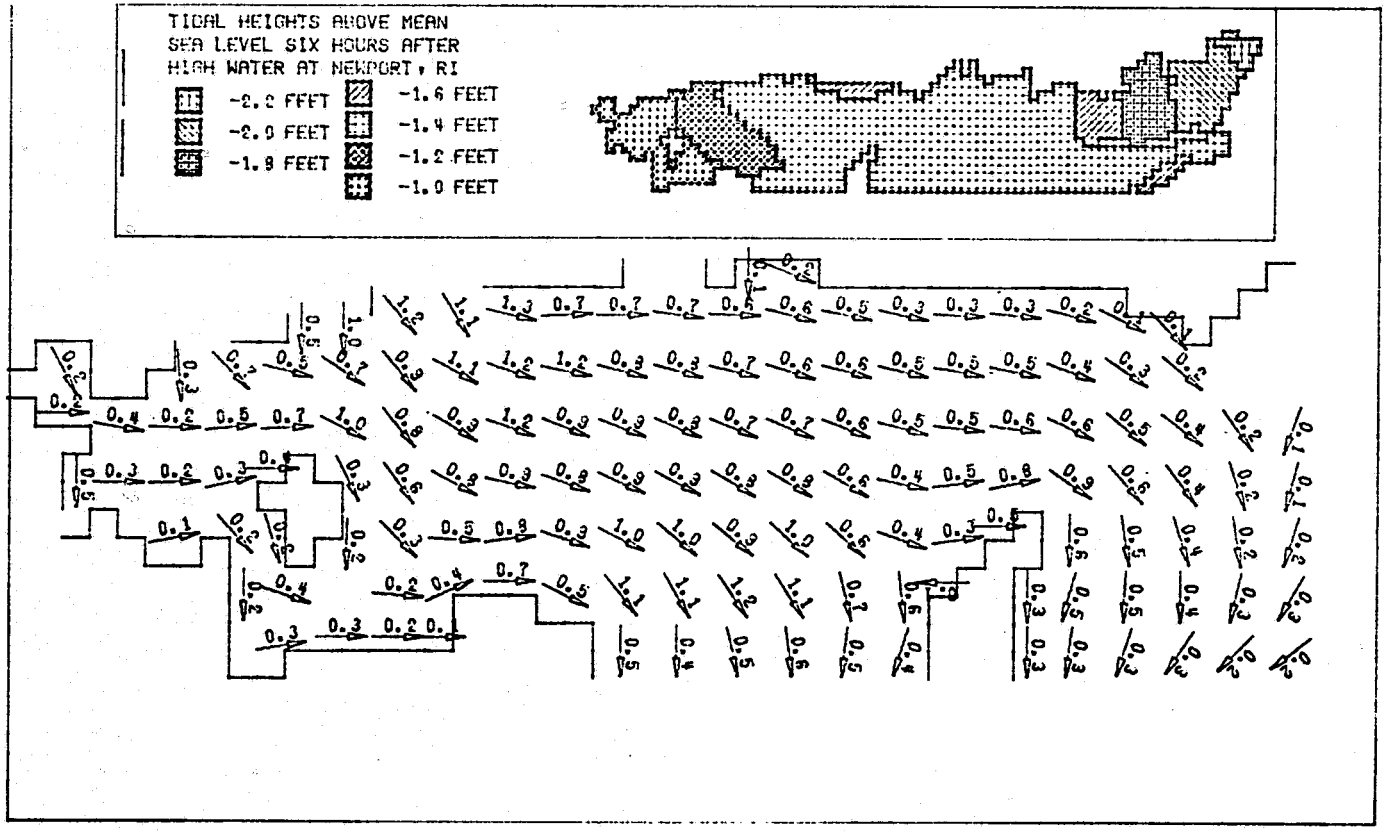

FIGURE 9.9 **Tidal Currents for Block Island Sound in Knots Six Hours After High Water at Newport, RI**

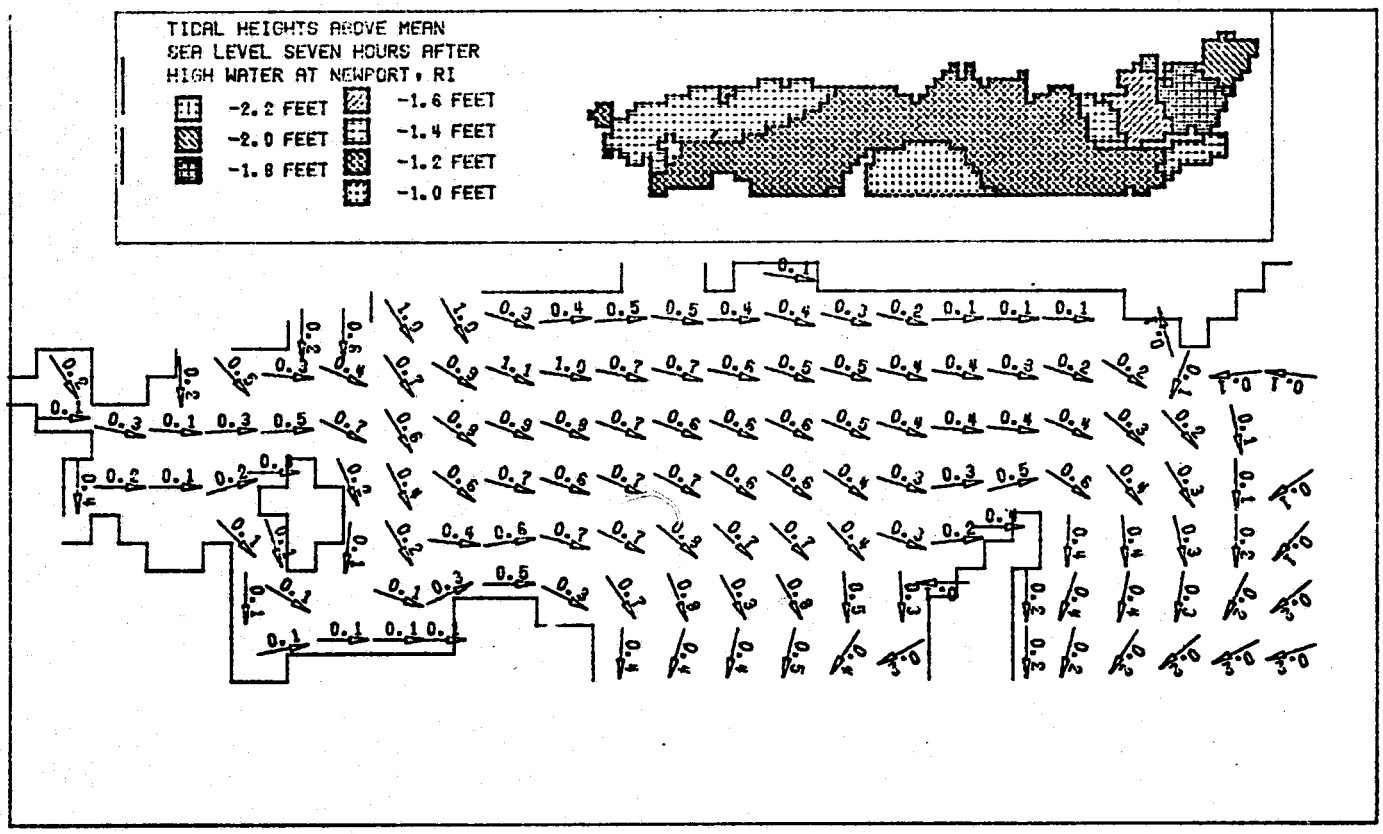

FIGURE 9.10 **Tidal Currents for Block Island Sound Seven Hours After High Water at Newport, RI**

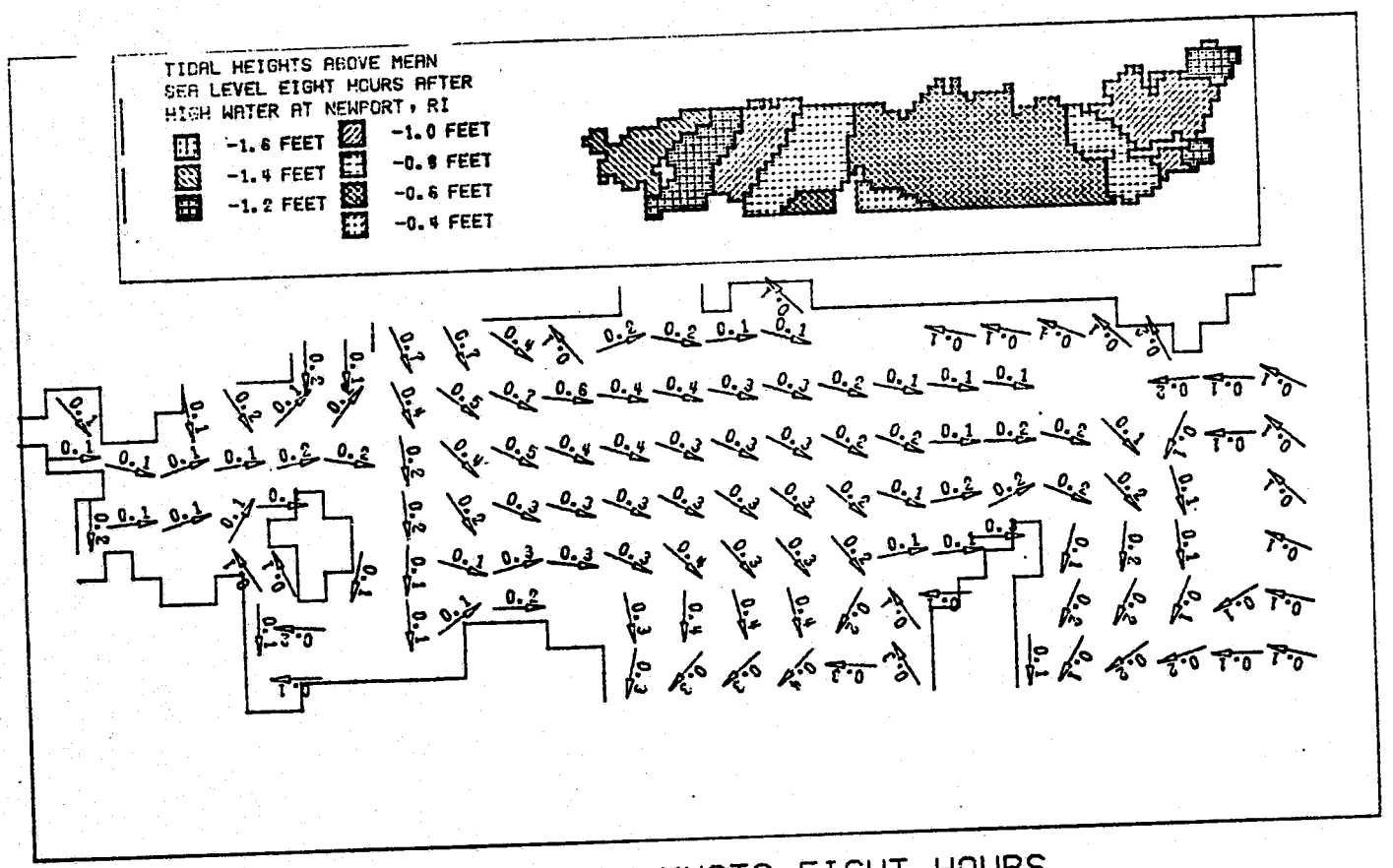

FIGURE 9.11 Tidal Currents for Block Island Sound in Knots Eight Hours After High Water at Newport, RI

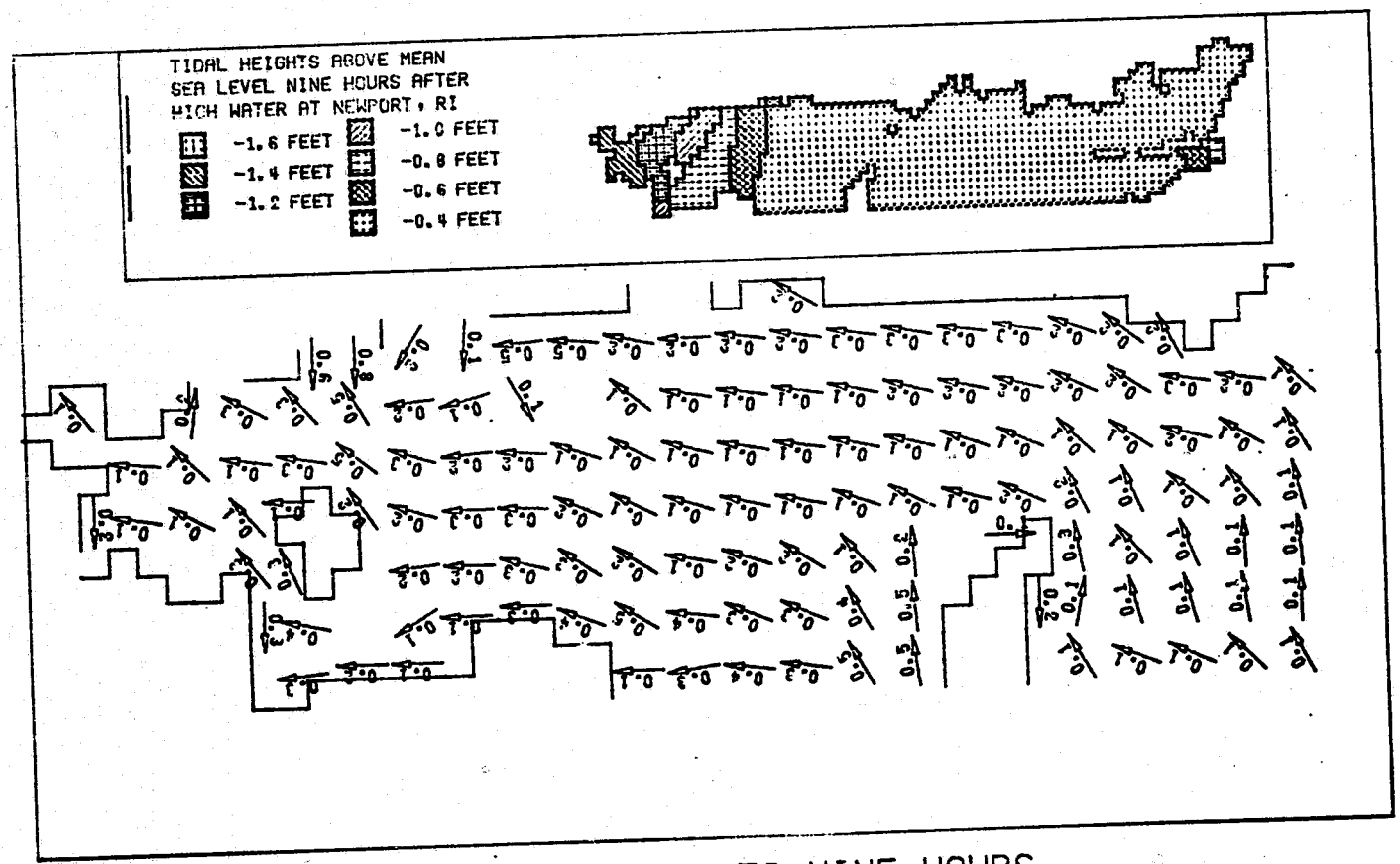

FIGURE 9.12 **Tidal Currents for Block Island Sound in Knots Nine Hours After High Water at Newport, RI**

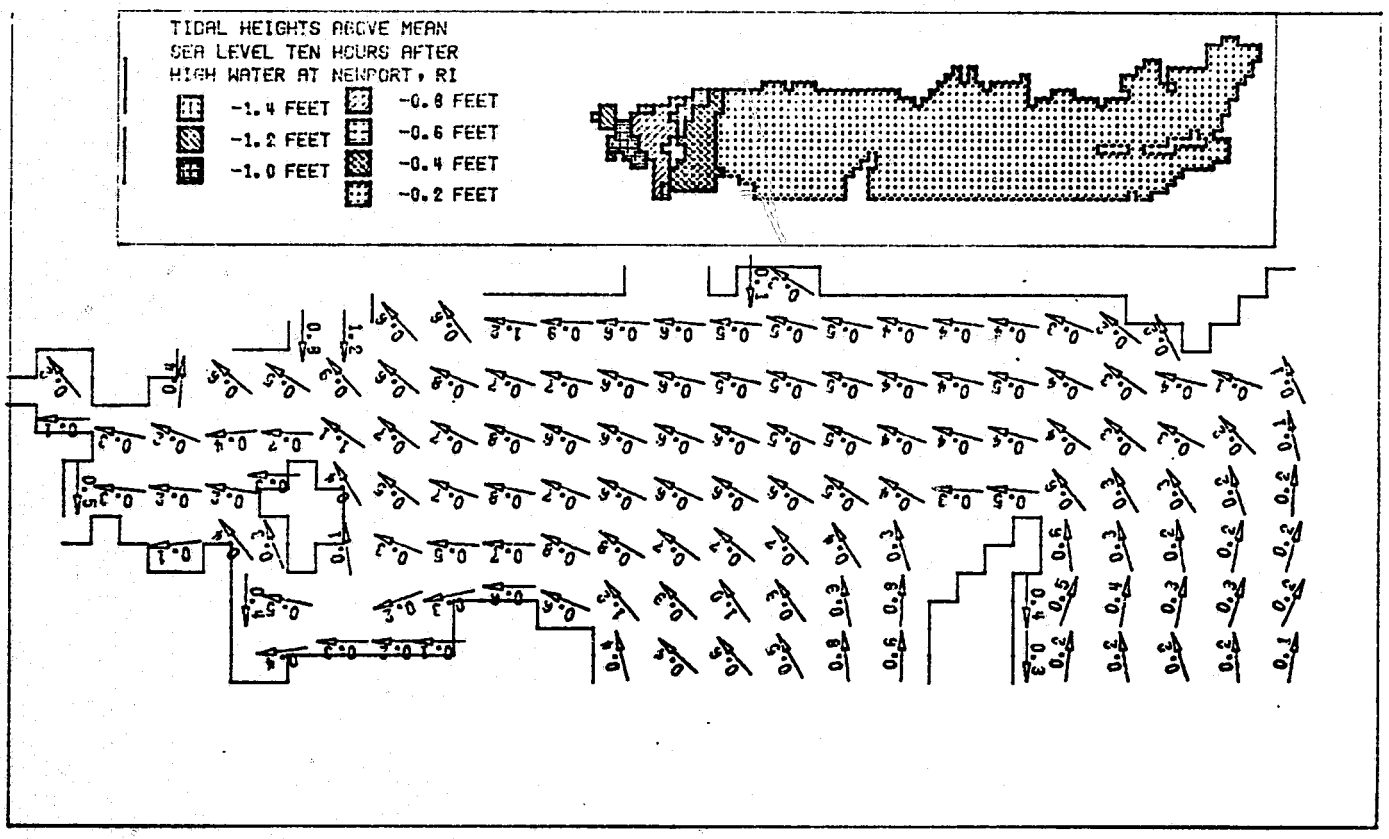

FIGURE 9.13 **Tidal Currents for Block Island Sound in Knots Ten Hours After High Water at Newport, RI**

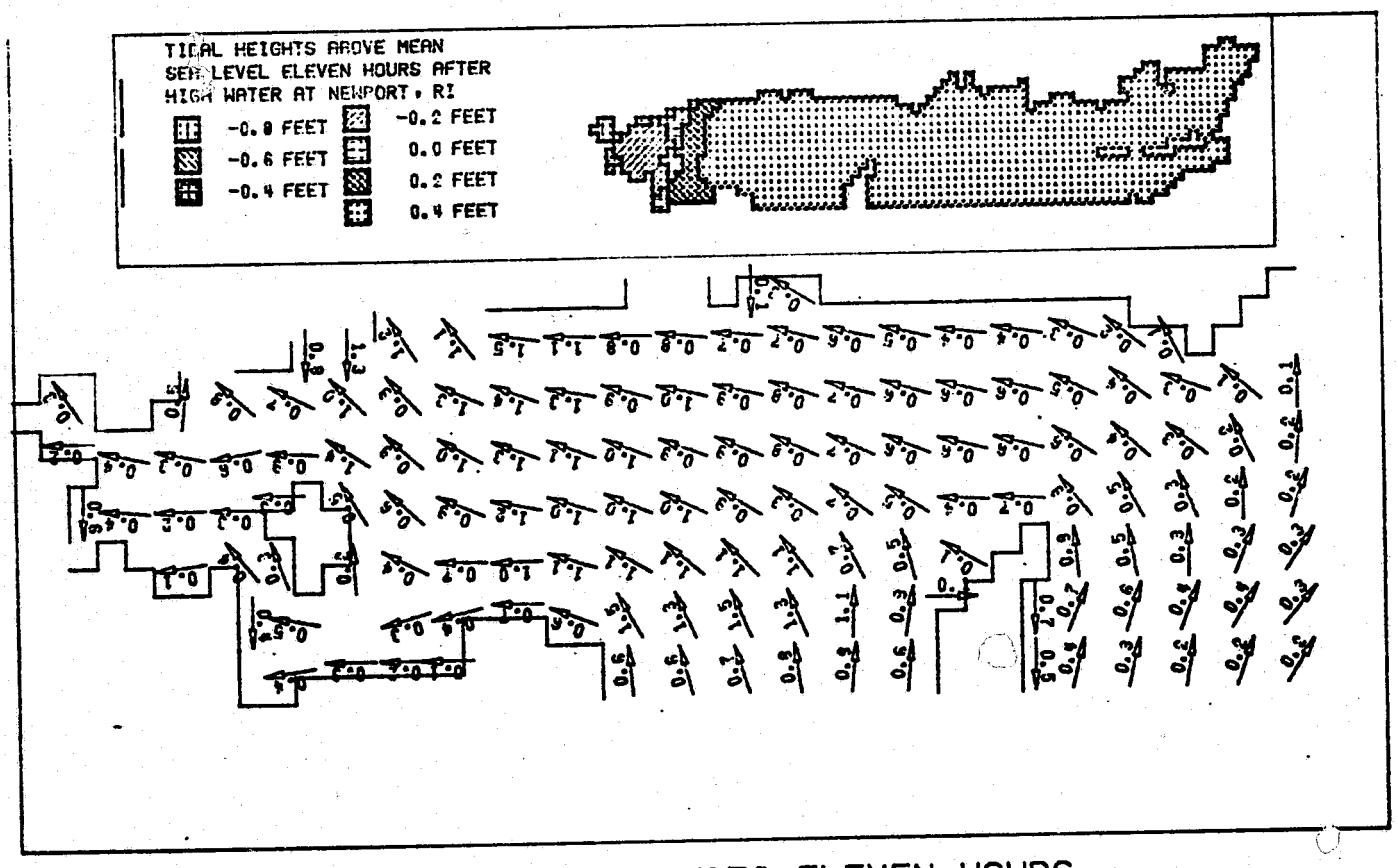

FIGURE 9.14 Tidal Currents for Block Island Sound in Knots Eleven Hours After High Water at Newport, RI

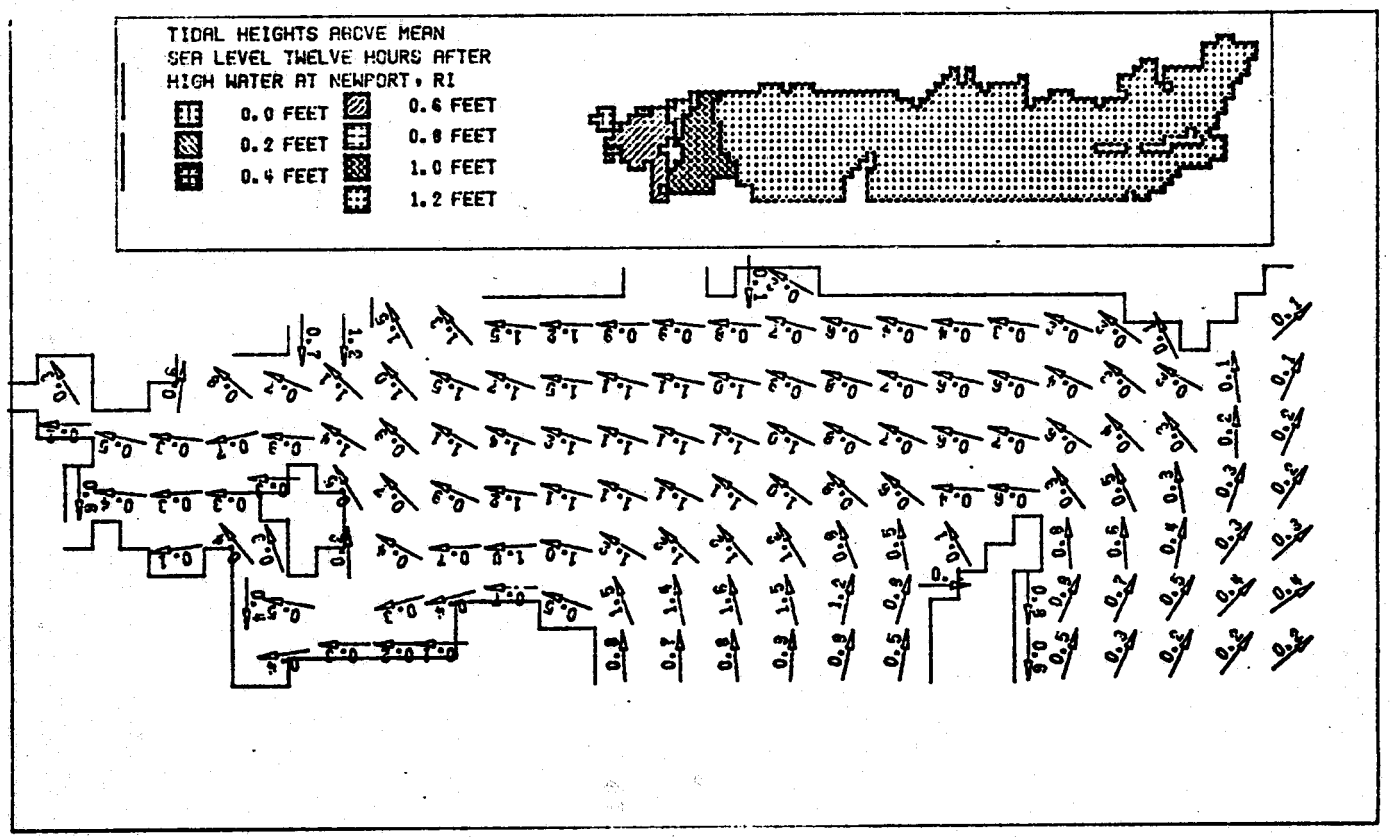

FIGURE 9.15 **Tidal Currents for Block Island Sound in Knots Twelve Hours After High Water at Newport, RI**

Figures 9.16 through 9.30 show model predictions for one through thirteen hours after high water at Newport in hourly increments. Figure 9.29 shows the concentrations at 5 tidal cycles after discharge began at approximately slack water. As expected from observing the velocity field, the waste cloud displays a predominantly along-the-shore motion that responds directly to the flooding and ebbing of the current in the area. The increase in concentration in the outfall area is easily seen.

Using essentially the same input as for the two-dimensional vertically-averaged concentration model (see Table 9.1) the three-dimensional mass transport model was used to simulate the same release, but the waste was discharged at mid-depth. Figures 9.30 through 9.34 present concentration contours at nondimensional levels 2 (at sea bottom) through 6 (sea surface) for one hour after high water at Newport. The vertical distribution of waste is clearly seen. Figures 9.35 through 9.39 show similar plots for six hours after discharge began, while Figures 9.40 through 9.44 give the concentration distribution at twelve hours after waste release. The vertical stratification and increase in concentration with time are readily apparent. Comparison of the three-dimensional predictions to the vertically-averaged case show similar behavior with predominant along-the-shore pollutant transport. Results of these three-dimensional predictions indicate

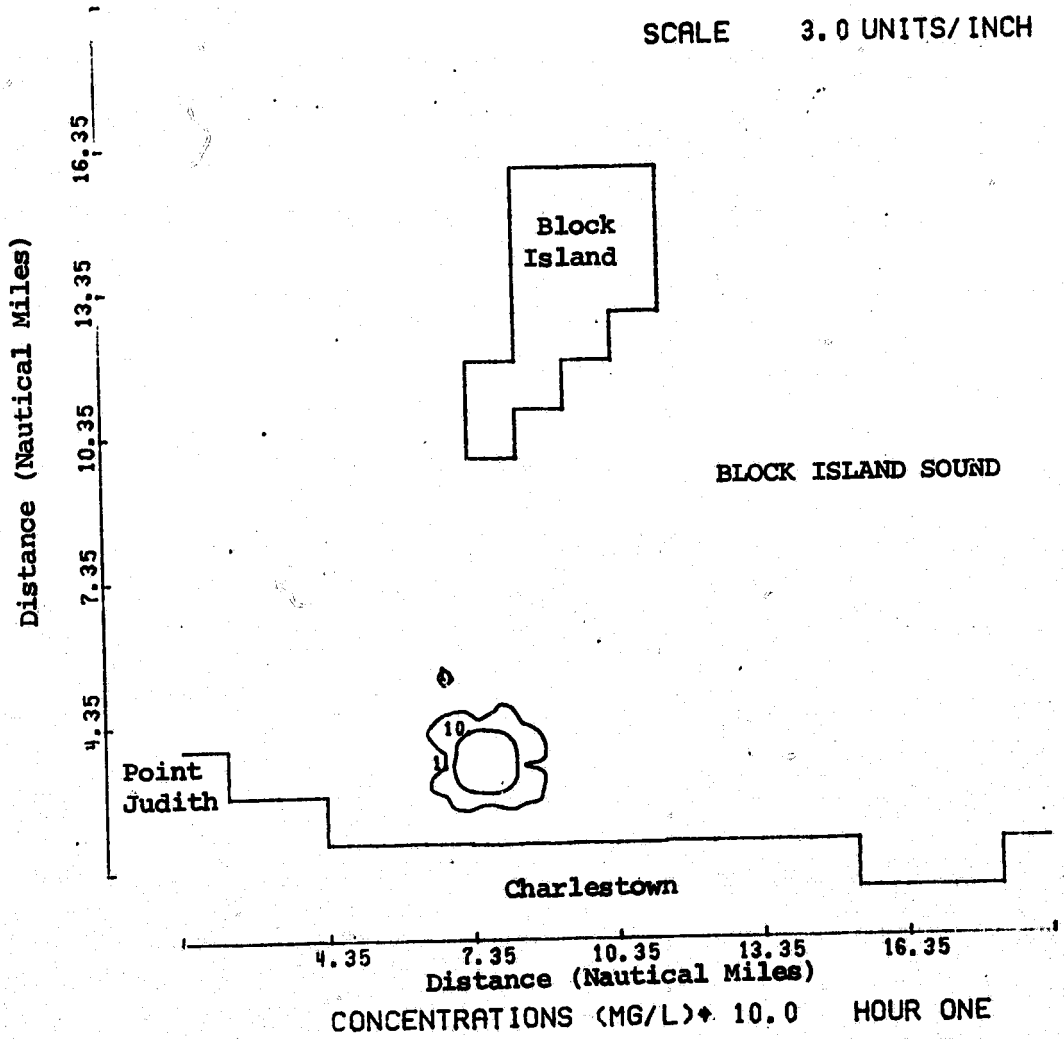

FIGURE 9.16 Concentration (mg/l) Contours for Continuous Release Predicted by Vertically Averaged Concentration Model One Hour After High Water at Newport, R.I.

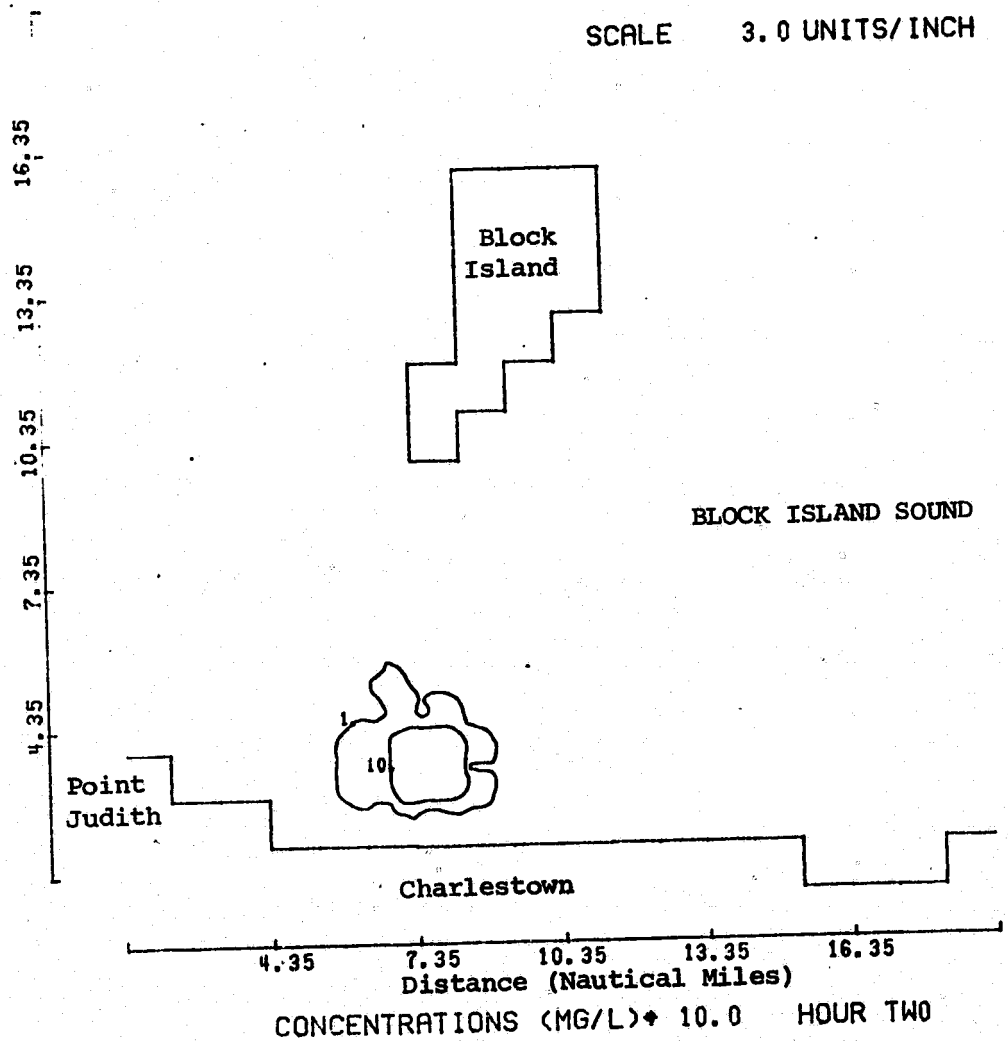

FIGURE 9.17 Concentration (mg/l) Contours for Continuous Release Predicted by Vertically Averaged Concentration Model Two Hours After High Water at Newport, R.I.

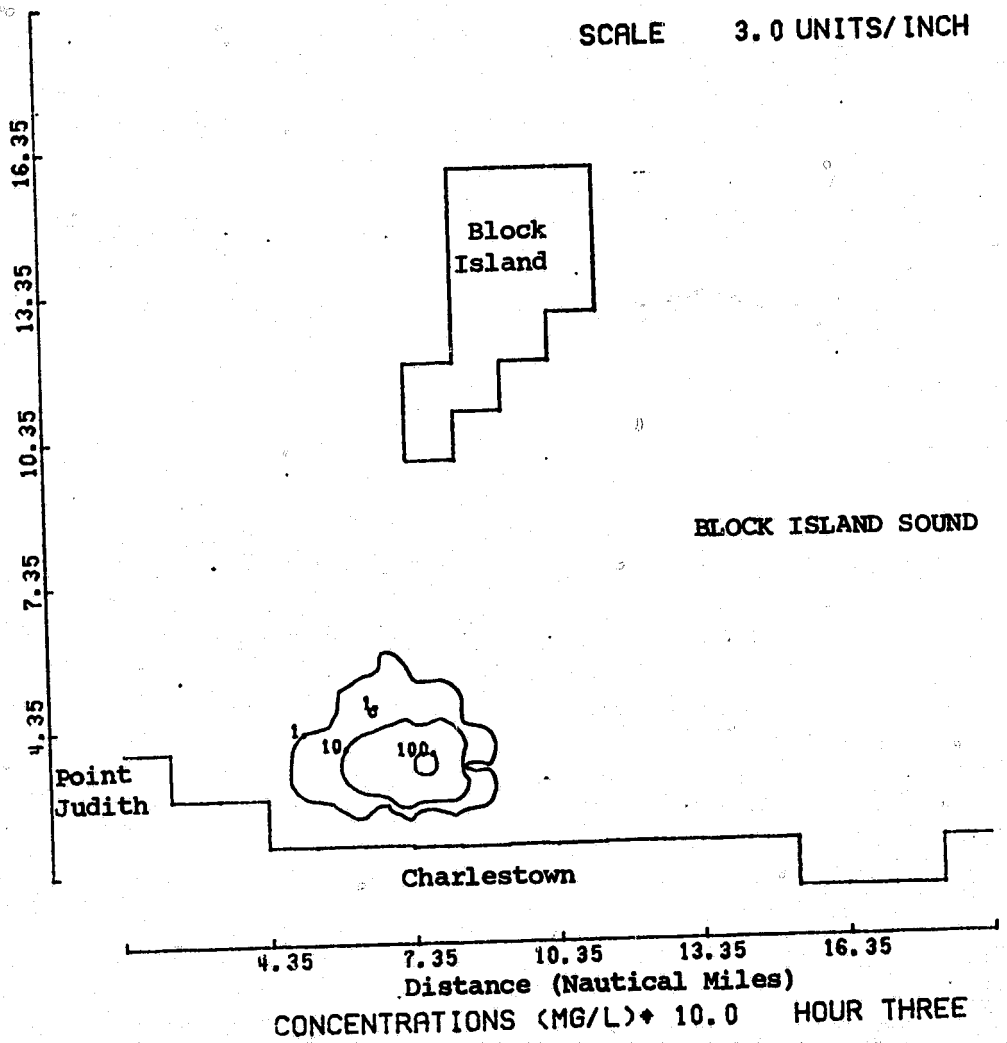

FIGURE 9.18 Concentration (mg/l) Contours for Continuous Release Predicted by Vertically Averaged Concentration Model Three Hours After High Water at Newport, R.I.

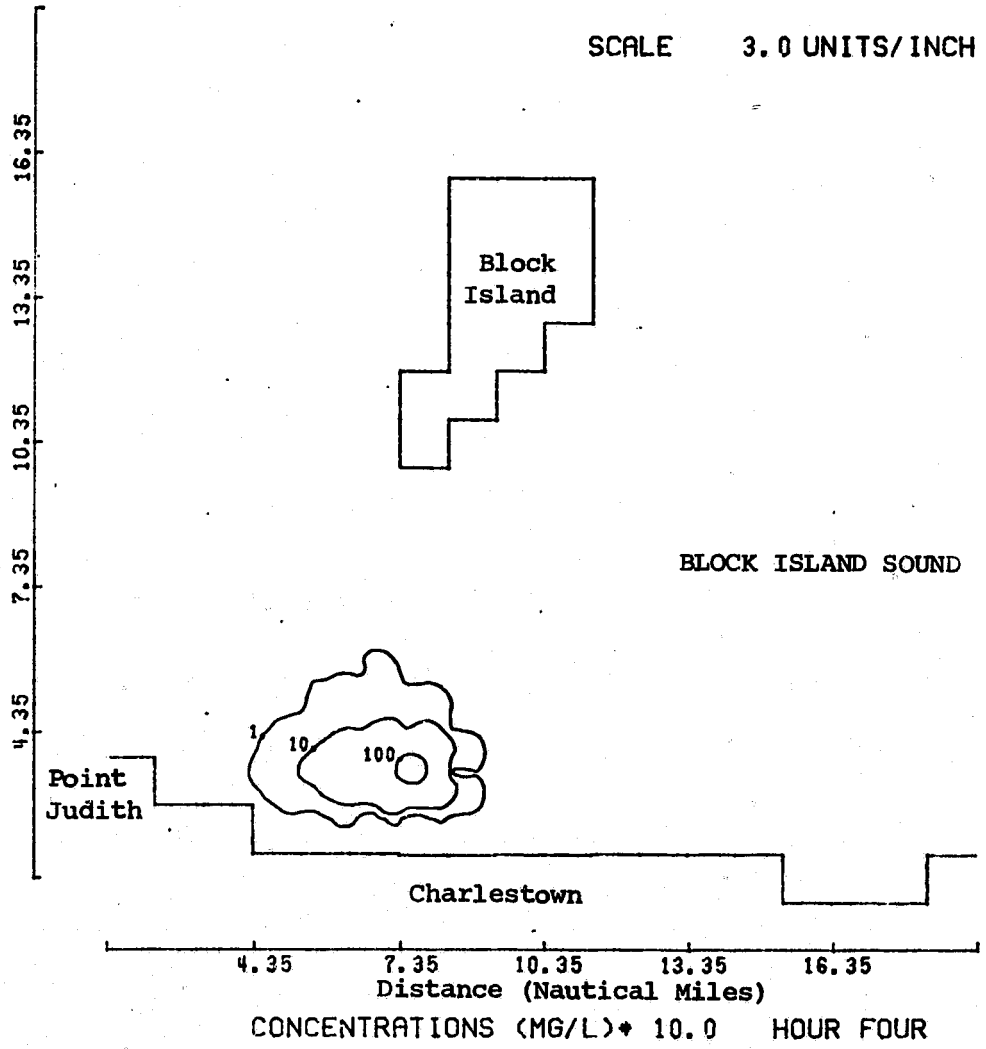

FIGURE 9.19 Concentration (mg/l) Contours for Continuous Release Predicted by Vertically Averaged Concentration Model Four Hours After High Water at Newport, R.I.

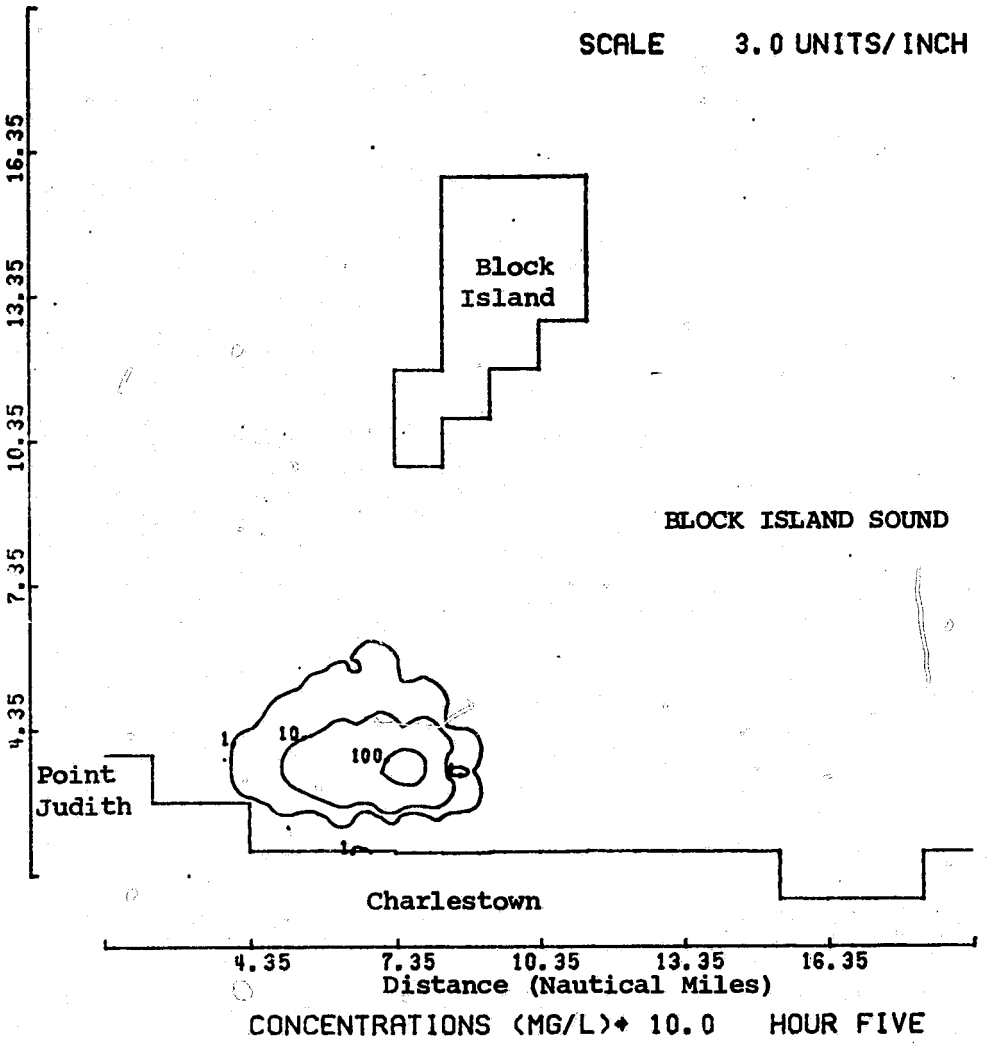

FIGURE 9.20 Concentration (mg/l) Contours for Continuous Release Predicted by Vertically Averaged Concentration Model Five Hours After High Water at Newport, R.I.

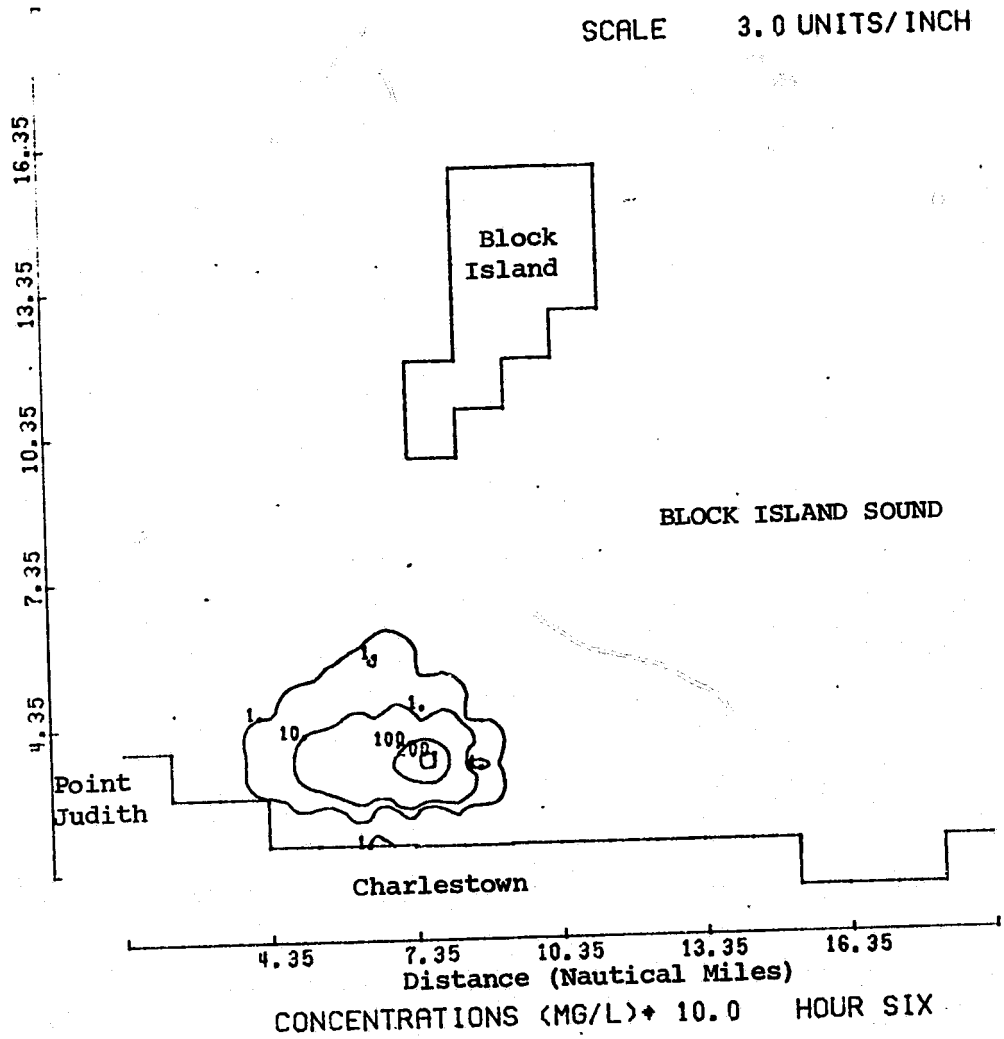

FIGURE 9.21 Concentration (mg/l) Contours for Continuous Release Predicted by Vertically Averaged Concentration Model Six Hours After High Water at Newport, R.I.

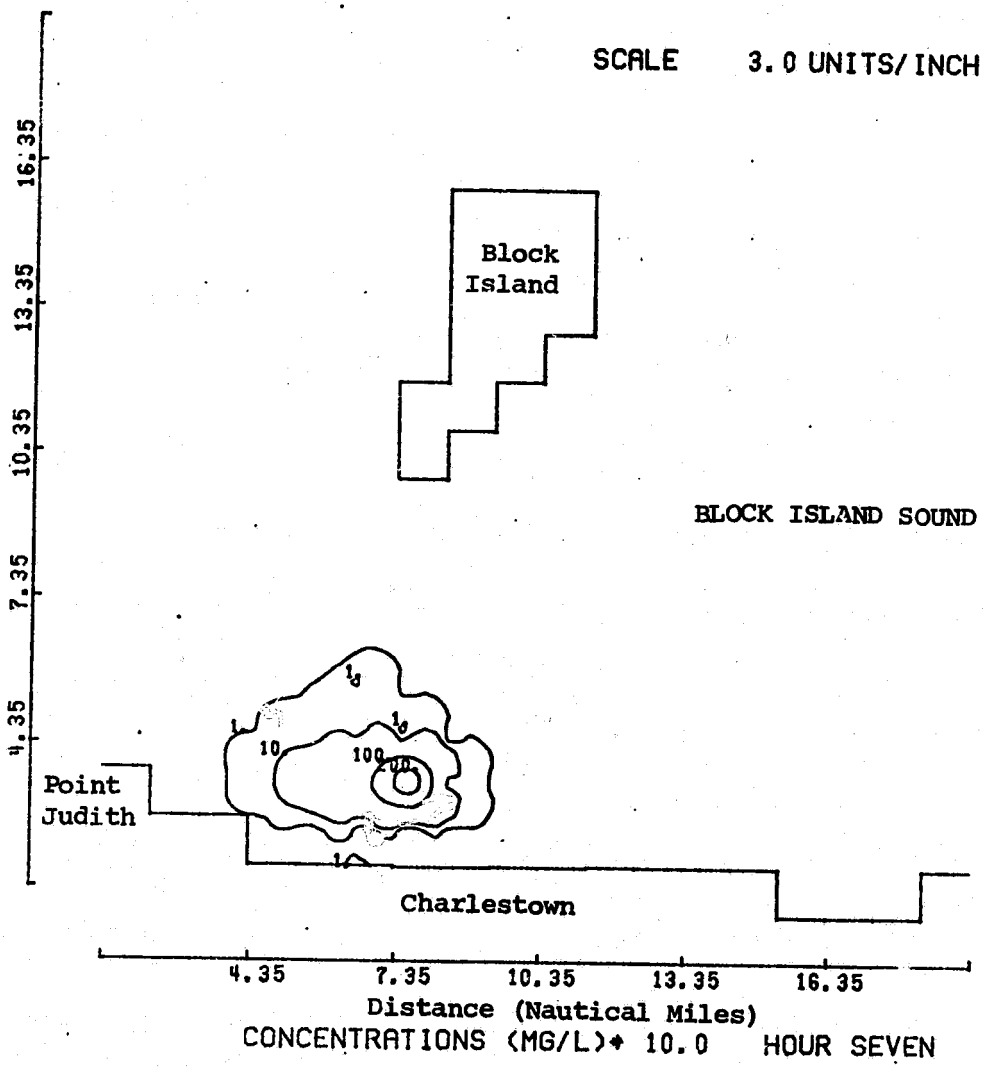

FIGURE 9.22 Concentration (mg/l) Contours for Continuous Release Predicted by Vertically Averaged Concentration Model Seven Hours After High Water at Newport, R.I.

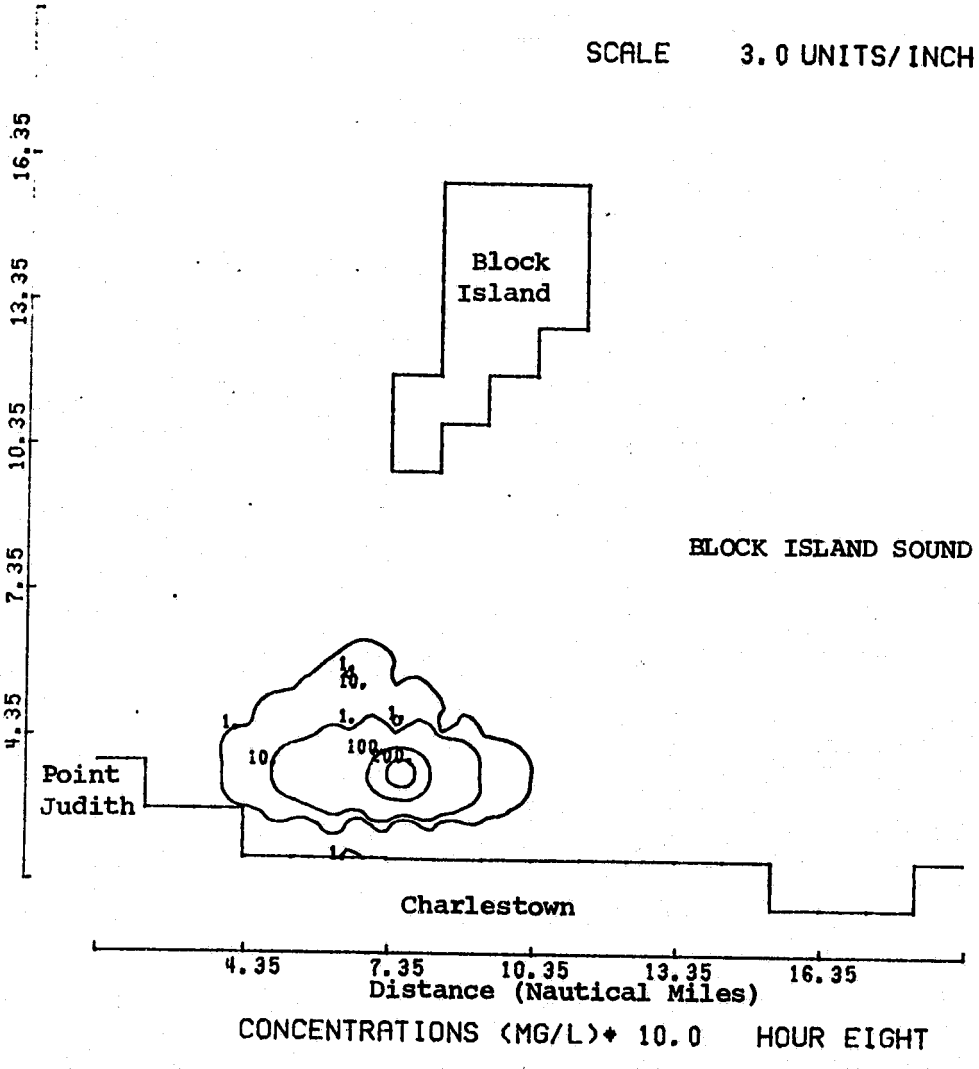

FIGURE 9.23 Concentration (mg/l) Contours for Continuous Release Predicted by Vertically Averaged Concentration Model Eight Hours After High Water at Newport, R.I.

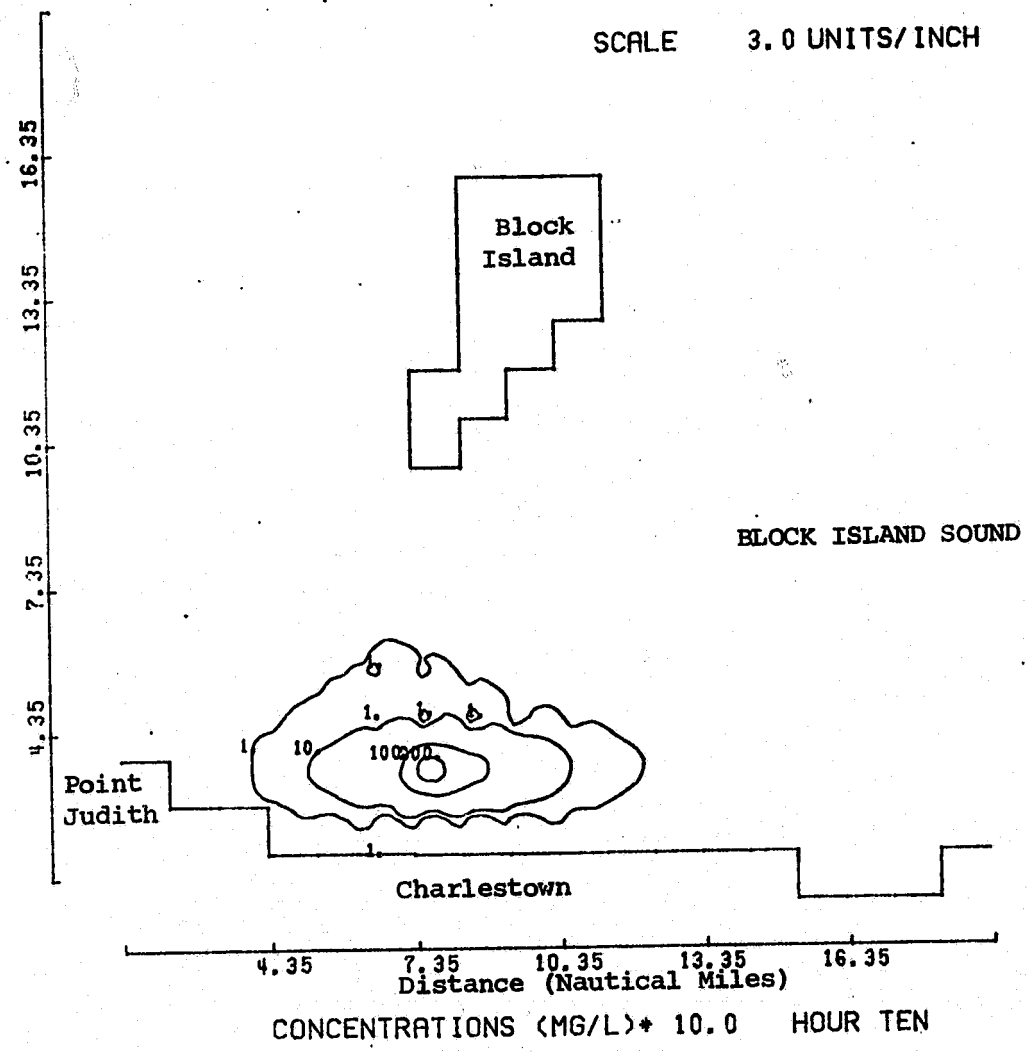

FIGURE 9.25 Concentration (mg/l) Contours for Continuous Release Predicted by Vertically Averaged Concengration Model Ten Hours After High Water at Newport, R.I.

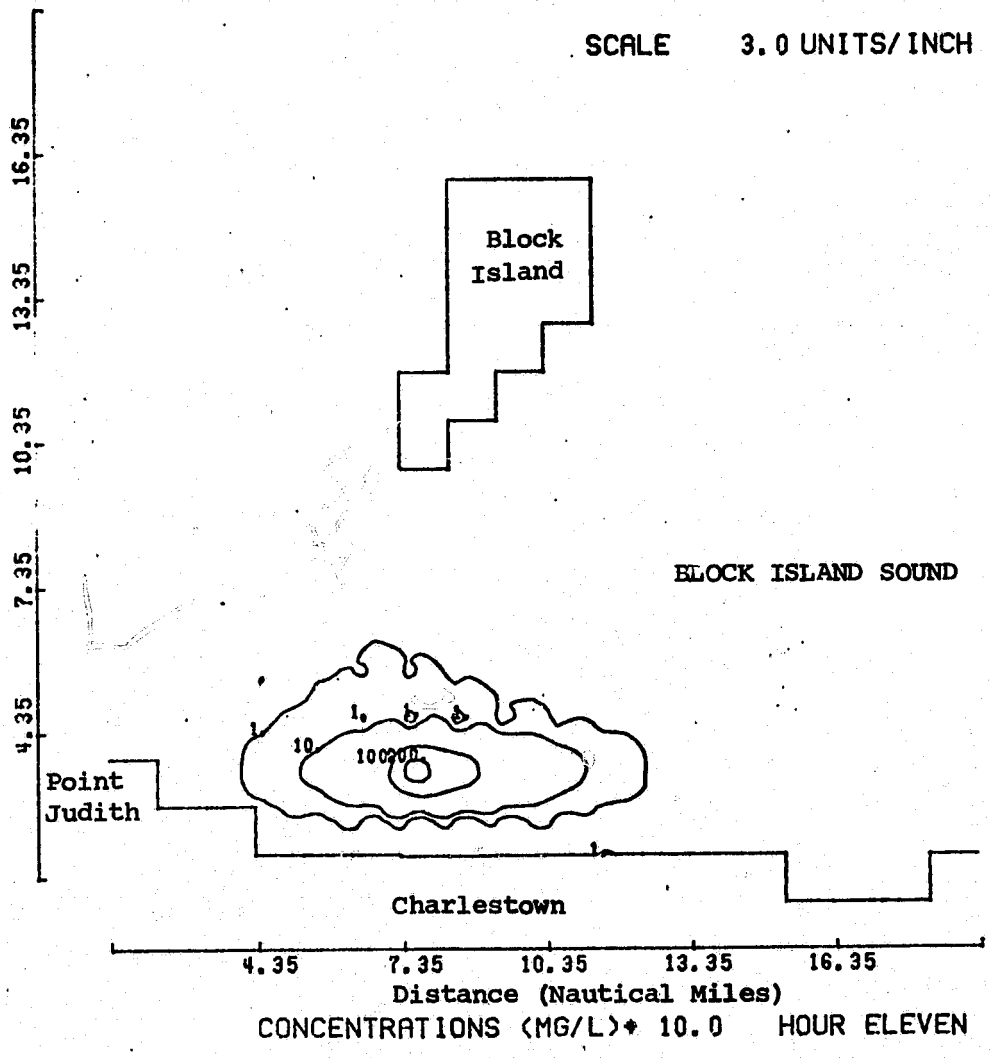

FIGURE 9.26 **Concentration (mg/l) Contours for Continuous Release Predicted by Vertically Averaged Concentration Model Eleven Hours After High Water at Newport, R.I.**

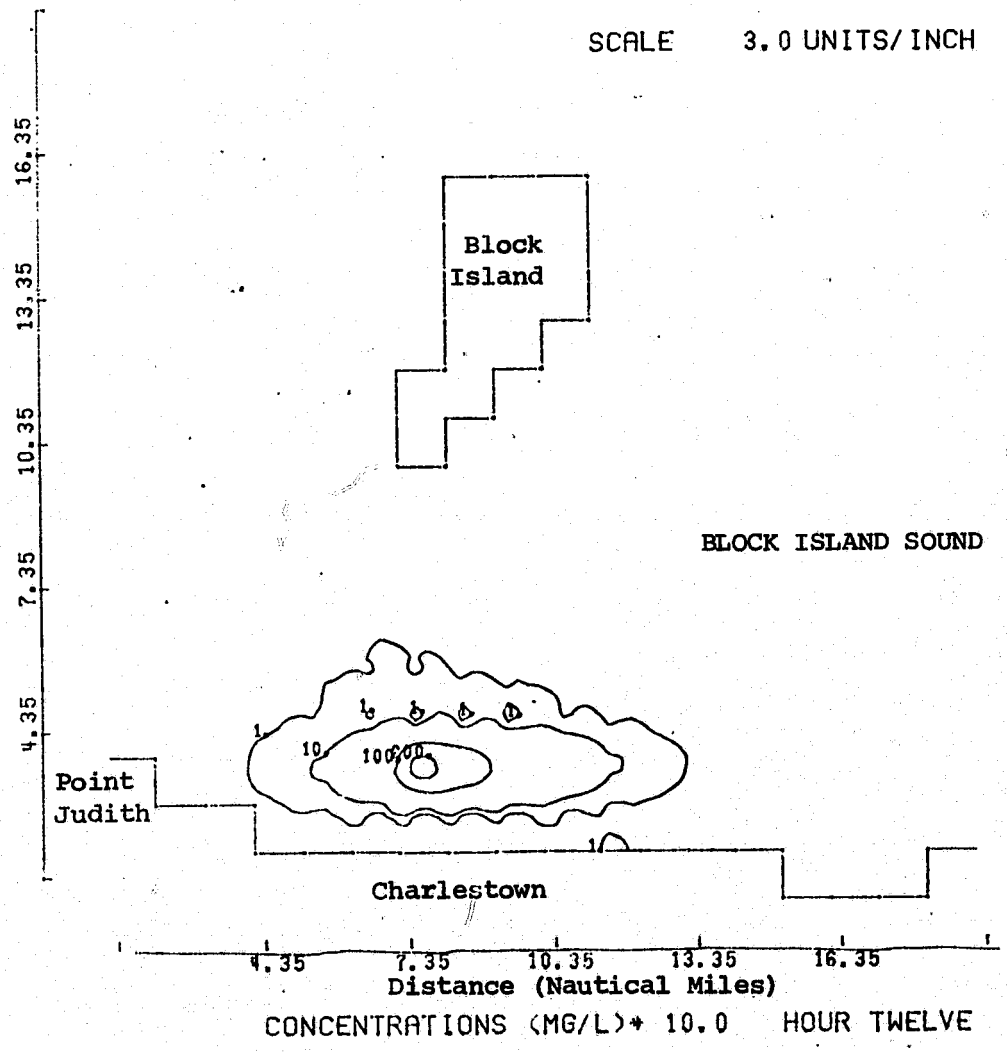

FIGURE 9.27 Concentration (mg/l) Contours for Continuous Release Predicted by Vertically Averaged Concentration Model Twelve Hours After High Water at Newport, R.I.

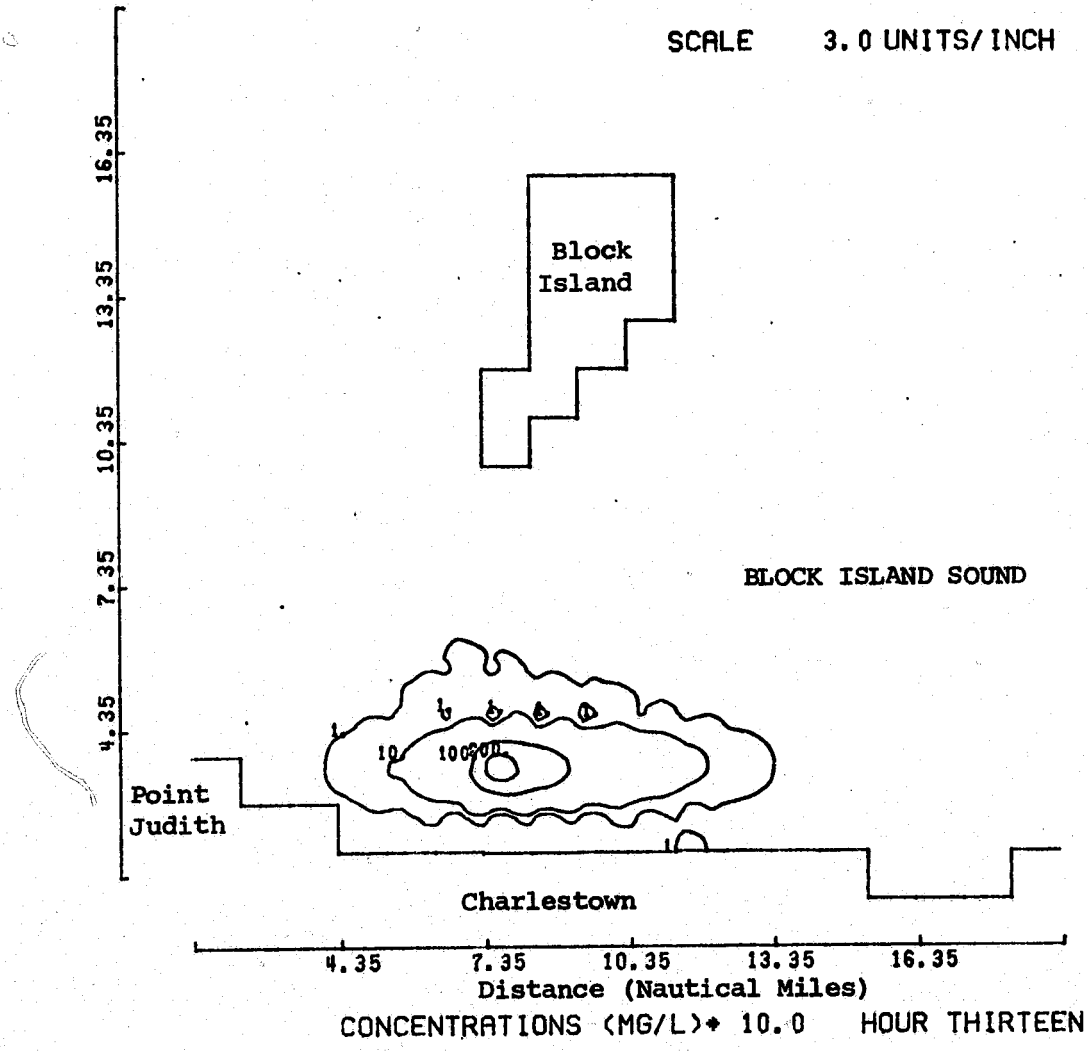

FIGURE 9.28 Concentration (mg/l) Contours for Continuous Release Predicted by Vertically Averaged Concentration Model Thirteen Hours After High Water at Newport, R.I.

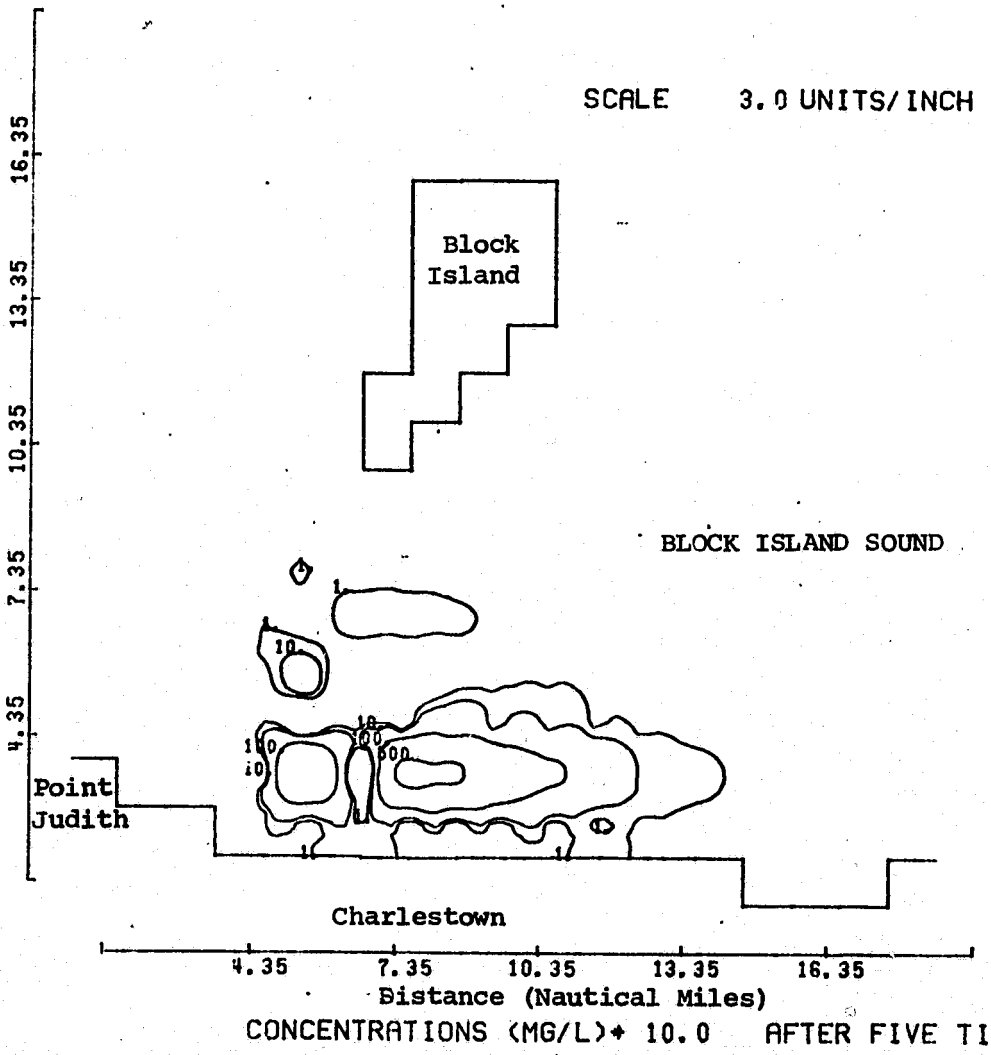

FIGURE 9.29 Concentration (mg/l) Contours for Continuous Release Predicted by Vertically Averaged Concentration Model Five Tidal Cycles After High Water at Newport, R.I.

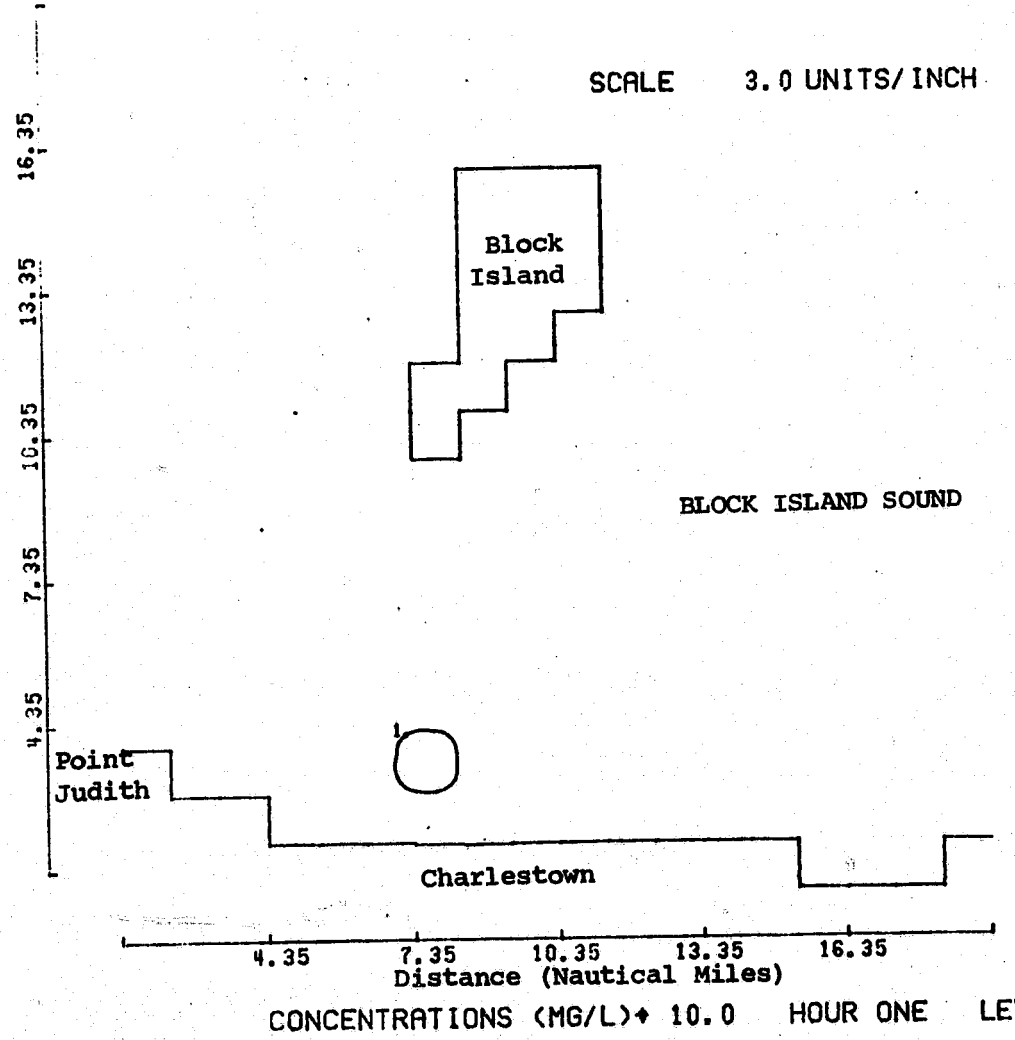

FIGURE 9.30 Concentration (mg/l) Contours for Level-2 for Continuous Release Predicted by the Three Dimensional Concentration Model One Hour After High Water at Newport, R.I.

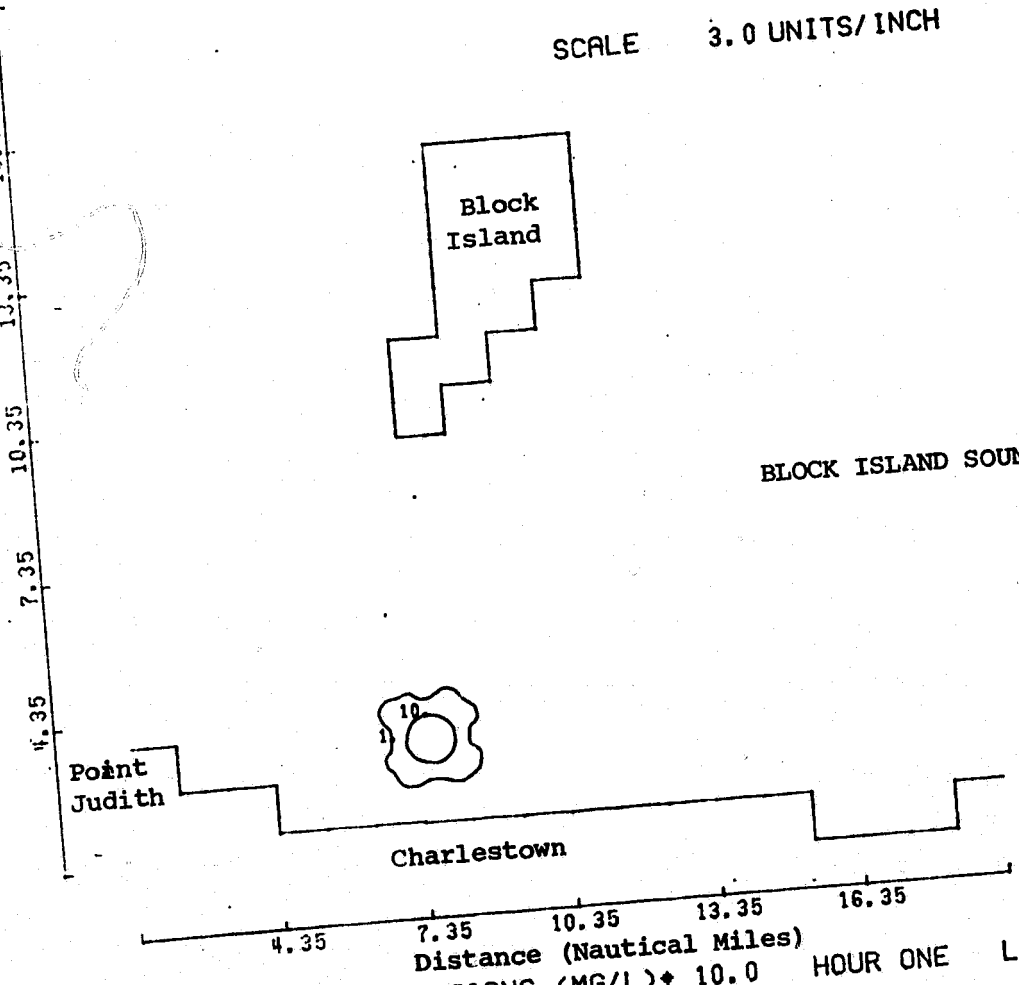

FIGURE 9.31 Concentration (mg/l) Contours for Level-3 for Continuous Release Predicted by the Three Dimensional Concentration Model One Hour After High Water at Newport, R.I.

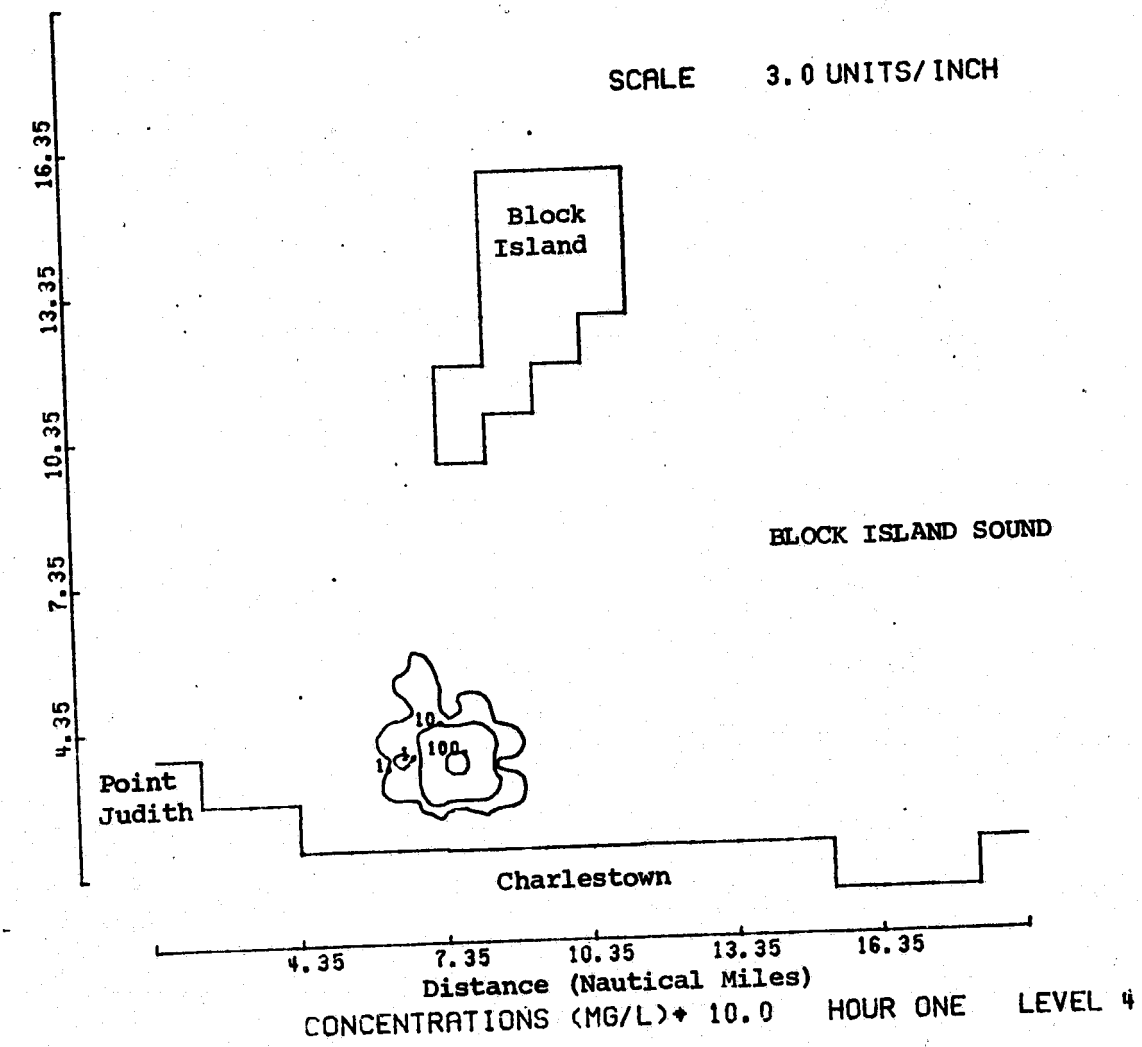

FIGURE 9.32 Concentration (mg/l) Contours for Level-4 for Continuous Release Predicted by the Three Dimensional Concentration Model One Hour After High Water at Newport, R.I.

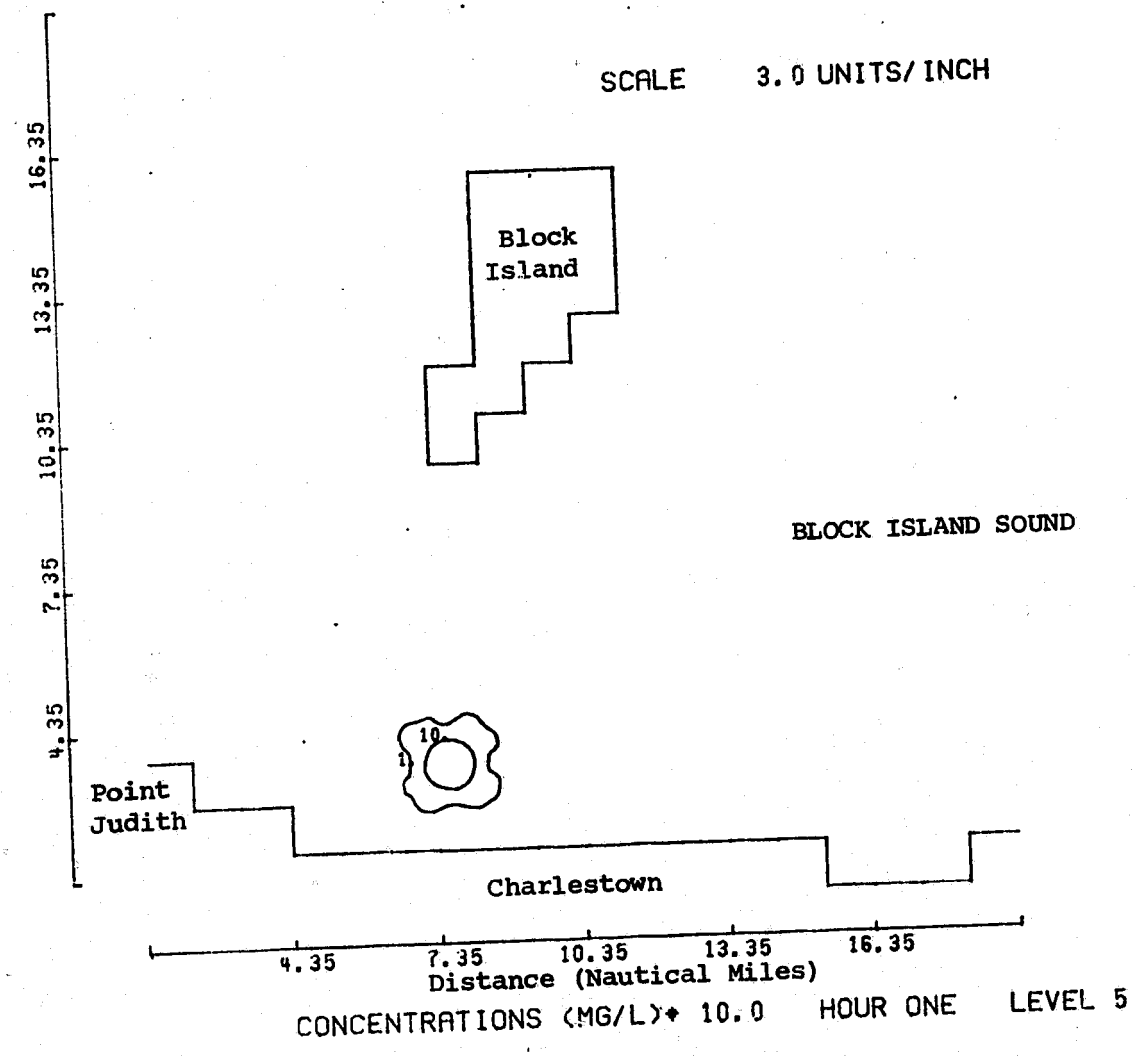

FIGURE 9.33 Concentration (mg/l) Contours for Level-5 for Continuous Release Predicted by the Three Dimensional Concentration Model One Hour After High Water at Newport, R.I.

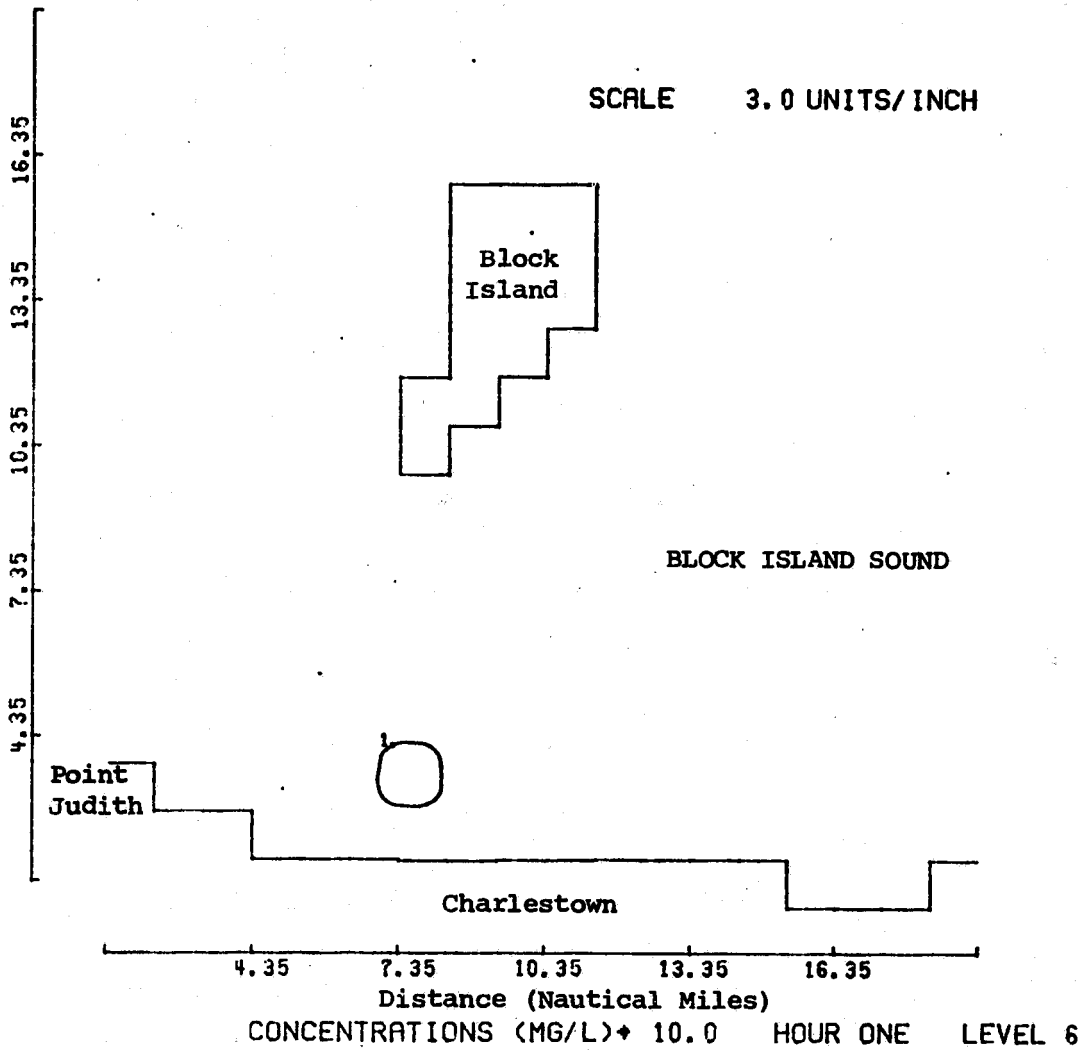

FIGURE 9.34 Concentration (mg/l) Contours for Level-6 Continuous Release Predicted by the Three Dimensional Concentration Model One Hour After High Water at Newport, R.I.

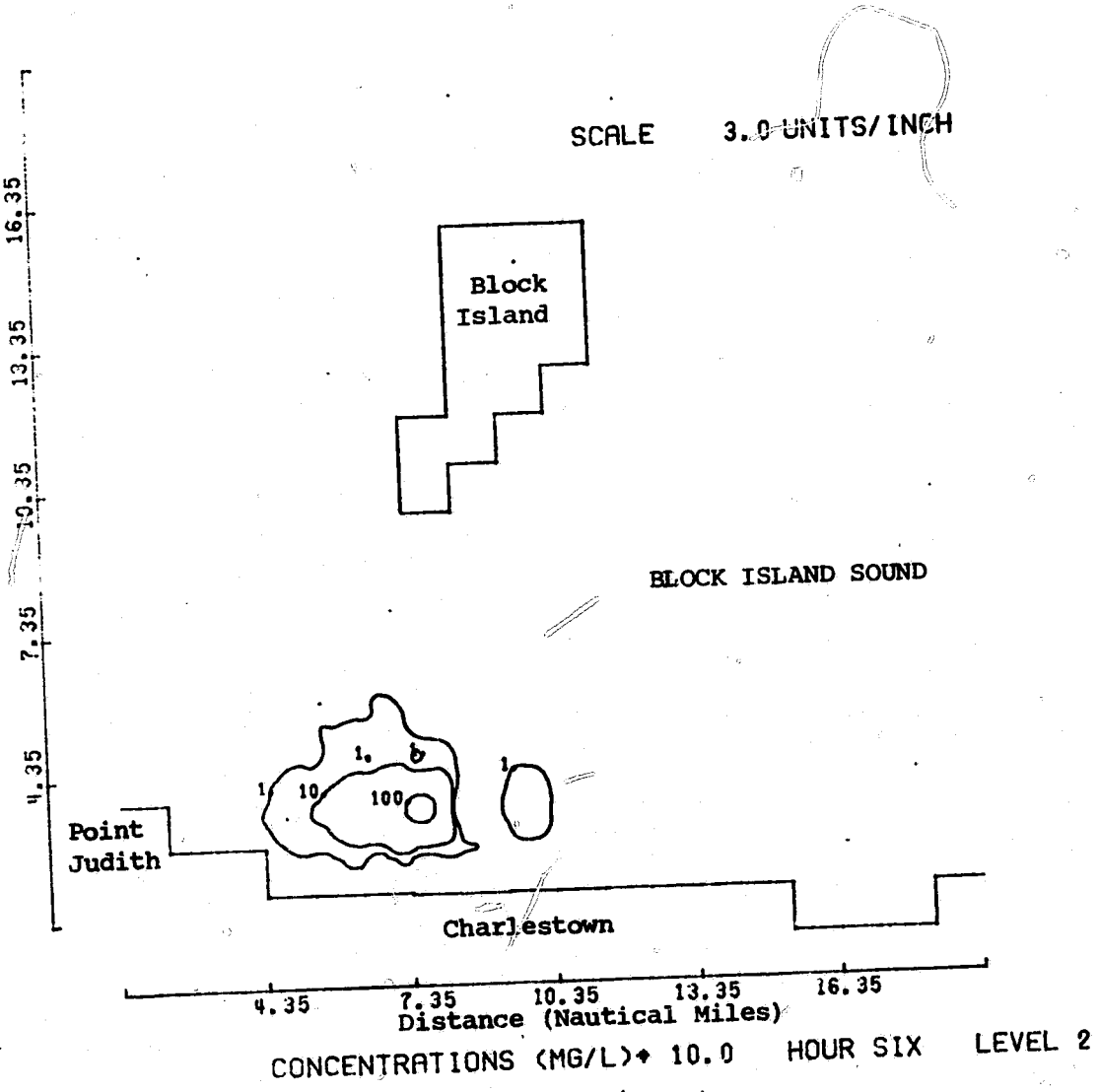

FIGURE 9.35 Concentration (mg/l) Contours for Level-2 for Continuous Release Predicted by the Three Dimensional Concentration Model Six Hours After High Water at Newport, R.I.

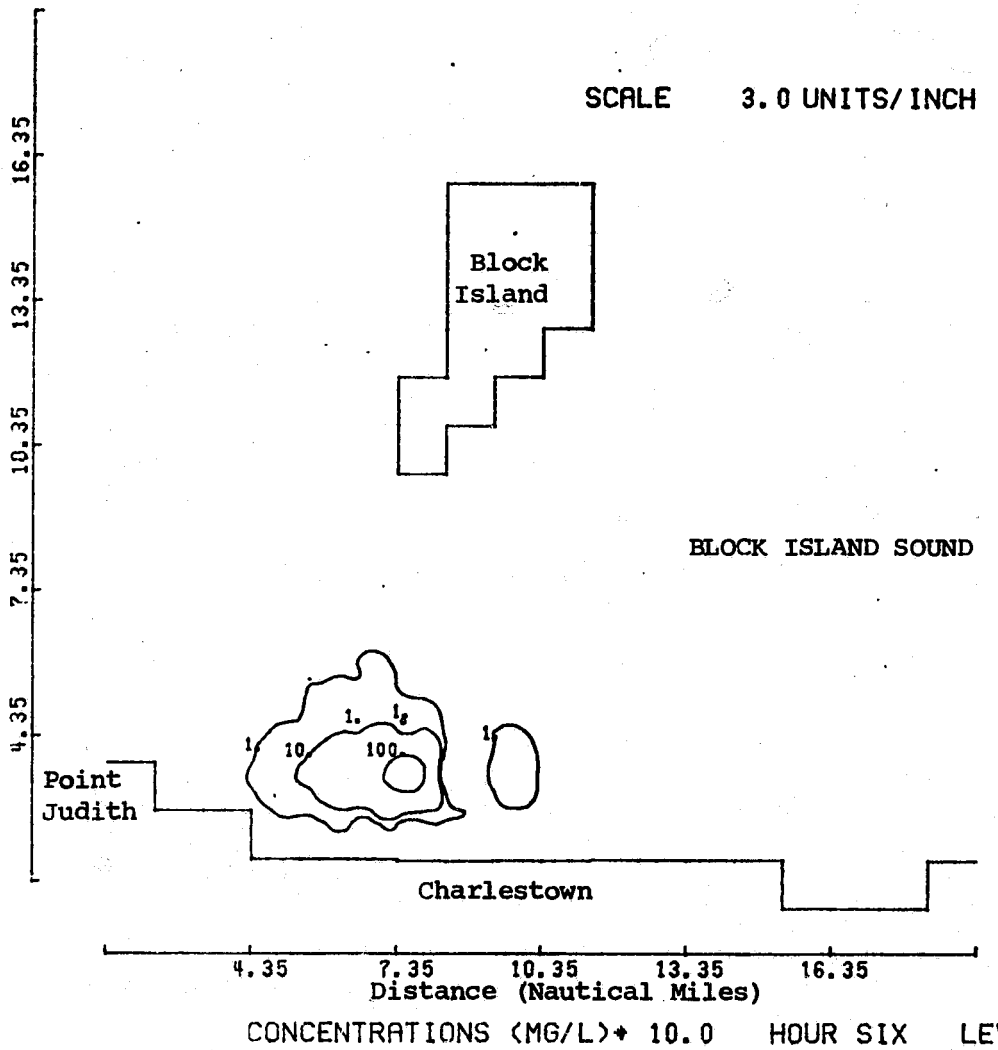

FIGURE 9.36 Concentration (mg/l) Contours for Level-3 for Continuous Release Predicted by the Three Dimensional Concentration Model Six Hours After High Water at Newport, R.I.

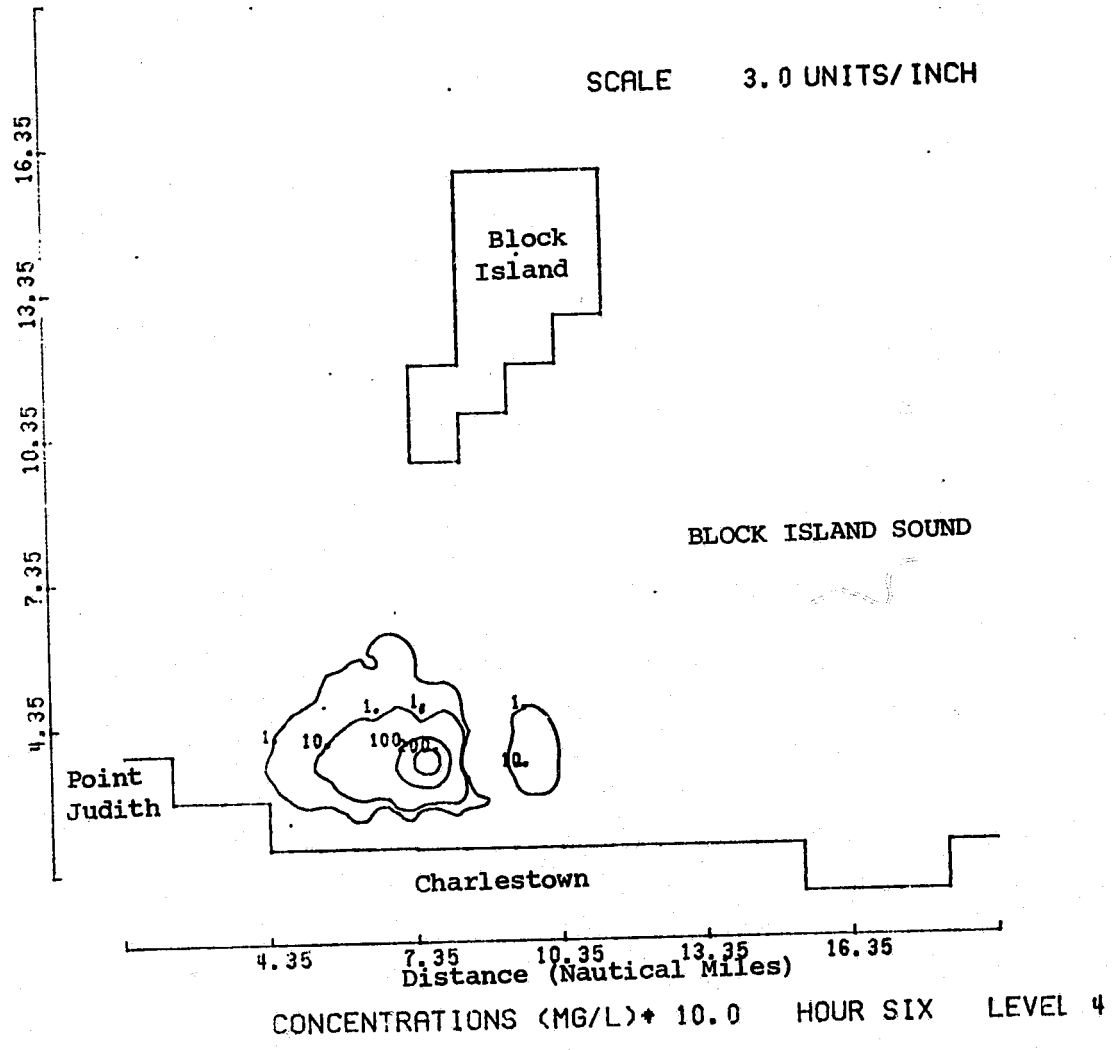

FIGURE 9.37 Concentration (mg/l) Contours for Level-4 for Continuous Release Predicted by the Three Dimensional Concentration Model Six Hours After High Water at Newport, R.I.

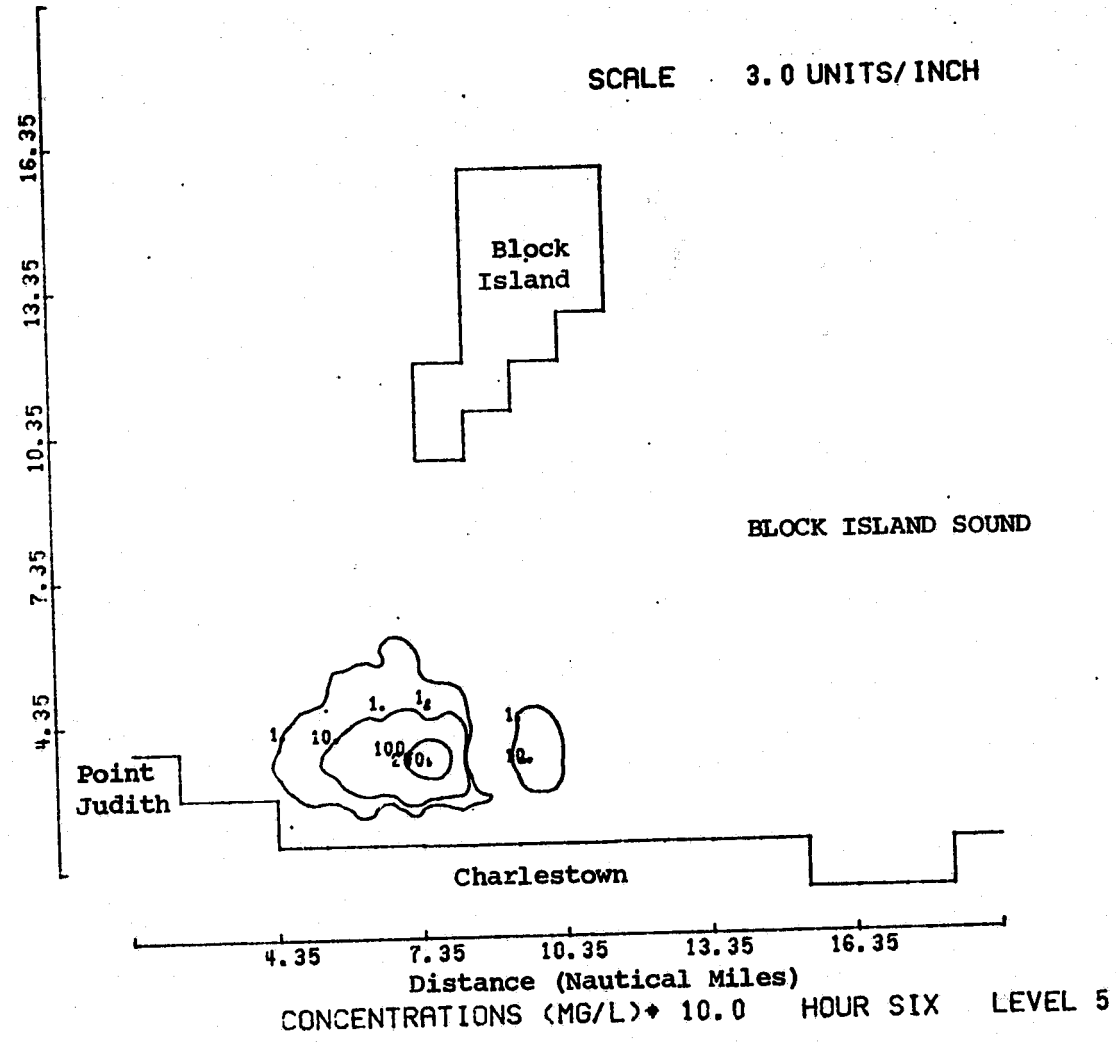

FIGURE 9.38 Concentration (mg/l) Contours for Level-5 for Continuous Release Predicted by the Three Dimensional Concentration Model Six Hours After High Water at Newport, R.I.

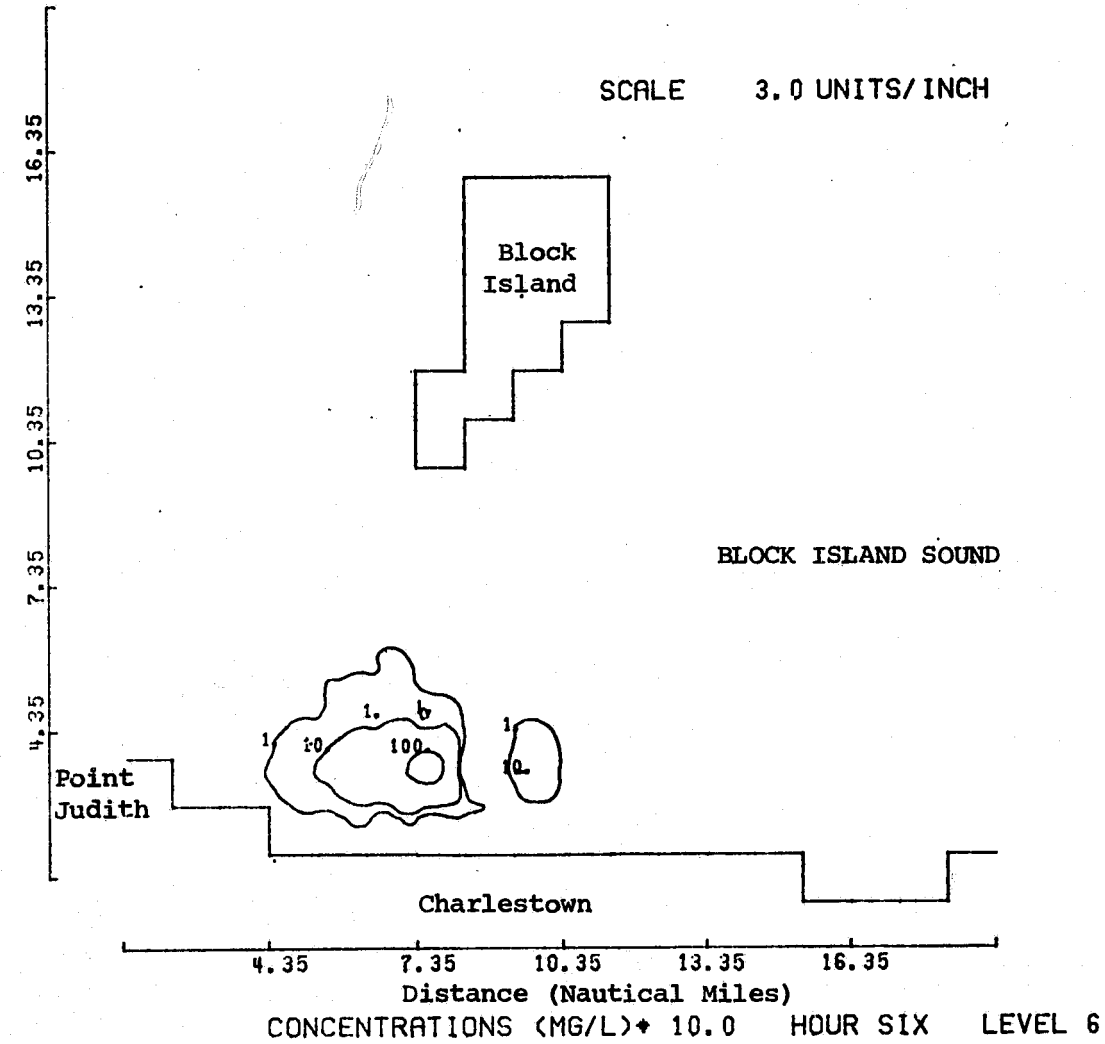

FIGURE 9.39 Concentration (mg/l) Contours for Level-6 for Continuous Release Predicted by the Three Dimensional Concentration Model Six Hours After High Water at Newport, R.I.

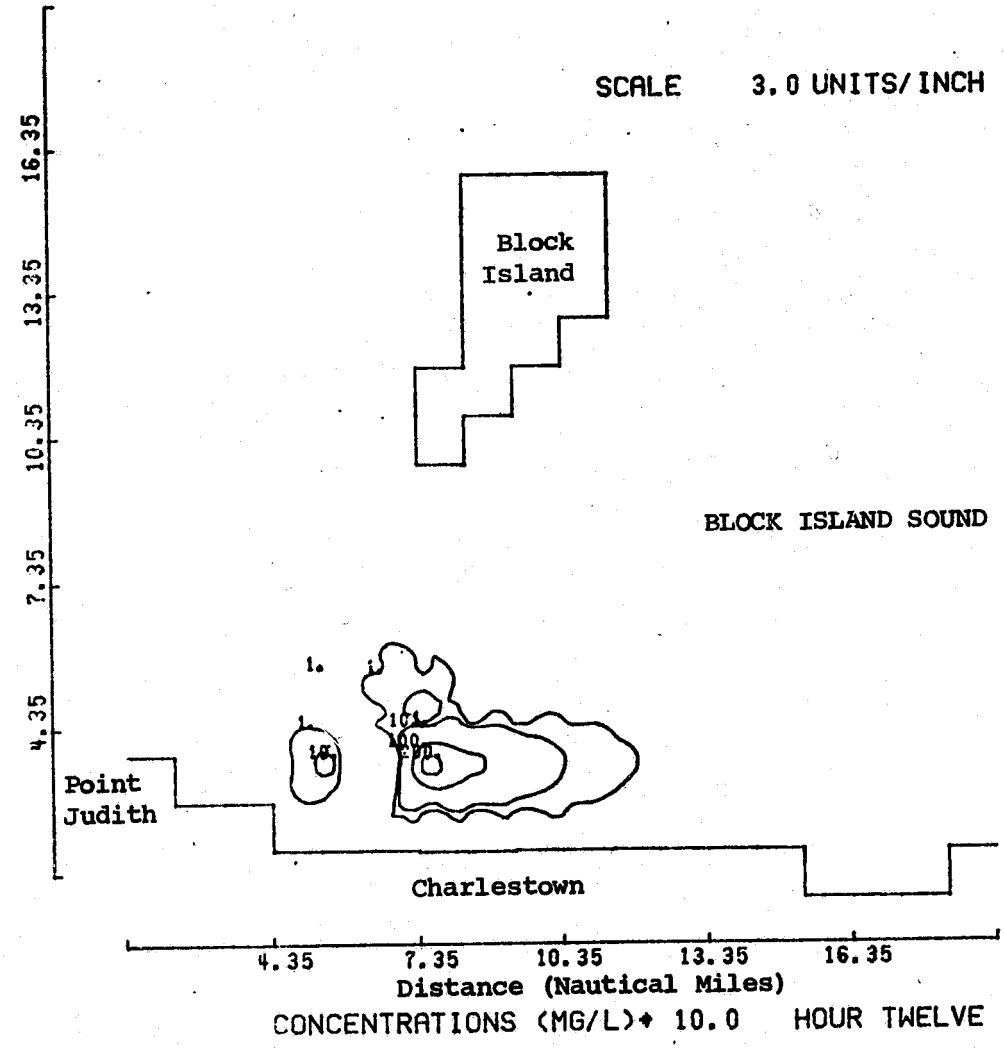

FIGURE 9.40 Concentration (mg/l) Contours for Level-2 for Continuous Release Predicted by the Three Dimensional Concentration Model Twelve Hours After High Water at Newport, R.I.

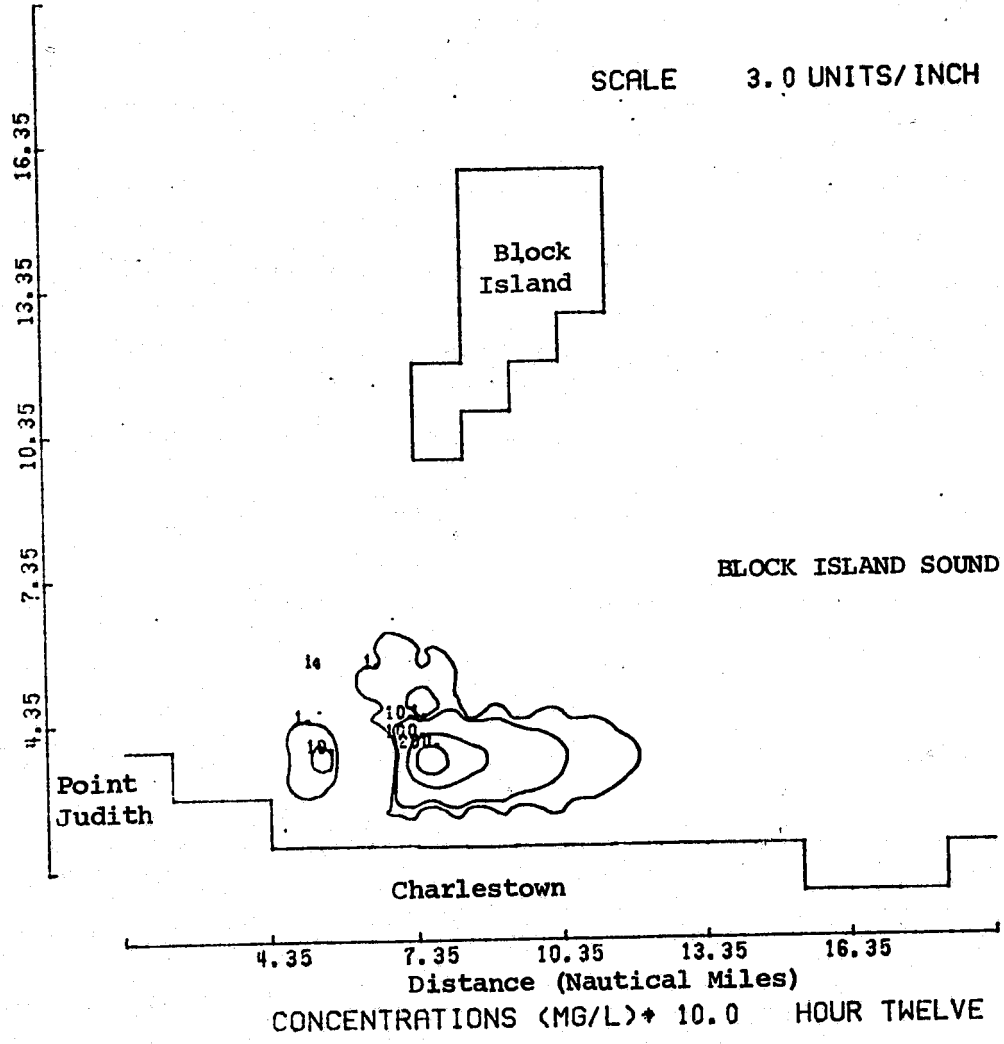

FIGURE 9.41 Concentration (mg/l) Contours for Level-3 for Continuous Release Predicted by the Three Dimensional Concentration Model Twelve Hours After High Water at Newport, R.I.

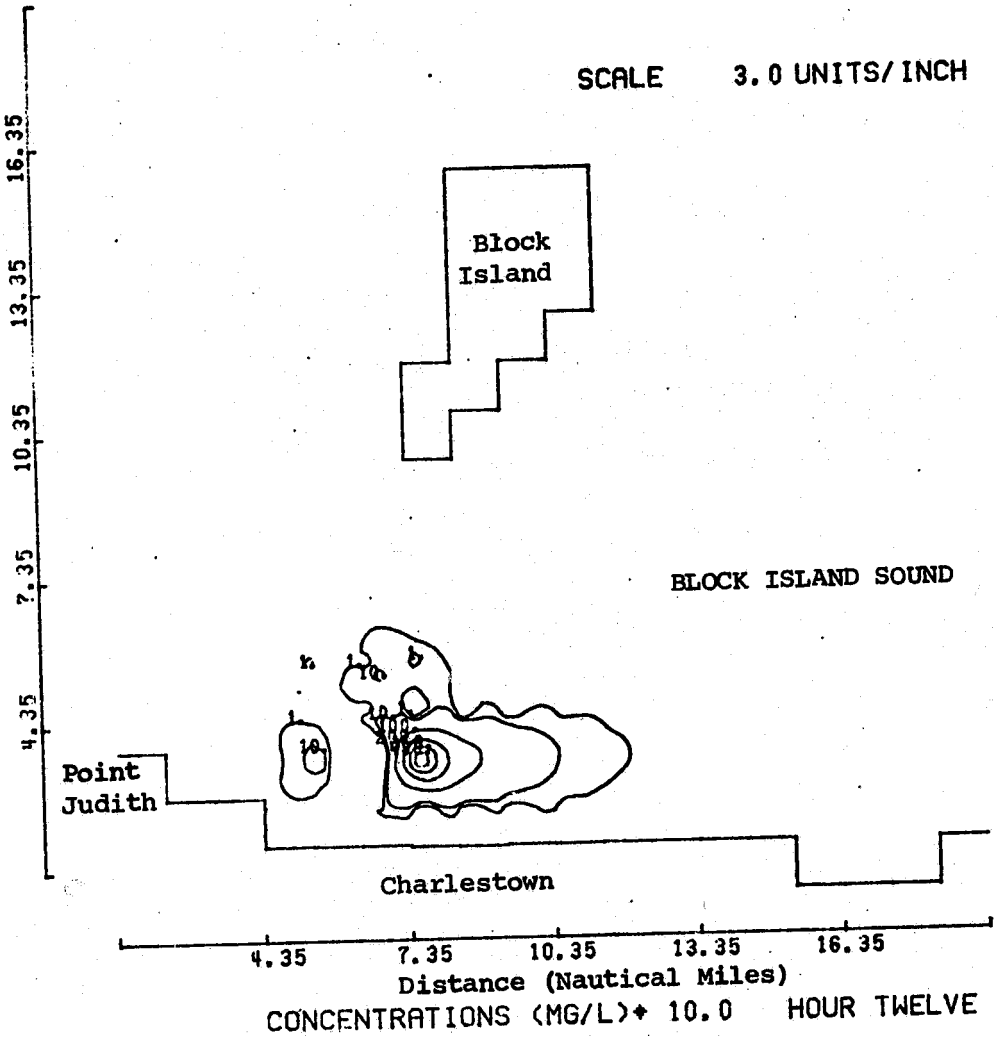

FIGURE 9.42 Concentration (mg/l) Contours for Level-4 for Continuous Release Predicted by the Three Dimensional Concentration Model Twelve Hours After High Water at Newport, R.I.

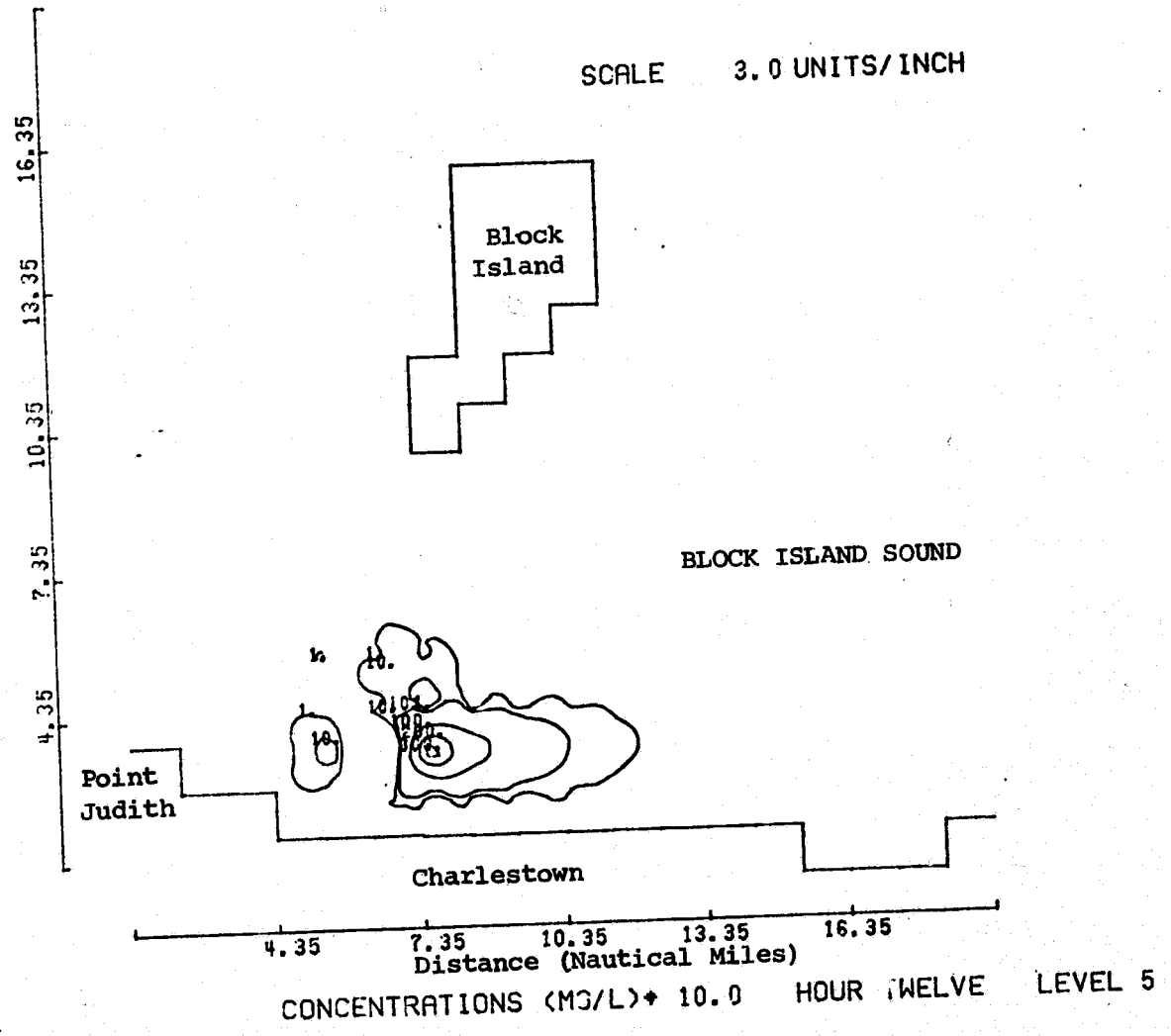

FIGURE 9.43 Concentrations (mg/l) Contours for Level-5 for Continuous Release Predicted by the Three Dimensional Concentration Model Twelve Hours After High Water at Newport, R.I.

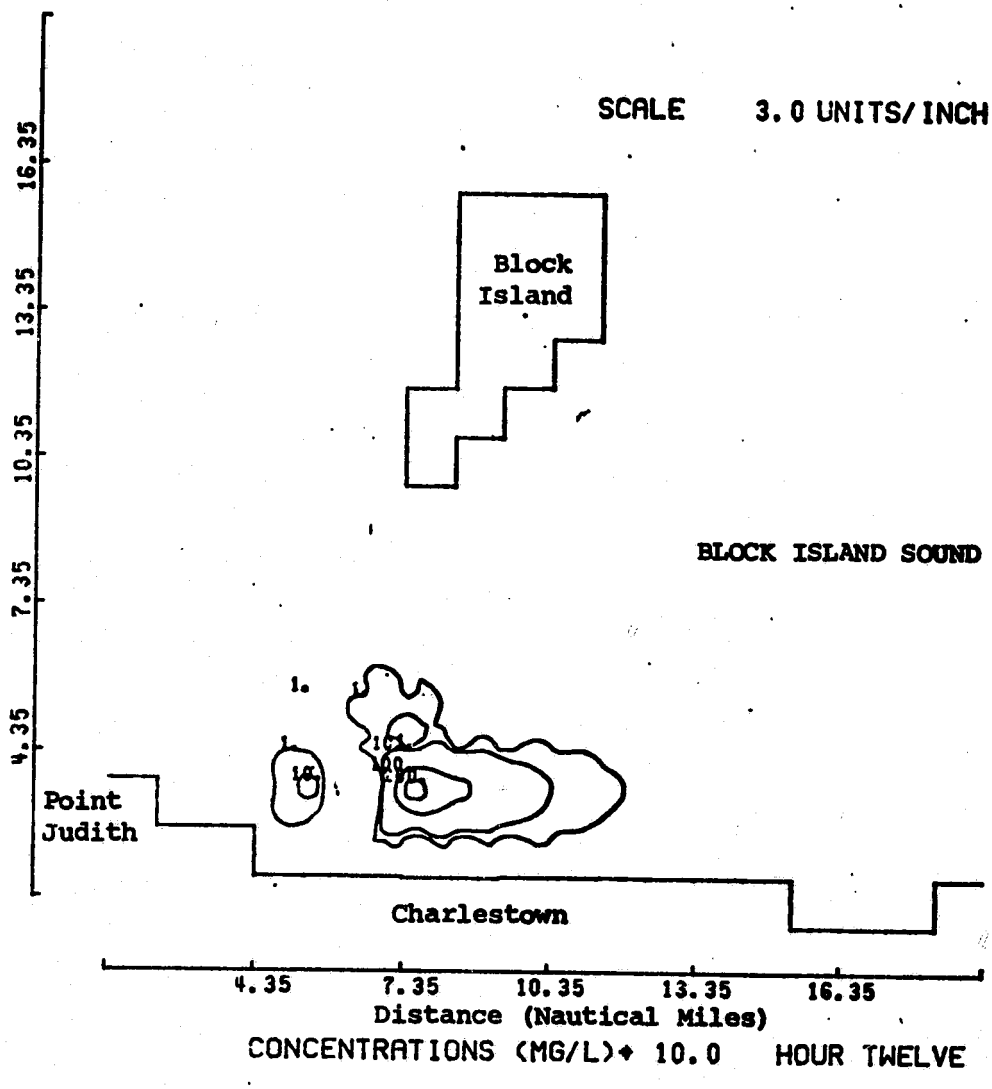

FIGURE 9.44 Concentration (mg/l) Contours for Level-6 for Continuous Release Predicted by the Three Dimensional Concentration Model Twelve Hours After High Water at Newport, R.I.

sharp concentration gradients along one side of contour plots. This is a direct result of the point-loading condition and its associated depression of the concentration field upstream of the discharge. This condition could be removed by introducing artificial dispersion upstream of the release, but it was felt that the worst case should be indicated to illustrate the effects of the problem for realistic coastal zone simulations.

Figures 9.45 through 9.49 display the three-dimensional results after five tidal cycles at approximately slack water. Comparison of these figures with those for the two-dimensional vertically-averaged case show almost exact comparison. This close agreement can be explained simply by noting that the three-dimensional model employed a vertical diffusion coefficient typical of a well-mixed area, and therefore the three-dimensional predictions should approach the two-dimensional case as time proceeds. The same effect has been noted for the estuary application, even though the diffusion coefficient indicated stratification, because the water was relatively shallow.

Additional complexity such as multiple-point time-varying loadings, multi-stage reaction mechanics, and stratification can be readily incorporated in the modeling scheme. With this capability it is felt that the modeling approach presented allows a more realistic prediction technique for pollutant transport in coastal

zone areas.

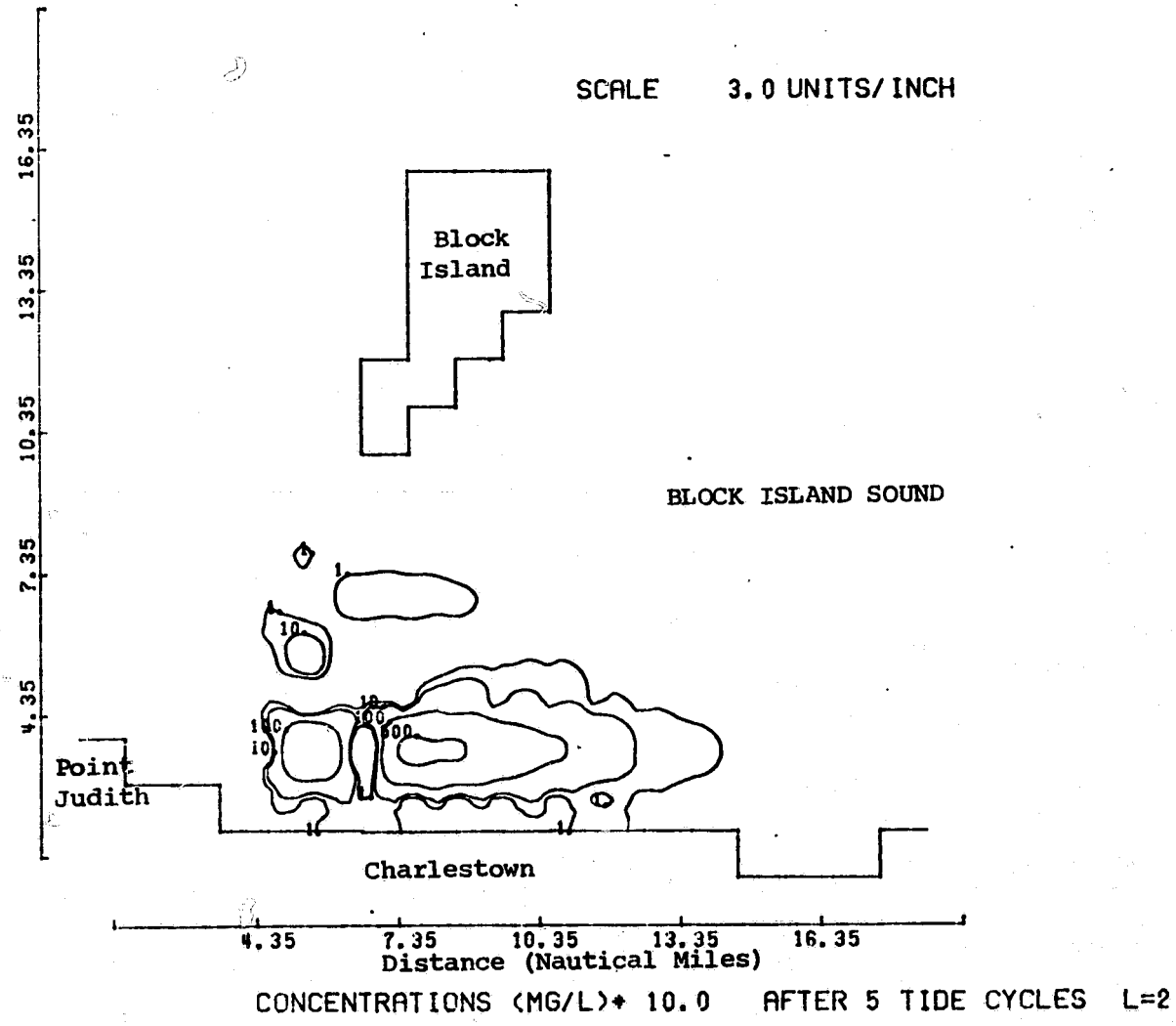

FIGURE 9.45 Concentration (mg/l) Contours for Level-2 for Continuous Release Predicted by the Three Dimensional Concentration Model Five Tidal Cycles After High Water at Newport, R.I.

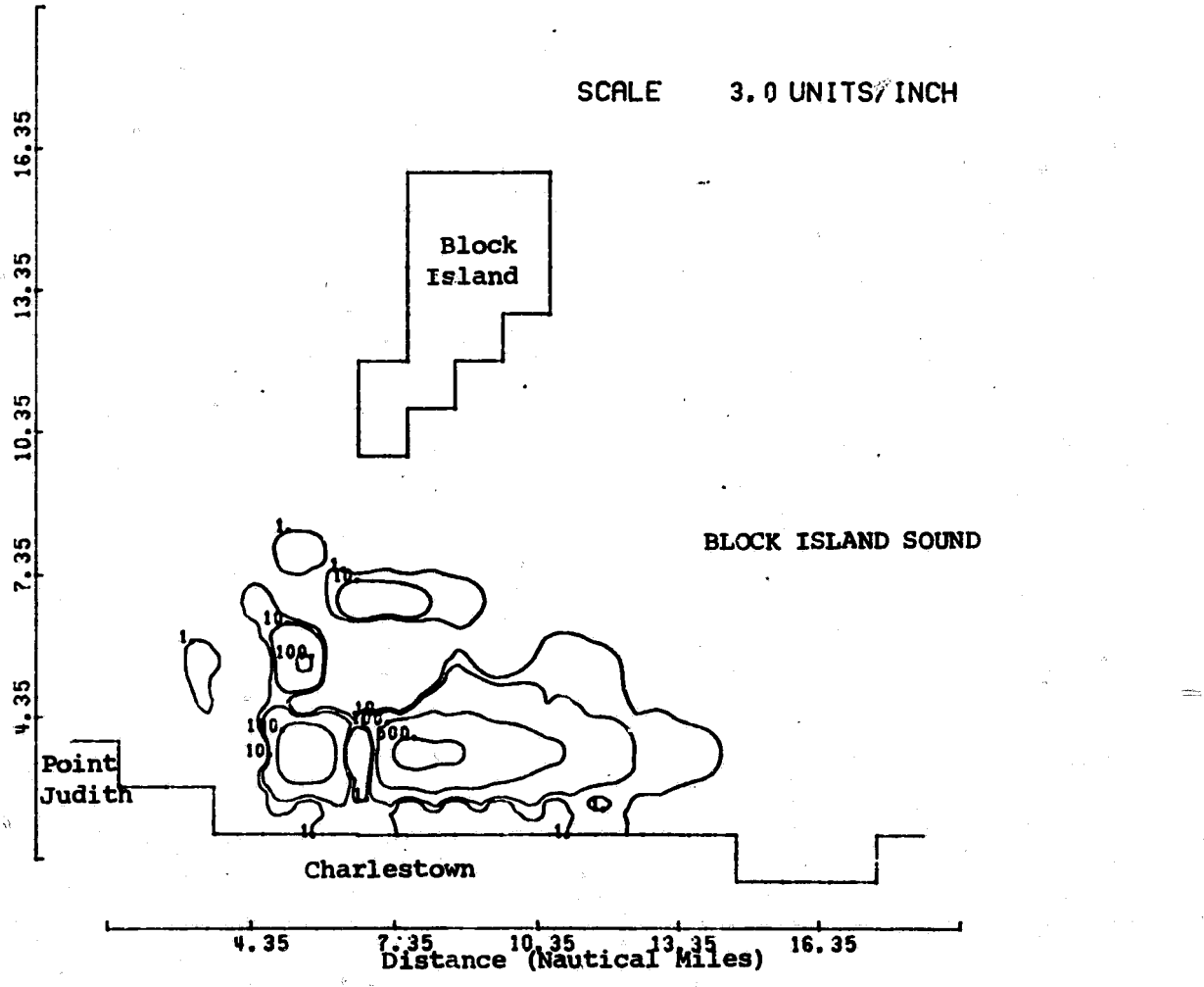

FIGURE 9.46 Concentration (mg/l) Contours for Level-3 for Continuous Release Predicted by the Three Dimensional Concentration Model Five Tidal Cycles After High Water at Newport, R.I.

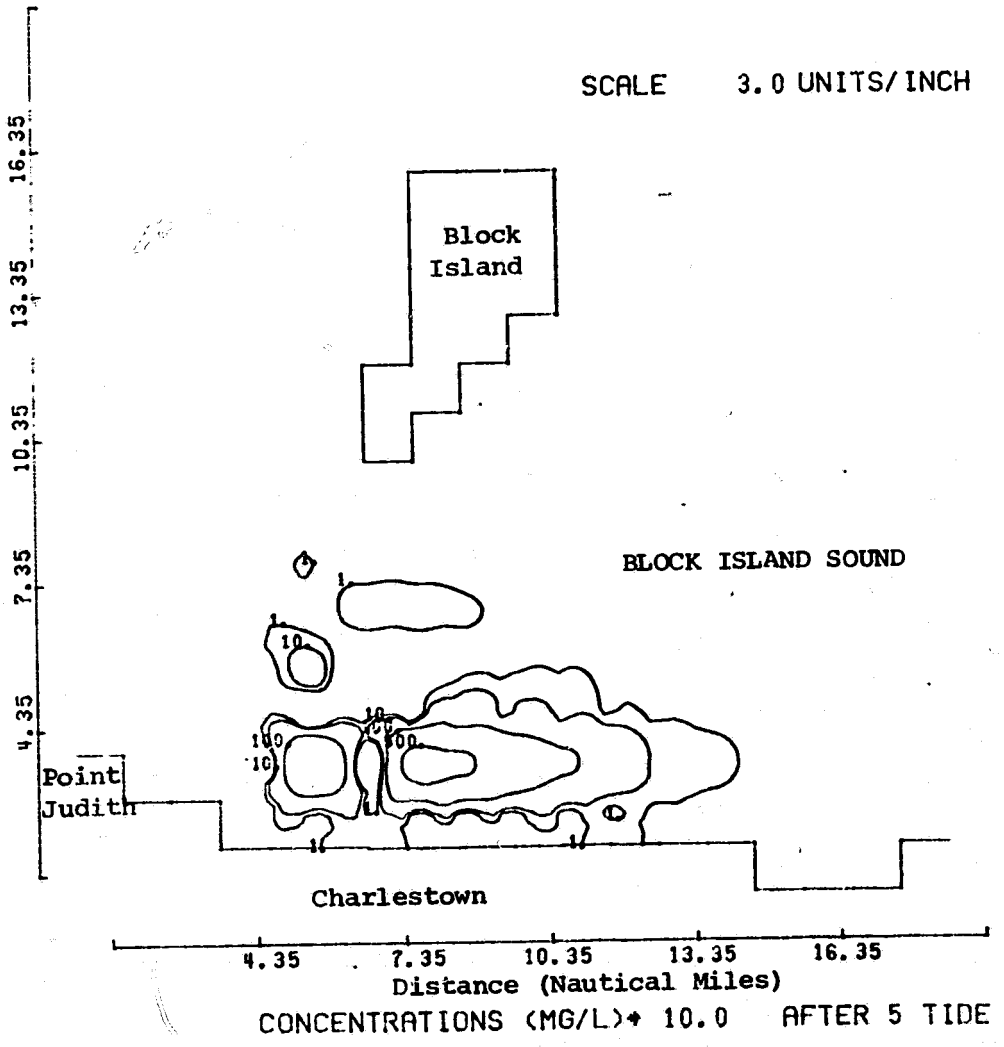

FIGURE 9.47 Concentration (mg/l) Contours for Level-4 for Continuous Release Predicted by the Three Dimensional Concentration Model Five Tidal Cycles After High Water at Newport, R.I.

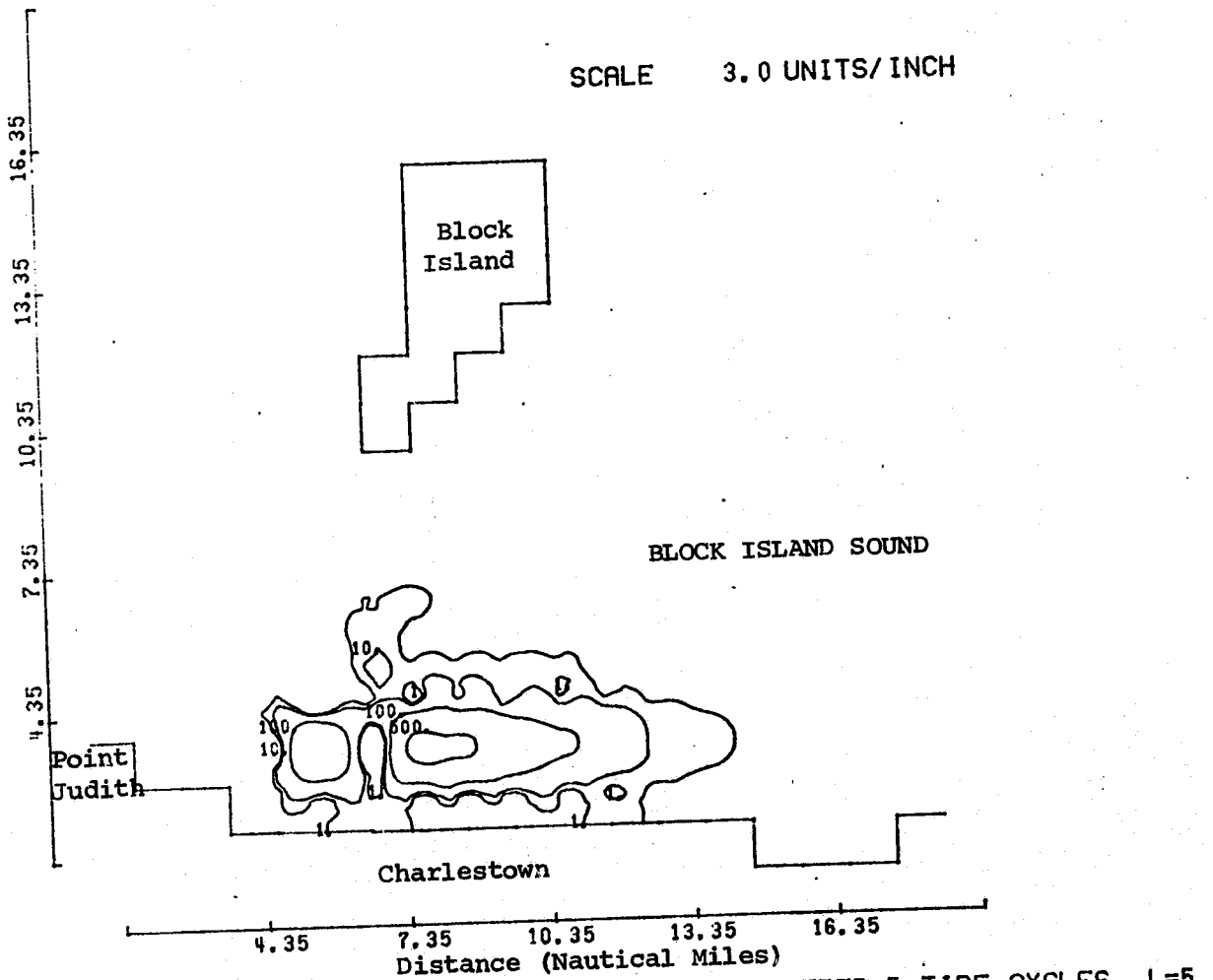

FIGURE 9.48 Concentration (mg/l) Contours for Level-5 for Continuous Release Predicted by the Three Dimensional Concentration Model Five Tidal Cycles After High Water at Newport, R.I.

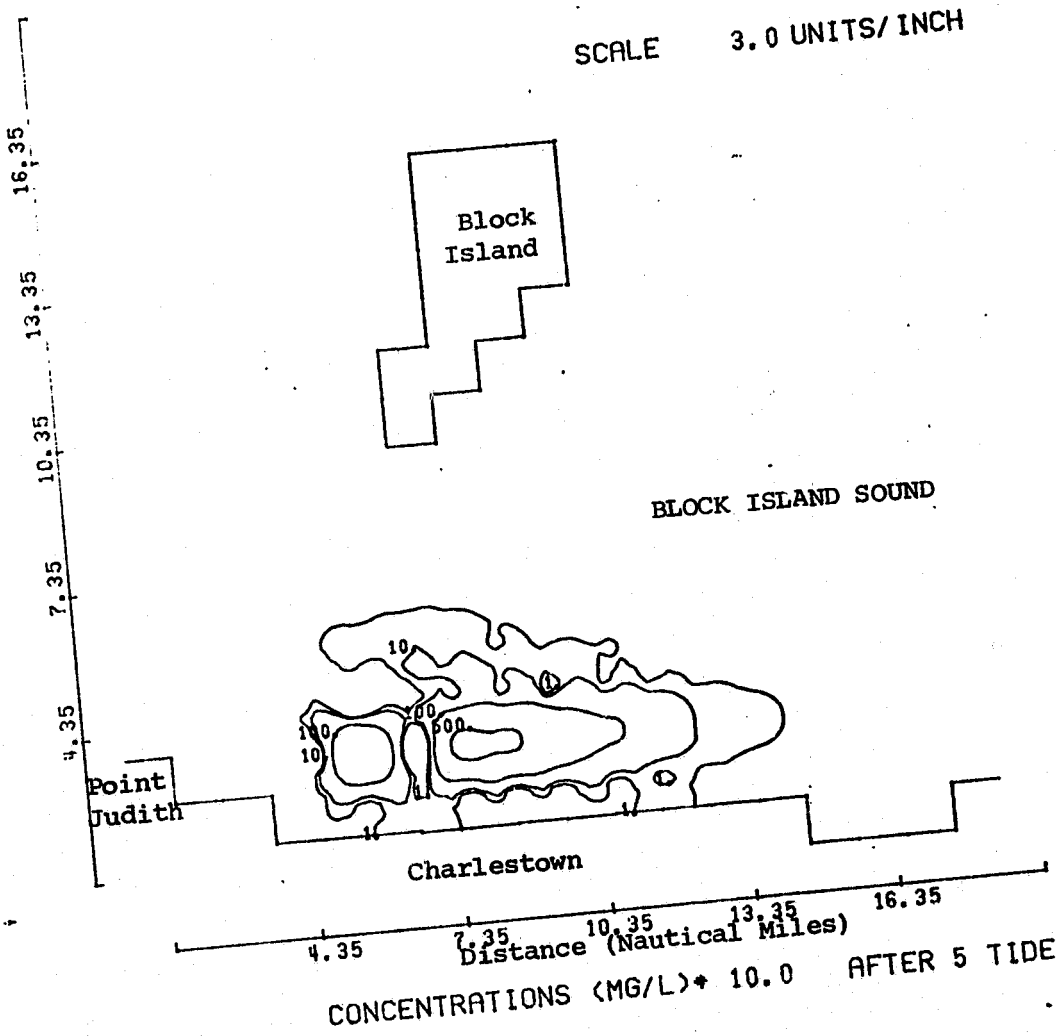

FIGURE 9.49 Concentration (mg/l) Contours for Level-6 for Continuous Release Predicted by the Three Dimensional Concentration Model Five Tidal Cycles After High Water at Newport, R.I.

X. CONCLUSIONS AND RECOMMENDATIONS

The computational accuracy and usefulness of the three-dimensional mass transport model have been demonstrated sucessfully by the investigations and applications herein. The capacity to define vertical as well as lateral variations has been seen to be valuable, particularly in short-term phenomena. Over longer periods of time, vertical variations are much reduced by diffusion, at least when using a vertically averaged two-dimensional model to obtain the hydrodynamic input.

The analytical investigations of dispersive and dissipative effects, performed for the one-dimensional mass transport equation with constant dispersion coefficients, have been verified numerically for the three-dimensional model.

The generation of computational discontinuities at extreme concentration gradients can be reduced, but not eliminated, by the method of adding artificial dispersion at appropriate times and places. Care must be taken that the increase in dispersion is not large enough to cause severe distortion of the concentration field in the area under study. The values used here for the overall dispersion coefficients appear from the verification attempt to represent very well the processes taking place in the the Providence River.

Two qualities of the model are particularly useful

in modeling of coliform bacteria distribution. The vertical resolution permits the incorporation of the effect of solar radiation, and the reaction matrix can accomodate a lag or growth phase. As the behavior of coliforms can vary widely depending upon the prevailing conditions, it is recommended that either field studies be made first in the area to be modeled, or the results of earlier studies be consulted.

If difficult boundary conditions, such as those at the Seekonk River, are seen to produce a significant mass conservation error, effort should be made toward reducing it. Elaboration upon the extrapolation technique is expected to help. A conclusion of this boundary condition research is that the major portion of the error in simulating a realistic pollutant transport problem is usually the error of the boundary approximation, and therefore more detailed understanding of those approximations is necessary.

The development of a steady-state mode of operation has provided an additional tool to predict water quality for complex constant flow areas. Comparison of model predictions to analytic solutions and a river confluence case have shown the present model scheme to be accurate and reasonably efficient. Further testing of this modeling approach should be performed by comparing predictions for multi-stage reacting constituents to data for a realistic steady-state coastal zone circulation system.

Coupling of the two-dimensional vertically averaged tidal hydrodynamics model to the three-dimensional water quality model for a typical open coastal area such as Block Island Sound has shown the feasibility and capability of the present approach. Application and verification of this approach should build more confidence and experience in the ultimate use of these models in coastal zone management. It is therefore recommended that the model be verified for a number of coastal zone pollutant transport problems.

In short, the three-dimensional mass transport model, as now developed, appears to be capable of handling almost any water quality problem currently under investigation. The major limitation is still in obtaining adequate data to verify the models, and in the refinement of various circulation models which may be used to obtain the hydrodynamic input. New models are under development which will enhance the usefulness of this model. Leendertse et al. (73) have developed a three-dimensional model incorporating the salt equation. This model has the additional capability of computing w, the vertical velocity component, as a function of the density variation due to salinity. In addition, Gordon and Spaulding (74) have developed a three-dimensional hydrodynamics model employing the same non-dimensional vertical coordinate used in this study. This model has been designed to interface directly with the three-dimensional water quality model. The coupling

of these two techniques should provide an effective tool for modeling complex pollutant transport in the coastal zone.

Although the information used in the Providence River application produced a reasonably good verification, it is hoped to have more field information than was available for this study. Vertical concentration profiles at river mouths, at a number of different states of the tide, would permit more accurate modeling of the river source levels. Any information on the time variation of outfall discharges would increase the value of the modeling effort. The lack of information on vertical diffusion coefficients requires some arbitrariness. Although field studies attempting to define D would be difficult and expensive, they would also increase the knowledge to be gained from modeling, by revealing the magnitude of vertical diffusion in the particular area of interest. As mentioned, field studies would also aid in the modeling of coliforms or other indicator bacteria.

The more information that is supplied to the model, the more it can produce. The computational methods have been shown to be accurate, stable, and very flexible. Here is a tool which can help fill many gaps in the knowledge of coastal transport problems.

REFERENCES

1. Goldstein, G.S., "Narrow River Failing Water Purity Tests", Narragansett Times, 22 August 1974, p. 1.

2. Pararas-Carayannis, G., Ocean Dumping in the New York Bight: An Assessment of Environmental Studies, U.S. Army C.E.R.C., TM No. 39, May 1973.

3. Mackay, Sludge Dumping in the Firth of Clyde, Marine Pollution Bulletin, 3-1:7, 1972.

4. Shelton, R., Sludge Dumping in the Thames Estuary, Marine Pollution Bulletin, 2-2:24, 1971.

5. Lukin, L., Limitations and Effects of Waste Disposal on an Ocean Shelf, EPA, 16070 EGF, December 1971.

6. Water Quality Standards Summary. Joint Publication by EPA, R.I. Department of Health, Division of Water Supply and Pollution Control. Government Printing Office, 1972.

7. "Voters Reject 9 of 12 Bond Proposals", The Providence Journal, 6 November 1974, p. A-2.

8. TRACOR, Inc., Estuaries Water Quality Modeling: An Assessment of Pollution Control Capabilities, EPA Contract 14-12-551, February 1971.

9. Thomann, R., Mathematical Model for Dissolved Oxygen, ASCE Journal, SA5, October 1963.

10. Thomann, R., Recent Results from a Mathematical Model of Water Pollution Control in the Delaware Estuary, Water Resources Research, 1-3:349, 1965.

11. Dailey, J. and D. Harleman, Numerical Model for the Prediction of Transient Water Quality in Estuary Networks, MITSG T-72-15, October 30, 1972.

12. Christodoulou, G., W. Leimkuhler, A. Ippen, Mathematical Models of the Massachusetts Bay, Part III. A Mathematical Model for the Dispersion of Suspended Sediments in Coastal Waters, MITSG T-74-14, January 31, 1974.

13. Guymon, F., V. Scott, and L. Herrmann, A General Numerical Solution of the Two-Dimensional Diffusion-Convection Equation by the Finite-Element Method, Water Resources Research, 6-6:1611, 1970.

14. Leendertse, J.J., A Water Quality Simulation Model for Well Mixed Estuaries and Coastal Seas: Volume I, Principles of Computation, The Rand Corporation, RM-6230-RC, Santa Monica, California, February 1970.

15. Spaulding, M.L., Laterally Integrated Numerical Water Quality Model, Ph.D. Thesis, University of Rhode Island, 1972.

16. Elliot, A., Douglas Point, A Study of Circulation and Mixing, Special Report 93, Reference 75-4, Chesapeake Bay Institute, Johns Hopkins University, May 1975.

17. Douglas, J., Alternating Direction Methods for Three-Space Variables, Numerische Mathematik, 4:41, 1962.

18. Hess, K. and F. White, A Numerical Tidal Model of Narragansett Bay, University of Rhode Island, Marine Technical Report No. 20, Kingston, R.I., 1974.

19. Leendertse, J., Aspects of a Computational Model for Long-Period Water-Wave Propagation, Rand Corporation, Santa Monica, California, RM 5294-PR, May 1967.

20. Gritton, E., A Water Quality Model for Well-Mixed Estuaries and Coastal Seas: Volume V, Jamaica Bay Rainstorms, The Rand Corporation, R-1010-NYC, New York City, N.Y., July 1972.

21. Canale, R.P., Model of Coliform Bacteria in Grand Traverse Bay, Journal of the Water Pollution Control Federation, 45-11:2358, November 1973.

22. "Bacteriological and Chemical Survey of Providence River", Unpublished Report, Rhode Island Department of Health, 1966.

23. Bird, R., W. Stuart and E. Lightfoot, Transport Phenomena, John Wiley and Sons, N.Y., N.Y., 1960.

24. Spaulding, M.L., Derivation of a Three-Dimensional Numerical Water Quality Model for Estuary and Continental Shelf Application, NASA Technical Memorandum X-71930, 1973.

25. Douglas, J. and J. Gunn, A General Formulation of Alternating Direction Methods, Numerische Mathematik, G:428, 1964.

26. Holley, E., Unified View of Diffusion and Dispersion, ASCE Journal, HYD., March 1969.

27. Orlob, G., Eddy Diffusion in Homogeneous Turbulence, ASCE Transactions, 126-I: 397, 1961.

28. Brooks, N., Diffusion of Sewage Effluent in an Ocean Current, in Waste Disposal in the Marine Environment, 246-267, 1960.

29. Foxworthy, J., Eddy Diffusivity and the Four Thirds Law in Near Shore Coastal Waters, University of Southern California, Report 68-1, 1968.

30. Okubo, A., Oceanic Diffusion Diagrams, Deep Sea Research, 18:789, August 1971.

31. Richardson, L., Some Measurements of Atmospheric Turbulence, Philosophical Transactions, Royal Society of London, Series 22(A), 1920.

32. Yudelson, J., A Survey of Ocean Diffusion Studies and Data, Cal. Tech. Memorandum 67-2, September 1967.

33. Koh, R. and Y. Chang, Mathematical Model for Barged Ocean Disposal of Wastes, EPA-66012-73-029, December 1973.

34. Guttman, N., and N. Huang, Calculation of Vertical Turbulent Diffusivity for a Stratified Shear Flow, Trans. AGU, 52-4:233, 1973.

35. Sastry, J. and A. Okubo, On the Prediction of the Probable Distribution of Concentrations from Hypothetical Radioactive Sources on the Continental Slope off the East Coast of the U.S., Part I, Chesapeake Bay Institute, Johns Hopkins University, 68-1, March 1968.

36. Ichiye, T., N. Bassin, and J. Harris, Diffusivity of Suspended Matter in the Carribean Sea, Journal of Geophysical Research, 77-33:6576, November 20, 1972.

37. Kullenberg, G., Vertical Diffusion in Shallow Waters, Tellus, 23-2:129, 1971.

38. Pritchard, D., The Movement and Mixing of Contaminants in Tidal Estuaries, Proceedings, First International Conference on Waste Disposal in the Marine Environment, E.A. Pearson, ED, 1960.

39. Holley, E., D. Harleman, and H. Fischer, Dispersion in Homogeneous Estuary Flow, ASCE Journal, HYD:1691, August, 1970.

40. Elder, J., The Dispersion of Marked Fluid in Turbulent Shear Flow, Journal of Fluid Mechanics, 5-4:554, May 1959.

41. Diachishin, A., Dye Dispersion Studies, ASCE Journal, 89-SA1:29, January 1963.

42. Mitchell, A. and G. Fairweather, Improved Forms of the Alternating Direction Methods of Douglas, Peaceman, and Rachford for Solving Parabolic and Elliptic Equations, Numerische Mathematik, 6:285, 1964.

43. Aziz, K., and J. Hellums, Numerical Solution of the Three-Dimensional Equations of Motion for Laminar Natural Convection, The Physics of Fluids, 10-2:314, February 1967.

44. Haight, F., Currents in Narragansett Bay, Buzzards Bay, and Nantucket and Vineyard Sounds, U.S.C. and G.S. Sp. Pub. No. 208, 1938.

45. Public Health Service Drinking Water Standards, Public Health Reports, 61:371, 1946.

46. National Shellfish Sanitation Program Manual of Operations, Public Health Service Publication No. 33, 1965.

47. Bonde, G., Bacterial Indicators of Sewage Pollution, International Symposium on Discharge of Sewage from Sea Outfalls, (Several Papers Cited from this Symposium*), Paper No. 5, London, August 30, 1974.

48. Public Health Activities Committee, Coliform Standards for Recreational Waters, ASCE Journal, 89-SA4:57, 1963.

49. Shuval, The Case for Microbial Standards for Bathing Beaches, (Same Symposium*), Paper No. 10.

50. Moore, B., The Case Against Microbial Standards for Bathing Beaches, (Same Symposium*), Paper No. 11.

51. Won, W. and H. Ross, Persistence of Virus and Bacteria in Seawater, ASCE Journal, 99-EE1:205, June 1973.

52. Dutka, B., Coliforms are an Inadequate Index of Water Quality, Journal of Environmental Hygience, 36-1:39, July-August 1973.

53. Graham, J. and J. Sieburth, Survival of Salmonella Typhi Murium in Artifical and Coastal Sea Water, Revue Internationale D'Oceanographic Medicale, 29, 1973.

54. Geldreich, E., Applying Bacteriological Parameters to Recreational Water Quality, J. Amer. Water Works Assoc., 62:113, 1970.

55. Hanes, N. and R. Tragala, Effect of Seawater Concentration on Survival of Indicator Bacteria, Water Pollution Control Federation Journal, 39-1:97, January, 1967.

56. Dufour, Alfred P., Personal Communications, September 1975.

57. Orlob, G., Viability of Sewage Bacteria in Seawater, Sewage and Industrial Wastes, 28:1147, September 1956.

58. Pike, E., Gameson, A., and D. Gould, Mortality of Coliform Bacteria in Sea Water Samples in the Dark, Revue International D'Oceanographic Medicale, 18-19:97, 1970.

59. Gameson, A. and J. Saxon, Field Studies on Affect of Daylight on Mortality of Coliform Bacteria, Water Research, 1-4:279, 1967.

60. Gameson, A. and D. Gould, Effects of Solar Radiation on the Mortality of Some Terrestrial Bacteria in Sea Water (Same Symposium*), Paper No. 22.

61. Mitchell, R. and C. Chamberlin, Factors Influencing the Survival of Enteric Microorganisms in the Sea: An Overview (Same Symposium*), Paper No. 25.

62. Ryan, P. and K. Stolzenbach, Environmental Heat Transfer, Parsons Laboratory, M.I.T., Report No. 156, September 1972.

63. Schenck, H. and A. Davis, A Turbidity Survey of Narragansett Bay, Ocean Engineering, 2:168, 1973.

64. Rhode Island Department of Health, Division of Water Supply and Pollution Control, Unpublished Information, 1966-1975.

65. Frederiksen, R., Our Dirty Water, Reprints from The Providence Journal, October 1971.

66. U.R.I. Ocean Engineering Bay Watch Program, Unpublished Data, 1972.

67. Wachpress, E.L., Iterative Solutions of Ellystic Systems, Prentice Hall, New Jersey, 1966.

68. Gordon, R. and M. Spaulding, "Finite Difference Approximation to the Convective Transport Equation", ASCE Modeling 75, September 3-5, 1975, San Francisco, California.

69. Anasonlis, R.E. and N. McDonald, "A Study of Combustor Flow Computations and Comparison with Experiment", EPA-650/2-73-045, EPA National Environmental Research Center, December 1973.

70. Clear y, Robert W., and D.D. Adrian, "New Analytical Solutions for Dye Diffusion Equations", Journal of Environmental Engineering Division, ASCE, EE3, June 1973.

71. Tidal Current Charts - Block Island Sound - Eastern Long Island Sound, U.S. Department of Commerce, NOAA - National Ocean Survey, First Edition, 1971.

72. Leenderstee, J.J. and E.C. Gritton, "A Water Quality Simulation Model for Well Mixed Estuaries and Coastal Seas, Vol. II: Computational Procedures", The Rand Corporation, July 1971.

73. Leendertse, J., R. Alexander, and S. Lier, A Three-Dimensional Model for Estuaries and Coastal Seas: Volume I, Principles of Computation, The Rand Corporation, RA-1417-OWRR, December 1973.

74. Gordon, R. and M. Spaulding, "Development of a Three Dimensional Nondimensional Vertical Axis Hydrodynamics Model for Application to Coastal Seas and Estuary Areas", Sea Grant, University of Rhode Island (in preparation), 1975.